

# 7<sup>th</sup> International IP Workshop

Lund, Sweden, May 28<sup>th</sup> – 30<sup>th</sup>, 2024

## Book of Abstracts



# 7<sup>th</sup> International IP Workshop

Lund, Sweden, May 28<sup>th</sup> – 30<sup>th</sup>, 2024



**LUND**  
UNIVERSITY

**LTH**  
**FACULTY OF  
ENGINEERING**

*ISRN LUTVDG/(TVTG-3103)/1-136/(2024)*

## Scientific Committee

Adrian Flores Orozco, TU Vienna, Austria

Adrian Mellage, University Tübingen, Germany

Alex Furman, Technion, Israel

Angelos Almparis, Aarhus University, Denmark

Aris Nivorlis, Deltares, The Netherlands

Charles Bérbé, Technological University Montréal, Canada

Flore Rembert, University Orléans, France

Frédéric Nguyen, University Liège, Belgium

Léa Levy, Lund University, Sweden

Line Meldgaard Madsen, Aarhus University, Denmark

Matteo Rossi, Lund University, Sweden

Matthias Bücker, TU Braunschweig, Germany

Pauline Kessouri, BRGM Orleans, France

Sara Johansson, Lund University, Sweden

Thomas Günther, LIAG Hannover, Germany

Tina Martin, Lund University, Sweden

Torleif Dahlin, Lund University, Sweden

Virginie Leroux, SGU, Sweden

# Abstracts and poster for 7th International IP workshop in Lund, Sweden, May 28th – 30th 2024

Session 1: IP for mineral exploration

Session 2: Tackling ambiguity: Towards a more reliable interpretation of IP signals

Session 3: Characterization of contaminated subsurface and monitoring of dynamic processes

Session 4: From field data acquisition and processing to inversion

Poster number	Author	Title	Page #
S1_01	James Macnae	Simple circuits for IP effects	5
S1_02	Virginie Leroux	Measurements of spectral IP on mine tailings	7
S1_03	Veronique Naudet	Very low pH SIP signature of heap-bioleaching	9
S1_04	Kreith Dennis	Modeling of spectral induced-polarization measurements on cm-sized metallic spheres in sand-water mixtures	11
S1_05	Nuray Oncul	Enhancing Mineral Exploration Using Spectral Induced Polarization: Determining the Faradaic Effect for Electron-Conducting Minerals	13
S1_06	Regean Pitiya	SSIP measurements over a porphyry Cu-Au deposit	14
S1_07	Charles Bérubé	Machine learning of complex conductivity anisotropy	16
S1_08	Farid Ullah	Detection of a new Cu-polymetallic deposit by SSIP	18
S1_09	Francesco Dauti	Inductive Induced Polarization: integration with galvanic DCIP and joint inversion	20
S1_10	Jean-Luc Gagnon	Integration of rock anisotropy in the GEMTIP model	22
S1_11	Tina Martin	Superposition of IP signals measured on pyrite–sand mixtures	24
S2_01	Lukas Römhild	Tackling petrophysical ambiguities in IP-K relations by joint inversion of hydraulic tomography and induced polarization data	26
S2_02	Damien Jougnot	Complex conductivity in heterogeneous media, can we use simple mixing laws on SIP spectra?	28
S2_03	James Macnae	Intrinsic Clay IP using low frequency TDEM data	30
S2_04	Danney Glaser	Laboratory Scale Electromagnetic IP Signatures Using a Saw-Tooth Time-Domain Waveform	32
S2_05	Clément Casotti	Applying Induced Polarization to Characterize Nant des Granges Landslide, Bauges, France.	34
S2_06	Leroy Philippe	Can equivalent circuit models be used for the complex conductivity of clayey materials	36
S2_07	Klaudio Peshtani	On the Reliability of Constraining Surface Conductivity using Induced Polarization Measurements in Sedimentary Rocks	38
S2_08	Daniel Anthony Ciraula	Joint application of time-lapse induced polarization and reactive transport modeling to track subsurface H2S mineral storage at a geothermal site	40
S2_09	Marsel Janik	Modeling of membrane polarization for arbitrary electrolytes	42
S2_10	Andreas Hördt	Insights into the structural properties of frozen rock, from fitting a 2-component model to high-frequency SIP laboratory data	44

<b>S2_11</b>	Glebe Ruth	Impact of Pore-Water Velocity on the Spectral Induced Polarization Response of Granular Materials	45
<b>S2_12</b>	Youzheng Qi	On the relationship between quadrature and surface conductivities: A pseudo-constant ratio	47
<b>S2_13</b>	Ermis Proestakis	Complex conductivity of diatomites from Fur Formation saturated with NaCl and KCl solutions	49
<b>S2_14</b>	Klitzsch Norbert	Is it possible to assess the quality of carbonates using IP?	51
<b>S2_15</b>	Abdoul Nasser YACOUBA	Characterization of electrical properties of Beauce Limestones (O-ZNS, France) from SIP measurement	52
<b>S2_16</b>	Luca Peruzzo	Spectral Induced Polarization and Mise-a-la-masse for studying plant roots and root water uptake	54
<b>S2_17</b>	Shany Ben Moshe	On the fate and transport of heavy metals in calcareous soils – a spectral induced polarization study	57
<b>S2_18</b>	Tina Martin	Estimating hydraulic properties from IP and NMR measurements at field and laboratory scale	58
<b>S3_01</b>	Cora Strobel	Reactive process monitoring via joint induced polarization and transport modeling – new insights from cation exchange experiments	60
<b>S3_02</b>	Rahmani Dadenjani, Ali	Tracking ammonium cation exchange in landfill waste using spectral induced polarization (SIP)	61
<b>S3_03</b>	Na Hao	Spectral induced polarization characterization on the landfill leachate contaminated groundwater remediation using permeable reactive materials	63
<b>S3_04</b>	Siyuan Qiang	Quantitative evaluation of the effect of pore water morphology on complex conductivity saturation exponents of porous media saturated by two immiscible fluid phases	65
<b>S3_05</b>	Deqiang Mao	Unveiling the characteristics of ZVI-AC-sand mixtures in remediating contaminated groundwater using spectral induced polarization	67
<b>S3_06</b>	Jian Meng	Quantitation of solid waste deposits through time domain induced polarization signatures	69
<b>S3_07</b>	Flore Rembert	Direct observation and petrophysical modeling of calcite dissolution with microfluidics and spectral induced polarization	71
<b>S3_08</b>	Robinson Judith L	Investigating soil organic matter complexation using SIP in microfluidic and column scale experiments	73
<b>S3_09</b>	Davide Melegari	ERT and TDIP survey for mapping of leachate plumes: application to a MSW landfill in central Italy	76
<b>S3_10</b>	Sonya Altzitser	Organic Pollutant Oxidation on Manganese Oxides in Soils - The Role of Calcite Indicated by Geoelectrical and Chemical Analysis	79
<b>S3_11</b>	Sonya Altzitser	Impact of Natural and Synthetic Polymers on Soil Stability: Insights from SIP and Chemical Analysis	81
<b>S3_12</b>	Marco Vasconez Maza	Monitoring metal mobility in mine tailings during electrokinetic forcing using spectral induced polarisation	83
<b>S3_13</b>	Uriel Zohore	Experimental and numerical characterization of toluene transport and bioremediation processes using spectral induced polarization	85
<b>S3_14</b>	Hamdi Omar	A new experimental setup for combination of SIP measurements with X-ray $\mu$ CT scanning: an application to the Gunnuhver geothermal system in Iceland	87

<b>S3_15</b>	Nicolette Filippone	Exploring the Biogeobattery Phenomenon: Implications of Induced Polarization and Magnetic Susceptibility	89
<b>S3_16</b>	Shoker Abbas	Electrical Characterization of Foam Used in Decontamination: Correlation between Foam Drainage and Resistivity	90
<b>S3_17</b>	Arne Mansfeld	The complex electrical response to NaHCO <sub>3</sub> diffusion in non equilibrium systems.	92
<b>S3_18</b>	Emerson, Hilary P	Monitoring of sulfur modified iron oxidation with spectral induced polarization	94
<b>S3_19</b>	Lee Slater	Spectral induced polarization signals of soils contaminated by aqueous film forming foam (AFFF) releases	96
<b>S3_20</b>	Reyhaneh Norooz	DCIP monitoring of Älvkarleby test embankment dam	98
<b>S3_21</b>	Torleif Dahlin	DCIP monitoring of a MAR infiltration pond at Vomb	100
<b>S3_22</b>	Ijaz Ahmed	Electrical Detection of Groundwater Leakage Channels by Spread Spectrum Induced Polarization (SSIP) Geophysical Method, Fuquan, Guizhou, China	102
<b>S4_01</b>	Haoran Wang	Capacitive coupling in spectral electrical impedance tomography (sEIT) measurements with a centralized multiplexer	104
<b>S4_02</b>	Schulz, Raphael	Induction effect removal for High-Frequency Induced Polarization data	106
<b>S4_03</b>	Sugand, Madhuri	High-frequency induced polarisation: Data inversion and ice-relaxation modelling	108
<b>S4_04</b>	Fereydoun Sharifi	IP-distorted Transient Electromagnetic data modelling	110
<b>S4_05</b>	Lore Vanhooren	The use of Reciprocals for TDIP in volcanic areas	112
<b>S4_06</b>	Khuram Naveed	Variational Mode Decomposition for Estimating Uncertainties in Time-domain Induced Polarization Data	114
<b>S4_07</b>	Stefano Galli	Investigating induced polarization in Floatem Data	116
<b>S4_08</b>	Arcangela Bollino	Inversion of galvanic time-domain IP data in terms of Debye-Warburg decomposition	118
<b>S4_09</b>	Jian Chen	Three-dimensional vector finite element forward modeling and inversion for airborne electromagnetic data considering induced polarization effect	121
<b>S4_10</b>	Gianluca Fiandaca	Closing the gap between galvanic and inductive induced polarization: EEMverter, a new modelling tool for Electric and Electromagnetic data	123
<b>S4_11</b>	Alessandro Signora	Joint inversion of E&EM data with IP modelling: The HydroGeosITe case study	125
<b>S4_12</b>	Nicole Sullivan	EEMstudio: a QGIS plugin for processing and modelling of electric and electromagnetic data with focus on induced polarization	127
<b>S4_13</b>	Rujun Chen	Principle and application of array spread-spectrum IP technique for large depth of exploration	129
<b>S4_14</b>	Thomas Günther	Inverting time-domain induced polarization field data using Debye discretization	131
<b>S4_15</b>	Matteo Rossi	Processing of Time-Domain Induced Polarization datasets with reciprocal measurements	133
<b>S4_16</b>	Aris Nivorolis	An open-source suite for deployment of automated DCIP monitoring: towards real-time monitoring applications	135

# Simple circuits for IP effects

James Macnae CD3D Pty Limited & RMIT University, Melbourne, Australia.

Mechanistic and mathematical models of IP are valuable tools for the characterization of materials. Equivalent circuits can however assist in the intuitive understanding of the electrical and electromagnetic response of polarizable minerals located within a non-polarizable host or under conductive cover.

Some Questions and GENERALISED Answers (Yes No Maybe)

	Q	A	Notes/References
1	Are conceptual electronic circuits useful?	M	Pelton et al, (1978), Weller and Slater (2022), Lou and Wu (1989)
2	Does a spectral response define an equivalent circuit?	N	Definitely not due to Kirchoff Equivalence (Weller and Slater, 2022)
3	Are resistivity Cole-Cole, conductivity Cole-Cole and other dispersive models equally good to fit data?	Y	Tarasov and Titov (2013), Kozhevnikov & Antonov (2020), Fiandaca et al. (2018)
4	Is the Cole-Cole conductivity time-constant (from $\mathbf{J} = \sigma\mathbf{E}$ ) the “simplest” for characterising physical reality?	Y	I have changed my mind from a different opinion expressed by Macnae (2015) and agree with Tarasov and Titov (2013) and Kozhevnikov and Antonov (2020)
5	Can we represent a finite IP target in background or under cover with a simple circuit?	Y	Lou and Wu (1989) seminal paper with (as far as I can ascertain) no citations in last 25 years! Lou spelled Luo in other publications.

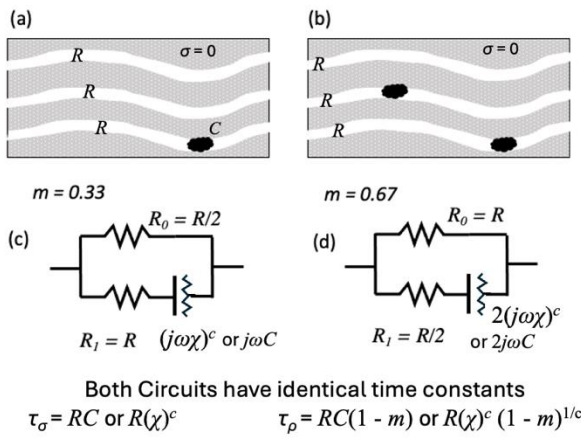


Figure 1: The “blocked” pore model.

Pelton’s conceptual “blocked pore” model shown in 2D above has (Fig. 1) chargeability  $m = (\sigma_\infty - \sigma_0)/\sigma_\infty$  as a fraction of blocked pores assuming block has “infinite” conductivity at high frequency, zero at low frequency and host is perfectly resistive. This circuit “scales” in that the time constant of a set of these circuits in 3D is the same as that of the individual circuits shown (Macnae and Zorin, 2022).

Formulated in conductivity  $\sigma = 1/\rho$ , [ $\mathbf{J} = \sigma\mathbf{E}$ ], the time constant  $\tau_\sigma$  for an applied Voltage step is independent of  $m$  and thus the concentration of polarizable material.  $\tau_\sigma$  is a function of product of resistance  $R$  and  $C$  or  $\chi$  in equivalent circuit, but  $\tau_\rho$  measuring the time constant of the voltage response after a current step also related to chargeability  $m$  (Fig. 1).  $m$  is mathematically just the fraction of blocked pores in this simple model. If all pores are blocked,  $m = 1$ .

## Swiss Cheese Model (Park et al., 2019)

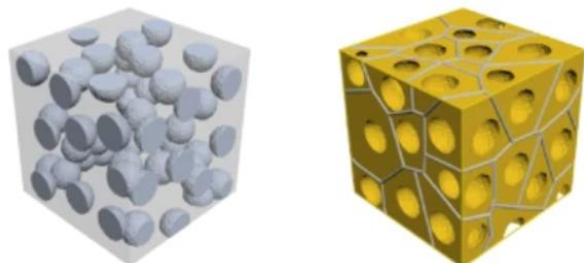


Figure 2: Spheres in background model.

In the 3D distributed sphere model (Fig 2), chargeability  $\mathbf{m}$  for volume fraction  $v$  given by  $\mathbf{m} = 9v/(2 + 5v + 2v^2)$ , provided the spheres are perfectly polarizable (Wong, 1979). The simple electrical circuit equivalent is identical to the blocked pore case (Fig 1), with resistance  $R$  related to resistivity. The time constant  $\tau_\sigma \propto D/d^2$  for practical sulphide cases with  $D$  active ion diffusivity and  $d$  particle diameter. Frequency dependence  $c = 1$  (“Debye”) if no chemical reactions take place, and  $c = 0.5$  (“Warburg”) if  $d$  is constant and reactive ions are present in the surrounds of the polarizable sphere (Wong, 1979). For mineral exploration  $c \leq 0.5$  is critical indicator of sulphides rather than coupling or EM responses, which can often be fit with  $c = 1$  responses;  $\tau_\sigma > 0.1$  s typical for economic sulphides

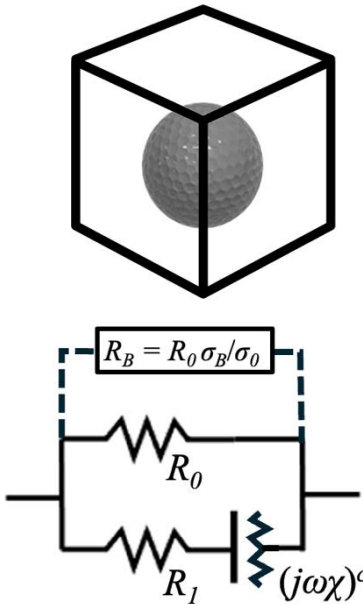


Figure 3:

Externally (field) measured IP spectra can be very different from internal (target) spectra. Consider the case of a polarizable sphere ( $\mathbf{m}$ ,  $\tau_\sigma$ ,  $c$ ,  $\sigma_\infty$ ) in a non-polarizable background of conductivity  $\sigma_B$  (Fig 3). What current do we measure as a function of frequency when an E field is applied to the outside of the box, and as a result what is the spectrum of the galvanic current flow? This problem has a solution given in Lou and Wu (1989), who also provide an equivalent circuit for the case of a sphere in a half-space. The circuit is identical for the polarizable target itself, with an added arm in parallel that accounts for the effect of return currents that can flow in the surrounding half-space as well as within the target.

Without the host, the “matched to target” chargeability is given by  $\mathbf{m} = R_0 / (R_0 + R_1)$ , and the time constant  $\tau_\sigma$  given by  $\tau_\sigma = \chi(R_0 + R_1)^{1/c}$ . With the parallel resistor  $R_B$  in place to represent the host, the apparent time constant  $\tau_a$  that would be measured from surface is:  $\tau_a = \chi(R_1 + R_0 / (1 + \sigma_B / \sigma_0))^{1/c}$ . As shown convincingly in Lou and Yu (1989), the ratio of  $\tau_a$  to  $\tau_\sigma$  can be many orders of magnitude when the background has very different conductivity to the target and  $c$  is small; which is commonly the case for IP targets in mineral exploration. Inversion of finite bandwidth data is as a result not always reliable.

**Conclusions:** The analysis and circuits discussed are simplified, but with physical (including electronic) understanding the response of realistic mineral exploration responses can be better understood. Simple circuits help predict that conductivity Cole-Cole  $\tau_\sigma$  is the most unencumbered of IP time-constant definitions, being independent of chargeability  $\mathbf{m}$ . Resistivity defined time-constant  $\tau_\rho$  and the Fiandaca et al (2018) hybrid  $\tau_\phi = \sqrt{(\tau_\sigma \tau_\rho)}$  are both dependent on  $\mathbf{m}$ . This conclusion applies to both conceptual 2D and 3D models, and to models of IP targets in less-polarizable host rocks.

## References

- Fiandaca, G., Madsen, L., and Maurya P, 2018, Near Surface Geophysics 16 (4), 385-399.
- Kozhevnikov, N. and Antonov, E, 2020,. Geophysical Prospecting, 69, 872-877.
- Lou, Y. and Wu, Z., 1989, SEG, An Overview of Exploration Geophysics in China -1988, 303-331.
- Macnae, J., 2015,. Geophys, J. Int., Vol.202(1), 529-532
- Macnae J. and Zorin, N., 2023, Geophysics 88, No 2.
- Park, S., Hwang, J., Park, G, and Ha, J., 2019. Nature Communications 10(1):2357.
- Pelton, W.H., Ward, S.H., Hallof, P.G., Sill, W.R. and Nelson, P.H., 1978.. Geophysics, 43, 588–609.
- Tarasov, A. & Titov, K., 2013, Geophys. J. Int., 195, 352-356.
- Weller A. and Slater, L., 2022, Geophysics, 87, E393–E399.
- Wong, J, 1979. Geophysics 44, 1245-1269.

# Measurements of spectral IP on mine tailings

Virginie Leroux<sup>1</sup>, Lena Persson<sup>1</sup>, Patrick Casey<sup>1</sup>, Mehrdad Bastani<sup>1</sup>, Cecilia Brolin<sup>1</sup>, Tina Martin<sup>2</sup>

<sup>1</sup>SGU, Geological Survey of Sweden, virginie.leroux@sgu.se

<sup>2</sup>Department of Engineering Geology, Lund University, tina.martin@tg.lth.se

## Introduction

In 2021 and 2022 the Geological Survey of Sweden (SGU) carried out a governmental assignment aiming at assessing the critical raw material resources still present in mining waste throughout the country. As part of the project detailed geophysical investigations were conducted on several tailing dams.

## Method

The tailings sites are all situated in the old mining district of Bergslagen and contain residuals of the extraction of iron and base metals by crushing and gravity techniques on several types of ores. The exploitation of these sites ceased in the 1980s. SGU mapped eight of the tailings using time-domain ERT-IP and tTEM among other geophysical techniques (see Camitz et al. 2024 and Casey et al. 2024). At each tailings site samples from at least two boreholes were collected at every meter and were subjected to detailed geochemical analysis. Spectral IP response for frequencies between  $10^{-3}$  and  $10^4$  Hz was measured in the laboratory on 10 samples, taken at five of the sites and collected at two different depths in each borehole. These samples were sieved to 4 fractions to determine the distribution of grain sizes.

The characteristics of the samples are summarized in the table below.

Site	Ore	Estimated depth of water table	Median grain size in $\mu\text{m}$	Depth of samples
Morkulltjärnen (Yxsjöberg)	W and Cu	<3m	ca 125 >63 and <125	Y1: 2-3m Y2: 8-9 m
Jan-Matsdammen	Fe-oxide apatite	>11m	>200 >200	G1: 1-2 m G2: 5-6 m
Blötberget	Fe-oxide apatite	>9m	>125 and <200 ca 63	Bb1: 6-7 m Bb2: 10-11m
Stollberg	Pb-Zn and Fe-Mn	>12m	>63 and <125 >63 and <125	S1: 4-5 m S2: 15-16 m
Bäckegravan	Fe and cu	0-7m	>63 and <100 >45 and <63	B1: 4-5 m B2: 8-9 m

Table 1: Some specifications of the collected samples subjected to SIP laboratory measurements.

## Results

The observed chargeabilities are between 50 and 400 mV/V. The resistivity and phase spectra vary among and within the sites, but all the measured spectral IP responses can be easily fitted to a Cole-Cole (Pelton) type model (Fig. 1).

Since deeper samples generally contain more water, the resistivity seems related to both water content and to the composition of the material (Fig. 1A, 1B and 2). The peak of the phase is generally displaced towards the higher frequencies when the grain size is finer (Fig 1A & Table 1). Within each borehole the chargeability (intensity of IP response) seems to increase with increased Fe content for all samples except for the samples collected at Stollberg where the effect of Pb content seems to be more significant (Fig 2).

## Conclusions

These results helped evaluating results from field measurements with ERT-IP and tTEM (see Madsen et al. 2023, Casey et al. 2024, Bastani et al. 2023). Measurements on more samples are needed to investigate the relation with water content, grain size, mineral and chemical composition. It would help to better understand the applicability of IP for mineral exploration in such sandy materials.

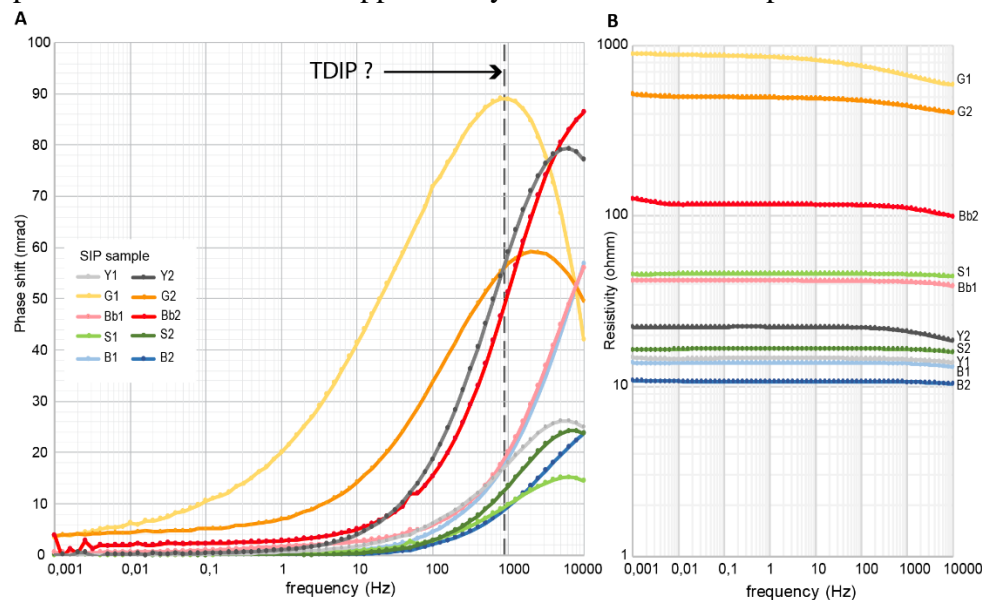


Figure 1: Laboratory measured spectral IP responses (phase (A) and resistivity (B)) of the samples in five sites and at two different depths. The dashed line indicates the maximum frequency resolved by the ground time-domain IP (TDIP) measurements.

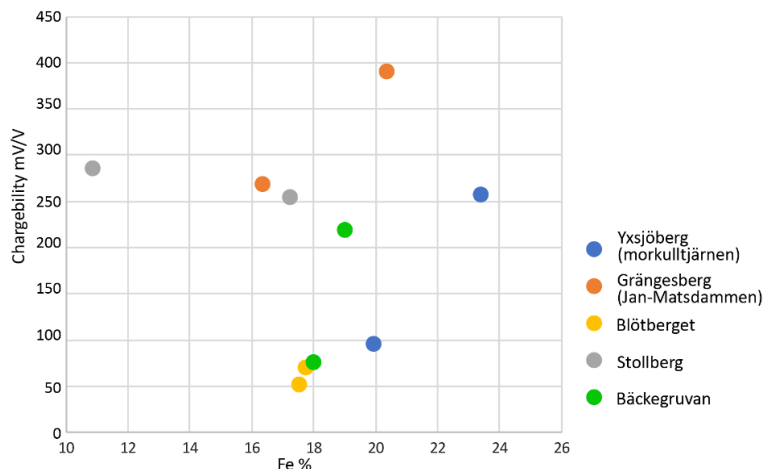


Figure 2: Chargeability versus iron content (in percent of the mass)

## References

- Bastani, M., Brolin, C., Persson, L., Leroux, V., Martin, T., & Maurya, P., 2023. Ground geophysical measurements made on mine tailings in Sweden. Case studies and lessons learned. NSG 2023, 29th European Conference Meeting of Environmental and Engineering Geophysics (5 p.), EAGE.
- Camitz, J., Rauséus, G., Jönberger, J., Persson, L., Sopher, D., & Bastani, M., 2024. Secondary ressources directive. Characterisation of mining waste in central and southern Bergslagen, SGU rapport 2024:23 . (Available at [www.SGU.se](http://www.SGU.se)).
- Casey, P., Brolin, C., Persson, L., Sopher, D., Leroux, V., & Persson, S., 2024. Secondary ressource directive. Characterisation of mining waste in central and western Bergslagen, Sweden, SGU-rapport 2024:02. (Available at [www.SGU.se](http://www.SGU.se)).
- Madsen, L., Asif, M., Maurya, P., Kühl, A., Domenzain, D., Jensen, C., Martin T., Bastani M., Persson, L., 2023. Comparison of tTEM-IP and ERT-IP: Cases from mine tailing sites in Sweden. NSG 2023 29th European Meeting of Environmental and Engineering Geophysics (5 p). EAGE.

# Very low pH SIP signature of heap-bioleaching

Véronique Naudet<sup>1</sup>, Alexis Maineult<sup>2</sup>, Philippe Leroy<sup>3</sup>, Nicolas Florsch<sup>4</sup>, Jochen Petersen<sup>5</sup>

<sup>1</sup> I2M, Bordeaux University, France, [veronique.naudet-maillet@u-bordeaux.fr](mailto:veronique.naudet-maillet@u-bordeaux.fr)

<sup>2</sup> Laboratoire de Géologie, Ecole Normale Supérieure / CNRS UMR8538, PSL Research University, 75005 Paris, France.

<sup>3</sup> BRGM, French Geological Survey, 45060 Orléans, France

<sup>4</sup> UMI 209 UMMISCO, Sorbonne University, Paris, France

<sup>5</sup> Department of Chemical Engineering, University of Cape Town, South Africa.

## Introduction

Heap bioleaching is a technology for recovering copper from low-grade ores. It aims to create conditions in an aerobic biopile of ore material that are conducive to these natural phenomena to achieve the desired mineral dissolution. The Induced Polarization (IP) method could be useful in heap bioleaching to identify areas of high and low water saturation within the heap, or to detect solution flow patterns and microbial effectiveness. We tested the Spectral Induced Polarization (SIP) method in lab. experiments at pH 1, mainly to determine its feasibility in such acidic conditions.

## Materials and Experimental Conditions

Two rectangular cells (8x10 cm in section and 40 cm in height) were packed with heterogeneous acid agglomerated chalcocite (particle size distribution from 20 mm down to sub- $\mu\text{m}$ ). The cells were continuously aerated at 420 mL/min and crossed by a fed solution ( $\approx 5 \text{ L/m}^2/\text{h}$ ) composed of distilled water, sulfuric acid, ferrous iron and ferric iron to support bacterial growth in a medium. This fed solution was sprinkled form the top of the cells onto the bed and withdrawn at the bottom. The experiments were carried out under unsaturated conditions, at room temperature (22°C), under aerobic conditions ( $E_h=450 \text{ mV}$ ) and very acid conditions (pH=1). Cell 1 was inoculated with a culture of iron- and sulfur- oxidizing bacteria just at the beginning of the SIP monitoring, whereas cell 2 was inoculated 28 earlier. Cell 1 is considered to contain young bacteria and cell 2 mature bacteria.

SIP measurements were made with a SIP-Fuchs II system from 0.1 to 10000 Hz. Four nonpolarizing Cu/CuSO<sub>4</sub> electrodes were inserted into the centre of each cell through pierced rubber septum corks at 5 cm intervals. Ideally fluid sampling, geochemical measurements and total effluent volume should have been recorded during the experiment but due to logistical constraints this was not possible. Therefore, we only present preliminary SIP results from two cells over a 5 days period.

## Results

Figure 1 is a plot of the minus phase shift between injected current and measured voltage (-phi) as a function of frequency at 3 different times during the experiment. All spectra show a dispersion around 2 kHz. This could be related to the clay introduced between the electrodes and the heterogeneous medium to improve electrical contact. Prior to bacterial inoculation, we performed SIP measurements under abiotic conditions trying to determine the particular frequency signature associated with this electrode/clay/grain interface. We found a “clay dispersion” around 500 Hz which could not explain the 2 kHz dispersion.

Only the spectra without bacteria (day 1, cell 1, Fig. 1.c.) shows a dispersion around 5 Hz. This could be due to the presence of pyrite at the beginning of the experiment before the bacterial action.

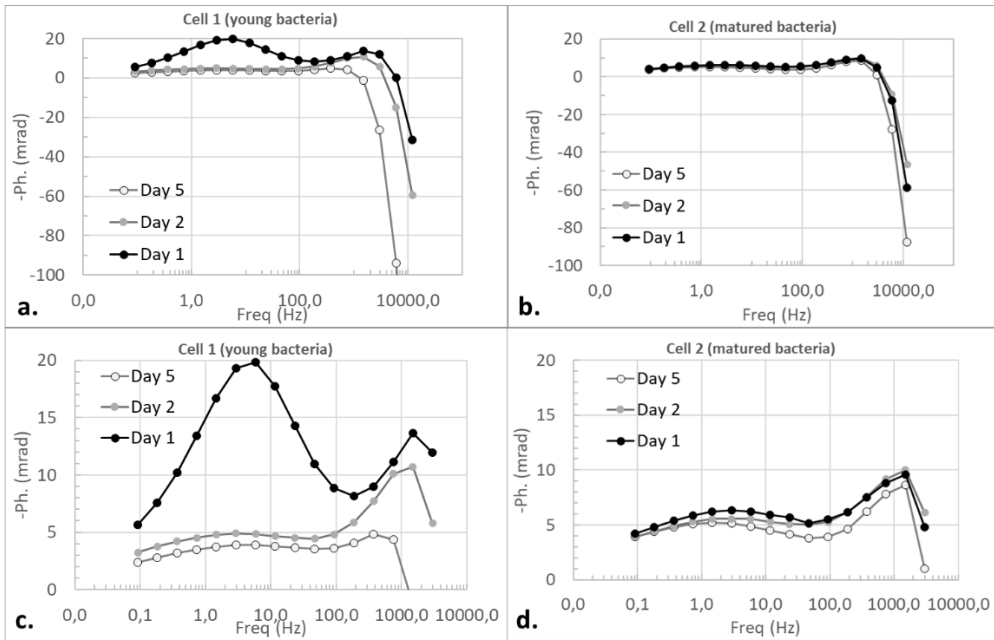


Figure 1. Minus phase shifts measured on (a) cell 1 with young bacteria inoculated day 1 and on (b) cell 2 with matured bacteria inoculated 28 days before, i.e. at a more advanced stage of the heap-bioleaching process. (c) and (d) are the same data represented until 3 kHz.

As we do not have biogeochemical analyses it is difficult to go too far in interpreting this dispersion. A phase decrease over time is observed in all cells and particularly in cell 1 (Fig. 1.c), which has just been inoculated. This could be a reflection of bacterial action during the heap-leaching process. At very high frequencies ( $>5$  kHz), the phase drops dramatically to positive values. This could be due to cable or electrode effects (Slater and Wang, 2019), but previous mathematical computations using CR1Dmod and CR1Dinv (Ghorbani *et. al.* 2009) show that cable effects cannot induce such a signature at our frequencies and scale. We therefore suggest that the positive phase may be due medium or process related and can be explained by the very acidic pH of the medium. Indeed, at such an extreme pH with a high concentration of protons in the bulk water that could be adsorbed on the solid surface, the surface charge may be positive, inducing anion accumulation in the electrical double layer and an associated positive phase.

## Conclusion

While these preliminary lab experiments have large gaps, especially in biogeochemical monitoring, they have raised new scientific questions that we did not expect, especially the positive phase at high frequency. We expect to improve our understanding of these data through modelling and new experiments.

## References

- Ghorbani, A., Camerlynck, C., and Florsch, N., 2009. CR1Dinv: A Matlab program to invert 1D spectral induced polarization data for the Cole–Cole model including electromagnetic Effects. *Computers & Geosciences*, 35(2), 255–266. doi:10.1016/j.cageo.2008.06.001
- Slater, L. D., and C. Wang (2019), Extending accurate spectral induced polarization measurements into the kHz range: modelling and removal of errors from interactions between the parasitic capacitive coupling and the sample holder, *Geophysical Journal International*, 218(2), 895–912, doi:10.1093/gji/ggz199.

# Modeling of spectral induced-polarization measurements on cm-sized metallic spheres in sand-water mixtures

Dennis Kreith<sup>1</sup>, Katrin Breede<sup>2</sup>, Zeyu Zhang<sup>2</sup>, Andreas Weller<sup>2</sup>, Matthias Bücker<sup>1</sup>

<sup>1</sup> Institute of Geophysics and Extraterrestrial Physics, TU Braunschweig, Germany, [d.kreith@tu-braunschweig.de](mailto:d.kreith@tu-braunschweig.de)

<sup>2</sup> Institute of Geology and Paleontology, TU Clausthal, Germany

The detection of metallic particles has been an important field in applied geophysics for several decades, e.g. in the exploration of mineral deposits. Induced polarization measurements are a highly suitable geophysical method due to the high polarizability of metallic particles.

To correctly interpret field and laboratory data, a thorough understanding of the underlying conduction and polarization mechanisms is necessary. Such understanding can be achieved by combining laboratory measurements under well-controlled experimental conditions with theoretical models describing the basic physical processes at the micro scale. However, matching theoretical model predictions with real measured data can be challenging as models often consider idealized situations, are based on largely simplified assumptions and exhibit a large number of model parameters that are hard to be constrained by experimental measures.

We compare experimental spectral induced-polarization data of one single metallic sphere with a diameter of 9.5 mm, embedded in a sand-water mixture with the prediction of theoretical models. The response of a spherical metallic particle can be described by the analytical model of Wong (1979), which considers one metallic sphere in an electrolyte solution. Bücker et al. (2019) presented a numerical model, extending the model of Wong (1979) by the influence of a static surface charge.

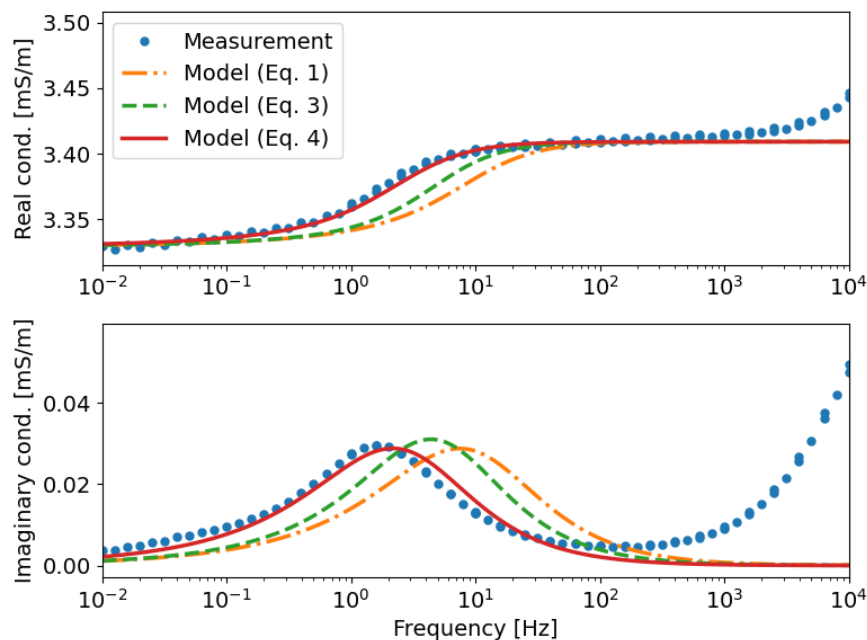


Figure 1: Measured complex conductivity spectrum (blue dots) of one single stainless-steel sphere with a diameter of 9.5 mm. The sphere is embedded in a sand-water mixture with a porosity of 40.15 % and a fluid conductivity of 11.5 mS/m. The solid lines show the modelled conductivity spectra of this system with different approaches for consideration of the formation factor.

We use the numerical model of Bücker et al. (2019), which we extend to be able to consider the influence of dissolved metal ions with valences  $>1$  as expected for real metal ions (e.g., Fe(II), Fe(III)). Figure 1 shows the polarization response of our model along with a corresponding laboratory measurement.

To fit the low-frequency value of the real conductivity, we adjust the modelled complex conductivity  $\sigma_{\text{mod}}$  with the formation factor  $F = 3.43$  that is calculated as the ratio between the DC-limit of the measured real conductivity and the bulk electrolyte conductivity of 11.5 mS/m. The formation factor takes the influence of the sand into account in which the metal sphere is embedded.

We use three different approaches to include the formation factor in our model: In a first approach, we divide the modelled conductivity spectrum by  $F$  (orange dash-dotted line in Figure 1)

$$\sigma_{\text{eff}}(\omega) = \frac{\sigma_{\text{mod}}(\omega)}{F}, \quad (1)$$

while the actual simulation is carried out assuming a sphere immersed in an electrolyte of conductivity

$$\sigma_0 = 2\mu e N_A c_0 = 11.5 \text{ mS/m}. \quad (2)$$

Here,  $\mu$  is the ion mobility,  $e$  is the elementary charge,  $N_A$  is the Avogadro constant, and  $c_0$  is the bulk electrolyte concentration.

In two other approaches, we include the formation factor already during the simulation process by either adjusting the ion concentration to an effective ion concentration

$$c_{0,\text{eff}} = \frac{c_0}{F} \quad (3)$$

(green dashed line in Figure 1) or the ion mobility to an effective ion mobility

$$\mu_{\text{eff}} = \frac{\mu}{F} \quad (4)$$

(red solid line in Figure 1). It is also possible to combine the latter approaches (not shown here), leading to results, which fall in between these two limiting cases.

A comparison of the three modeling approaches with the measured conductivity spectrum indicates that adjusting the ion mobility provides the best fit of model and measured data. Please come to our poster to discuss the implications of this finding!

## References

- Bücker, M., Undorf, S., Flores Orozco, A. and Kemna, A., 2019. Electrochemical polarization around metallic particles – Part 2: The role of diffuse surface charge. *Geophysics*, 84, E57-E73.
- Wong, J., 1979. An electrochemical model of the induced-polarization phenomenon in disseminated sulfide ores. *Geophysics*, 44, 1245-1265.

# Enhancing Mineral Exploration Using Spectral Induced Polarization: Determining the Faradaic Effect for Electron-Conducting Minerals

Nuray Oncul<sup>1</sup>, John Kingman<sup>2</sup>, Lee Slater<sup>1,3</sup>

<sup>1</sup>*Department of Earth and Environmental Science, Rutgers University Newark, NJ, USA, no171@scarletmail.rutgers.edu*

<sup>2</sup>*Terrigena Ltd., Hong Kong,*

<sup>3</sup>*Pacific Northwest National Laboratory, Energy and Environment Directorate, Richland, USA*

Investigating economically valuable electron-conducting minerals has become increasingly important due to the rising demand for these essential resources. Spectral Induced Polarization (SIP) is a geophysical method extensively utilized for investigating mineral deposits. It involves measuring the complex impedance across various frequencies to assess the subsurface characteristics. In the presence of electron-conducting minerals and under an applied alternating electrical field, both non-faradaic effects and faradaic effects occur at the metal-solution interface. Under non-faradaic conditions, the charge can only accumulate and is unable to traverse the interface. However, under faradaic conditions, the faradaic current can effectively cross the phase boundary through electron transfer in the presence of redox-active ions. This faradaic process leads to a non-linear SIP response. Recent research on SIP has primarily focused on non-faradaic polarization effects, with the faradaic effect largely ignored. In this study, the significance of the faradaic effect was examined across a range of electron-conducting minerals. Laboratory measurements were performed on synthetic mixtures containing electron-conducting minerals and sand, simulating both veinlet and disseminated mineralization. We find that veinlet mineralization yields significantly stronger faradaic SIP effects compared to disseminated mineralization. Furthermore, considering different mineralization, while certain minerals exhibit strong faradaic effects, others (such as graphite) show no significant faradaic response. Additional laboratory experiments revealed that rock samples with various textural and mineralogical characteristics exhibited distinct faradaic signatures in their SIP responses. Observing these distinctive effects in both synthetic and rock samples encourages the utilization of faradaic signatures to enhance interpretation of SIP measurements.

# SSIP measurements over a porphyry Cu-Au deposit

Regean Pitiya<sup>1</sup>, Rujun Chen<sup>\*1</sup>, Lunkai Yang<sup>2</sup>, Qingling Xiao<sup>3</sup>, Haojie Zhang<sup>1</sup>, Shuang Cheng<sup>4</sup>

<sup>1</sup> School of Geosciences and Info-Physics, Central South University, Changsha 410083, China, [chruijun12358@gmail.com](mailto:chruijun12358@gmail.com)

<sup>2</sup> Institute of Geochemical Exploration and Marine Geological Survey, Jiangsu Geological Bureau, China

<sup>3</sup> School of Earth Sciences, Hebei GEO University, Shijiazhuang, Hebei, China

<sup>4</sup> Giant Sequoia Artificial Intelligence Technology (CHANGSHA) Limited, China

Porphyry deposits that are exposed to the surface are mostly found and mined in large porphyry provinces around the world. The metallogenic potential of concealed porphyry deposits is thought to be just as favorable by some mineralogists as that of exposed deposits. Increasing the success rate for discovering such concealed deposits is important to maintain a steady supply of critical commodities needed in the shift to green technology. To improve the discovery rates, modern mineral exploration utilizes advanced multi-method techniques that integrate a wide range of geoscience data and information to generate complex and high-resolution exploration models. Geophysical methods are crucial in this type of exploration, as they allow for non-invasive, systematic measurements and generally have considerable depth penetration. They provide 2D and 3D physical models of geological information. One such geophysical methods, which is most effective in porphyry exploration on the prospect scale is the induced polarization (IP) method. The IP image both the chargeability and electrical conductivity. Individual rock units and alteration products associated with porphyry deposits render them detected with IP surveys. Pyrite, chalcopyrite, and bornite alter chargeability; and significant mineralization and fluid filled fractures will affect the electrical conductivity. In recent years a new frequency-domain IP method called the spread-spectrum induced-polarization (SSIP) approach was introduced. This method uses pseudorandom m-sequence as a broadband signal for the injected primary current with power in the frequency range of 1/16 – 1 Hz. In addition, the method allows synchronous real-time full-waveform acquisition and real-time data-quality monitoring of massive SSIP receivers. This is based on the integrated spread spectrum communication technology of ZigBee wireless sensor network and GPS timing (Liu et al., 2017). The SSIP technique has been successfully applied to mineral and groundwater exploration, and the depth of exploration is more than 1 km.

Here we present pole-dipole SSIP results from field experiment on the hidden Chating porphyry copper-gold deposit in Anhui Province, China. The deposit was recently discovered hosted in quartz diorite porphyry, surrounded by marble and/or limestone and overlaid by a shallow volcanic cover (Xu et al., 2022). A 1840m long SSIP survey line oriented north to south through the main ore body of Chating mining area with the measurement point distance and pole distance of 40m was deployed. A total of 48 SSIP sounding points were designed and transceiver maximum distance of 2500m. Since the SSIP method use 16 frequencies for signal transmission, we tested and selected appropriate base frequencies. 1/4Hz and 1/16 Hz were selected as the base frequencies. The 1/16Hz presented smaller electromagnetic coupling but the difference in rock and ore polarizability was slightly smaller. Strong electromagnetic coupling was evident at 1/4 Hz but the polarizability difference of rock and ore was larger. The obtained SSIP chargeability and resistivity inversion results are shown in Figure 1 for the

two selected frequencies. The obtained resistivity tomograms (Figure 1a and c) present only a conductive shallow layer with thickness increasing towards the north, overlaying a resistive layer. The resistivity does not distinguish the ore bodies' location from the known marble. The chargeability results on the other hand show distinct IP anomalies. The 1/4Hz tomogram (Figure 1b) is characterised by high IP chargeability body of  $\eta \geq 5\%$  (IP1) that is discriminated from the surrounding rocks (marble). This anomaly is consistent with the location of Cu-Au mineralization in quartz diorite porphyry and crypto-explosive breccia body revealed by drill data. For the 1/16Hz tomogram (Figure 1d), the shallow IP anomaly (IP2) extending north is likely caused by the wide spread pyrite-sericite.

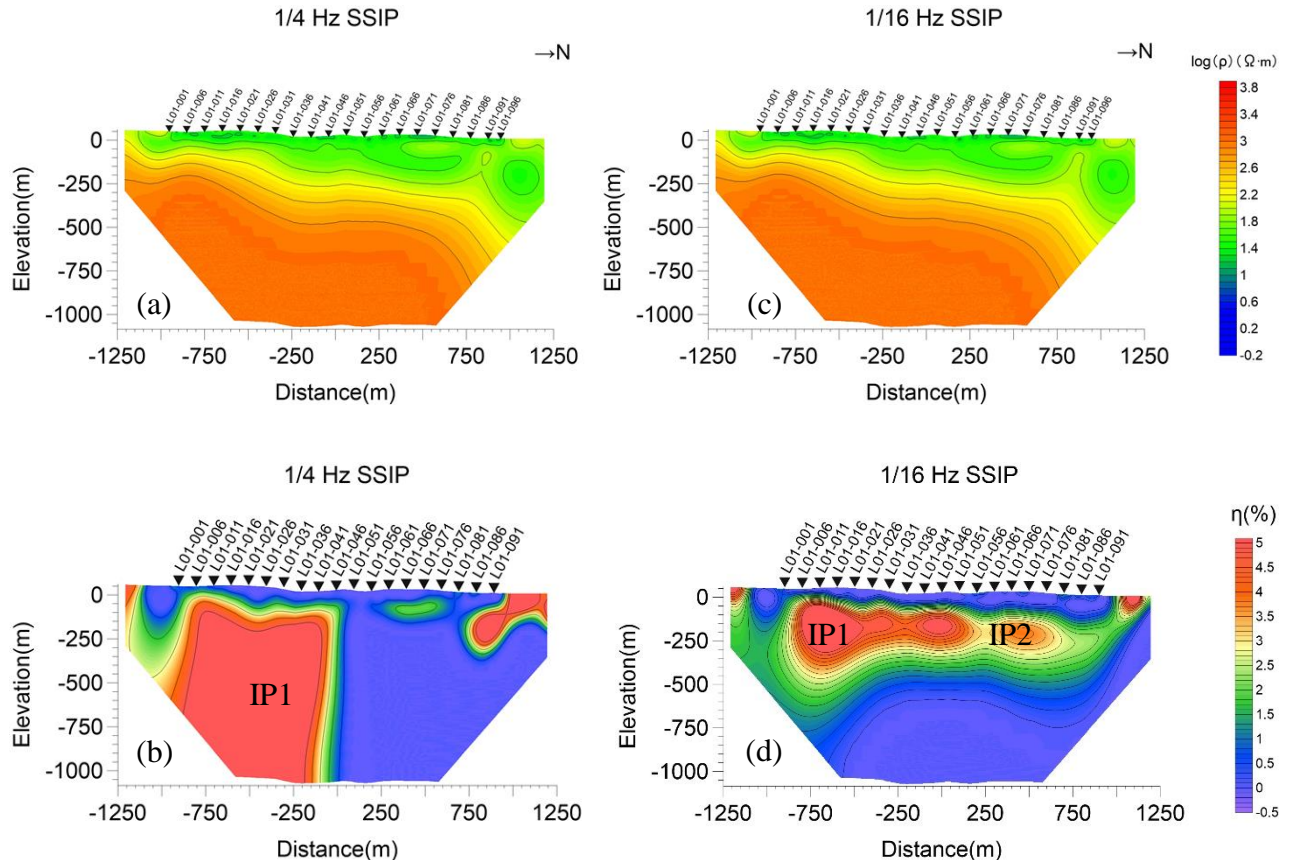


Figure 1: Location of porphyry Cu-Au detected by SSIP. (a) The 2D resistivity tomogram derived from the apparent complex resistivity data at a frequency of 1/4 Hz. (b) The 2D IP chargeability tomogram at 1/4 Hz. (c) The 2D resistivity tomogram at 1/16 Hz. (d) The 2D IP chargeability tomogram at 1/16 Hz.

To conclude, in this work we show the feasibility of the SSIP method at detecting a concealed porphyry copper-gold deposit under a thin overburden. The IP chargeability data prove to discriminate well the porphyry deposit from the barren rocks than the resistivity data. In general, the SSIP method has great application in the exploration of porphyry deposits.

## References

- Liu, W., Chen, R., Cai, H., Luo, W. and Revil, A. 2017. Correlation analysis for spread-spectrum induced-polarization signal processing in electromagnetically noisy environments. *Geophysics*, 82, E243-E256.
- Xu, X.-Y., Xu, X.-C., Xie, Q.-Q., Fu, Z.-Y., Lu, S.-M. and Zhao, L.-L. 2022. Geological features and ore-forming mechanisms of the Chating Cu–Au deposit: A rare case of porphyry deposit in the Middle–Lower Yangtze River metallogenic belt. *Ore Geology Reviews*, 144, 104860.

# Machine learning of complex conductivity anisotropy

Charles L. Bérubé<sup>1</sup>, Jean-Luc Gagnon<sup>2</sup>

<sup>1</sup>*Department of civil, geological and mining engineering, Polytechnique Montréal, Canada, [charles.berube@polymtl.ca](mailto:charles.berube@polymtl.ca)*

<sup>2</sup>*Department of engineering physics, Polytechnique Montréal, Canada*

**Abstract.** We formulate the generalized effective medium theory of IP with a neural network to efficiently model the complex conductivity of anisotropic rocks. We validate the results against published solutions for simplified rock models. Simulations with anisotropic rock models show that the neural network is up to 100,000 faster than numerical integration methods.

## Introduction

The generalized effective medium theory of IP (Zhdanov, 2008) models the complex conductivity of rocks at their bulk scale. While this model does not describe IP mechanistically at the pore and grain scales, it stands out by accounting for polarizable mineral inclusions of any shape and orientation in three dimensions. However, the effective medium theory requires solving the depolarization tensor integrals of every inclusion in a given rock model, which is numerically demanding for anisotropic rocks. Thus, modelling the IP signals of realistic rock models typical of ore deposits may necessitate excessive computation times, especially when dealing with numerous mineral types and geometries. We aim to streamline anisotropic IP simulations by estimating the depolarization tensors with machine learning, effectively replacing numerical integration.

## Methods

The proposed neural network (NN) approximates the volume ( $\boldsymbol{\Gamma}$ ) and surface ( $\boldsymbol{\Lambda}$ ) depolarization tensors of mineral inclusions given anisotropy parameters ( $A, B, C, D$ ).  $A$  and  $B$  are normalized ratios describing the shape anisotropy of triaxial ellipsoid inclusions, whereas  $C$  and  $D$  convey the conductivity anisotropy of the host rock. The output of our NN with  $L = 4$  hidden layers is

$$(\boldsymbol{\Gamma}, \boldsymbol{\Lambda}) = \mathbf{W}^{(L+1)} \mathbf{a}^{(L)} + \mathbf{b}^{(L+1)},$$

where the output of the  $l^{\text{th}}$  hidden layer is

$$\mathbf{a}^{(l)} = \text{SiLU}(\mathbf{W}^{(l)} \mathbf{a}^{(l-1)} + \mathbf{b}^{(l)}),$$

and where  $\mathbf{W}$  and  $\mathbf{b}$  are respectively the NN's weight matrices and bias vectors. SiLU denotes the element-wise sigmoid linear unit activation function. The input layer is the special case of

$$\mathbf{a}^{(0)} = (A, B, C, D).$$

Additional details on the anisotropic depolarization tensor integrals, training data generation, and NN optimization strategy are available in Bérubé & Gagnon (2024).

## Results

The NN accurately predicts the depolarization tensor integrals with up to four significant digits for moderately anisotropic rocks and two significant digits for highly anisotropic rocks. Moreover, the mean absolute percentage error between the NN-predicted IP response and the numerical integration solution for a test rock model is  $(0.04 \pm 0.03)$  %. In addition to the validation experiments, we present examples of complex anisotropic rock models and their corresponding NN-predicted IP signatures. For rocks with numerous inclusions, the NN is up to 100,000 times faster than Simpson's rule integration if aiming for a comparable accuracy with both methods (Figure 1).

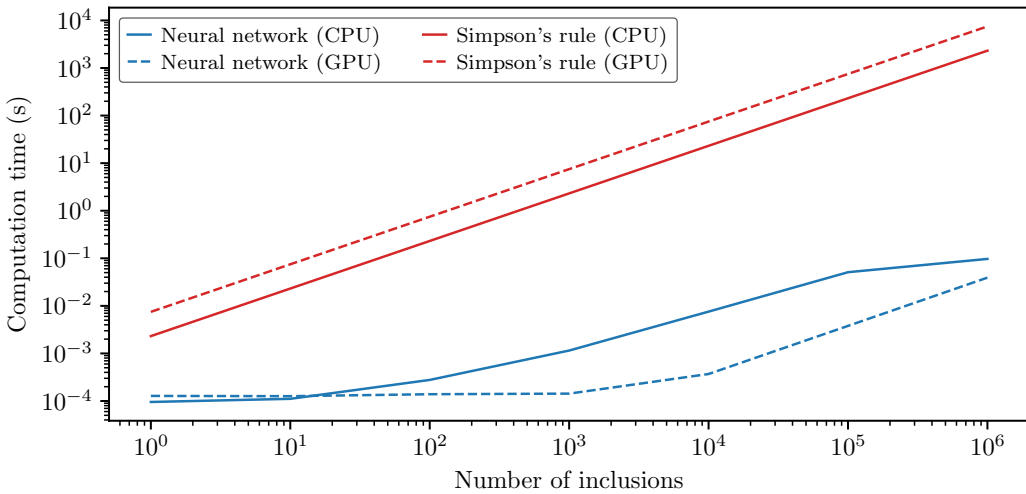


Figure 1: Comparison of neural network and Simpson's rule computation times as a function of mineral inclusion number.

We leverage the efficiency of the NN to conduct new experiments on IP anisotropy. Our results show that highly anisotropic rocks deviate from the expected relationship between chargeability and polarizable mineral content. We observe a similar result concerning critical frequency and host rock conductivity. Finally, the NN's Jacobian provides the relative sensitivity of the depolarization tensors to the anisotropy parameters. The inclusion shape anisotropy is, on average, more important than the host rock anisotropy for determining depolarization tensors (Table 1).

Depolarization tensor	Inclusion shape anisotropy	Background conductivity anisotropy
Volume	47.8 %	52.2 %
Surface	64.5 %	35.5 %

Table 1: Average relative sensitivity indices of the depolarization tensors with respect to anisotropy parameters.

## Conclusions

Our machine learning approach streamlines IP modelling for anisotropic rocks. We use the NN to analyze the IP responses of anisotropic host rocks with triaxial inclusions, a significant contribution over existing solutions for isotropic host rocks with spheroidal inclusions. The NN is a fast and precise alternative to numerical integration for solving depolarization tensors, making it practical to simulate the IP responses of increasingly realistic rock models with limited computational resources.

## References

- Bérubé, C.L., Gagnon, J.-L., 2024. Anisotropic induced polarization modeling with neural networks and effective medium theory. *arXiv:2402.11313 [physics.geo-ph]*. <https://doi.org/10.48550/arXiv.2402.11313>
- Zhdanov, M., 2008. Generalized effective-medium theory of induced polarization. *Geophysics* 73, F197–F211. <https://doi.org/10.1190/1.2973462>

# Detection of a new Cu-polymetallic deposit by SSIP

Farid Ullah<sup>1</sup>, Zhou Xin<sup>\*2</sup>, Chen Rujun<sup>\*1</sup>, Yang Lunkai<sup>2</sup>, Yao Hongchun<sup>1</sup>, Hu Hao<sup>2</sup>, Chen Siwen<sup>1</sup>, Wang Quanggong<sup>1</sup>

<sup>1</sup> School of Geosciences and Info-Physics, Central South University, Changsha 410083 China, chrujun12358@gmail.com

<sup>2</sup> Institute of Geochemical Exploration and Marine Geological Survey, Jiangsu Geological Bureau, China, 66535649@qq.com

Spread spectrum induced-polarization (SSIP) method is a relatively new geophysical method based on the technology of spread-spectrum communication and change in type of signal used for the injected (primary) current unalike that used in traditional frequency domain induced polarization (FDIP). That is, instead of the using classical rectangular current waves with boxes of constant durations, the SSIP use m-sequence signal(Liu et al., 2017, Liu et al., 2016). The new method is steadily gaining applications in underground water exploration, groundwater monitoring and mineral exploration. Recent and ongoing exploration work in the Gaochun District, Jiangsu Province, China, has detected new Cu-polymetallic deposits through the application of this new method among others. Hence in this paper, we report on the discovery results of the applied SSIP method.

In June of 2022, we conducted SSIP surveys in Gucheng-Yaxi Area, Gaochun District, Jiangsu Province, China. A SSIP profile with the length of 3300m was established on which potential electrodes were planted at a constant spacing of 40m. The pole-dipole sounding was used for which the initial current electrode spacing was set to 80m, then subsequently increased each time until the entire profile was covered. There were 29 current injections inside and outside the receiver array to ensure the high resolution of near-surface structures.

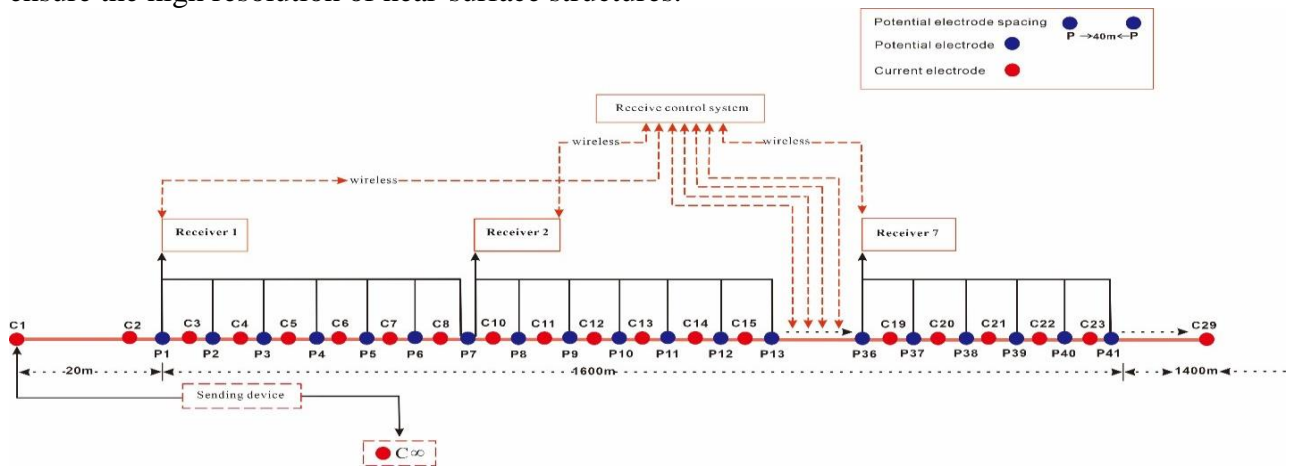


Figure 1 Schematic diagram of SSIP for pole-dipole sounding

We performed 2dimensional (2D) inversion for property of SSIP polarizability and resistivity and the results are presented in Figure 1.

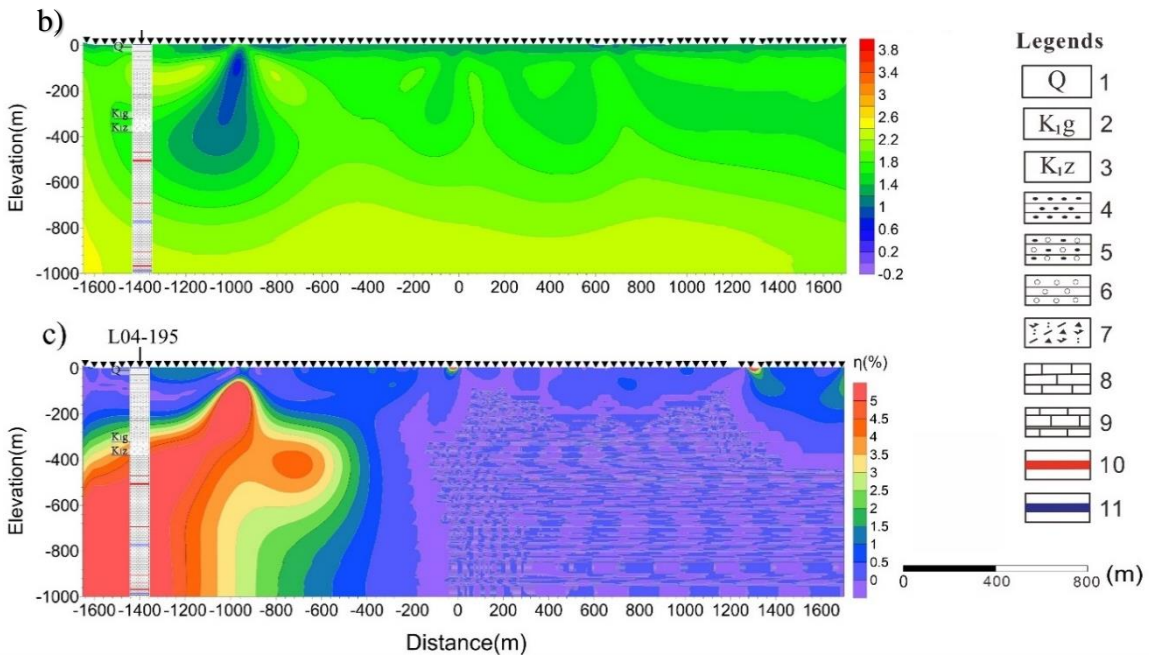


Figure 2 SSIP inversion results from a Cu-polymetallic deposit. (b) The resistivity model. (c) The chargeability model. 1; Quaternary, 2; Lower Cretaceous Ganhe Formation, 3; Lower Cretaceous Zhongfencun Formation, 4; Silt stone, 5; Glutenite, 6; Conglomerate, 7; Dacite volcanic breccia, 8; Limestone, 9; Marble, 10; Pb-Zn ore body, 11; Cu-Au ore body

The 2D SSIP inversion results for the resistivity model clearly show a low resistivity anomaly centered at the point distance -1000m and extend from surface to 600 depth. The same anomalous structure is observed to be present in the IP chargeability model having the highest chargeability distinct from the sounding area. The low resistivity- high chargeability characteristic of this structure suggested a favorable mineralization location and a drill hole was established for verification. The drillhole encountered mineralization between 400 m and 1201.97m depth. The ore bearing rock is mainly marble rock mass in which mineralization occurs interspaced at varies depth. Furthermore, during the verification, a thick mineralized dolomite zone, 13 polymetallic veins containing copper, lead, zinc, gold, and silver were encountered, with individual vein thickness ranging from approximately 0.15m to 3.4m and a cumulative thickness of 17.03m. The main lithology in the order from the surface is as follows: quaternary layer with a thickness of about 100 m, K1g with 200 m thickness, K1z with a thickness of about 100m, and from 400 m to 1201.97 is marble from the Triassic (T1).

In summary, this study demonstrated the successful detection of a new polymetallic deposit by SSIP method among others in a new area without enough prior information. For the first time, through borehole verification, the lithology of the study area is revealed which is essential to guide further exploration in the periphery area.

## References

- LIU, W., CHEN, R., CAI, H. & LUO, W. 2016. Robust statistical methods for impulse noise suppressing of spread spectrum induced polarization data, with application to a mine site, Gansu province, China. *Journal of Applied Geophysics*, 135, 397-407.
- LIU, W., CHEN, R., CAI, H., LUO, W. & REVIL, A. 2017. Correlation analysis for spread-spectrum induced-polarization signal processing in electromagnetically noisy environments. *Geophysics*, 82, E243-E256.

# Inductive Induced Polarization: integration with galvanic DCIP and joint inversion

F. Dauti<sup>\*,1</sup>, A. Viezzoli<sup>2</sup>, G. Fiandaca<sup>1</sup>

1 The EEM Team for Hydro & eXploration, Dep. of Earth Sciences A. Desio, Università degli Studi di Milano, Via Botticelli 23, Milano (Italy)

2 Emergo s.r.l., Via XX Settembre 12, Cascina (Pisa), Italy

\*francesco.dauti@unimi.it

With this contribute we present a case study of integration between ground DCIP and the inductive Induced Polarization extracted from the airborne EM measurements. To do this we worked with data acquired by the PanGlobal mining company, in Spain, constituted by 17 ground DCIP lines overlapped by an airborne EM survey.

The two datasets have been modelled with a consistent modelling procedure within EEMverter (Fiandaca et al., 2024): a 2D forward response formulation for the full-decay DCIP data and a 1D modelling for the TEM data, modelling transmitter waveform and receiver transfer function.

Regarding the model-space parametrisation, we used the Maximum Phase Angle (MPA) Cole-Cole re-parametrisation (Madsen et al., 2018) for both galvanic and inductive data, to reduce equivalencies between the parameters. Furthermore, in order to minimize the poorly-resolved inversion parameters, no vertical variability was allowed for spectral parameters.

The results of this approach are presented in *Figure 1a* and *1b*, showing a comparison between the ground DCIP (*1a*) and the airborne chargeability models (*1b*). A very good correlation is clearly visible from the figure. In *figure 1c*, a comparison between the known mineralization model and the airborne chargeability model (in yellow) is presented.

Moreover, a joint inversion between the two entire datasets has been performed. The results are visible in *Figure 2*, showing an improvement in the lateral resolution of the retrieved chargeability model.

In conclusion, it is possible to effectively retrieve the chargeability from airborne EM measurements when the model-space is properly constrained and to effectively jointly model ground and airborne IP data. These findings open the way for a radical change in mineral exploration with electric and electromagnetic methods: the AEM method can be used to guide the ground exploration also for finding chargeability anomalies, and then the joint inversion of AEM and ground IP data can further enhance the resolution of the imaging results.

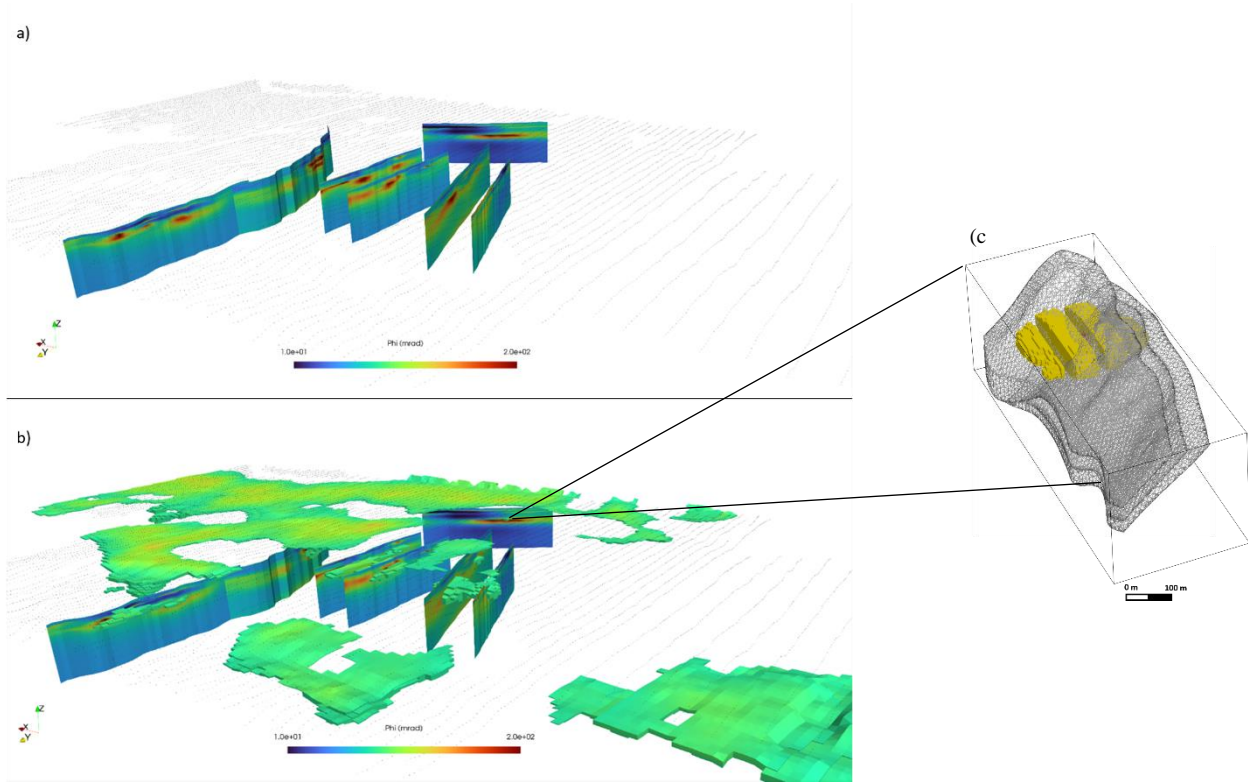


Figure 1. a) Example of ground DCIP phase results and, in dashed line, the AEM survey flown above; b) Partial Ground DCIP vs Airborne IP phase results; c) Airborne chargeability model (yellow) vs known mineralization (grey).

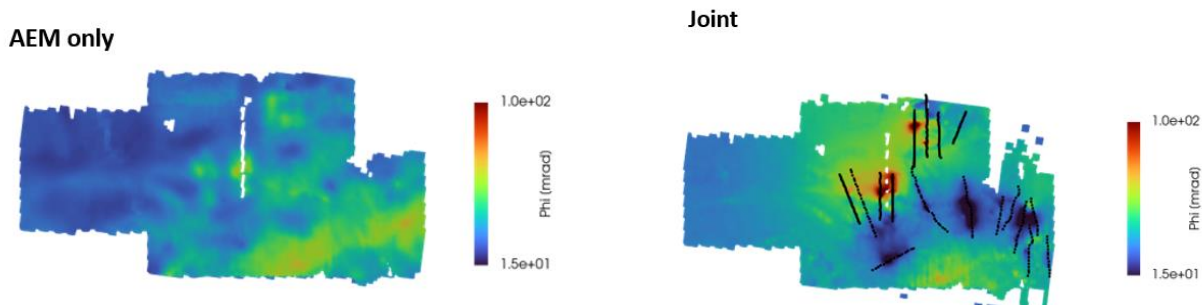


Figure 2. Comparison between AEM only model (on the top) and Joint Inversion model (on the bottom) for a chargeability slice at 60 m of depth.

## References

- Fiandaca, G., Zhang, B., Chen, J., Signora, A., Dauti, F., Galli, S., Sullivan, N.A.L., Bollino, A., Viezzoli, A. (2024). Closing the gap between galvanic and inductive induced polarization: EEMverter, a new modelling tool for Electric and Electromagnetic data. *7th international IP workshop, 28-30 May 2024, Lund, Sweden*.
- Madsen, L.M., Fiandaca, G., Maurya, P.K. (2018), Re-parameterisations of the Cole–Cole model for improved spectral inversion of induced polarization data. *Near Surface Geophysics*, 16: 385-399.
- Inverno, C. & Díez-Montes, (2015). Introduction and Geological Setting of the Iberian Pyrite Belt. 10.1007/978-3-319-17428-0\_9.

# Integration of rock anisotropy in the GEMTIP model

Jean-Luc Gagnon<sup>1</sup>, Charles L. Bérubé<sup>2</sup>

<sup>1</sup>Department of engineering physics, Polytechnique Montréal, Canada, [jean-luc.gagnon@polymtl.ca](mailto:jean-luc.gagnon@polymtl.ca)

<sup>2</sup>Department of civil, geological and mining engineering, Polytechnique Montréal, Canada

**Abstract.** We extend the generalized effective medium theory of induced polarization (GEMTIP) to model the complex conductivity of anisotropic host rocks containing triaxial ellipsoid inclusions. This extension involves numerically solving the depolarization tensors of the inclusions, for which the integrands are unstable in the case of highly anisotropic rocks. We show that adaptive sampling outperforms uniform sampling for solving the depolarization tensors of highly anisotropic rocks.

## Introduction

The electrical properties of rocks are often described by an effective complex-valued conductivity tensor, comprised of a host medium conductivity  $\sigma$  and an anomalous conductivity  $\Delta\sigma$  describing the polarization of mineral inclusions. The GEMTIP model (Zhdanov, 2008), takes the Stroud formulation of the effective conductivity and improves it by adding new a term, which describes the accumulation of charges on the boundary between the host and inclusion media when a current is applied. Our contribution aims to further extend this model by integrating the Green's function for anisotropic conductivity and triaxial ellipsoidal inclusions in the effective medium conductivity.

## Theory and methods

The integration of host rock conductivity and inclusion shape anisotropy parameters in the GEMTIP model modify the volume ( $\Gamma$ ) and surface ( $\Lambda$ ) depolarization tensors. Following Bérubé et Gagnon (2024), the anisotropic volume depolarization tensor of inclusion  $l$  is

$$\boldsymbol{\Gamma}_l = \frac{abc}{4\pi\sqrt{\sigma_x\sigma_y\sigma_z}} \mathbf{T} \int_0^{2\pi} \int_0^\pi \frac{d\theta d\phi \sin \theta}{|\mathbf{R}'|^3} \mathbf{n}' \mathbf{R}',$$

and its anisotropic surface depolarization tensor is

$$\boldsymbol{\Lambda}_l = -\frac{abc}{4\pi\sqrt{\sigma_x\sigma_y\sigma_z}} \int_0^{2\pi} \int_0^\pi \frac{d\theta d\phi \sin \theta}{|\mathbf{R}'|^5 |\mathbf{n}'|} \mathbf{Q}',$$

where  $a, b, c$  are the semi-axes lengths of the ellipsoid in the  $x, y, z$  directions,  $\sigma_x, \sigma_y, \sigma_z$  are the host rock conductivities in those directions,  $\mathbf{n}'$  is the vector normal to the ellipsoid and

$$\mathbf{T} = \text{diag}(\sigma_x, \sigma_y, \sigma_z)^{-1/2}.$$

In addition,  $\mathbf{R}' = \mathbf{r}' \mathbf{T}$ , where  $\mathbf{r}'$  is an arbitrary position vector and  $\mathbf{Q}' = (-3(\mathbf{R}' \mathbf{R}') + |\mathbf{R}'|^2 \mathbf{I}) \mathbf{n}' \mathbf{n}' \mathbf{T}^2$ , with  $\mathbf{I}$  being the identity matrix. We calculate the depolarization tensors using the *torchquad* Python library and its GPU-accelerated implementation of Simpson's rule.

## Results

The anisotropic GEMTIP model is validated in two ways. First, estimates of  $\Gamma$  are compared with its solutions involving elliptical integrals of the first and second kinds, in the case where  $\sigma_x \neq \sigma_y \neq \sigma_z$  and  $a \neq b \neq c$ . Second, estimates of  $\Lambda$  are compared with the solutions of Zhdanov (2018) in the special case of isotropic host rocks and spheroidal inclusions ( $\sigma_x = \sigma_y = \sigma_z$  and  $a \neq b = c$ ). We also analyze the accuracy of  $\Gamma$  as a function of anisotropy parameters  $A = b/a$ ,  $B = c/a$ ,  $C = \sigma_y/\sigma_x$  and  $D = \sigma_z/\sigma_x$ , and the accuracy of  $\Lambda$  as function of spheroid eccentricity. Last, we show that non-uniform sampling of the integrand functions using dynamic programming improves the accuracy with which  $\Gamma$  and  $\Lambda$  are estimated, also as a function of  $A, B, C$  and  $D$ .

## Conclusion

We develop a fully anisotropic IP model using the GEMTIP framework. Results show that our development is consistent with previous research that considers only special cases of anisotropy. The proposed adaptive sampling method for solving the depolarization tensors surpasses traditional techniques in accuracy and improves modelling the electrical properties of anisotropic rocks. Applications of precise computations of depolarization tensors are also interesting in other fields, such as frequency-domain electromagnetic analysis of rocks and soils or designing magnetic field probes with magnetic cores made of sophisticated effective media.

## Références

- Bérubé, C.L., Gagnon, J.-L., 2024. Anisotropic induced polarization modeling with neural networks and effective medium theory. *arXiv:2402.11313 [physics.geo-ph]*. <https://doi.org/10.48550/arXiv.2402.11313>
- Zhdanov, M., 2008. Generalized effective-medium theory of induced polarization. *Geophysics* 73, F197–F211. <https://doi.org/10.1190/1.2973462>
- Zhdanov, M. S., V. Burtman, M. Endo, and W. Lin, 2018. Complex resistivity of mineral rocks in the context of the generalised effective-medium theory of the induced polarisation effect. *Geophysical Prospecting* 66, 798–817. <https://doi.org/10.1111/1365-2478.12581>

# Superposition of IP signals measured on pyrite–sand mixtures

Tina Martin<sup>1</sup>, Andreas Weller<sup>2</sup>,

<sup>1</sup>*Engineering Geology, Lund University, Sweden, tina.martin@tg.lth.se*

<sup>2</sup>*Clausthal University of Technology, Clausthal-Zellerfeld, Germany*

## Introduction:

Induced polarization (IP) has proven to be an invaluable tool in ore deposit exploration. IP spectra, measured across a wide frequency range, offer insights into the material properties of ores, slags, and other residual materials from mining and processing operations. However, most studies have focused on single fractions with fixed grain sizes. In our experiments with sand–pyrite mixtures, we aim to investigate how varying size of pyrite particles affects IP signals despite having the same volume fraction.

In this study, we compare IP spectra recorded for samples with either a single grain radius fraction (referred to as E-samples) or two different grain radii fractions (referred to as Z-samples). These spectra are then fitted to Pelton models. Additionally, we employ a Debye decomposition method to analyze the complex conductivity spectra and derive a relaxation time distribution (RTD).

## Material & methods:

As described in Martin & Weller (2023), we examined 11 unconsolidated pyrite–sand mixtures. The pyrite grain radius varied across the samples, ranging from 31 to 1000 µm, while the quartz sand grain radius varied between 56 and 178 µm. We prepared six samples consisting of a single pyrite grain radius mixed with sand (E-samples), and five samples containing two different grain radii within the sand (Z-samples). The pyrite mineral content in the mixtures with a single pyrite grain radius was 2.75 vol.%, while the mixtures with two pyrite grain radii consisted of 2.75 vol.% of the lower and an additional 2.75 vol.% of the larger pyrite grain radius, resulting in a total percentage of 5.50%.

## Results & Discussion:

We recorded the IP spectra for all samples within the frequency range of 1 mHz to 1 kHz and removed the high-frequency electromagnetic coupling effects. For the E-samples, we observed an increase in resistivity amplitude and a decrease in phase maxima, which shifts to lower frequencies, as the pyrite particle radii increased. For the Z-samples, similar trends were noted, with the spectra widening and the maximum shifting to higher frequencies as the difference in radii between the two pyrite grain fractions increased. Both the E- and Z-samples, with symmetric phase spectra, were fitted to the standard Pelton model. The Z-samples were fitted to a double Pelton model. Upon increasing the pyrite grain radii from sample E 01 to E 06, we observed an increase in resistivity ( $\rho$ ), a decrease in chargeability ( $m$ ), and a significant increase in relaxation time ( $\tau$ ). The  $c$ -exponent of the Pelton model remained relatively constant, varying within a narrow range between 0.75 and 0.80. Similar trends were observed for the Z-samples, showing an increase in resistivity with increasing radii of the fraction of smaller pyrite grains.

In Fig. 1, we present the superposition of all samples. It is evident that for most spectra, there are moderate deviations between the measured and mathematically predicted superposition. The superposition aligns best for sample Z 05, which contains two pyrite fractions with similar grain radii (last row). In this case, the validity of mathematical superposition is well confirmed for the phase spectra. Additionally, a good agreement is observed between the mathematically predicted and measured superposition for the imaginary conductivity and RTD.

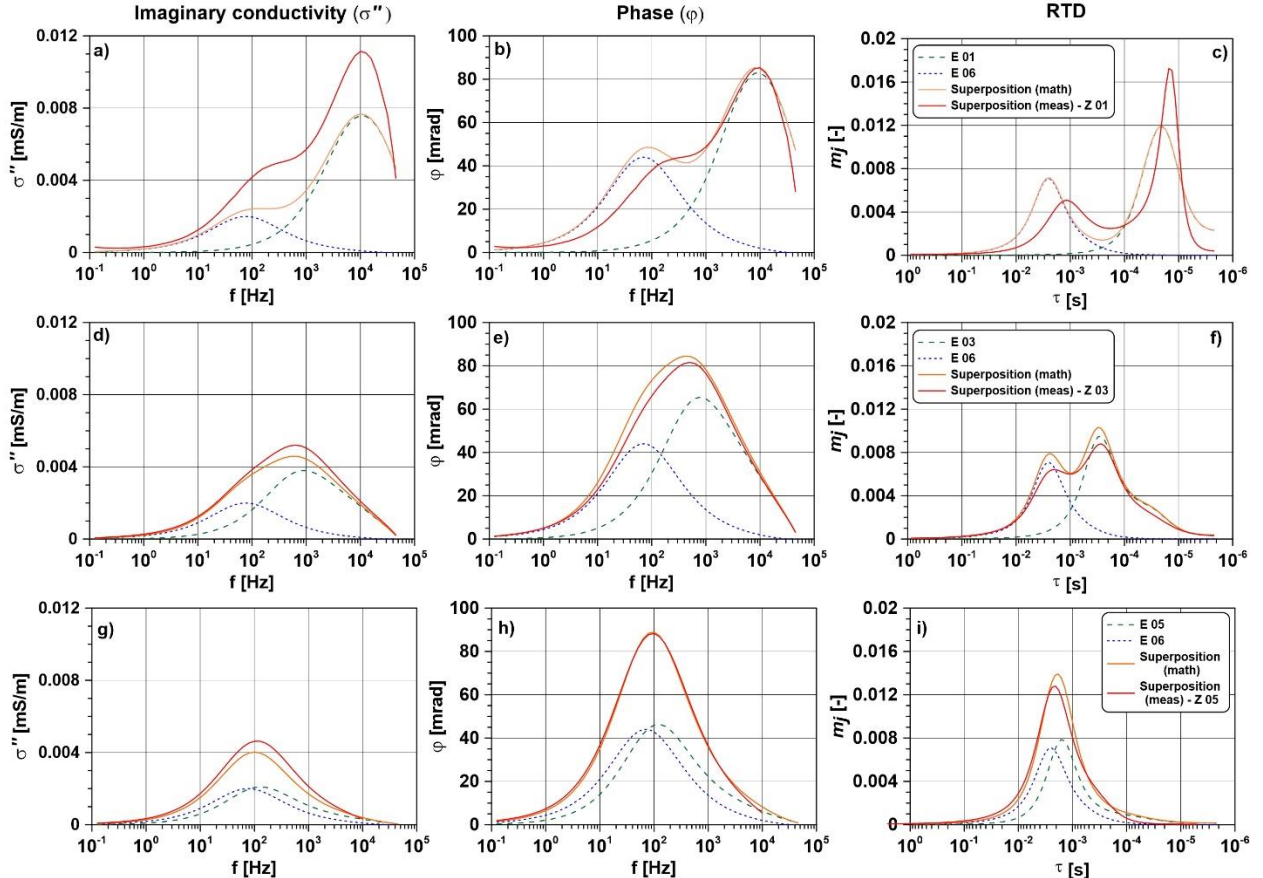


Figure 1: Superposition spectra from samples with varying pyrite grain radii for imaginary conductivity ( $\sigma''$ , left column), phase shift ( $\phi$ , middle column), and the Relaxation Time Distribution (RTD) from Debye decomposition (right column). Note the  $\tau$ -axis is inverted, ranging from larger to lower values.

### Conclusion:

Comparing IP spectra obtained from sand-pyrite mixtures with single grain radius fractions and those with two fractions of different grain radii offers valuable insights into the validity of superposition of IP spectra and the resulting IP parameters. Assuming an equal volume fraction, the pyrite-sand mixture with smaller grain size causes stronger effects in the spectra of imaginary conductivity, phase, and RTD. The chargeability observed in a sand mixture with two grain radius fractions is lower than the mathematical superposition by simply adding the chargeability values of the two single grain size mixtures. This discrepancy is particularly noticeable when considering fractions with a large grain size ratio. This observation confirms that chargeability is not simply an IP parameter that can be summed up for all constituents.

### References

- Martin, T. and A. Weller, 2023 Superposition of induced polarization signals measured on pyrite–sand mixtures. Geophysical Journal International, 234, 699–711

# Tackling petrophysical ambiguities in IP-K relations by joint inversion of hydraulic tomography and induced polarization data

Lukas Römhild<sup>1\*</sup>, Gianluca Fiandaca<sup>2</sup>, Peter Bayer<sup>1</sup>

<sup>1</sup>Applied Geology, Institute of Geosciences and Geography, Martin Luther University Halle-Wittenberg

<sup>2</sup>The EEM Team for Hydro & eXploration, Department of Earth Sciences ‘‘Ardito Desio’’, Università degli Studi di Milano

\* Corresponding Author: [lukas.roemhild@geo.uni-halle.de](mailto:lukas.roemhild@geo.uni-halle.de)

Accurate and high-resolution information about hydraulic conductivity K within an aquifer is an essential precondition for modeling groundwater flow and transport processes correctly. Based on the similarities between groundwater flow and electrical conduction in porous media, petrophysical relations linking hydraulic and IP parameters have been derived from laboratory experiments (Revil et al. 2012; Weller et al. 2015), and those can be used to infer a highly resolved K-distribution from the measured IP data. However, the applicability of such equations to specific site conditions remains ambiguous, and inherent scatter or bias in the petrophysical laws may introduce additional uncertainties to the IP-based K-estimates. Tackling these ambiguities can be considered crucial for establishing IP as a tool for imaging K-heterogeneities in the field.

In contrast, hydrological methods, such as hydraulic tomography (HT), are based on pumping tests, and they typically yield more reliable K-estimates, because those can be inferred directly from the hydraulic processes. However, these tests are time-consuming and expensive, so that data are mostly sparse and structural features can only be imaged with very limited spatial resolution. Based on the complementary abilities of the two approaches, a joint inversion procedure for both HT and IP data has been developed. Within this approach, a travel time inversion is applied to the HT data (Brauchler et al. 2003), while the IP inversion is based on a full-decay time-domain forward response (Fiandaca et al. 2012, 2013), as well as a re-parameterization of the Cole-Cole model to invert for K directly (Martin et al. 2021; Römhild et al. 2022).

We test the new inversion procedure, as well as individual HT and IP inversions, on a simple synthetic model, and thereby illustrate how the imaging results can be improved by combining the

complementary sensitivities of both methods within the joint inversion (Figure 1). It is also shown how the novel approach can correct biases within the petrophysical relations automatically, by taking into account both the reliable K-information from hydraulic tests and the high-resolution structural information from IP. The quality of the different inversion results is assessed by using the structural similarity index (SSIM), which underlines the robustness of the joint inversion compared to using the data individually. Therefore, we conclude that the combined application of HT and IP within field surveys and a subsequent joint inversion of both data sets has the potential to improve our understanding of hydraulically relevant subsurface structures, and thus the reliability of groundwater modeling results.

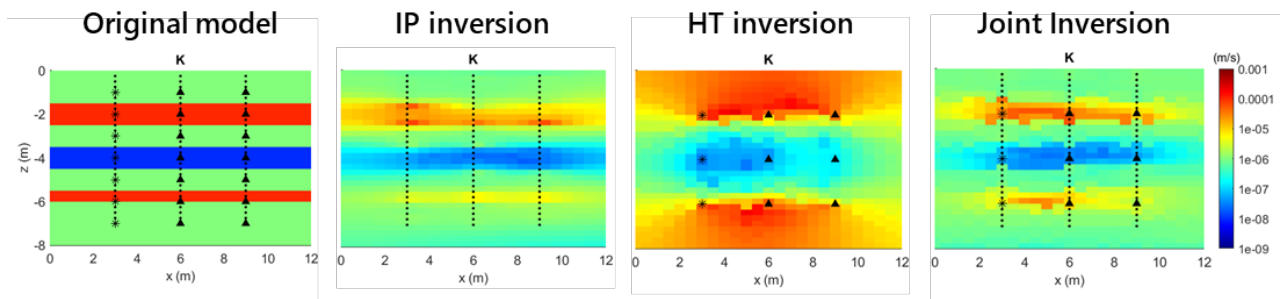


Figure 1: Inversion results of IP, HT and joint inversion for a horizontally layered synthetic model. Black dots represent DCIP electrode positions, asterisks HT source positions, and triangles HT receiver positions, distributed in three boreholes.

## References:

- Brauchler, R., Liedl, R. and Dietrich, P. (2003): A travel time based hydraulic tomography approach. *Water Res. Research*, 39(12), 1370.
- Fiandaca, G., Auken, E., Christiansen, A.V. and Gazoty, A. (2012): Time-domain-induced polarization: Full-decay forward modeling and 1D lateral constrained inversion of Cole-Cole parameters. *Geophysics*, 77(3), 213-225.
- Fiandaca, G., Ramm, J., Binley, A., Gazoty, A., Christiansen, A.V. and Auken, E. (2013): Resolving spectral information from time domain induced polarization data through 2-D inversion. *Geophysical Journal International*, 192, 631-646.
- Martin, T., Pauw, P.S., Karoulis, M., Mendoza, A., Günther, T., Medlgaaard Madsen, L., Maurya, P.K., Doetsch, J., Rejkjaer, S., Dahlin, T. and Fiandaca, G. (2021): Inversion of Hydraulic Conductivity from Induced Polarisation, Part B: Field Examples from Five Countries. Conference Proceedings, NSG2021 1st Conference on Hydrogeophysics, Aug 2021, Volume 2021, p.1–5.
- Revil, A., Koch, K., and Holliger, K. (2012): Is it the grain size or the characteristic pore size that controls the induced polarization relaxation time of clean sands and sandstones? *Water Resour. Res.*, 48, W05602.
- Römhild, L., Fiandaca, G., Hu, L., Meyer, L. and Bayer, P. (2022): Imaging hydraulic conductivity in near-surface aquifers by complementing cross-borehole induced polarization with hydraulic experiments. *Advances in Water Resources*, 170, 104322.
- Weller, A., Slater, L., Binley, A., Nordsiek, S., and Xu, S. (2015): Permeability prediction based on induced polarization: Insights from measurements on sandstone and unconsolidated samples spanning a wide permeability range. *Geophysics*, 80(2), D161–D173.

# Complex conductivity in heterogeneous media, can we use simple mixing laws on SIP spectra?

Aida Mendieta<sup>1,2</sup>, Alexis Maineult<sup>1</sup>, Philippe Leroy<sup>3</sup>, Matéo Leroy<sup>1</sup>, Damien Jougnot<sup>1</sup>

<sup>1</sup> Sorbonne Université, CNRS, EPHE, UMR 7619 METIS, 75005 Paris, France ; damien.jougnot@upmc.fr

<sup>2</sup> Université de Paris, Institut de Physique du Globe de Paris, CNRS, 75005 Paris, France

<sup>3</sup> BRGM, French Geological Survey, Water, Environment, Process and Analysis Department, 45060 Orléans, France.

## Tackling heterogeneity? Let's mix!

An old say in French is “C'est dans les vieux pots que l'on fait la meilleure soupe” (i.e., best soups are made in old pots) and, in this contribution, we decided to try the old cuisine of mixing laws to tackle geometrical heterogeneities. Analogous circuits in parallel and series are indeed very effective to obtain various equivalent properties (see the example of equivalent hydraulic conductivity in Renard and de Marsily, 1997). But what about complex properties such as the frequency dependent electrical conductivity that one measures with Spectral Induced Polarization (SIP)?

In this contribution we decided to test the effectiveness of three mixing laws through a series of experiments on synthetic samples made of well-characterized clay material.

### Synthetic clay sample geometries and complex conductivity

In order to test the ability of mixing laws to provide accurate equivalent complex conductivity, we proposed an experimental set-up containing meso-scale heterogeneities. In this study, meso-scale refers to an intermediate scale that is larger than the pore scale and smaller than the measurements scale footprint (i.e., related to the electrode spacing in SIP, see Jougnot, 2020).

In this study, we used two types of clay material characterized previously by Mendieta et al. (2021), a red montmorillonite and an illite. Figure 1a, b, c, and d present the different geometries created to test different mixing laws using the sample holder presented in Fig. 1e: (a) perfectly mixed montmorillonite and illite, (b) organized in series, (c) and (d) organized in parallel with Illite on the top or montmorillonite on the top, respectively. Measurements were conducted with the SIP Fuchs III from 1 mHz to 20 kHz with the current injected between C1 and C2 and the potential measured in P1 and P2 (Fig. 1e). These measurements later compared to three classical mixing laws, the so-called Wiener bounds, i.e., the model in parallel (Reuss, 1929) and the model in series (Voigt, 1910), and the self-consistent approach proposed by Hashin (1968).

Table 1: Classical mixing laws to test and compare to the experimental data (Figure 1f and g)

In parallel (Reuss, 1929)	In series (Voigt, 1910)	Self-consistent (Hashin, 1968)
$\sigma_R^* = \left( \frac{c}{\sigma_1^*} + \frac{1-c}{\sigma_2^*} \right)^{-1}$	$\sigma_V^* = c\sigma_1^* + (1-c)\sigma_2^*$	$\sigma_{SC}^* = \sigma_2^* + \frac{3c\sigma_2^*}{3\sigma_2^* + (1-c)(\sigma_1^* - \sigma_2^*)}(\sigma_1^* - \sigma_2^*)$

Where  $\sigma^*$  is the complex conductivity of the material 1 (illite) and 2 (montmorillonite), and  $c$  ( $c = 0.5$ ) is the volumetric proportion of material 1 with respect to the whole volume.

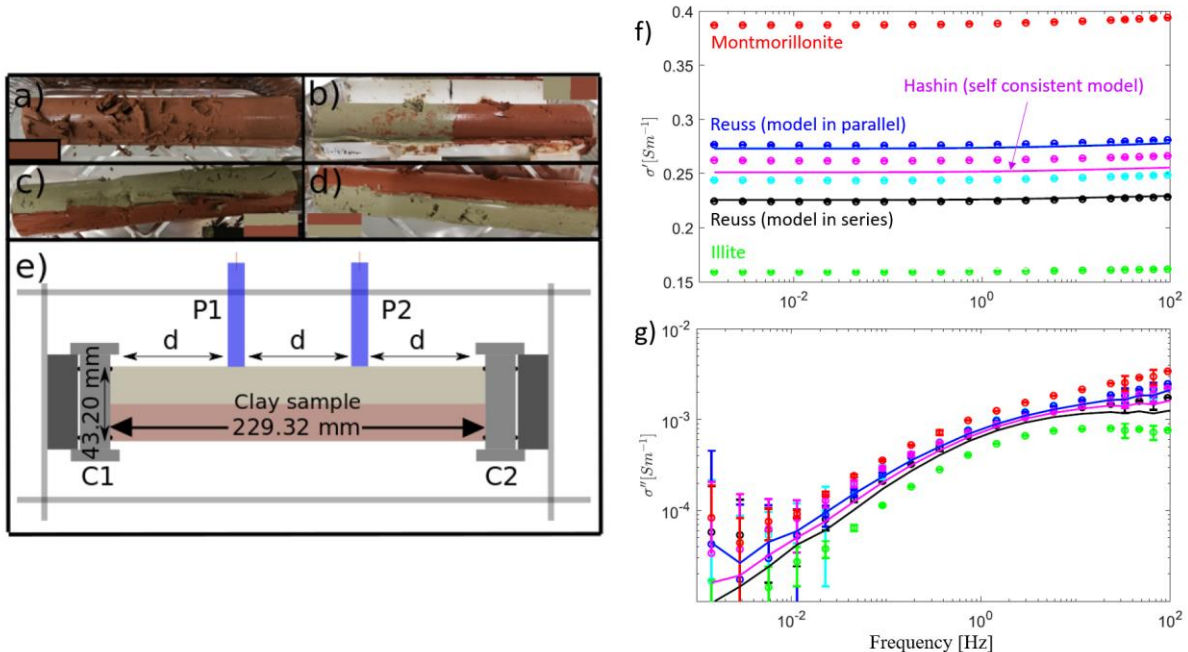


Figure 1: Heterogeneous samples made of montmorillonite and illite: (a) well-mixed, (b) in serie, (c) and (d) in parallel. (e) Sample holder for SIP measurements. (f) and (g) experimental results and the corresponding mixture law models for the real and the imaginary part of the complex electrical conductivity (modified from Mendieta et al., 2023).

The results of the SIP measurements of the homogeneous and heterogeneous mixtures are presented in Fig. 1f and g. First, as expected, one can clearly see that the equivalent complex conductivity measured on the composite samples are distributed in between the two individual clay types, illite and montmorillonite.

Figures 1f and g also clearly show that the mixture law prediction from Table 1 compare really favorably with our experimental results (for the real and imaginary part). The only unexpected exception is for the sample in parallel with the illite placed on top (light blue line in Fig. 1f and g).

This work showed that the mixing laws are effective to provide equivalent complex conductivity for heterogeneous media. Since many natural media are organized in layers, this opens up a way to improve or simplify IP modelling for various applications from reservoir properties to Critical Zone studies.

## References

- Hashin, Z. (1968). Assessment of the self consistent scheme approximation: conductivity of particulate composites, *J. Composite Mater.*, 2(3), 284–300.
- Jougnot, D. (2020). Developing hydrogeophysics for critical zone studies, importance of heterogeneities and processes at the mesoscopic scale. Sorbonne Université, Paris.
- Mendieta, A., Jougnot, D., Leroy, P., & Maineult, A. (2021). Spectral induced polarization characterization of non-consolidated clays for varying salinities—An experimental study. *Journal of Geophysical Research: Solid Earth*, 126(4), e2020JB021125.
- Mendieta, A., Maineult, A., Leroy, P., & Jougnot, D. (2023). Spectral induced polarization of heterogeneous non-consolidated clays. *Geophysical Journal International*, 233(1), 436-447.
- Renard, P., & De Marsily, G. (1997). Calculating equivalent permeability: a review. *Advances in water resources*, 20(5-6), 253-278.
- Reuss, A. (1929). Berechnung der Fließgrenze von Mischkristallen auf Grund der Plastizitätsbedingung für Einkristalle, *Zeitschrift für Angew. Math. Mech.*, 9(1), 49–58.
- Voigt, W., (1910). *Lehrbuch der Kristallphysik*, Teubner-Verlag, Leipzig, Germany.

# Intrinsic Clay IP using low frequency TDEM data

James Macnae<sup>1</sup> and Kate Hine<sup>2</sup>

<sup>1</sup>CD3D Pty Limited & RMIT University, Melbourne, Australia. <sup>2</sup>Mitre Geophysics, Brisbane, Australia

In ground G galvanic IP surveys (GIP) with typically 0.125 Hz base frequency (8 sec period), clays produce small chargeability anomalies that are mostly regarded as background and ignored in the search for larger responses from sulphides. While the intrinsic physical properties (using a Cole-Cole CC resistivity parameterization) of sulphides have long been known (Pelton et al., 1978), the intrinsic IP properties of clays have only been comprehensively investigated more recently (e.g. Revil et al., 2023). Airborne and ground time-domain electromagnetic TEM surveys have chosen to use very low base frequencies in recent years in mineral exploration surveys. The late-time TEM data are frequently affected by IP responses, appearing as negatives in coincident-loop z component or in the horizontal component in Slingram geometry. Many authors have speculated that these inductive IP responses may be sulphide indicators, without a thorough analysis of TEM sensitivity to the expected physical properties of sulphide targets.

Conventional ground GIP surveys for sulphide targets have difficulty estimating IP parameters other than chargeability, as the injected current and voltage measurements are made in overlying regolith rather than in the target itself. As a result, geometrical target knowledge or accurate inversion is needed to extract intrinsic target IP properties, and successful field case histories of spectral IP in mineral exploration are virtually non-existent compared to laboratory physical property measurements. Because inductive source TEM systems have limited bandwidth compared to laboratory measurements, and because in-situ measurements are complicated with induced currents being a function of the environment rather than being directly injected, intrinsic IP parameter estimation of a sulphide target from induced TEM is even less certain.

It is however possible to estimate CC conductivity parameters of the regolith or near-surface relatively easily from sampled TEM data, whether ground or airborne, under the assumption of either a geometrically thin regolith (Macnae, 2016) or a layered earth (Kaminski and Viezzoli, 2017).

Conductive layers occur most commonly in the shallow regolith overlying a resistive basement, and as a result it is possible to simultaneously model and thus fit their EM and IP responses as the clays (if moistened) are often both the only EM secondary field source and the IP source. In extensive mineral exploration surveys, I have analysed the observed responses from B field and dB/dt (coil sensor) data collected in Aeris Resources Triton Project in NSW, Australia. Figure 1 is an example of the fit to an observed inductive source TEM decay by inversion using thin-sheet parameters (Macnae, 2016).

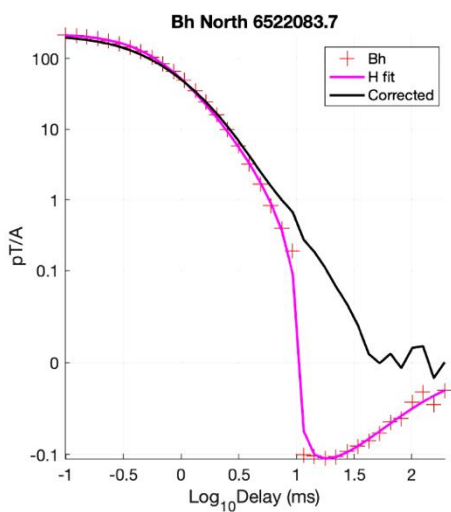
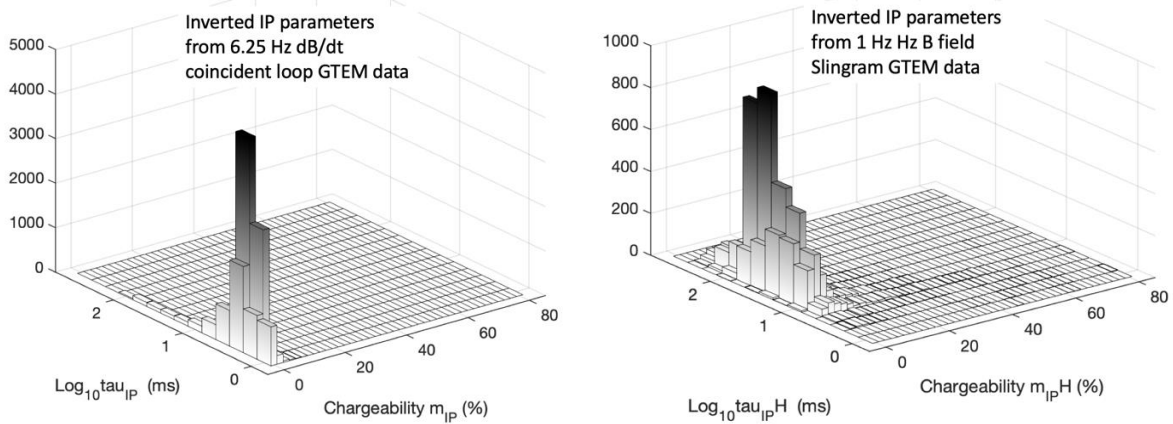


Figure 1: Example inverted fit of thin sheet model EM and IP components to 300 m Slingram separation 1 Hz B field GTEM data. The black curve is an estimate of the EM response without IP.

When we analysed the results of numerous inductive source TEM data over Australian regolith by plotting onto histograms (Figure 2) it initially surprised us that 1 Hz B field data provided IP time constant estimates ( $\sim 30$  msec) that were 10 times longer than dB/dt collected at 6.25 Hz base frequency (IP time constant estimates about 2 to 3 ms). Other examples show that dB/dt data tends to estimate time constants of about half the value estimated by B field data at the same base frequency. Figure 3 shows that the characteristic frequency (related to inverse time constant) from inversion of inductive source TEM data samples a rather flat region of laboratory measured intrinsic IP response (imaginary component of conductivity). The result of the limited TEM bandwidth sampling is a biased estimate of the intrinsic IP response. By coincidence, 1 Hz B field data appears

to have inverted  $\tau_{IP}$  consistent with laboratory measurements, whereas 6.25 Hz dB/dt data leads to an inverted estimate that is an order of magnitude “wrong”.



*Figure 2. Histograms of fitted IP chargeability and time constant from thousands of ground GTEM soundings over regolith in the general Triton area, NSW, Australia.*

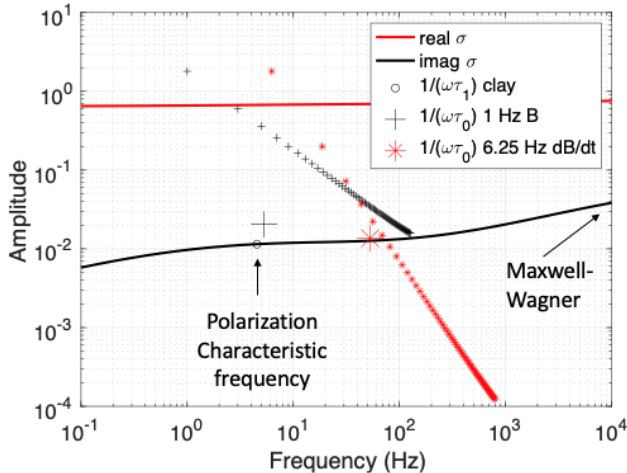


*Figure 3. Plot of dual Cole-Cole response derived from clay conductivity (Revil et al, 2023) as a function of frequency. The small black circle shows the characteristic frequency of the polarisation effect. Small crosses and stars show the frequency content of 1 Hz B field and 6.25 Hz dB/dt 50% duty cycle ground GTEM systems. The large cross and asterisk show the time constant and chargeability estimates of the median IP response inverted from recent Australian surveys. Time constants are  $\tau_\sigma$*

IP characteristic frequency  $\{=1/(2\pi\tau_\sigma)\}$  for regolith clays that is within the first few harmonics of the TEM transmitter base frequency.

Refining our understanding of the spectrum of IP frequencies has important implications for improving effectiveness of EM surveys: IP effects often either mimic or suppress basement responses, and this work shows that the magnitude of the effect depends not just on the ground properties and survey geometry but also on the type of receiver and frequency. Incorporating the IP characteristic frequency for a specific survey into any attempts to derive Cole-Cole model should help produce a better model, limiting the chance that EM signals are mistaken as IP effects and vice versa. With further development this method may prove to be useful additional processing tool to help better resolve true ground conductivity beneath polarizable regolith.

- Kaminski, V. and Viezzoli, A., 2017, Modeling induced polarization effects in helicopter time-domain electromagnetic data: Field case studies, *Geophysics* 82: B49-B61.
- Macnae, J., 2016, Quantitative estimation of intrinsic induced polarization and superparamagnetic parameters from airborne electromagnetic data. *Geophysics* 81: E433-E446.
- Pelton, W.H., Ward, S.H., Hallof, P.G., Sill, W.R. and Nelson, P.H., 1978. Mineral discrimination and removal of inductive coupling with multifrequency IP. *Geophysics*, 43, 588–609.
- Revil A., Ghorbani, A., Jougnot, D. and Yven, B., 2023, Induced polarization of clay-rich materials — Part 1: The effect of desiccation. *Geophysics* 88, MR195-MR210

# Laboratory Scale Electromagnetic IP Signatures Using a Saw-Tooth Time-Domain Waveform

Dan R. Glaser<sup>1,2</sup>, Randall Reynolds<sup>1,3</sup>, Fridon Shubitidze<sup>3</sup>, Ben Barrowes<sup>1</sup>, and Lee Slater<sup>2,4</sup>

<sup>1</sup>*USACE ERDC Cold Regions Research & Engineering Laboratory, USA, [danney.r.glasner@erdc.dren.mil](mailto:danney.r.glasner@erdc.dren.mil)*

<sup>2</sup>*Department of Earth & Environmental Sciences, Rutgers University-Newark, USA*

<sup>3</sup>*Thayer School of Engineering, Dartmouth University, USA*

<sup>4</sup>*Pacific Northwest National Laboratory, Energy and Environment Directorate, Richland, USA*

The induced polarization effect is a well-documented capacitive-like phenomenon associated with electrical and electromagnetic measurements of porous materials. With direct contact galvanic electrical measurements, the effect is associated with clay content and specific surface area of sediments and rocks, as well as certain metallic minerals, contaminants, and biological processes and media. The relaxation signature associated with IP is present in the frequency-domain and in the time-domain. Standoff electromagnetic induction (EMI) measurements also demonstrate induced polarization effects, most often observed at the field scale and in the time-domain. Here we present observations of induced polarization effects in time-domain electromagnetic measurements at the laboratory scale using both traditional square waveforms and saw-tooth waveforms.

We examine responses of various porous materials including soils with 13% kaolinite clay content, sand-pyrite mixtures, and small steel spheres. Measurements were obtained under both dry and saturated conditions for each sample. The steel sphere samples were also examined under three different volumes. The sand-pyrite mixtures were comprised of 10% pyrite, 90% Ottawa sand. Only very small IP responses were observed for these conditions, with no significant variation in signal observed between the square wave and saw-tooth wave signatures. Signatures associated with the 13% kaolinite clay content naturally occurring soil demonstrated clear IP signatures only in the saw-tooth signal mode, while the square wave signatures show a less pronounced signature observed near the noise floor. Finally, samples of small steel spheres were examined at three different masses: 150 g (small); 450 g (medium); and 750 g (large). Each sample was examined using square wave and saw-tooth wave transmitted signals and under both dry and saturated conditions.

The saw-tooth EMI (ST-EMI) repeatedly demonstrated improved signal response in the presence of both clay content and metallic particles as well as dry and saturated materials. Implications of such a laboratory design could allow for calibration of observed field signals and forward modeling of expected field signals in the presence of materials where induced polarization phenomena are likely, especially in low moisture conditions where galvanic measurements are limited.

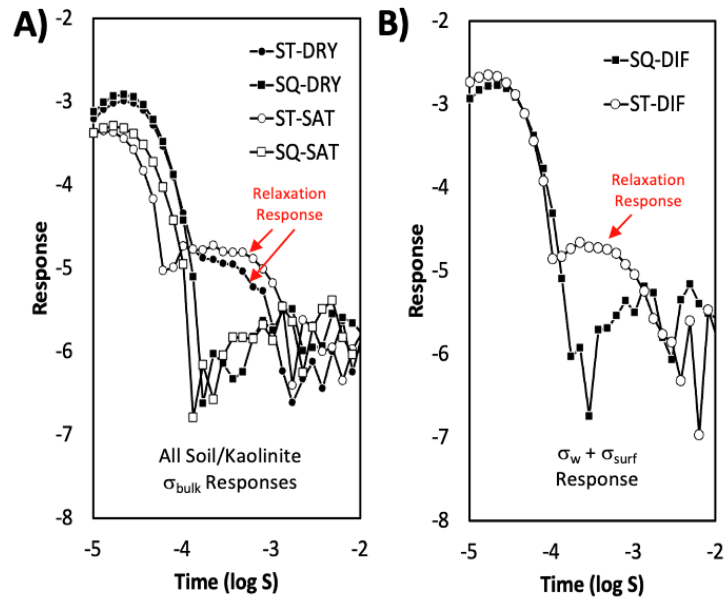


*Figure 1:* A) Time-domain electromagnetic induction response of saturated and dry soil with 13% kaolinite clay content. Square wave response is shown with open (saturated) and filled squares (dry), while saw-tooth wave response is shown with open (saturated) and filled circles (dry). B) Difference of the dry and saturated responses of both the square (squares) and saw-tooth (circle) transmitted wave-forms.

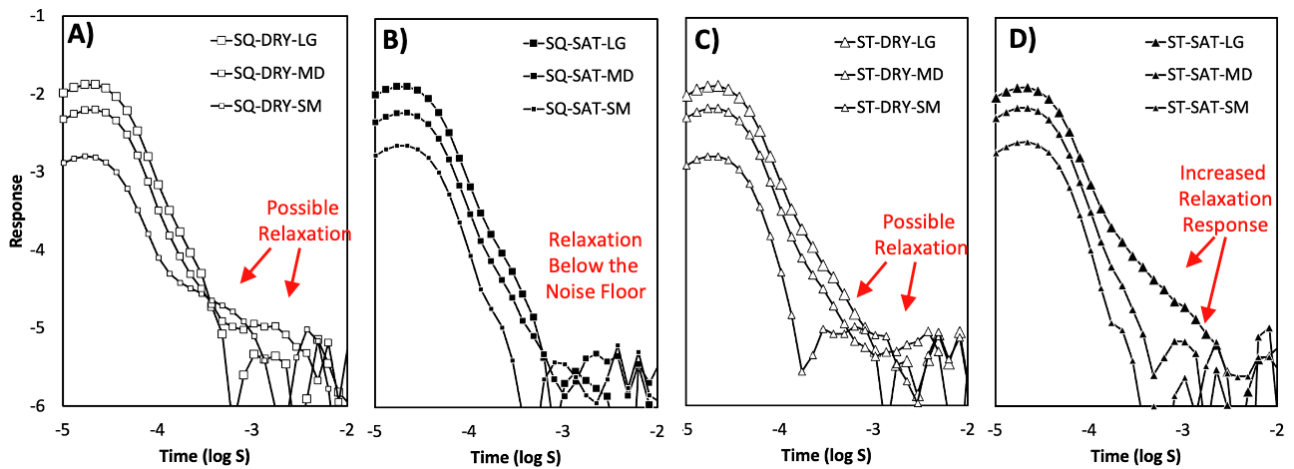


*Figure 2.* Time-domain electromagnetic induction response of three steel sphere masses using square wave and saw-tooth wave transmitted signals, results shown: A) square wave, dry samples; B) square wave, saturated samples; C) saw-tooth wave, dry samples; D) saw-tooth, saturated samples.

# Applying Induced Polarization to Characterize Nant des Granges Landslide, Bauges, France.

Casotti.C<sup>1</sup>, Revil.A,<sup>2</sup> Zhang X<sup>3</sup>, Su Z<sup>4</sup>?Guerini.M<sup>2</sup>

<sup>1</sup> Univ. Savoie Mont-Blanc GINGER CEBTP, EDYTEM, 73370 Le Bourget du Lac, France

<sup>2</sup> Univ. Savoie Mont-Blanc, CNRS, UMR CNRS 5204, EDYTEM, 73370 Le Bourget du Lac, France

<sup>3</sup> School of Safety Engineering, China University of Mining and Technology, Xuzhou 221116, China

<sup>4</sup> College of geophysics, China University of Petroleum, Beijing, 102249, China

## Introduction (site description)

The Nant des Granges landslide in the Bauges massif in the French Alps is one of the most significant and destructive landslides in the Alps. In 1931, this event ravaged 2 hamlets and left 3 abandoned, displacing a total of around 6 million cubic meters of material. This 900 m-long landslide is located in a syncline crowned by a massive Urgonian bed. The core of the landslide is made up of more recent, clayey materials, notably marked by morainic deposits on the surface, favouring landslides and mudflows.

## Methods

In order to understand how the landslide is embedded in the complex geology of the site, we decided to carry out a Time Domain Induced Polarization (TDIP) profile about 1900m long, with an inter-electrode spacing of 20m. The raw data were then filtered and inverted using the pyGIMLI open source package (Rücker et al., 2017).

As a first step in interpretation, we opted to use the scikit-learn python package (Pedregosa et al., 2011) with Gaussian Mixture Model (GMM) clustering technique applied to the standardized logarithms of normalized conductivity and chargeability. This approach is designed to facilitate the identification of different geological formations. The interpretation obtained then enables us to adapt the petrophysical models, based on the Stern layer model (Revil et al., 2017a, 2017b; 2017c ; Soueid Ahmed et al., 2020), to the specific characteristics of each group of similar formations. The petrophysical parameters concerned will be measured in the laboratory with Spectral Polarized Induction (SIP) tests carried out at different pore water conductivities. These measurements will be supplemented by cation exchange capacity (CEC) and Atterberg limit tests. In addition, the profile

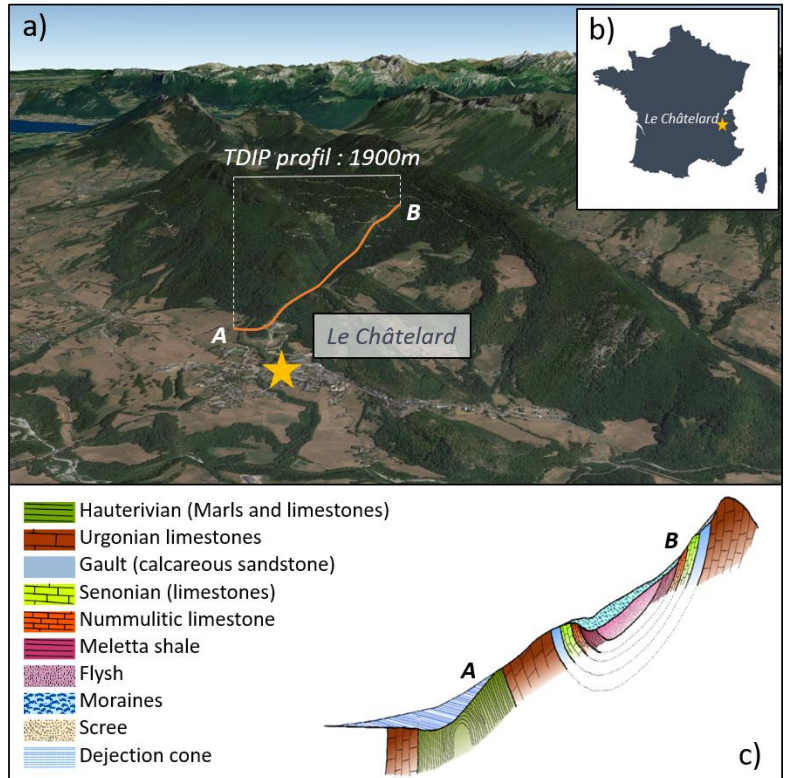


Figure 1: Google Earth 3D aerial view of the Nant des Granges syncline with TDIP profile location (a), Site location in France (b), Schematic reconstruction of the geological section (adapted from ONF/ Service RTM 73)

was doubled with Spontaneous Potential (SP) measurements to better understand the hydrogeology of the site.

## Results & Conclusion

The site studied has a complex geology, common in the Alps, characterized by a multitude of formations. With the help of a simple clustering technique TDIP measure highlight these different formations. This approach, combined with laboratory SIP tests, facilitated the precise and distinct adjustment of petrophysical modeling parameters, resulting in detailed tomograms of cation exchange capacity (CEC), water content and permeability.

These tomograms are particularly relevant to understanding landslides mechanics such as the one at Nant des Granges. It would now be interesting to compare these promising results with conventional geotechnical techniques such as borehole point testing (Atterberg limits, pressuremeter or borehole permeability tests).

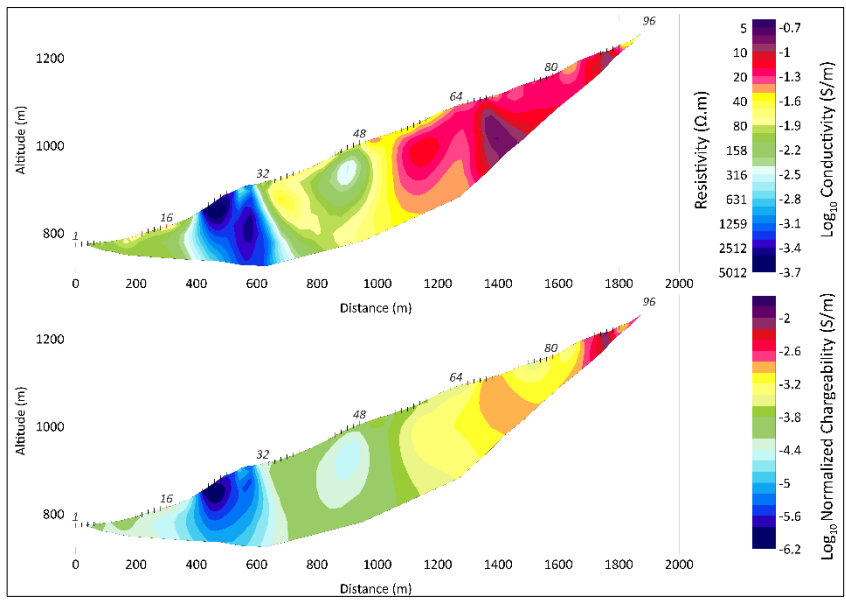


Figure 2: TDIP tomograms with electrical conductivity distribution (a) and normalized chargeability distribution (b). Blue part is associated with the Urgonian bed. High conductivity/normalized chargeability areas indicate flysch, marl, and moraine, which form the material source of the landslide.

## Reference

- Gunther, T., Rucker, C., n.d. Boundless Electrical Resistivity Tomography BERT 2 – the user tutorial.
- Revil, A., Breton, M.L., Niu, Q., Wallin, E., Haskins, E., Thomas, D.M., 2017a. Induced polarization of volcanic rocks. 2. Influence of pore size and permeability. *Geophys. J. Int.* 208, 814–825. <https://doi.org/10.1093/gji/ggw382>
- Revil, A., Coperey, A., Shao, Z., Florsch, N., Fabricius, I.L., Deng, Y., Delsman, J.R., Pauw, P.S., Karaoulis, M., de Louw, P.G.B., van Baaren, E.S., Dabekaußen, W., Menkovic, A., Gunnink, J.L., 2017b. Complex conductivity of soils: COMPLEX CONDUCTIVITY OF SOILS. *Water Resour. Res.* 53, 7121–7147. <https://doi.org/10.1002/2017WR020655>
- Revil, A., Le Breton, M., Niu, Q., Wallin, E., Haskins, E., Thomas, D.M., 2017c. Induced polarization of volcanic rocks – 1. Surface versus quadrature conductivity. *Geophys. J. Int.* 208, 826–844. <https://doi.org/10.1093/gji/ggw444>
- Rücker, C., Günther, T., Wagner, F.M., 2017. pyGIMLi: An open-source library for modelling and inversion in geophysics. *Computers & Geosciences* 109, 106–123. <https://doi.org/10.1016/j.cageo.2017.07.011>
- Soueid Ahmed, A., Revil, A., Abdulsamad, F., Steck, B., Vergnial, C., Guihard, V., 2020. Induced polarization as a tool to non-intrusively characterize embankment hydraulic properties. *Engineering Geology* 271, 105604. <https://doi.org/10.1016/j.enggeo.2020.105604>

# Can equivalent circuit models be used for the complex conductivity of clayey materials?

Philippe Leroy<sup>1</sup>, Alexis Maineult<sup>2</sup>, Aida Mendieta<sup>3</sup>, Damien Jougnot<sup>4</sup>

<sup>1</sup> BRGM, French Geological Survey, 45060 Orléans, France, p.leroy@brgm.fr.

<sup>2</sup> Laboratoire de Géologie, Ecole Normale Supérieure / CNRS UMR8538, PSL Research University, 75005 Paris, France.

<sup>3</sup> Université de Paris, Institut de Physique du Globe de Paris, CNRS, 75005 Paris, France.

<sup>4</sup> Sorbonne Université, CNRS, EPHE, UMR 7619 METIS, 75005 Paris, France.

## Introduction

Clays are very abundant minerals in the Earth's crust and express a high conductivity response that can be measured at the scale of the geological formation by electrical and electromagnetic methods in geophysics. However, these minerals have a complex microstructure that renders difficult the quantitative petrophysical interpretation of electrical field measurements. In this study, we have developed a new approach to interpret measured spectral induced polarization (SIP) spectra on clay materials in terms of microstructural and electrical double layer properties including surface conductivity using an extension of the mechanistic model developed by Leroy et al. (2017) considering interlayer space and Maxwell-Wagner polarizations.

## Modeling strategy

With a minimum set of physical-chemical parameters to be optimized, i.e., the fraction of the counter-charge and cation mobility in the Stern layer, number of stacked solid layers per particle, and clay aggregate size distribution, a fitting procedure to experimental data is considered. Its aim is to reproduce the measured laboratory SIP spectra in the mHz to kHz frequency range on kaolinite, illite and montmorillonite muds at different NaCl concentrations reported by Mendieta et al. (2021).

## Results and discussion

We find that the conduction and polarization of the interlayer space of Na-montmorillonite (Na-Mt) suspensions should not be neglected. We also find that the surface conductivity concept may not apply to the diffuse layer of clays like Na-Mt because the thickness of the diffuser layer can be larger than Na-Mt particle thickness. We show that Archie's first law is enough for computing the electrical conductivity of clay muds when water conductivity is modeled considering the diffuse layer contribution (Figure 1, top). We also test the validity of the petrophysical model of Weller et al. (2013) based on equivalent circuit modeling that is commonly used to interpret laboratory and field SIP measurements on clays in terms of mineralogy, state and transport properties. Our model shows a frequency dependence and a more slightly salinity dependence of surface conductivity (Figure 1, bottom). It also confirms most of the assumptions of the petrophysical induced polarization model of Weller et al. (2013) for the surface conductivity of clay muds except when they contain a significant fraction of Na-Mt because, in this condition, imaginary surface conductivity may not be approximated by measured imaginary conductivity.

## Conclusion and perspective

Our modeling approach allows extracting surface conductivity from complex conductivity measurements on clayey materials in a more realistic way than petrophysical models based on equivalent circuit modeling. It needs more physical parameters to be adjusted than equivalent circuit models but it shows that equivalent circuit model assumptions regarding surface conductivity may not be valid in all situations especially when samples contain a large fraction of Na-Mt. Our study is a step forward to better understand the high conductivity response of clays from geophysical electrical measurements. The next step will be to use a purely numerical model to compute the complex conductivity of clay materials whose geometrical parameters will be constrained by high-resolution characterization measurements.

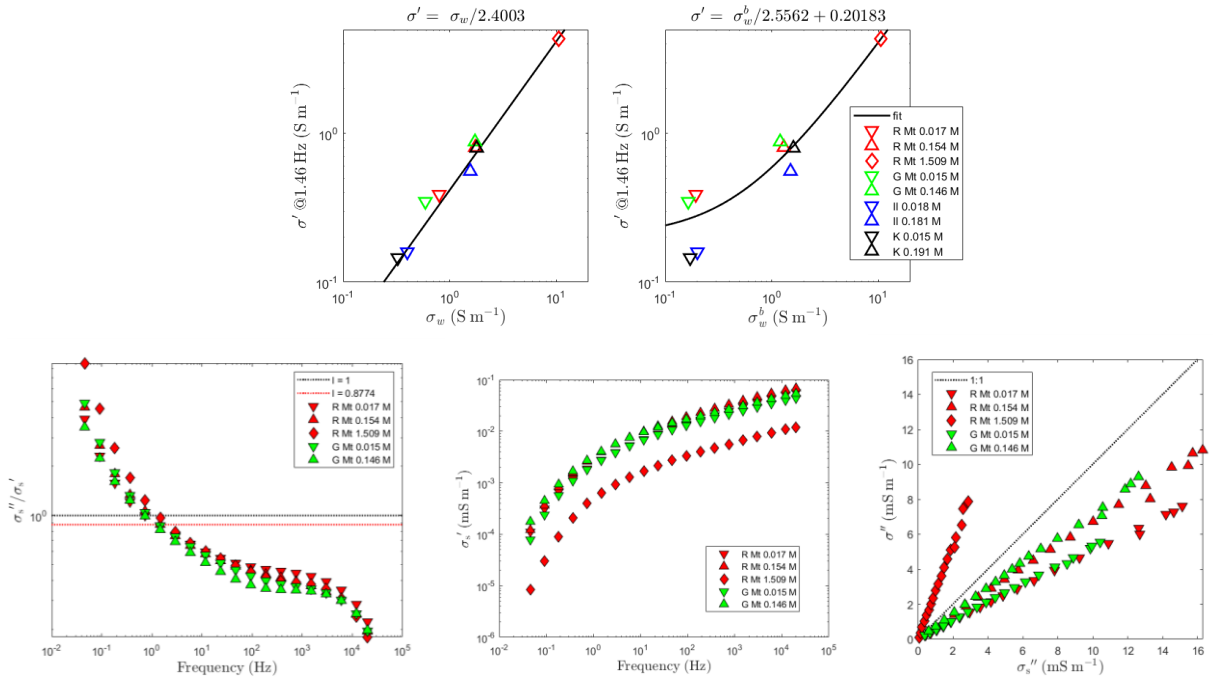


Figure 1: Top, real part of the measured complex conductivity as a function of the modeled water conductivity at different salinities (NaCl concentrations) considering diffuse layer and bulk water contributions (left) and solely bulk water contribution (right). Bottom, imaginary and real components of the modeled surface conductivity and measured imaginary conductivity of clay muds as a function of frequency and salinity.

## References

- Leroy, P., Weigand, M., Mériguet, G., Zimmermann, E., Tournassat, C., Fagerlund, F., Kemna, A. and Huisman, J.A., 2017. Spectral induced polarization of Na-montmorillonite dispersions. Journal of Colloid and Interface Science, 505, 1093-1110.
- Mendieta, A., Jougnot, D., Leroy, P. and Maineult, A., 2021. Spectral Induced Polarization Characterization of Non-Consolidated Clays for Varying Salinities-An Experimental Study. Journal of Geophysical Research: Solid Earth, 126.
- Weller, A., Slater, L. and Nordsiek, S., 2013. On the relationship between induced polarization and surface conductivity: Implications for petrophysical interpretation of electrical measurements. Geophysics, 78, D315-D325.

## On the Reliability of Constraining Surface Conductivity using Induced Polarization Measurements in Sedimentary Rocks

Klaudio Peshtani<sup>1</sup>, Lee Slater<sup>1,2</sup>

<sup>1</sup>*Department of Earth & Environmental Sciences, Rutgers University, Newark, [kpeshtani@gmail.com](mailto:kpeshtani@gmail.com)*

<sup>2</sup>*Energy & Environmental Directorate, Pacific Northwest National Laboratory, [lslater@newark.rutgers.edu](mailto:lslater@newark.rutgers.edu)*

In recent decades, substantial advancements have been made in understanding the induced polarization (IP) method, leading to improvements in interpreting hydraulic properties from electrical measurements. Distinguishing the effect of surface conduction from conduction through the electrolyte filling the interconnected pore spaces has been an ongoing challenge in interpreting field-scale electrical resistivity datasets. Previously proposed mechanistic models have suggested that this limitation can be overcome by utilizing the coefficient that describes the coefficient of the ratio between IP measurements and surface conductivity. In this study, we examine this proportionality coefficient ( $\ell$ ) through the relationship between IP parameters (imaginary conductivity and normalized chargeability) and surface conductivity for a sample group of 98 previously published sedimentary rocks, composed of sandstones, carbonates, and mudstones. A strong linear relationship is observed between the IP parameters and surface conductivity, as shown in Figure 1. The values of  $\ell$  vary significantly across each sample group. Predictions of the formation factor ( $F$ ) are best estimated using  $\ell$  values unique to the specific sample group, with mudstone samples showing no significant improvement. Conversely, employing separate  $\ell$  values from a previously published sample group of unconsolidated sediments and consolidated sandstones results in poor predictions of  $F$ . Additionally, using  $\ell$  coefficients from a sample group within this dataset with similar lithological properties moderately improves the estimation of  $F$ . No relationship is observed between the proportionality coefficient and the petrophysical parameters of the porous medium or iron mineralogy measured via magnetic susceptibility. Our results suggest that although IP measurements provide a valuable field-scale proxy for surface conductivity, using it to quantitatively improve the prediction of petrophysical parameters such as  $F$ , remains a significant challenge until this proportionality coefficient is better understood.

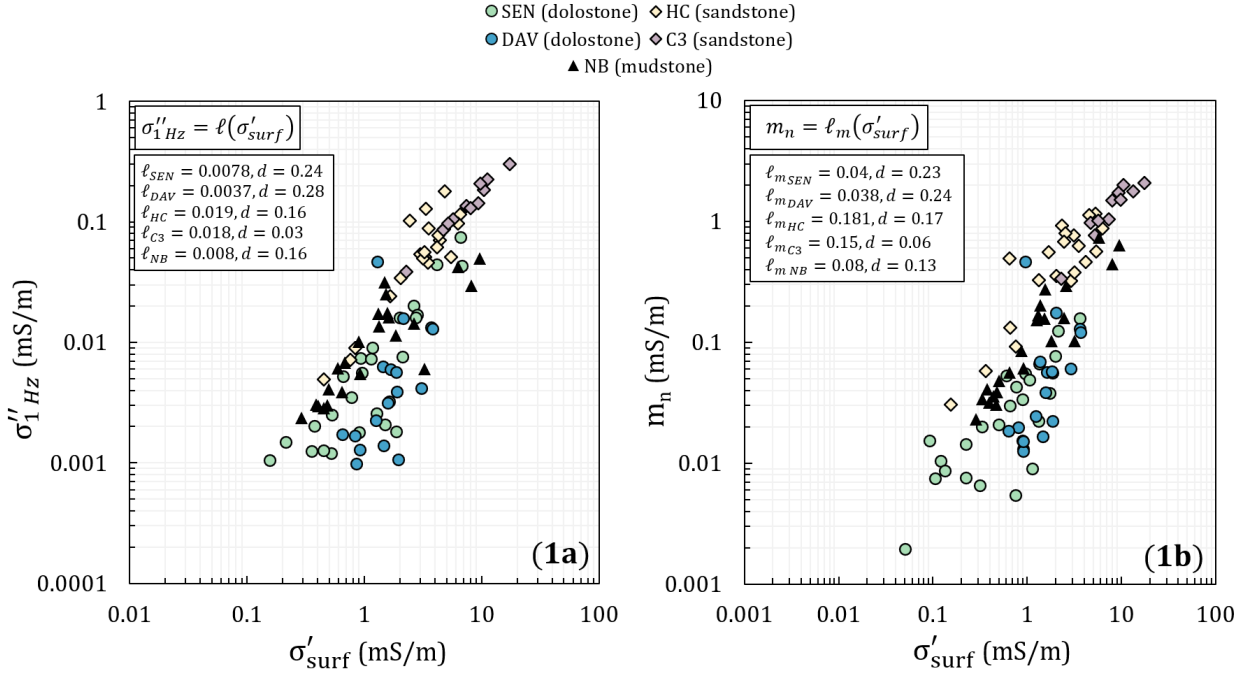


Figure 1: Relationship between IP parameters (imaginary conductivity  $\sigma''_{1\text{Hz}}$  and normalized chargeability  $m_n$ ) and surface conductivity ( $\sigma'_{\text{surf}}$ ) for 98 sedimentary samples (sandstone, carbonate, and mudstone): (a)  $\sigma''_{1\text{Hz}}$  versus  $\sigma'_{\text{surf}}$ ; (b)  $m_n$  versus  $\sigma'_{\text{surf}}$ . The  $d$ -value represents the logarithmic average of the best-fit linear trendline, with a lower  $d$ -value indicating a better fit.

# Joint application of time-lapse induced polarization and reactive transport modeling to track subsurface H<sub>2</sub>S mineral storage at a geothermal site

Daniel A. Ciraula<sup>1</sup>, Léa Lévy<sup>2</sup>, Gianluca Fiandaca<sup>3</sup>, Samuel W. Scott<sup>1</sup>, Barbara I. Kleine-Marshall<sup>4</sup>

<sup>1</sup> *NordVulk, Institute of Earth Sciences, University of Iceland, Reykjavik, Iceland, email: dac11@hi.is*

<sup>2</sup> *Engineering Geology, Lund University, Lund, Sweden*

<sup>3</sup> *Department of Earth Sciences “Ardito Desio”, University of Milan, Milan, Italy*

<sup>4</sup> *GeoZentrum Nordbayern, Friedrich-Alexander-Universität Erlangen-Nürnberg, Erlangen, Germany*

Hydrogen sulfide (H<sub>2</sub>S), contained in Icelandic geothermal production fluids, is emitted during geothermal energy production at flash steam power plants. Starting in January 2021, a subsurface storage initiative was implemented to reduce H<sub>2</sub>S emissions at the Nesjavellir geothermal power station (SW Iceland). In this process, the H<sub>2</sub>S gases are captured, dissolved into geothermal wastewater, and injected into the subsurface. Upon injection, the H<sub>2</sub>S-rich wastewater interacts with the highly reactive basaltic host rock to mineralize iron sulfides (e.g., pyrite and pyrrhotite). Although H<sub>2</sub>S mineralization in basalt host rocks provides a solution to reduce geothermal H<sub>2</sub>S emissions, the process must be effectively monitored to avoid potential adverse environmental impacts, such as the acidification of the groundwater system.

The time-domain induced polarization (TDIP) geophysical method is sensitive to the volume of pyrite and other metallic minerals in the subsurface, thus the method could be applied to directly measure H<sub>2</sub>S mineralization (Lévy et al., 2019; Martin and Weller, 2023; Revil et al., 2015). In this study, we explore the application of borehole and ground-based time-lapse TDIP data as a scalable and cost-effective solution to monitor industrial-scale H<sub>2</sub>S injection. Furthermore, we couple the TDIP surveying with reactive transport models to evaluate the time-lapse geophysical inversion results, identify the geochemical parameters controlling the effectiveness of H<sub>2</sub>S mineralization, and improve the resolution of time-lapse TDIP geophysical inversions.

Through the joint approach of time-lapse TDIP surveying and reactive transport modeling, we gain insight into the fate of injected H<sub>2</sub>S. Increases in the borehole TDIP response following H<sub>2</sub>S injection suggest that H<sub>2</sub>S mineralization is effective under the current injection conditions. This finding is supported by 1D reactive transport models of radial flow near the injection boreholes, which reveal that pyrite formation is favored at early stages of basalt alteration upon H<sub>2</sub>S injection. Additionally, the distribution of borehole TDIP changes is related to zones of increased fluid flow in the 1D reactive transport models, and the magnitude of the H<sub>2</sub>S mineralization near the boreholes is found to be limited, in part, by the iron supply from basalt dissolution and by large permeabilities.

The monitoring of H<sub>2</sub>S mineralization is expanded to a larger spatial extent through a ground-based time-lapse TDIP survey along 1.2 km long lines surrounding the injection wells. The time-lapse TDIP inversion scheme requires flexible gridding of model parameters and forward calculations to account for differences in electrode layouts between the surveys, and the simultaneous inversion of the sequential datasets to impose time-lapse constraints (Fiandaca et al., 2023, 2015). Preliminary inversion results do not recover any time-lapse TDIP changes. To better understand these findings, 3D reactive transport simulations and TDIP forward simulations are used to constrain the expected

$\text{H}_2\text{S}$  mineralization and corresponding IP response changes. Furthermore, various methods are explored that couple the reactive transport simulations to the time-lapse TDIP inversions. Through this coupling, we explore how time-lapse geophysical inversions can be directly constrained by the underlying physical and chemical processes controlling the subsurface changes.

## References

- Fiandaca, G., Doetsch, J., Vignoli, G., Auken, E., 2015. Generalized focusing of time-lapse changes with applications to direct current and time-domain induced polarization inversions. *Geophys J Int* 203. <https://doi.org/10.1093/gji/ggv350>
- Fiandaca, G., Zhang, B., Chen, J., Signora, A., Dauti, F., Galli, S., Sullivan, N.A.L., Bollino, A., Viezzoli, A., 2023. Closing the gap between galvanic and inductive methods: EEMverter, a new 1D/2D/3D inversion tool for electric and electromagnetic data with focus on induced polarisation, in: AEM 2023: Short Abstracts, Preview, 2023:225. pp. 52–66. <https://doi.org/10.1080/14432471.2023.2236352>
- Lévy, L., Maurya, P.K., Byrdina, S., Vandemeulebrouck, J., Sigmundsson, F., Árnason, K., Ricci, T., Deldicque, D., Roger, M., Gibert, B., Labazuy, P., 2019. Electrical resistivity tomography and time-domain induced polarization field investigations of geothermal areas at Krafla, Iceland: Comparison to borehole and laboratory frequency-domain electrical observations. *Geophys J Int* 218. <https://doi.org/10.1093/gji/ggz240>
- Martin, T., Weller, A., 2023. Superposition of induced polarization signals measured on pyrite-sand mixtures. *Geophys J Int* 234. <https://doi.org/10.1093/gji/ggad091>
- Revil, A., Florsch, N., Mao, D., 2015. Induced polarization response of porous media with metallic particles -Part 1: A theory for disseminated semiconductors. *Geophysics* 80. <https://doi.org/10.1190/GEO2014-0577.1>

# Modeling of membrane polarization for arbitrary electrolytes

Janik Marsel<sup>1</sup>, Dennis Kreith<sup>1</sup>, Matthias Bücker<sup>1</sup>

<sup>1</sup>Institute for Geophysics and Extraterrestrial Physics, TU Braunschweig, Germany, [j.marsel@tu-braunschweig.de](mailto:j.marsel@tu-braunschweig.de)

One model explaining the polarization processes that lead to the frequency dependence of the complex conductivity in geologic materials is membrane polarization. It is linked to the polarization of the ions dissolved in the pore water and takes place in the pore space of the rock or sediment under investigation. One prerequisite for the occurrence of membrane polarization is the presence of an electrical double layer (EDL) covering the pore surface. In pore constrictions, the unequal concentrations of differently charged ions in the diffuse layer of the EDL lead to a difference in the transport rates for the different ions.

While previous models of membrane polarization usually assume symmetric and monovalent electrolytes, we now present a model of membrane polarization that can take any electrolyte into account, in particular multivalent and asymmetric electrolytes.

The membrane polarization of Marshall and Madden (1959) serves as a starting point. This model considers a one-dimensional sequence of active and passive zones (pore constrictions and wide pores, respectively). We extend their model to be able to include more than two ion species with arbitrary valences. This is accomplished by setting up an ion-transport equation (Nernst-Planck equation) for each ion species in the electrolyte. All Nernst-Planck equations are coupled via a Poisson equation, which connects variations in the electrical potential to electrical charges resulting from unbalanced ion concentrations. The Nernst-Planck-Poisson system of partial differential equations is then solved by a semi-analytical method. In this solution we also include effective mobilities of ions, introduced by Bücker and Hördt (2013) to take the different average concentrations of cations and anions in pores into account, which we modify to work with multiple ions and arbitrary valences as well.

We compare our model predictions to the existing analytical solution of the model by Bücker and Hördt (2013) for the limiting case of a monovalent electrolyte (see Fig. 1) and further validate it with a numerical finite element simulation for the case of multivalent, asymmetric electrolytes. We observe a good agreement of the new semi-analytical model with the corresponding numerical and analytical solutions. Furthermore, the model predictions for valences larger than 1 (see Fig. 2), show that even small concentrations of ions with valence 2 increase the magnitude of the membrane polarization significantly.

Our new model thus represents an important step towards integrating additional relevant aspects into a more and more complete membrane polarization model.

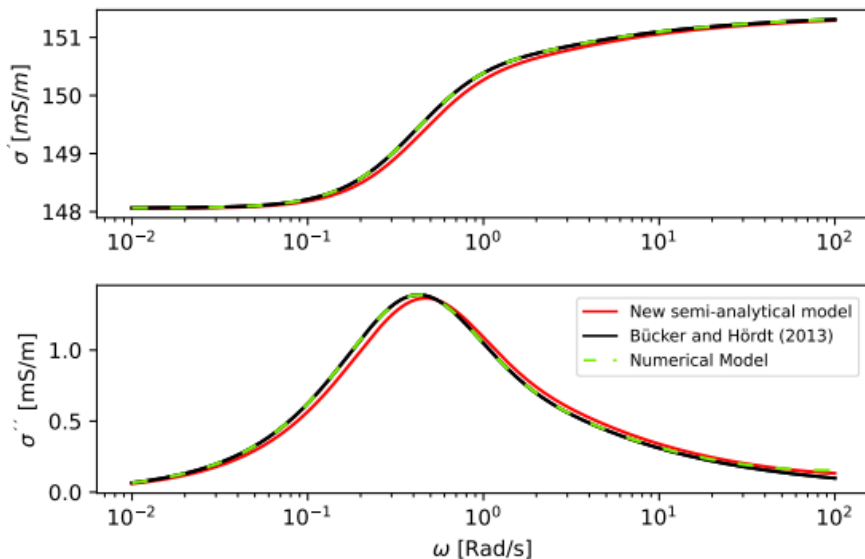


Figure 1: Comparison of real (upper panel) and imaginary conductivity (lower panel) of the model by Bücker and Hördt (2013), the numerical model (COMSOL) and the new semi-analytical model for a monovalent electrolyte with two ions. All three models match fairly well. Parameters used: radius narrow pore = 0,2  $\mu\text{m}$ , radius wide pore = 2  $\mu\text{m}$ , length narrow pore = 10  $\mu\text{m}$ , length wide pore = 90  $\mu\text{m}$ , Temperature = 293 K, relative permittivity = 80 (water), zeta potential = -100 mV, ion mobilitys (both ions) = 50 nm/s\*m/v, equilibrium concentrations (both ions) = 1 mol/m<sup>3</sup>, charge = e, -e

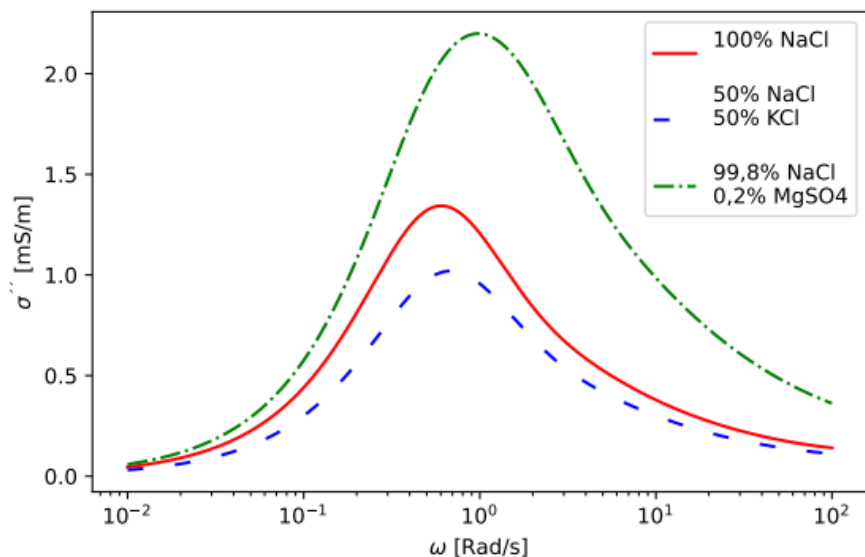


Figure 2: Polarization response (imaginary conductivity) for one mol of ions per m<sup>3</sup> in three different electrolyte solutions: While neither NaCl nor KCl contain ions with valences larger than 2, both Mg and SO<sub>4</sub> have a valence of 2. Even the small portion of 0,2% MgSO<sub>4</sub> causes an increase by a factor of almost 2 of the polarization magnitude compared to pure NaCl. All other model parameters as in Figure 1.

## References

- Marshall, D. J., Madden, T. R. (1959). Induced polarization, a study of its causes, Geophysics, XXIV NO.4, p. 790–816.
- Bücker, M., Hördt, A. (2013). Analytical modelling of membrane polarization with explicit parametrization of pore radii and the electrical double layer. Geophysical Journal International 194, p. 804–813.

# Insights into the structural properties of frozen rock from fitting a 2-component model to high-frequency SIP laboratory data

Andreas Hördt<sup>1</sup>, Jonas K. Limbrock<sup>2</sup>, Madhuri Sugand<sup>1</sup>, Andreas Kemna<sup>2</sup>

<sup>1</sup>*Institute of Geophysics and extraterrestrial Physics, TU Braunschweig, Germany, a.hoerdt@tu-bs.de*

<sup>2</sup>*Institute of Geosciences, Geophysics Section, University of Bonn, Germany*

High-frequency spectral induced polarization (HFIP) is an emerging method in permafrost research because of its potential to provide essential information about the properties of frozen ground. In the frequency range up to 200 kHz, ice exhibits a temperature-dependent characteristic relaxation that may be expressed in terms of the relative electric permittivity changing from values  $\approx 90$  to  $\approx 3$ . To extract quantitative information, such as ice content, from the measured impedance spectra, Zorin and Ageev (2017) suggest a model that describes the complex, electrical conductivity of an ice-containing material. The model consists of two components: the ice and the “matrix”, which includes all non-ice components (like minerals and residual liquid water). The conductivity of the bulk medium is calculated as a weighted power mean of the two components, where the ice content is the weight and the power is a structural parameter that theoretically varies between -1 and +1, corresponding to the two extremes of serial and parallel circuit arrangement of the two components.

Here, we test the applicability of the model with a set of laboratory data previously described in Limbrock et al. (2020). We focus on three samples, the impedance of which has been measured in a frequency range between 0.01 Hz and 45 kHz, and a temperature range between -40°C and +20 °C. Using a hybrid approach with trial-and-error forward modelling and a constrained inversion, we obtain reasonable fits to the data wherein the essential spectral features of the spectra, such as bumps in the phase spectra, are well reproduced. The model parameters are in the range that can be expected from the known ice relaxation and from porosity measurements.

One key observation is that the structural parameter is not necessarily limited to positive values, and may decrease with decreasing temperature. This means that the ice and the non-ice components do not mix in a random fashion but arrange in a specific way that may be characterized with HFIP measurements. Another important observation is that the ice relaxation itself may not dominate the spectral shape but rather Maxwell-Wagner polarization, which depends only on the low-frequency limit of the ice permittivity.

## References

- Limbrock, J., Weigand, M., and Kemna A., 2020. Improved thermal characterization of alpine permafrost sites by broadband SIP measurements. EGU-2020-20081.
- Zorin, N. and Ageev, D., 2017. Electrical properties of two-component mixtures and their application to high-frequency IP exploration of permafrost, Near Surface Geophysics, 15, 603 – 613.

# Impact of Pore-Water Velocity on the Spectral Induced Polarization Response of Granular Materials

Ruth Glebe<sup>1</sup>, Nimrod Schwartz<sup>2</sup>, Dennis Kreith<sup>1</sup>, Matthias Bücker<sup>1</sup>

<sup>1</sup> Institute of Geophysics and Extraterrestrial Physics of TU Braunschweig, Germany, [ruth.glebe@tu-bs.de](mailto:ruth.glebe@tu-bs.de)

<sup>2</sup> Soil and Water Sciences of Hebrew University of Jerusalem, Israel

The low-frequency spectral induced polarization (SIP) response of granular media is usually attributed to the polarization and relaxation of the electrical double layer covering mineral grains (e.g., Bücker et al., 2019). However, most of the models describing double-layer polarization do not consider possible changes in the SIP signal due to moving pore fluid.

Recently, Tsukanov et al. (2021) examined the impact of pore-fluid velocity on the SIP signal of soil samples. Their measurements showed a decrease of both, chargeability and time constant (both determined by fitting a Cole-Cole model) with increasing fluid velocity. The same authors also suggest an extension of the numerical double-layer polarization model of Bücker et al. (2019) to predict the effect of pore-fluid velocity on the SIP response of a single spherical mineral grain. Although experimental and numerical modeling results show similar general trends, the numerical simulations clearly overestimate the effect of pore water velocity on the SIP signal. As a possible explanation, the authors discuss the slip boundary condition at the mineral surface, which leads to an overestimation of the fluid velocity at the solid-liquid interface when solving the Stokes equation.

This work aims to further investigate the effect of surface properties of mineral grains, such as hydrophobicity, on the effect of the pore-water velocity on the SIP signal. We also present a further development of the numerical double-layer polarization model, which removes some important limitations of earlier numerical models.

SIP data was collected in the laboratory at different pore-water velocities. Two soil types, as well as several oxides were investigated. One example is Hamra soil, an Israeli soil mainly consisting of sandy loam with a reddish color, which was also used in the study by Tsukanov et al. (2021). With increasing pore-water velocity, the position of the phase peak shifts to higher frequencies and the magnitude of the phase peak decreases. These results confirm the experimental findings by Tsukanov et al. (2021).

In order to study the effect of surface hydrophobicity on the SIP signal, the soils were treated with palmitic acid at different concentrations. Figure 1 shows the SIP results for Hamra soil treated with several concentrations of palmitic acid. The general trends, i.e., the shift of the peak position to higher frequencies and the decrease of the peak magnitude with the velocity, are still observable. However, the strength of the effect of fluid velocity decreases with the concentration of palmitic acid, and thus the degree of hydrophobicity. This observation supports the hypothesis of Tsukanov et al. (2021), who reason that the influence of the velocity on the SIP signal depends on the slippage at the solid-liquid interface.

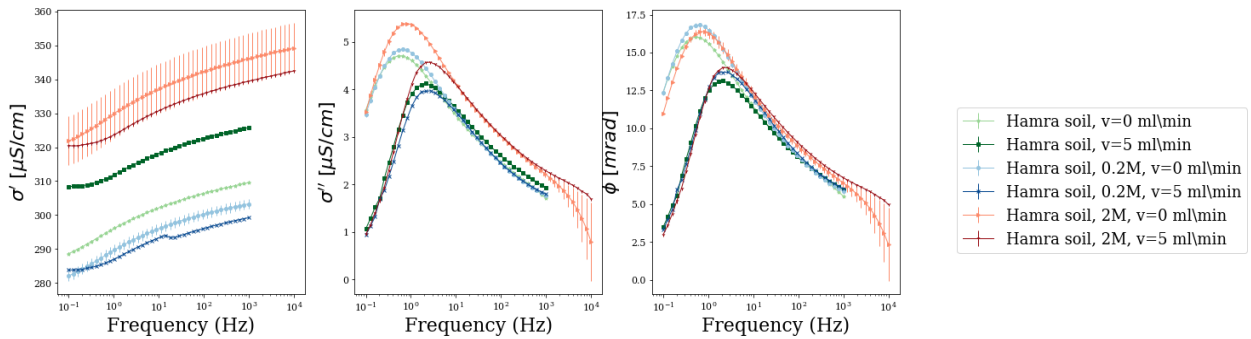


Figure 1: SIP response of Hamra soil for different pore-fluid velocities and different concentrations of the palmitic acid used to increase the hydrophobicity of the mineral surfaces. Left: in-phase conductivity, center: quadrature conductivity, right: phase angle. Increasing darkness correlates with increasing pore-water velocity.

The numerical model by Tsukanov et al. (2021) was extended to better account for the effect of fluid flow on the configuration of the electrical double layer covering the spherical mineral grain. Instead of assuming a fixed surface (zeta) potential and letting the flow field act on the diffuse layer only, a simple surface-complexation model was added, which allows to fix the total surface charge and calculate the distribution of charges into Stern and diffuse layer under the influence of the flow field. First modelling results shown in Figure 2 follows the same general trends as the experimental data but no longer require the assumption of Stern-layer charges being dragged around the mineral by the fluid-flow field.

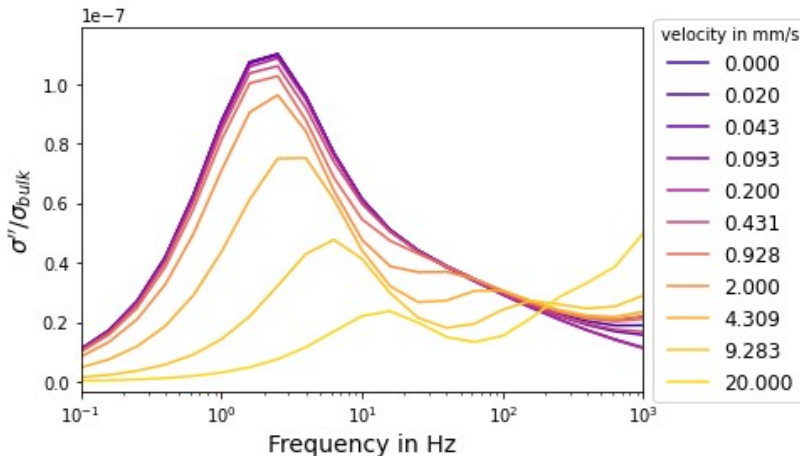


Figure 2: Modelled SIP response (quadrature conductivity normalized by bulk conductivity of the fluid) for several pore-water velocities. Lighter colors indicate larger velocities. The model consists of a single grain with a radius of 5  $\mu\text{m}$  in the center of a cylindrical pore with a radius of 250  $\mu\text{m}$  and a length of 250  $\mu\text{m}$  with a fluid conductivity of 9.65 mS/m. Without flow, a zeta potential of -81.2 mV and a Stern-layer surface charge density of 1.11 mC/m<sup>2</sup> were calculated.

All in all, we were able to confirm a dependence of the SIP lab measurements on the pore-water velocity. Furthermore, we were able to improve an existing numerical model for the SIP response, which takes fluid flow into account by incorporating a simple surface-complexation model. In the future, our improved model will be used to examine the dependence of the SIP signal on surface parameters, such as the total surface charge and its partitioning into Stern and diffuse layer.

## References

- Bücker, M., Flores Orozco, A. Undorf, S. and Kemna, A., 2019, On the role of Stern- and diffuse-layer polarization mechanisms in porous media. *Journal of Geophysical Research: Solid Earth*, 5656-5677.
- Tsukanov, K., Assa, I. and Schwartz, N., 2021, Modeling and experimental study of the effect of pore water velocity on the spectral induced polarization signature in porous media. *Water Resources Research*, 57.

# On the relationship between quadrature and surface conductivities: A pseudo-constant ratio

Youzheng Qi<sup>1</sup>, Yuxin Wu<sup>1</sup>

<sup>1</sup>*Earth and Environmental Sciences Area, Lawrence Berkeley National Laboratory, USA, Youzheng.Qi@lbl.gov*

## Abstract

Despite that multi-salinity experiments are routinely performed in laboratory induced polarization (IP) measurements to separate bulk water and surface conductivities with the gain of true formation factor  $F$ , this is impractical to realize in the fieldwork. One promising way to mitigate such a tough situation is to estimate the surface conductivity from quadrature conductivity on the presumption that there is a universal ratio between (i.e.,  $l \propto \sigma'' / \sigma_s$ ). However, recent independent rock and soil

/

measurements from different IP groups worldwide have obtained quite distinct ratios from each other, which makes the existence of such a constant ratio debatable. Here we scrutinize the conduction and polarization mechanisms within rocks and soils and prove that the ratio  $l$  shall be pseudo-constant and it is indeed a function of salinities, frequencies, and mineral types. Instead of  $l$ , we present another ratio directly from the effective electrical double layer (EDL) such that the new ratio excludes the salinity and frequency effects and could offer more quantitative applications.

## Theory

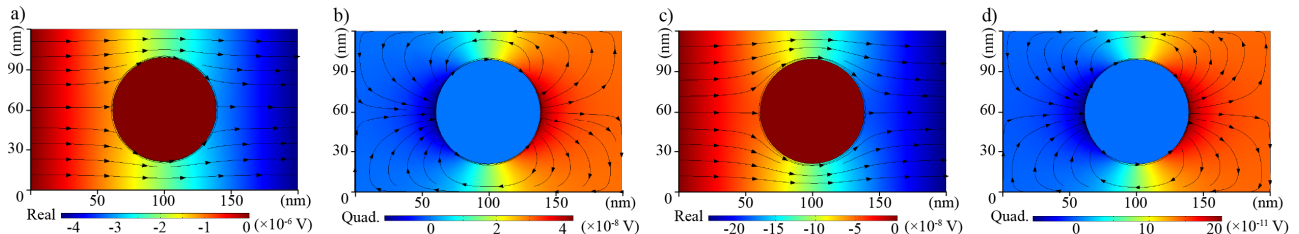


Figure 1: Grain-scale simulations testify that both real and quadrature voltages  $V$  and currents  $I$  distribute in the water. (a) and (b) are the real and quadrature distributions at low salinity ( $0.05 \text{ S/m}$ ), while (c) and (d) are those at high salinity ( $1 \text{ S/m}$ ), respectively. Note that  $V$  (in color scales) and  $I$  (in black arrowed lines) bear the same information since they are perpendicular to each other.

The philosophy of employing quadrature conductivity to assess surface conductivity can be backdated to the pioneering work of Börner (1992) and has been widely used in the IP community since the exceptional work of Weller et al. (2013). Considering the introduction of  $l = \sigma'' / \sigma_s$  in Börner (1992) lies in the ascription of these two components merely to the EDL, this foundation shall be revisited. A micro-scale grain-scale simulation at low- and high-salinity is performed in Figure 1 where it evidences that both the real and quadrature field distribute in the water, that is, the surface and quadrature conductivities are hybrid properties under the interplay of EDL and water. Although EDL is the original source, this by no means imply that these two components will only link to EDL since in IP measurement, electrodes do not directly connect to EDL and it is actually the total field in water that is measured, such field including the background field and the anomaly field disturbed by EDL.

## Simulations

Petrophysical models embracing such EDL-and-water coupling are the three-resistor (TR) model, Bruggeman-Hanai-Sen (BHS) model (Sen et al., 1981), Weller-Salter model (Weller et al., 2013), and the model recently developed by Qi & Wu (2024). Waxman-type model shall be excluded here because it empirically treats EDL and water as two separate conductors that contradicts the Maxwell's equations. Figure 2 demonstrates the simulated surface and quadrature conductivities from BHS and the model of Qi & Wu (2024) with constant EDL. Similar to each other, they both illustrate that although surface and quadrature conductivities behaves very similar, the resulting ratio between each other is still salinity-dependent, as both are compound properties including EDL and water properties.

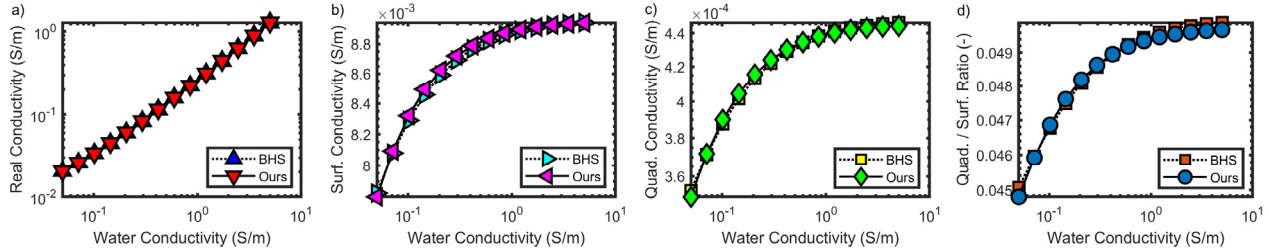


Figure 2: Simulated IP curves with BHS model and the model of Qi & Wu (2024). (a), (b), (c), and (d) are real conductivity, surface conductivity, quadrature conductivity, and the ratio between quadrature and surface conductivities, respectively. Note that with three-resistor model or Weller-Slater model, similar curves can also be obtained, albeit the other two models need more model parameters.

## Experiments

Most rock and soil experiments, including the original work of Börner (1992), have discovered this ratio is verily salinity-dependent, which is unfortunately neglected mostly because this dependence is weak at intermediate salinities. As to the frequency dependency, its exclusion mostly stems from the postulation that constant-phase-angle (CPA) model governs the IP responses of rocks and soils, but, by contrast, more experiments shows that Cole-Cole or Debye-decomposition model dictates the IP curves rather than CPA, which is also underpinned by the landmark theory of Schwarz (1962), both confirming that this ratio is frequency-dependent.

## Discussions and Conclusions

Given the fact that both surface and quadrature conductivities are composite properties under the interplay of EDL and water, to separate which, it shall be plausible to introduce another ratio between quadrature and surface conductivity of the effective EDL rather than of the bulk rock and soil. The effective complex conductivity of EDL can be extracted from TR, Weller-Slater, BHS or the model of Qi & Wu (2024). As to the frequency dependency, the characteristic frequency rather than 1 Hz is suggested since EDLs behave as Cole-Cole rather than CPA model, with which, the newly obtained ratio excludes salinity and frequency influences and will be only related to the specific mineral type.

## References

- Börner, F.D., 1992. Complex conductivity measurements of reservoir properties. Advances in Core Evaluation III (Reservoir Management). Gordon and Breach Science Publishers, London.
- Qi, Y., and Wu, Y., 2024. Induced polarization of clayey rocks and soils: Non-linear complex conductivity models, in revision.
- Sen, P. N., Scala, C., and Cohen, M. H., 1981. A self-similar model for sedimentary rocks with application to the dielectric constant of fused glass beads. Geophysics, 46(5), 781-795.
- Schwarz, G., 1962. A theory of the low-frequency dielectric dispersion of colloidal particles in electrolyte solution. The Journal of Physical Chemistry, 66(12), 2636-2642.
- Weller, A., Slater, L., and Nordsiek, S., 2013. On the relationship between induced polarization and surface conductivity: Implications for petrophysical interpretation of electrical measurements. Geophysics, 78(5), D315-D325.

# Complex conductivity of diatomites from Fur Formation saturated with NaCl and KCl solutions

E. Proestakis<sup>1</sup>, L.T.P. Meireles<sup>2</sup> and I. L. Fabricius<sup>1</sup>

<sup>1</sup>Department of Environmental and Resource Engineering, Technical University of Denmark, Kgs. Lyngby, Denmark.

<sup>2</sup>Equinor, Sandslia, Norway

Corresponding author email: ermpr@dtu.dk

## Introduction

Induced polarization in rock samples arises from the interaction between mineral surfaces and ions in pore water when subjected to an electrical field. In addition to the rocks containing conducting and semiconducting grains, induced polarization is also evident in rocks with high internal surface area. In our study, we investigated the effect of NaCl and KCl solutions on complex conductivity signals of an Eocene diatomite sample with high internal surface area from the Fur Formation in Denmark.

## Method

Prior to sample testing, we validated our complex conductivity setup using electronic circuits and various brines. Our tests demonstrated reproducibility of electrical conductivity within a 1% margin, while phase shift error fluctuated below 0.1 mrad below 1kHz. At higher frequencies, capacitive coupling effects were significant and modeled out using a single Cole-Cole relaxation model (Pelton et al., 1978). We saturated the sample and conducted complex conductivity measurements at four increasing bulk water conductivities using KCl solutions. Then, we diluted the sample with deionized water and repeated measurements at similar bulk water conductivities using NaCl solutions.

## Results, Discussion and Conclusions

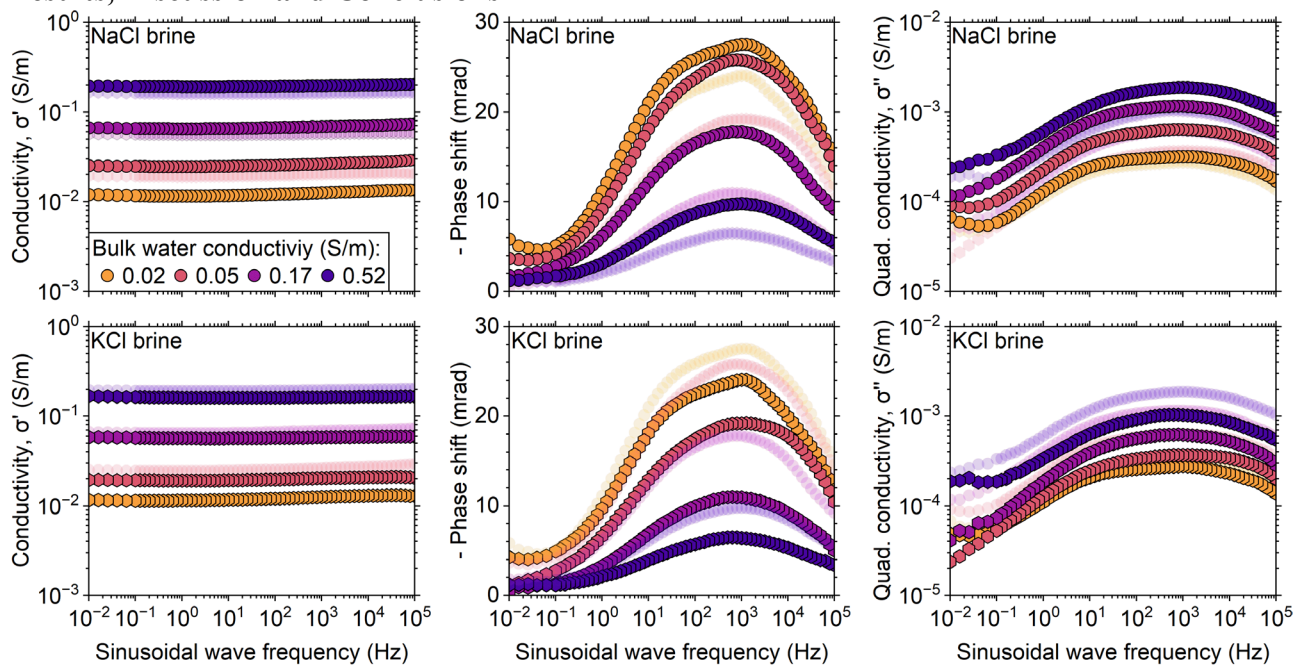


Figure 1: Conductivity, phase shift, and quadrature conductivity of Fur sample versus frequency, with top plots show results with NaCl brine and bottom plots with KCl brine. Background transparent data represent the results of the other electrolyte for comparison. The sample has a measured porosity of 72%, a grain density of  $2.04 \text{ g/cm}^3$ , and an internal surface area per bulk volume of  $13 \text{ m}^2/\text{cm}^3$ .

When salts are introduced to water, they dissolve into ions and become solvated by water molecules. Submerging a typical mineral in an aqueous solution exposes the surface charges that attract water and ions from the solution and a more concentrated region of ions around the surface forms, referred to as the electrical double layer (EDL). Given that the pH of the excess brine used to saturate the sample dropped from 7 to 6.5-4.5, it is plausible that  $\text{K}^+$  and  $\text{Na}^+$  respectively exchanged adsorbed  $\text{H}_3\text{O}^+$  in the EDL.

Within the EDL, surface forces can interact with hydrated ions, causing their gradual dehydration as concentration increases (Heuberger et al., 2017). This process enhances ordering and reduces the mobility of ions within the EDL. Consequently, with increasing concentration and decreased ion mobility within the EDL, the predominant transmission of current shifts from the surface to bulk water. The Gibbs free energy of hydration for  $\text{K}^+$  is -305 kJ/mol, while for  $\text{Na}^+$  it is -385 kJ/mol (Marcus, 1991). Due to the weaker hydration of  $\text{K}^+$  than  $\text{Na}^+$ , the transition of current transmission from the surface to the bulk water occurs at a lower concentration in KCl solutions than in NaCl solutions. As a result, for similar bulk water conductivity, the sample saturated with KCl solutions exhibits lower conductivity than when saturated with NaCl solutions (Figure 1). This causes a higher Archie's porosity exponent ( $m$ ) derived from a single-point measurement for KCl brine (Figure 2).

As current transmission increasingly occurs in the bulk water with increasing concentration, information regarding surface effects diminishes. Consequently, the magnitude of phase shift and chargeability progressively declines, although an increase in quadrature conductivity with concentration is still observed. The chargeability profile in the KCl-saturated state is shifted towards lower bulk water conductivity as compared to the NaCl-saturated state, reflecting the difference in Gibbs free energy of hydration between  $\text{K}^+$  and  $\text{Na}^+$ .

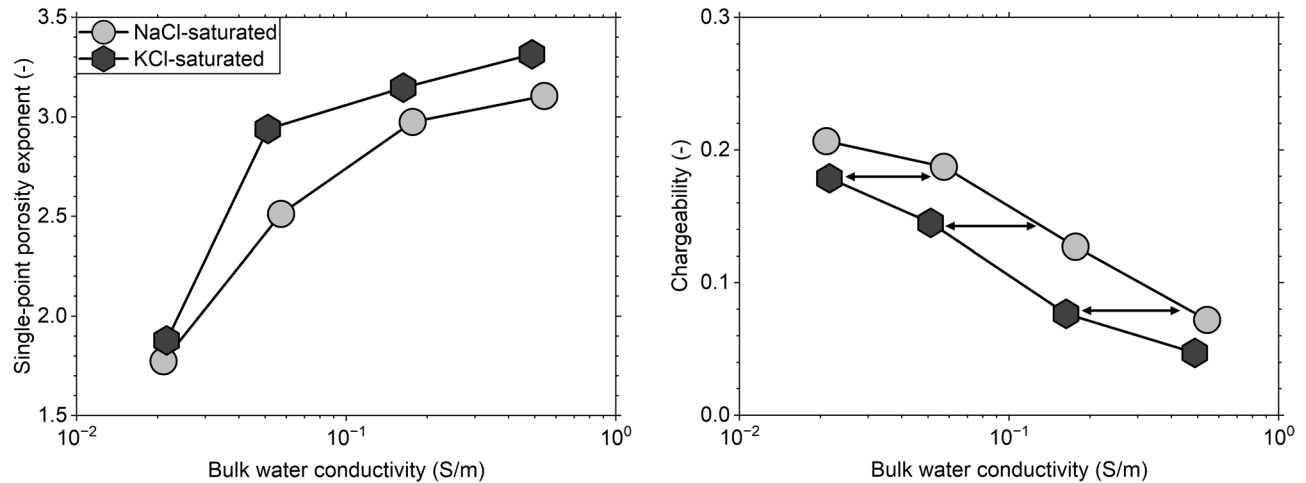


Figure 2: Left: Archie's porosity exponent ( $m$ ) versus bulk water conductivity for NaCl and KCl brines. Right: Chargeability using a single Cole-Cole relaxation model.

## Acknowledgements

The authors acknowledge the Danish Offshore Technology Center for funding this research.

## References

- Heuberger, M.P., Zachariah, Z., Spencer, N.D., Espinosa-Marzal, 2017. Collective dehydration of ions in nano-pores. *Physical Chemistry Chemical Physics*, 19, 13462–13468.
- Marcus, Y., 1991. Thermodynamics of solvation of ions. Part 5.—Gibbs free energy of hydration at 298.15 K. *Journal of the Chemical Society*, 87, 2995–2999.
- Pelton, W.H., Ward, S.H., Hallof, P.G., Sill, W.R. and Nelson, P.H., 1978. Mineral discrimination and removal of inductive coupling with multifrequency IP. *Geophysics*, 43, 588–609.

# Is it possible to assess the quality of carbonates using IP?

Norbert Klitzsch<sup>1</sup>, Lothar Ahrensmeier<sup>1</sup>, Nicolai Thüns<sup>2</sup>,

<sup>1</sup> Computational Geoscience, Geothermics, and Reservoir Geophysics, RWTH Aachen University, Germany,

*nklitzsch@eonerc.rwth-aachen.de*

<sup>2</sup> AixMinerals, Germany

Carbonate rock, i.e. limestone and dolomite, is often used as building material and construction aggregate, but also in industrial processes, e.g. in metallurgy and glass production. For many applications, the mineralogical purity of the carbonate rock, i.e. its calcium carbonate or dolomite content, is crucial. For carbonate deposits overlain by unconsolidated sediments, minerals can infiltrate into the carbonate's fracture network. These are mainly clay minerals as they are easily transported by water and can therefore infiltrate particularly well. As a result, they influence the mineralogical composition of the mined carbonate. To meet the purity requirements, one would like to assess the purity of the carbonate, at least qualitatively, before mining.

For the exploration of carbonate deposits electrical resistivity tomography (ERT) is a commonly used method that benefits from the high contrast between the resistivity of unconsolidated sediment and carbonate. ERT is however applied for the spatial delineation between overburden and carbonate rock, but not for assessing the quality of the latter.

We investigate whether the induced polarization (IP) method can be used for assessing the purity of carbonates. Specifically, we test the hypothesis that the imaginary conductivity and normalized chargeability are correlated with the clay content of the carbonate. This correlation is expected because the clay content determines the carbonates inner surface area and its cation exchange capacity (CEC). These two variables in turn correlate with the mentioned IP parameters, which was shown for both sandstones and unconsolidated sediments (e.g., Weller and Slater 2015, Revil et al. 2017).

To test our hypothesis, we measured two IP profiles in a dolomite quarry and obtained samples from the underlying wall. On these samples, we measured CEC and SIP. Additionally, we determined the clay mineral content of 10 selected samples using the XRD analyses.

The results of this study, specifically whether IP measurements can be utilized to assess the quality of carbonates, will be presented at the IP workshop.

## References

- Revil, A., Coperey, A., Shao, Z., Florsch, N., Fabricius, I.L., Deng, Y., Delsman, J.R., Pauw, P.S., Karaoulis, M., de Louw, P.G.B., van Baaren, E.S., Dabekaußen, W., Menkovic, A., Gunnink, J.L., 2017. Complex conductivity of soils. *Water Resour. Res.* 53 (8), 7121–7147. doi.org/10.1002/2017WR020655.
- Weller, A., Slater, L.D., 2015. Induced polarization dependence on pore space geometry: Empirical observations and mechanistic predictions, *J. of Appl. Geophysics*. doi.org/10.1016/j.jappgeo.2015.09.002

# Characterization of electrical properties of Beauce Limestones (O-ZNS, France) from SIP measurement.

A.N. Yacouba<sup>1,2</sup>, J. Deparis<sup>2</sup>, C. Mallet<sup>1</sup>, P. Leroy<sup>2</sup>, D. Jougnot<sup>3</sup>, M. Azaroual<sup>1,2</sup>

<sup>1</sup>ISTO, UMR 7327, univ Orleans, CNRS, BRGM, OSUC, F-45071, Orléans, France

<sup>2</sup>French geological survey, BRGM, F-45100, Orleans, France

<sup>3</sup>Sorbonne University, CNRS, EPHE, UMR 7619 METIS, F-75005 Paris, France

## Introduction

Water needs is tremendously and continuously increasing, driven by climate change and world population growth. In this context, hydrogeophysics can provide insightful non-intrusive information about groundwater activities. This study considers the Beauce aquifer (O-ZNS platform, France), where its lacustrine limestone vadose zone is characterized by multi-scale heterogeneities. They are defined by the overall complex pore structures and enhanced by diagenetic reactions and weathering processes. This leads to uncertainties for electrical properties estimation, which could be used to predict hydraulic parameters compulsory for flow models and helping aquifer management. In this study, we used complex conductivity measurement combined with other petrophysical analysis in order to relate these properties and ultimately infer the influence of weathering/fracturing on their prediction.

## Materiel and methods

The vadose zone of Beauce aquifer is an extremely complex porous and fractured medium mainly composed by lacustrine limestones (i.e., Beauce Limestones). This vadose zone can be subdivided in two layers: (1) the soil and the unconsolidated limestones and (2) the consolidated limestone on which we focus this study. In order to investigate rock with different (micro) structures, we further subdivided this consolidated limestone into four different facies (A, B, C and C') from which a total of 16 sample were cored. Spectral Induced Polarization (SIP) measurements (Binley and Slater, 2020) were carried out on 8 samples (of 4 cm diameter and ~10 cm length) with the SIP-LAB-IV apparatus using a 4-electrode setup (Jougnot et al., 2010). SIP measurements were performed on fully saturated samples at three different NaCl concentrations with the following conductivities (at 25 °C) 21.4, 86.9 and 956 mS/m, respectively. The sample have been also characterized in term of porosity, permeability and acoustic velocities, together with microstructural analysis.

## Results and discussion

We first considered a single frequency (1.46 Hz) to compute the formation factor (*FF*) and surface conductivity from in-phase conductivity. Yielding to formation factor from 86 to 378 and surface conductivity ranging between 0.0008 and 0.022 S/m. A cementation exponent (*m*) was then calculated according to Archie's law. Afterwards, we defined for each samples, the ratio between the two component of the complex surface conductivity ( $\sigma_{\text{surf}}^*$ ) as introduced by Börner et al (1996). The result is then compared (figure 1) to that of the datasets used by Weller et al. (2013). Beauce Limestones ratio values vary from 0.08 to 0.45 and are globally higher compare to those found by Weller et al. (2013) (0.01 to 0.13) and Börner et al. (1996) (0.01 to 0.15) for silicoclastic materials.

The second interpretation approach considered the entire spectrum of complex conductivity and interpreted from fitting a double Cole-Cole model. In general, the SIP spectra are well fitted, especially the quadrature conductivity where the fitting is almost perfect. In total, 7 fitting parameters among which chargeability ( $M$ ) and relaxation time ( $\tau$ ) are obtained and analysed. Both chargeability and relaxation time show some discrimination according the four defined facies.

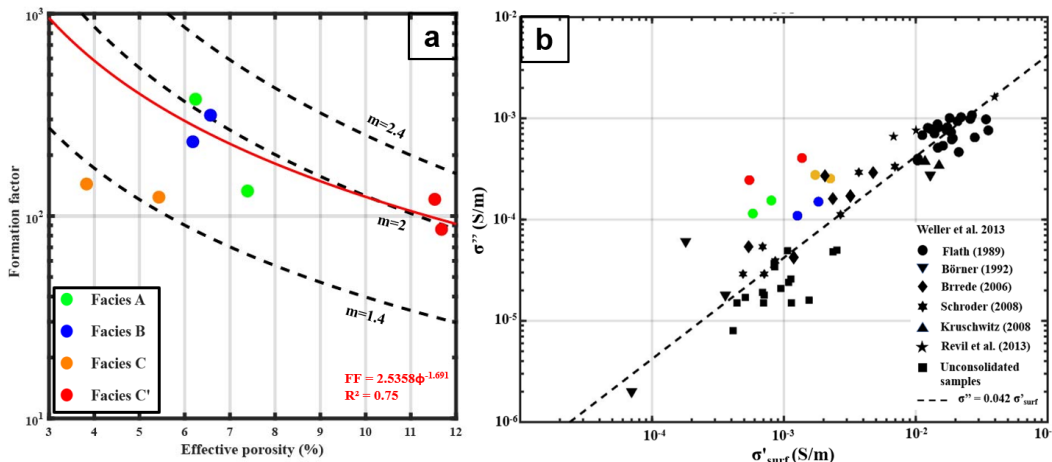


Figure 1. Cementation exponent of Beauce Limestones. a) Plot of FF versus effective porosity: dashed lines: Archie's models with different cementation exponent. Red line: Winsauer (1952)'s model. b) Relationship between quadrature conductivity and surface conductivity for Beauce Limestones compared to siliciclastic dataset from Weller et al. (2013). The quadrature conductivity and surface conductivity were defined at frequency of 1.46 Hz and water conductivity of 86.9 mS/m.

## Conclusion and perspectives

The SIP method provides interesting and relevant parameters that are related to pore structures and transport properties, helping us to better characterize carbonate samples than using only the real part of the electrical conductivity. The next step of this work is to predict Beauce Limestones permeability. By using on one hand, the first approach element ( $FF$ ,  $m$  and  $\sigma'^{*surf}$ ) and on the other hand the fitting parameters ( $M$ ,  $\tau$ ) based on petrophysical models more often limited to siliciclastic rocks (Binley and Slater, 2020). The influence of the complex pore structure of our weathered and fractured limestones will be also studied. Finally, we will assess a possible relationship between these complex electrical properties and acoustic velocities.

## References

- Binley, A., Slater, L., 2020. Resistivity and induced polarization: Theory and applications to the near-surface earth. Cambridge University Press. <https://doi.org/10.1017/9781108685955>
- Börner, F.D., Schopper, J., Weller, A., 1996. Evaluation of transport and storage properties in the soil and groundwater zone from induced polarization measurements1. Geophysical prospecting 44, 583–601. <https://doi.org/10.1111/j.1365-2478.1996.tb00167.x>
- Jougnot, D., Ghorbani, A., Revil, A., Leroy, P., Cosenza, P., 2010. Spectral induced polarization of partially saturated clay-rocks: A mechanistic approach. Geophysical Journal International 180, 210–224. <https://doi.org/10.1111/j.1365-246X.2009.04426.x>
- Weller, A., Slater, L., Nordsiek, S., 2013. On the relationship between induced polarization and surface conductivity: Implications for petrophysical interpretation of electrical measurements. Geophysics 78, D315–D325. <https://doi.org/10.1190/geo2013-0076.1>
- Winsauer, W.O., 1952. Resistivity of Brine-Saturated Sands in Relation to Pore Geometry. AAPG Bulletin 36, 253–277. <https://doi.org/10.1306/3D9343F4-16B1-11D7-8645000102C1865D>

# Spectral Induced Polarization and Mise-a-la-masse for studying plant roots and root water uptake

Luca Peruzzo<sup>1</sup>, Chunwei Chou<sup>2</sup>, Benjamin Mary<sup>3</sup>, Veronika Ivan<sup>1</sup>, Giorgio Cassiani<sup>1</sup>, Yuxin Wu<sup>2</sup>

<sup>1</sup>*Department of Geosciences, University of Padova, Italy, luca.peruzzo.1@unipd.it*

<sup>2</sup>*Earth and Environmental Sciences Area, Lawrence Berkeley National Laboratory, USA*

<sup>3</sup>*Consejo Superior de Investigaciones Científicas, Institute of Agricultural Sciences, Madrid, Spain*

This contribution elaborates on three recent studies in which we used Spectral Induced Polarization (SIP) and Mise-a-la-masse (MALM) to study plant roots and root water uptake (Peruzzo et al., 2020, 2021; Mary et al., 2020). Together, these studies aim to address long-lasting contradictions regarding the use of electrical signals measured in stem injection experiments as a proxy for root architectural traits and water pathways. On the one hand, numerous studies suggested and theoretically modelled the relationship between the impedance root signals and specific properties of the root system, such as the root surface area or total length. On the other hand, some authors have questioned the methodological soundness of such results and models, primarily pointing to possible proximal current leaking. In fact, the key point is whether the current from the stem injection reaches and thus can investigate the different parts of the root system, including the distal, fine, and more active roots.

This contribution first shows how commonly performed bioimpedance experiments with stem injection can be approached as MALM measurements by adding the imaging of the electric potential around the investigated root system. A combination of laboratory and field measurements confirm this possibility and successfully images the current pathways of different plant species and under variable soil water content. The plant species include herbaceous plants like wheat, pecan, and maize, but also grapevine.

While the results address the methodological gap and clarify the validity of the stem-injection bioimpedance experiments, the proposed approach is relatively time-consuming and strongly benefits from borehole electrodes, which in turn come with their own installation and processing difficulties.

For this reason, a variant of the traditional one-channel bioimpedance measurement is successively introduced. This approach takes advantage of the recent instrumental advances and uses three-channel SIP measurements (Fig. 1). The first channel only measures the response of the stem from the injection point to the soil surface, the second channel only measures the soil response, and the third channel measures the entire pathways, as typically done in previous studies. This way, it is possible to discern the impedance contributions of stem, root system, and soil. This three-channel measurements are significantly faster than MALM measurements and only require the instrumentation that is traditionally used in plant sciences.

The results show proximal current leakage in all the experiments performed with herbaceous roots, even if the roots were observed to extend more than several tens of centimeters. MALM and 3-channel SIP measurement agree on the depth of this proximal leaking region (Fig. 2). This ultimately provides evidence supporting the concerns on the general use of impedance measurements. On the contrary, the results from the grapevine experiments show that the current can travel within the root system for a significant length (Fig. 3), which was also used to monitor the root activity during infiltration experiments.

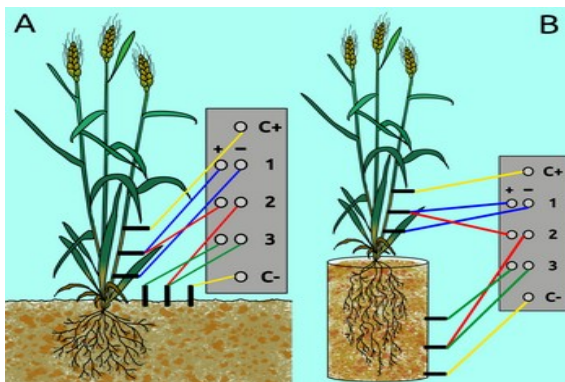


Figure 1: The three-channel setup that was used to measure the IP responses of stem, roots, and soil.

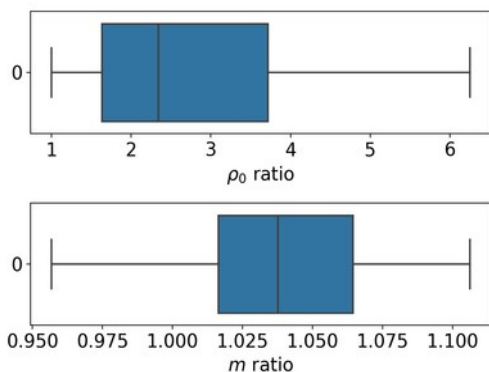


Figure 2: Statistical distribution of ratios between the root channel and stem channel, in terms of fitted Cole-Cole parameters. The figure shows that the current pathways have similar chargeability and that the low-frequency resistance is only a few times larger.

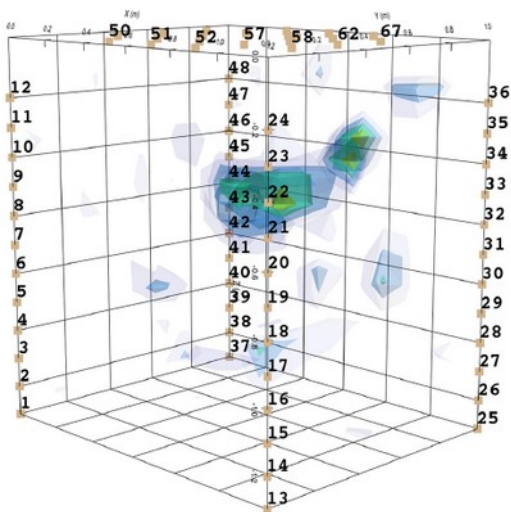


Figure 3: 3D setup used for the MALM measurements on the grapevines. The boreholes are 1.2 m deep. The current source density is shown within the volume, indicating deeper current pathways than in herbaceous plants.

## References

- Mary, B., Peruzzo, L., Boaga, J., Cenni, N., Schmutz, M., Wu, Y., Hubbard, S. S., & Cassiani, G. (2020). Time-lapse monitoring of root water uptake using electrical resistivity tomography and mise-à-la-masse: A vineyard infiltration experiment. *SOIL*, 6(1), 95–114. <https://doi.org/10.5194/soil-6-95-2020>

Peruzzo, L., Chou, C., Wu, Y., Schmutz, M., Mary, B., Wagner, F. M., Petrov, P., Newman, G., Blancaflor, E. B., Liu, X., Ma, X., & Hubbard, S. (2020). Imaging of plant current pathways for non-invasive root Phenotyping using a newly developed electrical current source density approach. *Plant and Soil*, 450(1-2), 567–584. <https://doi.org/10.1007/s11104-020-04529-w>

Peruzzo, L., Liu, X., Chou, C., Blancaflor, E. B., Zhao, H., Ma, X.-F., Mary, B., Iván, V., Weigand, M., & Wu, Y. (2021). Three-channel electrical impedance spectroscopy for field-scale root phenotyping. *The Plant Phenome Journal*, 4(1). <https://doi.org/10.1002/ppj2.20021>

**Send this pdf to: [induced.polarization@gmail.com](mailto:induced.polarization@gmail.com) and state the abstract title in the email header**

# On the fate and transport of heavy metals in calcareous soils – a spectral induced polarization study

Shany Ben Moshe<sup>1</sup>, Alex Furman<sup>1</sup>, ...

<sup>1</sup>Department of Environmental Engineering, Technion, Israel, [Benmoshe.shany@gmail.com](mailto:Benmoshe.shany@gmail.com)

The fate and transport of heavy metals in the soil have been intensively studied over the last decades due to its implications on public health and the environment. The mobility of heavy metals in the soil depends on the surface characteristics of the soil minerals and factors such as organic matter content, pore water pH and its composition, among others. Specifically, in calcareous soils, the introduction of heavy metals has been shown to induce dissolution of the calcite and formation of metal-based carbonate minerals. The study of such processes traditionally involves intensive sample collection and chemical analysis of multiple species. In this study, we use spectral induced polarization (SIP) for non-invasive monitoring of the transport of three heavy metals (Pb, Zn and Cu) through soils that contain calcite to different extents. Our experimental setup involves flow-through columns packed with different types of soil, through which the inflow solution is passed. Electrical potentials are recorded at three locations along the column and the outflow was collected in fractions and chemically analysed. The real part of the complex conductivity showed an initial increase followed by a gradual decrease in all three channels. The imaginary part decreased in a two-phase manner. For both the real and imaginary conductivities – the breakthrough of the metal was observed towards the stabilization of the conductivity decrease. The results indicate that both the real and the imaginary components of the complex conductivity are sensitive to the minerals' dissolution/precipitation. The conductivity values at the peak polarization frequency over time depict the progression of the dissolution/precipitation 'front' along the soil profile, as was confirmed by a PHREEQC model.

# Estimating hydraulic properties from IP and NMR measurements at field and laboratory scale

Tina Martin<sup>1</sup>, Thomas Günther<sup>2</sup>, Andreas Weller<sup>3</sup>, Andy Kass<sup>4</sup>, Denys Grombacher<sup>4</sup>, Christian Butron<sup>5</sup>, Alfredo Mendoza<sup>1</sup> and Torleif Dahlin<sup>1</sup>

<sup>1</sup>*Engineering Geology, Lund University, Sweden, tina.martin@tg.lth.se*

<sup>2</sup>*Leibniz Institute for Applied Geophysics, Hannover, Germany*

<sup>3</sup>*Clausthal University of Technology, Clausthal-Zellerfeld, Germany*

<sup>4</sup>*Hydrogeophysics Group, Aarhus University, Aarhus, Denmark*

<sup>5</sup>*Trafikverket, Gothenburg, Sweden*

## Introduction:

Protecting groundwater resources and preventing structural and environmental issues, especially in infrastructure projects, depends on adequate understanding of the groundwater dynamics. Traditionally, this understanding has been gleaned through costly and point-specific methods such as drillings followed by hydraulic tests. While reliable, these methods come with significant expenses and limited coverage. In our study, we employed geophysical methods such as Induced Polarization (IP) and Nuclear Magnetic Resonance (NMR) to tackle this challenge. These methods offer a way to gather information about the distribution of aquifer properties while minimizing the need for extensive drillings. By investigating various test sites in Sweden, we aimed to estimate hydraulic properties using IP and surface NMR. Additionally, we collected samples from these sites for laboratory analysis using the same methods.

## Test site and methods:

Our testsite Mjölkalånga is characterised by several layers of glacial and post-glacial sediments. The surface is characterised by agricultural areas with a low anthropogenic noise level. Apart from the geophysics HPT (hydraulic profiling tool) and slug tests were also conducted here to verify our results. The data of four DCIP (direct current resistivity and induced polarisation) profiles and 30 surface NMR soundings were collected. The data were processed afterwards and inverted. An approach based on the Debye decomposition was used to determine sections of hydraulic conductivity from time-domain IP data.

Additionally, samples were taken from the first meter of depth and analysed in the laboratory. Here, we conducted SIP, NMR, and hydraulic conductivity measurements using various sample holders.

## Results and discussion:

All four profiles, with profile 3 as an example shown in Fig. 1, exhibit distinct layers. The upper layers (8 to 10 m depth), display higher resistivity ( $> 500 \Omega\text{m}$ ), indicative of a sandy composition. Deeper sections of the profiles show a decrease in resistivity, suggesting a transition to more clayey materials ( $50 - 150 \Omega\text{m}$ ). The chargeability values in the upper 10 meters are generally low, gradually increasing to around 50 mV/V at greater depths. From these IP values, the calculated hydraulic conductivity falls within the range of  $10^{-3}$  to  $10^{-6} \text{ m/s}$ . Both the HPT and slug tests conducted along these profiles corroborate a highly permeable zone within the top 10 meters and a gradual decrease

of hydraulic conductivity below this zone. Comparing the hydraulic conductivity derived from IP measurements ( $K_{IP}$ ) with that from slug tests ( $K_{slug}$ ) reveals a good correlation. Furthermore, the NMR soundings indicate higher water content in the first few meters, while the transversal relaxation time ( $T_2^*$ ) shows a contrasting trend with lower values in the same depth range.

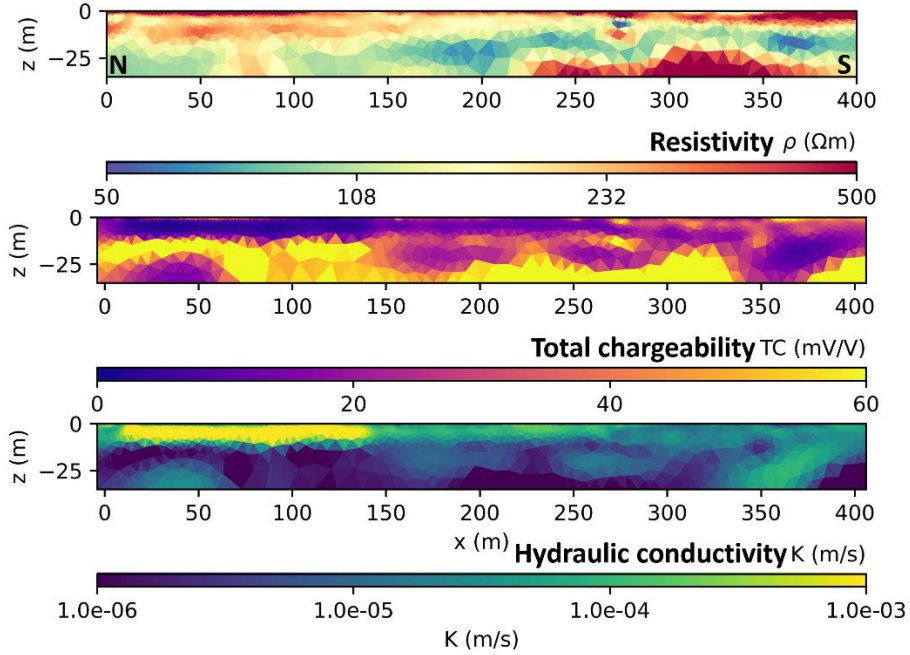


Figure 1: IP results for profile 3.

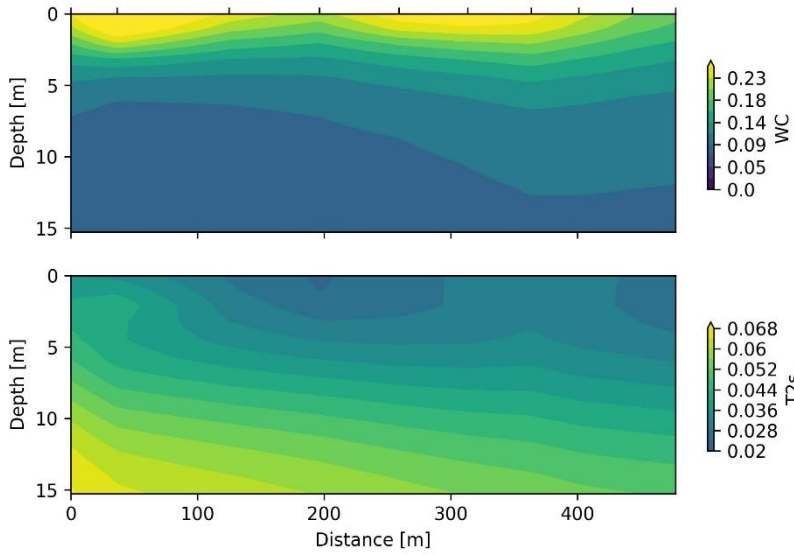


Figure 2: Surface NMR soundings for profile 3.

### Conclusion and outlook:

Initial findings demonstrate a good correlation between  $K_{IP}$  and  $K_{slug}$ , although ongoing tests with varied inversion algorithms are underway to enhance accuracy. The surface NMR soundings provide promising data, and the next phase involves calculating  $K$ -values from these measurements. Laboratory sample results exhibit a more favorable correlation compared to the field data. Subsequently, we plan to apply these methods in boreholes, coupled with various drilling and hydraulic logging techniques, to further validate the findings.

# Reactive process monitoring via joint induced polarization and transport modeling – new insights from cation exchange experiments

Cora Strobel<sup>1,2</sup>, Olaf A. Cirpka<sup>1</sup>, Adrian Mellage<sup>2</sup>

<sup>1</sup>Department of Geosciences, University of Tübingen, Tübingen, Germany, cora.strobel@uni-tuebingen.de

<sup>2</sup>Civil and Environmental Engineering, University of Kassel, Kassel, Germany

The promise of many geophysical monitoring methods is to provide a glimpse into the subsurface which largely remains a “black box” if only drill cores and water samples are available. Spectral induced polarization (SIP) in particular can provide valuable information about reactions that alter the surface chemistry/composition of the solid phase. This can be very valuable to fine-tune experiments and target sampling.

Sorption processes on organic matter are of particular importance for contaminant retardation and remediation applications. With its high surface area and a heterogeneous distribution of different sorption sites, organic matter is a strong sorbent for nutrients and/or contaminants in soils and sediments. In addition it also shows a strong polarization response (Strobel et al., 2023) thus making IP potentially sensitive for surface reactions on organic matter. In this work we explore how our current understanding of surface polarization can help to directly interpret IP data during cation exchange processes. We compare the IP response during the injection of a monovalent cation ( $\text{Na}^+$ ) and two divalent cations with different surface complexation strengths ( $\text{Ca}^{2+}$  and  $\text{Zn}^{2+}$ ) into columns with a calcite sand-peat mixture and  $\text{Ca}^{2+}$ -dominated pore water. We test whether a change in ion mobility on the surface is reflected in increasing (e.g. via  $\text{Na}^+$ ) or decreasing (e.g. via  $\text{Zn}^{2+}$ ) imaginary conductivity and whether we can monitor the moving front of cation exchange through the column using (S)IP.

We test the validity of our process understanding by comparing the qualitative IP interpretation with quantitative reactive transport models. Finally, we show how IP data can be incorporated into such models to better constrain solid-phase concentrations and provide an outlook on what is needed to successfully monitor reactions using IP by non-geophysicists.

## References

Strobel, C., Doerrich, M., Stieff, E. -H., Huisman, J.A., Cirpka, O.A., Mellage, A., 2023. Organic Matter

Matters—The Imaginary Conductivity of Sediments Rich in Solid Organic Carbon. *Geophysical Research Letters* 50, e2023GL104630.

# Tracking ammonium cation exchange in landfill waste using spectral induced polarization (SIP)

Ali Rahmani<sup>1</sup>, Laura Scharenberg<sup>1</sup>, David Laner<sup>1</sup> and Adrian Mellage<sup>1</sup>

<sup>1</sup>Civil and Environmental Engineering, University of Kassel, Germany. [Ali.Rahmani@uni-kassel.de](mailto:Ali.Rahmani@uni-kassel.de)

Landfill leachate poses a potential pollution threat to soil, surface water, and groundwater. Ammonium ( $\text{NH}_4^+$ ) is typically present at high concentrations in landfill leachate for extensive time periods (even decades after the end of waste deposition). Because ammonium is toxic at elevated levels in the environment and because of the formation of harmful nitrogen compounds, including nitrites and nitrates from nitrification (Halim et al., 2012; Liu et al., 2023; Raghab et al., 2013), ammonium-rich leachate needs to be treated before it can be released to the environment (Laner et al., 2011). In order to reduce mid- to long-term ammonium concentrations in landfill leachate, controlled mobilization of sorbed ammonium via cation exchange (e.g. with  $\text{K}^+$ ) could be an attractive option to remove ammonium while leachate is collected and treated and thereby shorten the need for extensive leachate management periods. Even though “controlled” (by the treatment of high concentrations of competing cations) the process relies on down-flow concentration sampling to detect its efficacy and remediation extent. Here, we test the application of spectral induced polarization (SIP), a non-invasive geophysical technique sensitive to ion exchange process in porous media (Hao et al., 2015; Vaudelet et al., 2011), as a sensing tool that offers can offer a potentially powerful real-time monitoring alternative to detect changes cation exchange without the need for down-flow monitoring. The objective of this study is to establish the sensitivity of the SIP signals towards cation exchange pre-treatment techniques that specifically target ammonium removal via exchange with  $\text{K}^+$  and divalent cations such as  $\text{Ca}^{2+}$ . The ultimate goal is to establish a robust framework for real-time monitoring at landfill sites, which is essential to implement effective management approaches to minimize the negative effects of high ammonium levels in landfill leachate.

## References

- Halim, A.A., Aziz, H.A., Johari, M.A.M., Ariffin, K.S., Bashir, M.J.K., 2012. Semi-Aerobic Landfill Leachate Treatment Using Carbon–Minerals Composite Adsorbent. *Environmental Engineering Science* 29, 306–312. <https://doi.org/10.1089/ees.2010.0204>
- Hao, N., Moysey, S.M.J., Powell, B.A., Ntarlagiannis, D., 2015. Evaluation of Surface Sorption Processes Using Spectral Induced Polarization and a  $^{22}\text{Na}$  Tracer. *Environ. Sci. Technol.* 49, 9866–9873. <https://doi.org/10.1021/acs.est.5b01327>
- Laner, D., Fellner, J., Brunner, P.H., 2011. Future landfill emissions and the effect of final cover installation – A case study. *Waste Management* 31, 1522–1531. <https://doi.org/10.1016/j.wasman.2011.02.022>

- Liu, N., Sun, Z., Zhang, H., Klausen, L.H., Moonhee, R., Kang, S., 2023. Emerging high-ammonia-nitrogen wastewater remediation by biological treatment and photocatalysis techniques. *Science of The Total Environment* 875, 162603. <https://doi.org/10.1016/j.scitotenv.2023.162603>
- Raghab, S.M., Abd El Meguid, A.M., Hegazi, H.A., 2013. Treatment of leachate from municipal solid waste landfill. *HBRC Journal* 9, 187–192. <https://doi.org/10.1016/j.hbrcj.2013.05.007>
- Vaudelet, P., Revil, A., Schmutz, M., Franceschi, M., Bégassat, P., 2011. Changes in induced polarization associated with the sorption of sodium, lead, and zinc on silica sands. *Journal of Colloid and Interface Science* 360, 739–752. <https://doi.org/10.1016/j.jcis.2011.04.077>

# Spectral induced polarization characterization on the landfill leachate contaminated groundwater remediation using permeable reactive materials

Na Hao<sup>1</sup>

<sup>1</sup>ZJU-Hangzhou Global Scientific and Technological Innovation Center, Zhejiang University, Hangzhou, China

Groundwater contamination caused by landfill activities has fueled the development of remediation strategies. Permeable reactive barriers (PRBs) are commonly applied in subsurface remediation because of their high removal effect and low costs. Spectral induced polarization (SIP) technique has been approved for its nondestructive ability to monitor the geochemical processes in porous media. Three application cases were presented here about the SIP technique applied for monitoring the contaminants remediation by permeable reactive materials at column scale.

The first study case was to apply SIP for monitoring iron remediation by limestone. The chemical analysis showed the pH of the porous fluid increased - attributed to the dissolution of limestone, which promoted the precipitation of iron. The micro computed tomography (CT) technique investigated the uneven distribution of the precipitates in the column, which indicated the existence of preferential flow. SIP signals revealed the quantity of the accumulated iron precipitates, which was proved by the chemical measurement and calculation. SIP signals also derived the time evolution of both the average precipitate size and size distribution, which elucidated the processes of precipitate crystal growth and aggregation during Fe flow-through. Above results suggest that SIP holds the promise of monitoring the engineering barrier performance.

The second application case was testing the remediation ability of activated carbon (AC) and biochar on lead (Pb), and SIP technique monitored the remediation process as well as revealing the interaction mechanisms. The calculated characteristic grain/pore size evolutions from SIP signals on AC, agreed well with the size of precipitates measured by SEM and mercury intrusion porosimetry (MIP) methods. The content increment process of the retained Pb on AC was also recorded via the magnitude increment of the imaginary conductivity. It showed that AC immobilizes through physical adsorption and precipitation, whereas complexation with functional groups is the remediation mechanism for biochar. Furthermore, the observed SIP responses of both AC and biochar are two orders of magnitude higher than those of typical natural soils or silica materials. This distinct difference is an additional advantage for the field application of SIP technique in PRB scenarios.

The last application case was about using SIP to monitor the  $Pb^{2+}$  and  $Cd^{2+}$  adsorption process by loess soils which are common and have been reported as effective material used in barrier for the removal of heavy metals. The column outflow aqueous geochemical analyses indicated a better retention capability of loess for  $Pb^{2+}$ , which was through precipitation induced by calcite dissolution and aqueous pH increment, as confirmed by SEM - EDS and XRD results. Cd retention took place mainly through ion exchange with  $Ca^{2+}$  and  $Mg^{2+}$  on the loess surface. The SIP signals showed a

continuous decrement on the magnitude of imaginary conductivity during both Pb<sup>2+</sup> and Cd<sup>2+</sup> flow-through, which was attributed to the total surface area and decrement of polarizable surface charges. The SIP signals differentiated the interactions between loess and Pb<sup>2+</sup>/ Cd<sup>2+</sup> by displaying a peak shift to a higher frequency on the imaginary conductivity spectra during Pb<sup>2+</sup> flow-through, attributing to calcite dissolution and proved by the high correlation ( $R^2 = 0.9366$ ) between the estimated dissolved calcite mass and the peak of imaginary conductivity. The above results suggest that loess has a great potential for field heavy metal remediation applications, and the SIP technique displays a promising capability of monitoring the remediation performance.

## References

- N. Hao, J. N. Cao, J. S. Ye, C. Zhang, C. Li, and B. Bate. Content and morphology of lead remediated by activated carbon and biochar: a spectral induced polarization study. *Journal of Hazardous Materials*, 2020, 411:124605.
- N. Hao, J. S. Ye, L. Zhao, M. Sun, Y. Y. You, Y. Peng, L. Zhao, and B. Bate\*. Evaluating iron remediation with limestone using spectral induced polarization and microscopic techniques, *Science of the Total Environment*, 2021, 149641.
- N. Hao\*, Y.Y. You, L.T. Zhan and B. Bate. "Evaluation of aqueous Cd<sup>2+</sup> and Pb<sup>2+</sup> removal by natural loess using spectral induced polarization and microscopic characterization." *Environmental Science and Pollution Research* 33(2022):29.

# Quantitative evaluation of the effect of pore water morphology on complex conductivity saturation exponents of porous media saturated by two immiscible fluid phases

Siyuan Qiang<sup>1</sup>, Xiaoqing Shi<sup>1\*</sup>, André Revil<sup>2</sup>, Xueyuan Kang<sup>1</sup>, Yalin Song<sup>1</sup>, Kun Xing<sup>1</sup>

<sup>1</sup>*Key Laboratory of Surficial Geochemistry of Ministry of Education, School of Earth Sciences and Engineering, Nanjing University, Nanjing 210023, China*

<sup>2</sup>*Université Grenoble Alpes, Université Savoie Mont Blanc, CNRS, UMR CNRS 5204, EDYTEM, 73370 Le Bourget du Lac, France*

The induced polarization (IP) method holds immense potentials for hydrogeophysical applications. Power-law relationships are typically used to estimate the subsurface water saturation from the complex conductivity obtained through IP method. However, the saturation exponents in the power-laws have been observed to vary with different geomaterials and wettabilities. Traditional experimental setups do not allow to visualize independently the water saturation and distribution in the pore space. Therefore, the physical interpretations of the variation of the saturation exponents values have remained unclear. We developed a novel 2D milli-fluidic micromodel using clay-coated glass beads that exhibit excellent visuality and high IP response (see Figure 1). Through experimental setups, we simultaneously determined the micromodel complex conductivity and acquired the corresponding pore-scale water distributions generated by drainage (oil displaces water) and displacement (water displaces oil) experiments. Additionally, finite-element numerical simulations of complex conductivity based on the upscaling of Electrical Double Layer (EDL) were conducted to reveal the saturation exponents under ideal pore water distributions. Results indicate that both the saturation exponents for in-phase and quadrature conductivities vary depending on non-aqueous phase ganglia size. The saturation exponents also exhibit power-law relationships with the change rate of pore water connectivity with saturation, which is calculated through the computation of the derivative of Euler characteristics. These findings provide a new physical explanation to the relationships between the saturation exponents and the microscopic pore water distribution.

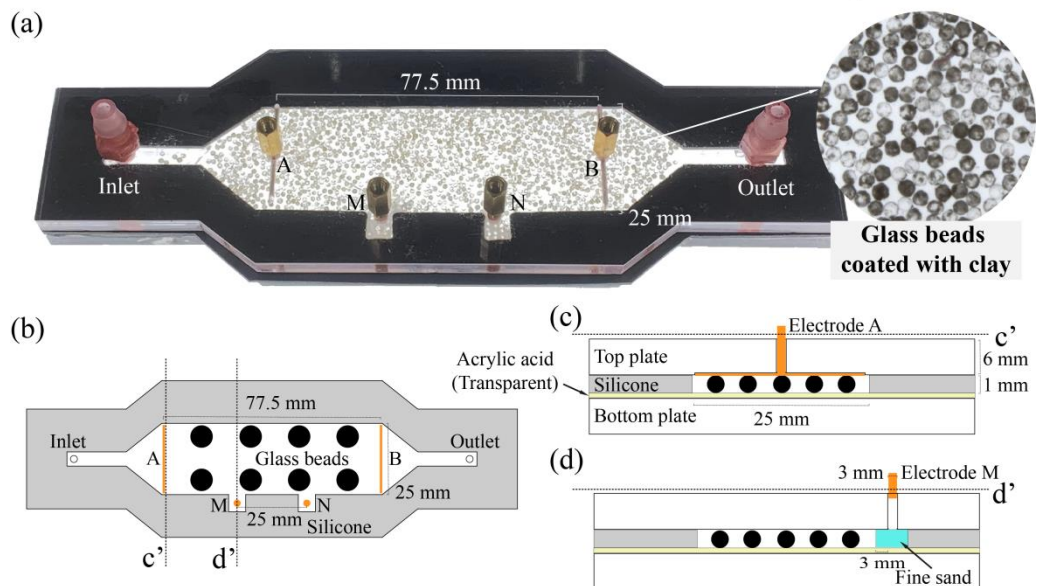


Figure 1: Sketch of the experimental setup. (a) Picture of the experimental micromodel without clamps. (b) Top view of the sketch of the micromodel. The dash lines correspond to the cross-section position for (c) the cross-section of the micromodel in line c' and (d) the cross-section of the micromodel in line d' .

# Unveiling the characteristics of ZVI-AC-sand mixtures in remediating contaminated groundwater using spectral induced polarization

Deqiang Mao<sup>1,\*</sup>, Xinmin Ma<sup>1</sup>, Nimrod Schwartz<sup>2</sup>, Chen Chao<sup>1</sup>, Kai Yang<sup>1</sup>, Xiaolei Guan<sup>1</sup>, Shiliang Liu<sup>1</sup>

<sup>1</sup> School of Civil Engineering, Shandong University, Jinan 250061, China, maoodeqiang@sdu.edu.cn

<sup>2</sup> The Institute of Environmental Sciences, The Hebrew University of Jerusalem, Rehovot 76100, Israel

The long-term performance of the permeable reactive barriers in remediating contaminated groundwater may diminish as a result of oxidation, precipitation on the particle surfaces, and pore space clogging. Evaluating its performance through monitoring could address this dilemma. We characterize the spectral induced polarization (SIP) response of zero valent iron (ZVI)-activated carbon (AC)-sand mixtures during remediating contamination. The chargeability exhibits a perfect linear relation to the volumetric concentration of ZVI (2.5-50%) and AC (2.5%-75%) with  $r = 0.99$ . However, the low-frequency electrical conductivity shows low sensitivity to the volumetric content of ZVI and AC. The relaxation time increases with the particle sizes. When these two particles are mixed, chargeability is approximated as a superposition of their individual values. In terms of phase values and frequencies of the phase peaks, it also exhibits this superposition effect. Furthermore, we conducted 720-hour SIP measurements on ZVI-AC-sand columns flushed with NaCl or NaNO<sub>3</sub> solutions. It suggests that precipitation of 0.06 mm thick sedimentation onto the ZVI surface induced by changes in redox chemistry observed in micromorphology images, resulting an increase in the normalized chargeability by 44.05%, the scaled relaxation time and Cole-Cole model exponent by 1098.99% and 23.11%. Compared to flow-through by NaCl solution, changes in these parameters are more pronounced for columns saturated with NaNO<sub>3</sub> solution, indicating the corrosion of ZVI. Our findings illustrate that induced polarization parameters vary in response to the chemical alteration of ZVI-AC-sand mixed media, showing the potential for noninvasive long-term monitoring of the reactive barriers.

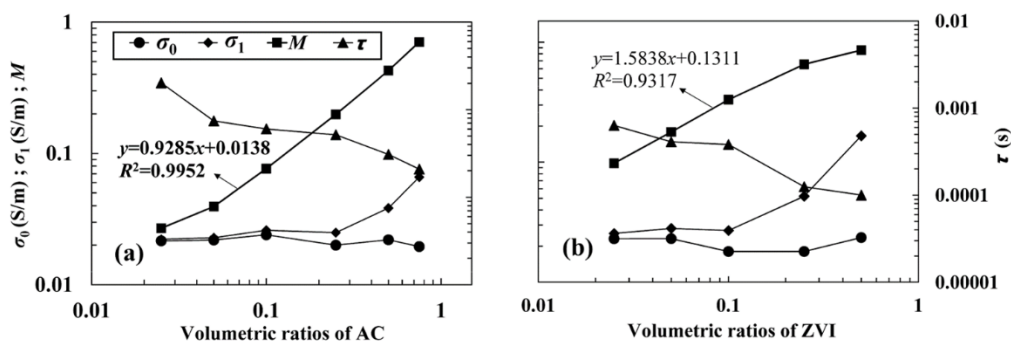


Figure 1: Cole-Cole model parameters for sand-ZVI/AC samples that vary from 0.25% to 50% ZVI volume concentration and 0.25% to 75% AC volume concentration.

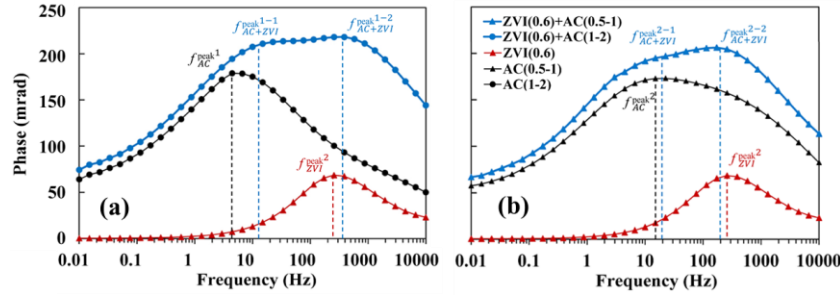


Figure 2: Phase spectra (0.01–10000 Hz) of samples under different particle size of ZVI and AC.

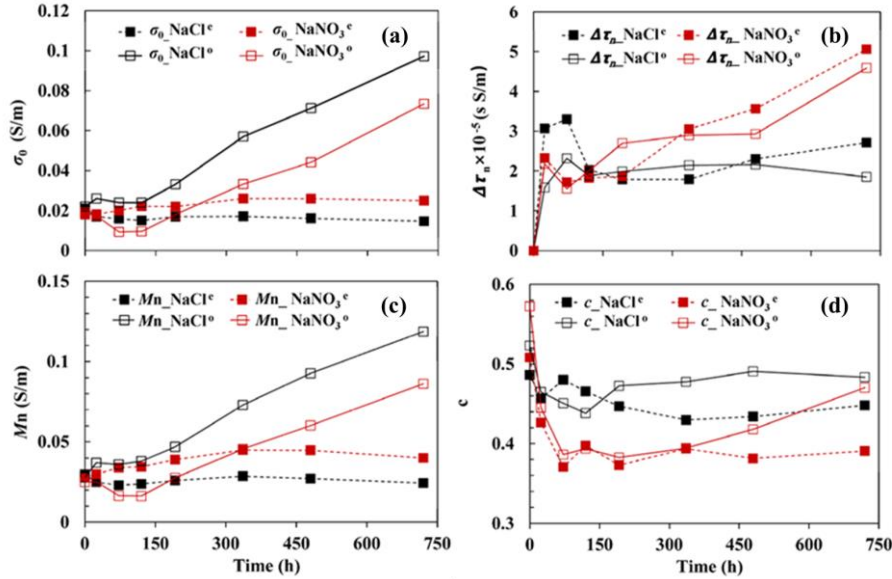


Figure 3: Cole-Cole model parameters of samples saturated with NaCl or NaNO<sub>3</sub> solution for 720-hour SIP measurements. The superscript 'o' represents saturated once, while the superscript 'e' represents resaturated each time.

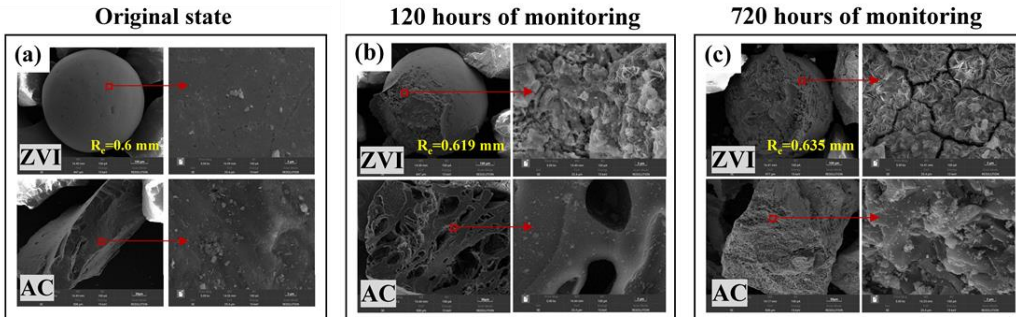


Figure 4: SEM images of the ZVI and AC on different monitoring time.

## References

- Bate, B., Ye, J., Cao, J., You, Y., Cao, J., Zhang, S., Zhan, L.T., Zhang, C., Hao, N., 2022. The mechanisms and monitoring of zeolite remediating chemical oxygen demand, NH<sub>4</sub><sup>+</sup>, and Pb<sup>2+</sup>. *J. Appl. Geophys.* 199, 104615.
- Hao, N., Ye, J., Zhao, L., Sun, M., You, Y., Zhang, C., Cao, J., Peng, Y., Zhang, S., Zhan, L.T., Chen, Y., Bate, B., 2021. Evaluating iron remediation with limestone using spectral induced polarization and microscopic techniques. *Sci. Total Environ.* 800, 149641.
- Slater, L.D., Choi, J., Wu, Y., 2005. Electrical properties of iron-sand columns: Implications for induced polarization investigation and performance monitoring of iron-wall barriers. *Geophysics*. 70 (4), G87-G94.
- Wu, Y., Slater, L., Versteeg, R., LaBrecque, D. 2008. A comparison of the low frequency electrical signatures of iron oxide versus calcite precipitation in granular zero valent iron columns. *J. Contam. Hydrol.* 95, 154-167.

# Quantitation of solid waste deposits through time domain induced polarization signatures

Jian Meng<sup>1</sup>, Ruijue Zhao<sup>1</sup>, Jing Li<sup>1</sup>, Yaxun Wang<sup>1</sup>, Shiliang Liu<sup>1</sup>, Deqiang Mao<sup>1,\*</sup>

<sup>1</sup>School of Civil Engineering, Shandong University, Jinan 250061, China, maodeqiang@sdu.edu.cn

Solid waste deposits are one of the leading environmental crises in soils and groundwater, and their negative impacts will continue for decades of years. In recent years, geophysical methods have been recognized as effective tools for providing imaging of environmental investigations. A time domain induced polarization (TDIP) survey was undertaken to map solid waste deposits and discriminate characteristic contaminants, supplemented by borehole logs and soil sample analysis. The whole dataset was inverted using a laterally constrained inversion scheme for reconstructing the electrical parameters of soils in terms of the integral chargeability constant phase angle model. The results reveal resistivity  $< 2 \Omega\cdot m$  or phase  $> 10$  mrad zones that show a good agreement with the extent of chromium-containing sludge or municipal solid waste. The thickness and location of waste types from surface measurements are further validated and quantified by borehole information. Four zones of solid waste deposits are discriminated with a total volume of 42,354.5 m<sup>3</sup>. IP responses also expose a linear relationship with concentrations of total chromium and total organic carbon. In conclusion, the non-invasive TDIP survey provides quantitative information for future land planning and remediation actions in the area.

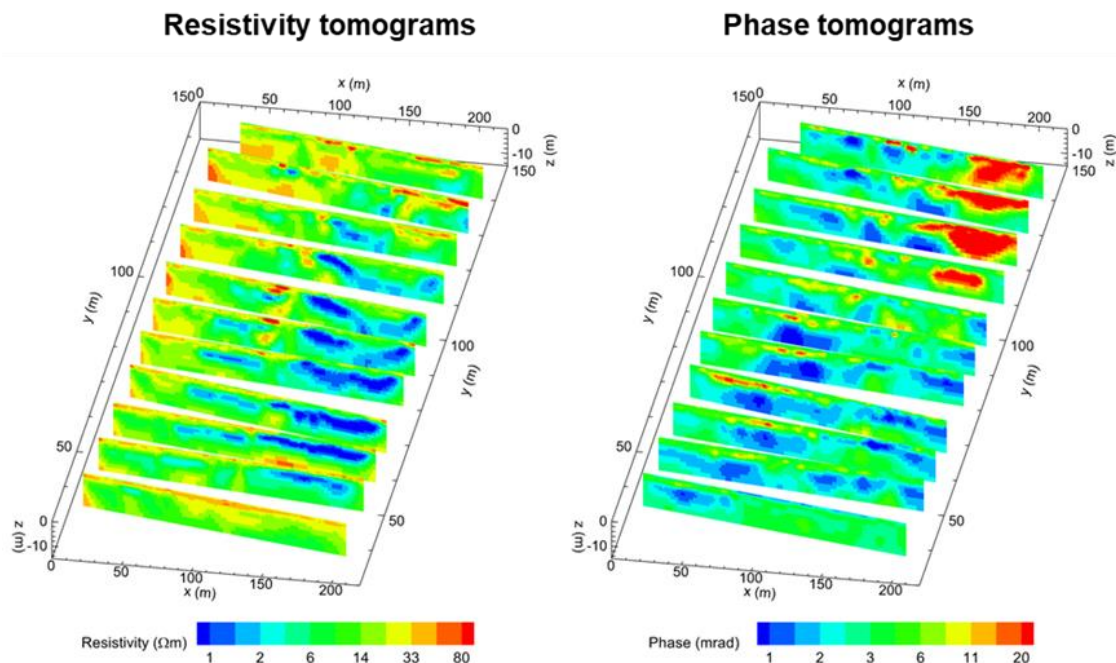


Figure 1: Three-dimensional view of resistivity and phase tomograms. The electrical features of low resistivity or high phase allow for depicting solid waste deposits.

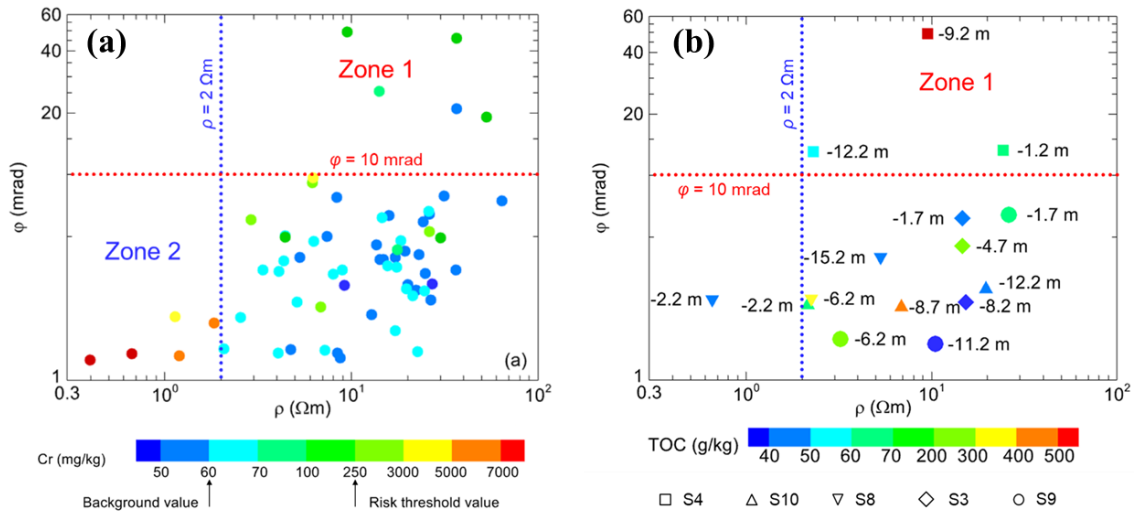


Figure 2: Correlation between electrical parameters and contaminant concentrations in soil samples. (a) Total chromium concentrations, (b) TOC concentrations. The colours of points are related to contaminant concentrations. Thresholds  $\rho = 2 \Omega\text{-m}$  and  $\varphi = 10$  mrad are marked with dotted lines for reference.

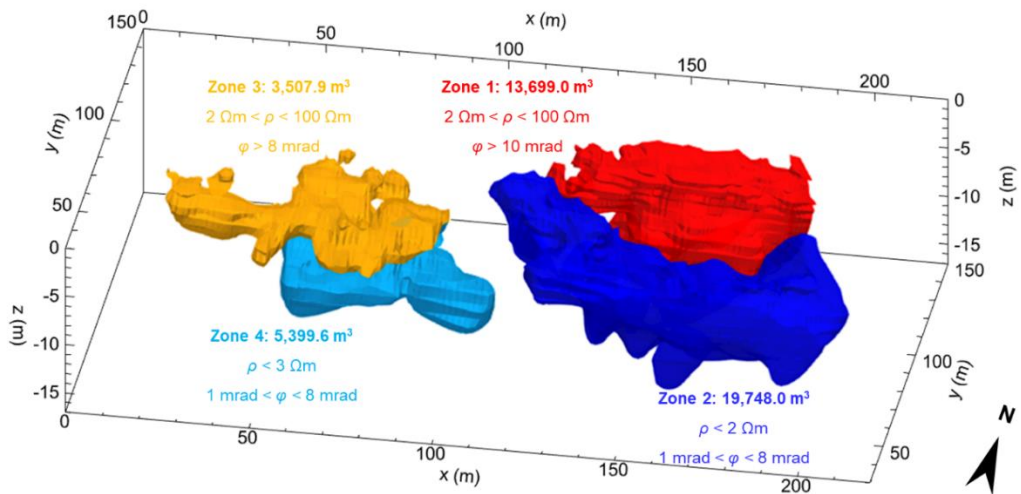


Figure 3: Four zones of solid waste deposits delineated with resistivity and phase values. The interpretation criteria for each zone are annotated, as well as the corresponding volumes. The total volume is 42,354.5  $\text{m}^3$ .

## References

- Balbarini, N., Rønde, V., Maurya, P., Klint, K.E., Christiansen, A.V., Fiandaca, G., Binning, P.J., Møller, I., Bjerg, P.L., 2018. Geophysics - Based Contaminant Mass Discharge Quantification Downgradient of a Landfill and a Former Pharmaceutical Factory. *Water Resour. Res.* 54, 5436–5456.
- Flores-Orozco, A., Gallistl, J., Steiner, M., Brandstätter, C., Fellner, J., 2020. Mapping biogeochemically active zones in landfills with induced polarization imaging: The Heferlbach landfill. *Waste Manage.* 107, 121–132.
- Olsson, P.-I., Fiandaca, G., Maurya, P.K., Dahlin, T., Auken, E., 2019. Effect of current pulse duration in recovering quantitative induced polarization models from time-domain full-response and integral chargeability data. *Geophys. J. Int.* 218, 1739–1747.
- Verma, S.K., Sharma, P.C., 2023. Current trends in solid tannery waste management. *Critical Reviews in Biotechnology.* 43 (5), 805–822.
- Wemegah, D.D., Fiandaca, G., Auken, E., Menyeh, A., Danuor, S.K., 2017. Spectral time-domain induced polarisation and magnetic surveying – an efficient tool for characterisation of solid waste deposits in developing countries. *Near Surf. Geophys.* 15, 75–84.

# Direct observation and petrophysical modeling of calcite dissolution with microfluidics and spectral induced polarization.

Flore Rembert<sup>1</sup>, Philippe Leroy<sup>2</sup>, Arnault Lassin<sup>2</sup>, Sophie Roman<sup>1</sup>

<sup>1</sup>Univ. Orléans, CNRS, BRGM, ISTO, OSUC, UMR 7327, F-45071 Orléans, France, flore.rembert@univ-orleans.fr

<sup>2</sup>BRGM, French geological survey, 45100 Orléans, France

We pioneer microscale geoelectrical acquisition with advanced microfabrication technologies to investigate hydrogeological processes using microfluidics that couple direct visualization of the pore scale dynamics with the geoelectrical response (Rembert et al., 2023). Geoelectrical monitoring gives information at various scales ( $\mu\text{m}$  to  $\text{m}$ ) about dynamic and reactive processes involving multiphase flow, solute transport, and mineral dissolution/precipitation, which rely on microscopic interactions. Yet, the field scale geophysical survey interpretation is challenging due to the superimposition of the couplings and the heterogeneity of the natural environment. We focus on developing electrical conductivity monitoring with the spectral induced polarization (SIP) method. The interpretation of the SIP signal is based on developing petrophysical models that relate the measured complex electrical conductivity to structural, hydrodynamical, and geochemical properties. State-of-the-art petrophysical models, however, suffer from a limited range of validity and presume many microscopic mechanisms to define macroscale parameters. Thus, direct observations of the underlying processes coupled with geoelectrical monitoring are keys for deconvoluting the signature of the bio-chemo-physical mechanisms at play and for using reliable models. Microfluidic experiments enable direct visualization of flows, reactions, and transport at the pore scale thanks to transparent micromodels coupled with high-resolution imaging techniques. Micromodels are pseudo-two-dimensional representations of the porous medium, ranging in complexity from single channels to replicas of natural rocks. Cutting-edge micromodels use reactive minerals to investigate the water-mineral interactions. Here, we investigate calcite dissolution, a key multiphase process of this ubiquitous mineral. Our micromodel is a channel containing a calcite grain in the middle. Thin gold electrodes are deposited on the bottom surface of the channel for SIP monitoring. We highlight the strong correlation between SIP response and dissolution through electrical signal examination and image analysis. In particular,  $\text{CO}_2$  bubbles generated by calcite dissolution play a critical role in the injected acid solution trajectory, the evolving calcite shape, and the observed decreasing real part of the complex conductivity. Then, we perform image processing to retrieve petrophysical parameters such as porosity and water saturation. These parameters are used as inputs to model the complex electrical conductivity with petrophysical modeling based on the concept of equivalent circuits representing bulk and surface conductivities. We show that the petrophysical model can be applied to pore-scale geoelectrical monitoring and is consistent with optical observations. We show that the time variations are linked to partially saturated conditions, pore water composition, and evolving

mineral surface state. These results demonstrate that the proposed technological advancement provides a breakthrough in understanding the subsurface processes through SIP monitoring.

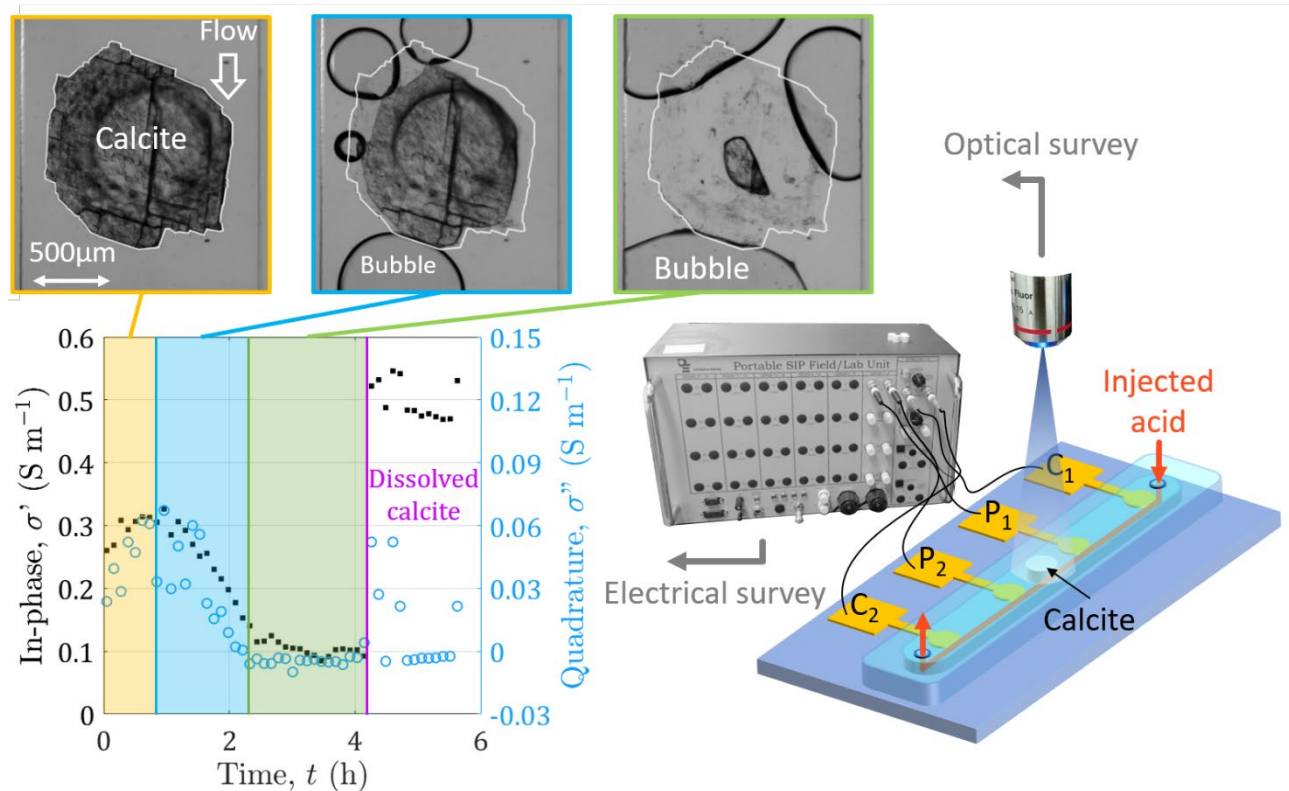


Figure 1: Optical survey with a SIP monitoring of calcite dissolution using microfluidics (frequency=2.5 Hz).

## References

- Rembert, F., Stoltz, A., Soulaine, C., Roman, S., 2023. A microfluidic chip for geoelectrical monitoring of critical zone processes. *Lab Chip* 23, 3433–3442. <https://doi.org/10.1039/D3LC00377A>

# Investigating soil organic matter complexation using SIP in microfluidic and column scale experiments

Judy Robinson<sup>1</sup>, Klaudio Peshtani<sup>1,2</sup>, Josh Torgeson<sup>1</sup>, Nikolla Qafoku<sup>1</sup>, Lee Slater<sup>1,2</sup>

<sup>1</sup>Pacific Northwest National Laboratory (PNNL), Richland, Washington (USA) [Judith.robinson@pnnl.gov](mailto:Judith.robinson@pnnl.gov)

<sup>2</sup>Rutgers University, Newark, New Jersey (USA)

---

The dynamics and interactions of soil organic matter (SOM) in subsurface environments are linked to the formation of organo-mineral complexes which affect or even control organic carbon (OC) stabilization in bioactive environments. Iron oxides (e.g., ferrihydrite) have been widely recognized to play an important role in preserving OC in soils. They have a high surface-area-to-volume ratio and exhibit high affinity for OC, resulting in the formation of stable Fe-OC compounds that can persist for millennia (Li et al., 2023). Typically, the distribution of Fe with OC is investigated with various laboratory spectroscopy and imaging techniques applied to discrete samples (cm to m scale) which can be labour intensive and costly. Having the ability to detect OC interactions with Fe oxides at the field-scale could help detect and/or quantify long-term SOM persistence. While there have been advancements to image SOM at the field scale using soil colour and machine learning algorithms (Gholizadeh et al., 2020) and self-potential measurements (Doro et al., 2022), spectral induced polarization (SIP) is another candidate technology to be explored because it is sensitive to electrostatic interactions and complexations between oppositely charged surfaces and ions. The goal of our research is to determine the pore network parameters that control the SIP response of the formation of organo-mineral complexes.

There have been limited studies investigating the sensitivity of SIP to OC interactions. Schwartz and Furman (2015) performed experiments where different percentages of peat (OC source) were mixed with a loamy sand soil (native or prewashed with NaCl) to have either  $\text{Ca}^{2+}$  or  $\text{Na}^+$  dominating the system. In both systems, it was found that as SOM content increased, the polarization (e.g., imaginary conductivity) and relaxation frequency using a Cole-Cole model fit decreased. The decrease in polarization was attributed to a decrease in ion-mobility due to cation bridging between the mineral surface and the OM. Contrary to this finding, other research has shown that as there are additional negatively charged, polarizable surface sites, the cation exchange capacity (CEC) increases and there is an increase in polarization (Revil, 2013; Slater & Lesmes, 2002; Waxman & Smits, 1968). In support of this finding within specific SOM studies, Mellage et al. (2022) and Strobel et al. (2023) found that an increase in SOM, measured by CEC and total organic carbon (TOC), respectively, manifested as an increase in the SIP polarization. These limited studies indicate there may be a more complicated relationship between the SIP response, the number of charged polarizable sites and ionic mobility.

In this work, the sensitivity of SIP to OC interactions with Fe oxides is being investigated in parallel microfluidic and column experiments to have a better mechanistic understanding of the SIP response to the formation of organo-mineral complexes. By varying pore scale properties within the pore network fabrication and using different diameter ceramic beads, this research aims to better understand how the SIP response is impacted by the formation of SOM complexes.

Using the Fe oxide, ferrihydrite, polydimethylsiloxane (PDMS) pore networks were spray coated for microfluidic experiments and ceramic beads were coated for column experiments. Ferrihydrite has a strong affinity (e.g., a large partitioning coefficient) for pentaglycine (PG) and was injected into the fluidic cell and columns, respectively. The PG was injected to create a simplified organic molecule that contains a fundamental amino acid component that contributes to SOM. As the PG was pulse-injected into the fluidic and column cells, SIP measurements were collected from 0.001 to 10,000 Hz. Chemical sampling of pH, fluid conductivity, TOC and Fe content were performed on fluid extracted during each injection. Experiments are on-going where we are varying the pore scale properties by using different sized ceramic beads and pore networks with varying parameters.

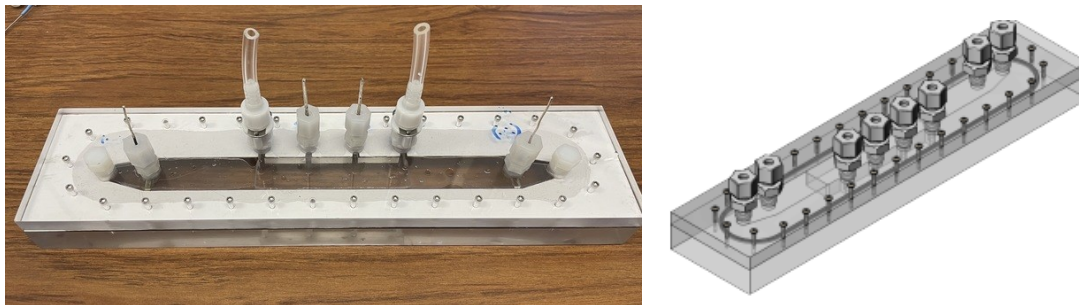


Figure 1. Fluidic cell (left) and schematic where SIP measurements are being collected.

**Send this pdf to: [induced.polarization@gmail.com](mailto:induced.polarization@gmail.com) and state the abstract title in the email header/subject.**

## References

- Pelton, W.H., Ward, S.H., Hallof, P.G., Sill, W.R. and Nelson, P.H., 1978. Mineral discrimination and removal of inductive coupling with multifrequency IP. *Geophysics*, 43, 588–609.
- Vinegar, H.J. and Waxman, M.H., 1984, Induced polarization of shaly sands. *Geophysics*, 49, 1267–1287.
- Doro, K. O., Stoikopoulos, N. P., Bank, C. G., & Ferris, F. G. (2022). Self-potential time series reveal emergent behavior in soil organic matter dynamics. *Sci Rep*, 12(1), 13531. <https://doi.org/10.1038/s41598-022-17914-5>
- Gholizadeh, A., Saberioon, M., Viscarra Rossel, R. A., Boruvka, L., & Klement, A. (2020). Spectroscopic measurements and imaging of soil colour for field scale estimation of soil organic carbon. *Geoderma*, 357. <https://doi.org/10.1016/j.geoderma.2019.113972>
- Li, Q., Hu, W., Li, L., & Li, Y. (2023). Interactions between organic matter and Fe oxides at soil micro-interfaces: Quantification, associations, and influencing factors. *Sci Total Environ*, 855, 158710. <https://doi.org/10.1016/j.scitotenv.2022.158710>
- Mellage, A., Zakai, G., Efrati, B., Pagel, H., & Schwartz, N. (2022). Paraquat sorption- and organic matter-induced modifications of soil spectral induced polarization (SIP) signals. *Geophysical Journal International*, 229(2), 1422-1433. <https://doi.org/10.1093/gji/ggab531>
- Revil, A. (2013). Effective conductivity and permittivity of unsaturated porous materials in the frequency range 1 mHz-1GHz. *Water Resources Research*, 49(1), 306-327. <https://doi.org/10.1029/2012WR012700>
- Schwartz, N., & Furman, A. (2015). On the spectral induced polarization signature of soil organic matter. *Geophysical Journal International*, 200(1), 589-595. <https://doi.org/10.1093/gji/ggu410>
- Slater, L., & Lesmes, D. (2002). Electrical-hydraulic relationships observed for unconsolidated sediments. *Water Resources Research*, 38(10), 33-46. <https://doi.org/10.1029/2001WR001075>

- Strobel, C., Doerrich, M., Stieff, E. H., Huisman, J. A., Cirpka, O. A., & Mellage, A. (2023). Organic Matter Matters—The Imaginary Conductivity of Sediments Rich in Solid Organic Carbon. *Geophysical Research Letters*, 50(23). <https://doi.org/10.1029/2023gl104630>
- Waxman, M. H., & Smits, L. J. M. (1968). Electrical Conductivities in Oil-Bearing Shaly Sands. In (Vol. 8).

# **ERT and TDIP survey for mapping of leachate plumes: application to a MSW landfill in central Italy**

D. Melegari<sup>1</sup>, G. De Donno<sup>1</sup>

<sup>1</sup> DICEA - "Sapienza" University of Rome, Italy

## **Introduction**

Landfill leachate is a highly polluted liquid with a high amount of toxic elements that can contaminate aquifers. Additionally, its uncontrolled accumulation in municipal solid waste (MSW) landfills located on slopes can represent an important risk since it can trigger instability phenomena. Therefore, mapping and monitoring the waste mass down to significant depths is required for the appropriate management of these landfill sites. Electrical resistivity tomography (ERT) and time-domain induced polarization (TDIP) are perfectly suited for this purpose given the electrical properties of leachate (highly conductive and chargeable) compared to the unsaturated waste mass and the surrounding materials, such as liners and covering soil (Leroux et al., 2010).

In the present study, we present an application in a real-case scenario of ERT/TDIP data for imaging leachate levels in a MSW landfill located in Central Italy.

## **Study area, data acquisition and processing**

The landfill is located on a steep slope in Central Italy, where the accumulation of leachate can lead to instability phenomena (Fig. 1a) and therefore the mapping of leachate plumes is pivotal for landfill management. To this end, ERT and TDIP data acquisition was performed on two chosen terraced steps with two profiles (L3 and L4 in Fig. 1a). Multiple-gradient (MG) arrays were used to acquire experimental datasets using the Syscal Pro resistivity-meter (IRIS Instruments) and stainless-steel electrodes spaced 5 m apart (line length = 250 m). We employed four stacks, a 50% duty cycle, a current injection time of 4 s and 20 gates to sample the TDIP decay curve logarithmically. Additionally, we logged leachate levels on three separate wells (SDI-04, SDI-05, and SDI-06) along L4.

We used the blocky inversion in the VEMI software (De Donno et al., 2017) to invert ERT/TDIP data for resistivity and integral chargeability. This software uses a Gauss-Newton inversion algorithm and the finite element method to solve the forward problem, while for chargeability forward modelling we use the non-linear approach (Method III after Oldenburg et al., 1994).

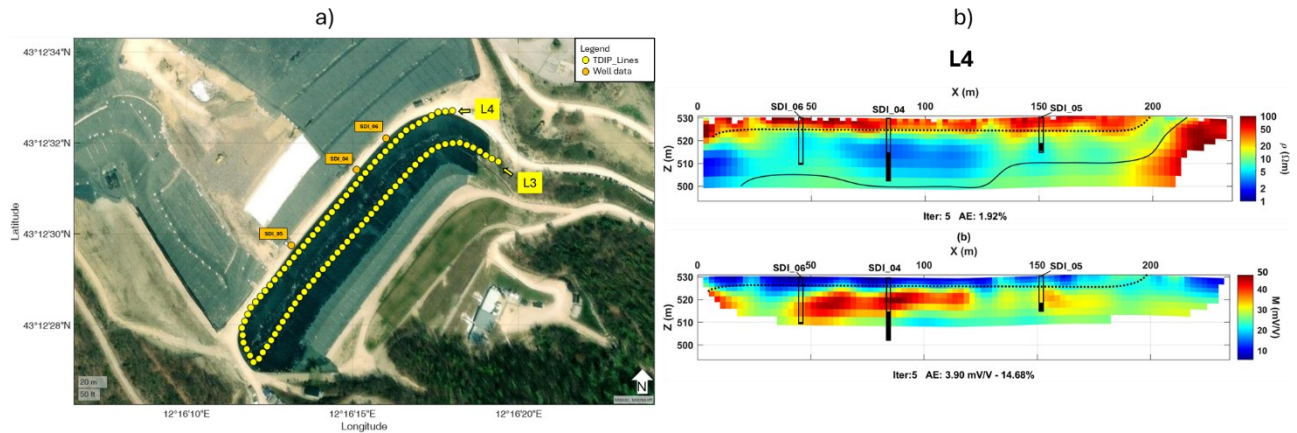


**Figure 1:** a) Aerial image of the municipal solid waste landfill in central Italy, with the location of the two investigated TDIP lines (L3-L4) and of the three piezometers (SDI-04,05,06); b) TDIP data inversion on the L4 line: resistivity model on the top and chargeability model on the bottom. The leachate levels logged in piezometers (SDI-04, SDI-05 and SDI-06) are marked with a black area, the supposed bottom of the landfill is represented by a black line and the separation between the first two layers is represented with a black dashed line.

## Results

The results for the profile L4 are shown in Figure 1b, in terms of resistivity and integral chargeability. For both models, we computed the model resolution matrix (Menke, 2012) and only pixels having values higher than 0.001 for the resistivity model and 0.05 for the chargeability model were selected. The models show three main layers in agreement with the expected stratigraphy of a landfill: i) a shallow layer (thickness around 5 m) showing relatively high resistivity ( $\rho > 20 \Omega\text{m}$ ) and very low chargeability ( $M < 10 \text{ mV/V}$ ), related to the presence of the covering soil; ii) a second layer (between 5 and 20-25 m) with low resistivity ( $\rho < 10 \Omega\text{m}$ ) and high chargeability ( $M > 20 \text{ mV/V}$ ), which reflects the presence of waste and leachate. This layer seems quite heterogeneous, with resistivity and chargeability changes both laterally and in depth due to a different saturation level within the waste mass; iii) a third layer, only visible on the resistivity model, where the resistivity slightly increases as an effect of the bottom liner acting as an insulator. The increase in resistivity is lower than expected due to the low resolution retrieved at the bottom of the model, while the resolution of the chargeability model is not enough to enlighten the whole cross-section down to the bottom liner.

When compared with well data, the resistivity model shows a good correlation between leachate levels (particularly in SDI\_04 well) and the most conductive zones ( $\rho < 5 \Omega\text{m}$ ). Conversely, the highest chargeability values are mostly located above the saturated zone (depths between 7 and 15 m), while lower values ( $M < 30 \text{ mV/V}$ ) are detected in the leachate accumulation areas. These findings suggest that resistivity is more effective for mapping leachate plumes compared to integral chargeability, which instead can be used to define more accurately the boundaries of the waste body.

## Conclusion

In this work, we presented a TDIP approach to upgrade leachate identification in municipal solid waste landfills. This approach can be effective for mapping leachate accumulation zones, as confirmed by the good match between the geophysical models and the leachate levels logged in wells. Future work will be focused on performing a full decay inversion of the acquired data to reduce the residual ambiguities and the depth resolution issue arising from integral chargeability.

## References

- Leroux, V., Dahlin, T., & Rosqvist, H. (2010, September). Time-domain IP and resistivity sections measured at four landfills with different contents. In Near Surface 2010-16th EAGE European Meeting of Environmental and Engineering Geophysics (pp. cp-164). European Association of Geoscientists & Engineers.
- De Donno, G., & Cardarelli, E. (2017). VEMI: a flexible interface for 3D tomographic inversion of time- and frequency-domain electrical data in EIDORS. *Near Surface Geophysics*, 15(1), 43-58.
- Menke, W. (2012). Discrete Inverse Theory. *Geophysical Data Analysis*. Academic Press.
- Oldenburg, D. W., & Li, Y. (1994). Inversion of induced polarization data. *Geophysics*, 59(9), 1327-1341.

# Organic Pollutant Oxidation on Manganese Oxides in Soils - The Role of Calcite Indicated by Geoelectrical and Chemical Analysis

Sonya S Altzitser<sup>1</sup>, Yael G Mishael<sup>1</sup>, Nimrod Schwartz<sup>1</sup>

<sup>1</sup> Department of Soil and Water Sci. The Robert H. Smith Faculty of Agriculture, Food, and Environment, The Hebrew University of Jerusalem, Israel ([Nimrod.schwartz@mail.huji.ac.il](mailto:Nimrod.schwartz@mail.huji.ac.il))

Phenolic pollutants pose significant environmental challenges, necessitating complex remediation and monitoring in heterogeneous subsurface environments. Adsorption-desorption and oxidation processes of phenolic pollutants have been well studied in controlled, buffered batch experiments. However, these conditions may not accurately represent the behavior in heterogeneous soil environments. Additionally, while SIP has been used to study adsorption-desorption on soil colloids, there is still a significant gap in understanding electrochemical reactions involving electron transfer processes during pollutant redox in the soil. Therefore, the objective of this work was to address the complex interactions between MnO<sub>2</sub> rich sandy soil, and phenolic pollutants, by developing and integrating a multidisciplinary approach that includes electric, microscopic, and chemical techniques. We studied hydroquinone, and benzoquinone behavior in sandy soil, and MnO<sub>2</sub> rich sandy soil by SIP signatures and chemical analysis in soil columns. Column experiments revealed distinct breakthrough curves for hydroquinone and benzoquinone in sandy soil and MnO<sub>2</sub> rich sandy soil columns. Hydroquinone flow through the MnO<sub>2</sub> rich sandy soil columns induced a constant decrease in  $\sigma''$ , as expected, due to oxidation processes in the system, resulting in a reduction in oxidizing and polarizing surfaces. On the other hand,  $\sigma'$  increased up to ~4 PVs and then decreased, which has correlated with pH, EC and Ca<sup>2+</sup> concentration measurements. Indeed,  $\sigma'$  is related to the bulk solution properties, i.e., an increase in ion concentration, mainly Ca<sup>2+</sup>, will result in an increase in  $\sigma'$ . Since these trends are not obtain in the control sandy soil columns (with hydroquinone flow), we suggest that hydroquinone oxidation by MnO<sub>2</sub> surfaces initiated a cascade of reactions, resulted in calcite dissolution and Mn<sup>2+</sup> precipitation. Further characterization of the soil using X-ray diffraction and SEM-EDS analysis supported the presence of and the reduction in MnO<sub>2</sub> and CaCO<sub>3</sub> content post-oxidation. Our findings highlight the sensitivity of SIP signatures to changes in soil properties and the potential of the multidisciplinary approach to understand the behavior of phenolic pollutants in natural soil systems.

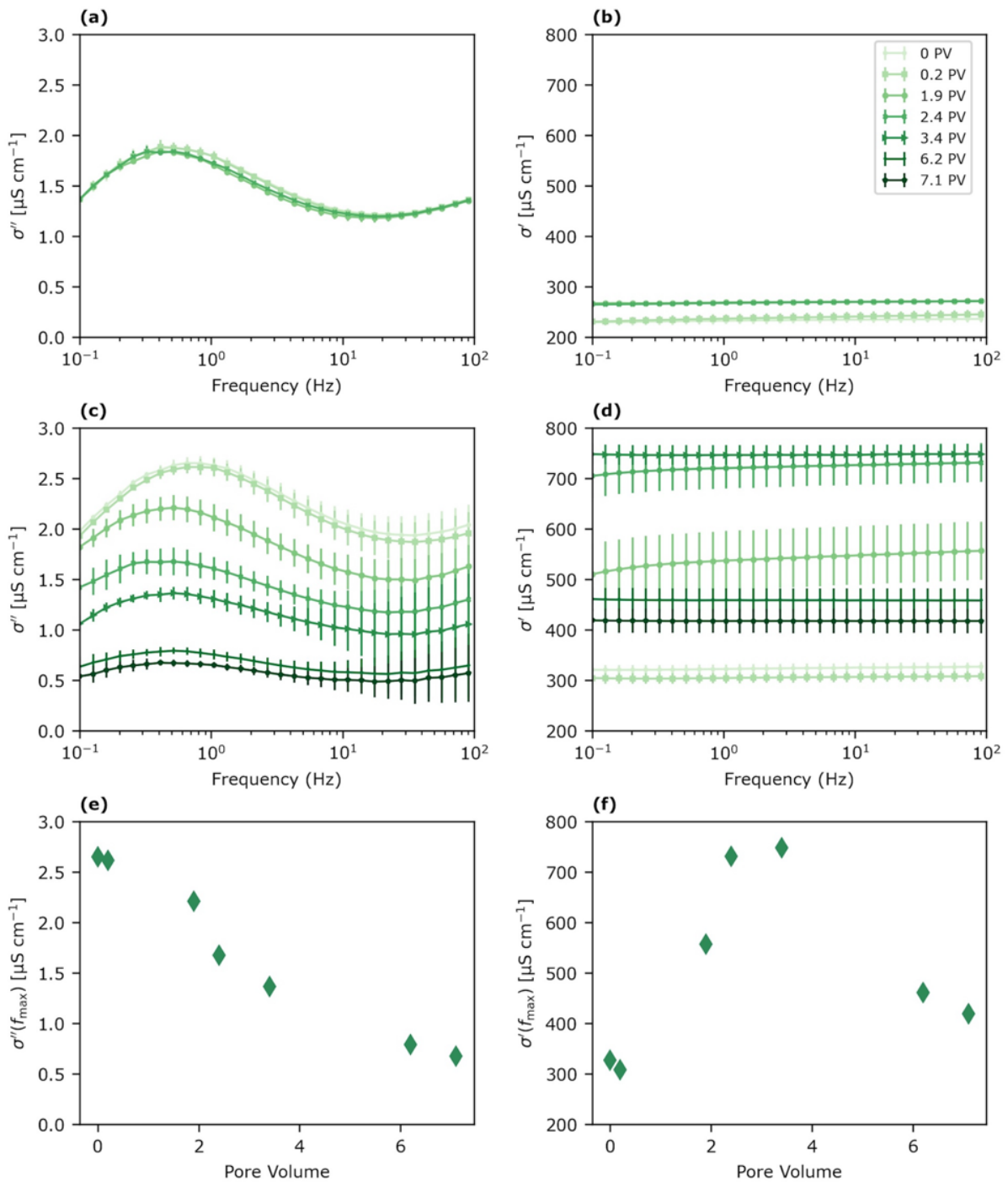


Figure 1. Quadrature ( $\sigma''$ ) and in-phase ( $\sigma'$ ) conductivity of sandy (a,b) and Mn-sandy soils (c,d) during hydroquinone oxidation.  $\sigma''$  (e) and  $\sigma'$  (f) at the peak frequency of Mn-sandy soil

# **Impact of Natural and Synthetic Polymers on Soil Stability: Insights from SIP and Chemical Analysis**

Sonya S Altzitser<sup>1</sup>, Yael G Mishael<sup>1</sup>, Nimrod Schwartz<sup>1</sup>

<sup>1</sup> Department of Soil and Water Sci. The Robert H. Smith Faculty of Agriculture, Food, and Environment, The Hebrew University of Jerusalem, Israel ([Nimrod.schwartz@mail.huji.ac.il](mailto:Nimrod.schwartz@mail.huji.ac.il))

Mucilage, a complex mixture of polysaccharides secreted by plant roots, significantly contributes to the natural soil environment by enhancing microbial activity, water retention, and nutrient exchange. Despite its critical role, the comprehensive impact of mucilage on soil stability has yet to be fully explored. In contrast, Polyacrylamide (PAM), a synthetic polymer widely used in agriculture for soil stabilization, has been shown to effectively reduce soil erosion and improve water infiltration. We propose that mucilage, similar to PAM, could significantly contribute to soil stabilization. This study aims to quantitatively assess the unique impacts of mucilage and PAM on soil stability, employing SIP measurements coupled with chemical analysis. SIP signals, sensitive to factors such as the electrical double layer or particle size, offer insights into particle aggregation and, consequently, soil aggregation. This comparative analysis seeks to illuminate the potential of mucilage as a natural alternative for soil stabilization. To assess the comparative effects of mucilage and PAM on soil stabilization, we prepared loess soil samples with varying concentrations of both substances (0.035% w/w and 0.175% w/w), alongside untreated control samples. Soil stability of the different treatments was assessed using Aggregate Durability Index (ADI) as formerly developed in our lab. SIP measurements were conducted on soil columns after ensuring saturated conditions and uniform density, using a PSIP impedance spectrometer. Chemical data was measured from soil solution via pH, EC, and ICP-AES on day 0 and day 20. Additionally, CO<sub>2</sub> emission, an indicator for microbial activity was measured by titration technique. Both control and mucilage treatments exhibited similar trends in  $\sigma'$  over time, starting with similar initial values. Notably, the treatment with high mucilage concentration demonstrated a significant increase in  $\sigma'$  by 23%, starting from day 3. This difference persisted, marking a distinct and sustained elevation above the increases observed in both the low mucilage concentration and control treatments through day 20. Solution chemistry analysis supported these observations, showing that while all treatments began with similar Ca<sup>2+</sup> levels and total cation sums on day 0, the high mucilage treatment experienced a substantial Ca<sup>2+</sup> concentration increase of 64%, compared to 32% and 28% increases for the low mucilage and control treatments, respectively. PAM treatments, irrespective of concentration, maintained stable  $\sigma'$  signatures for 10 days,

subsequently exhibiting a gradual increase up to day 20, culminating in a 46% enhancement. Based on our previous study, in calcareous soils an increase in  $\sigma'$  is primarily due to calcite dissolution. To explain these observations, we suggest that addition of organic carbon, derived from mucilage to the system results in augmenting microbial activity. CO<sub>2</sub> emission experiments, with low mucilage concentrations, showed that the microbial activity peaks after 3 days, result that coinciding with the onset of  $\sigma'$  increase. Enhanced microbial activity elevates CO<sub>2</sub> levels, potentially causing local acidification and, consequently, increase calcite dissolution. While PAM also contributes organic carbon to the soil, its impact on  $\sigma'$  was minimal, likely due to its effectiveness in soil stabilization and aggregation, which may inhibit calcite dissolution by trapping calcite surfaces within large aggregates. Mucilage, irrespective of concentration, initially increased  $\sigma''$  by ~10% compared to the control treatment, likely due to its negative net charge at pH=8. However,  $\sigma''$  began to decline in mucilage treatments after three days, mirroring control trends and CO<sub>2</sub> emission outcomes, whereas PAM  $\sigma''$  remained stable throughout the 20-day experiment. We speculate this  $\sigma''$  behavior is closely governed by calcite surface polarization, suggesting that enhanced calcite dissolution diminishes polarizing surfaces, resulting in a  $\sigma''$  decrease. Our findings highlight the sensitivity of SIP signatures to dynamic processes occurring in the soil and suggests the potential of mucilage as a sustainable alternative to synthetic polymers.

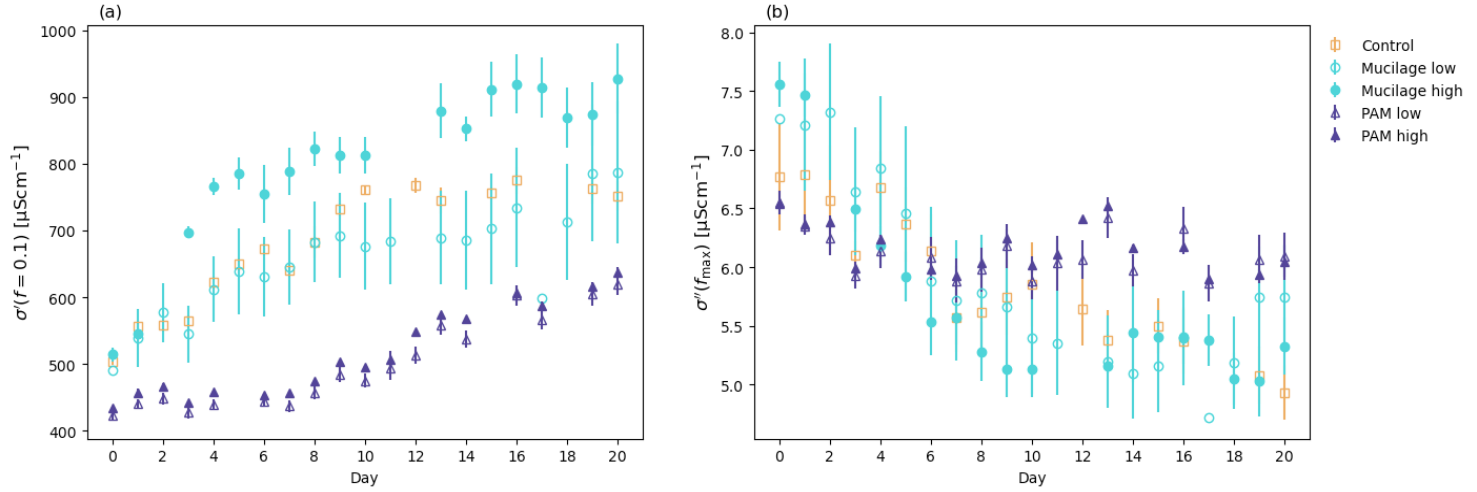


Figure 1. In-phase ( $\sigma'$ ) (a) and quadrature ( $\sigma''$ ) (b) conductivity at specific frequency, of loess soil treated with low (0.035% w/w) and high (0.175% w/w) concentrations of mucilage and PAM.

# Monitoring metal mobility in mine tailings during electrokinetic forcing using spectral induced polarisation

Marco Vasconez-Maza<sup>1</sup>, Russell Swift<sup>1,2</sup>, Reven Gibaga<sup>1</sup>, Yujie Yan<sup>3</sup>, Rich Crane<sup>3</sup>, Oliver Kuras<sup>1</sup>, Carlo Arcilla<sup>4</sup>, Gawen Jenkin<sup>5</sup>, Jonathan Chambers<sup>1</sup>

<sup>1</sup>*British Geological Survey, Nottingham, United Kingdom, [mvm@bgs.ac.uk](mailto:mvm@bgs.ac.uk)*

<sup>2</sup>*University of Liege, Belgium*

<sup>3</sup>*University of Exeter, Camborne School of Mines, United Kingdom*

<sup>4</sup>*Philippine Nuclear Research Institute, Philippines*

<sup>5</sup>*University of Leicester, United Kingdom*

**Abstract** Spectral induced polarisation (SIP) measurements were performed on copper mine tailings samples ( $20\text{ cm} \times 10\text{ cm} \times 10\text{ cm}$ ), which were saturated with 0.1M citric acid and subjected to an electrokinetic (EK) injection simulating a remediation process, using voltage gradient of 0.6 V/cm for 9 days. The real component of the complex conductivity measured  $85 \times 10^{-3}\text{ Sm}^{-1}$ . After the electrokinetic process was complete, it had fallen below  $70 \times 10^{-3}\text{ Sm}^{-1}$ . This observed reduction in the real part of the conductivity suggests metal mobility within the tailings, highlighting the potential of SIP as a sensitive tool for monitoring the mobilisation of metals during the EK process in mine tailings.

## Introduction

Approaching the management of old mine waste with innovation, this project reframes the narrative by considering it as a potential resource rather than a liability. By exploring the untapped value within these materials, particularly those containing copper residues, we aim to harness their inherent potential for economic and environmental benefit. This study centres on leveraging SIP as a monitoring tool to facilitate the transformation of discarded mine waste into a valuable resource. EK is a promising method for metal recovery. This method facilitates the removal of metals by applying an electric field between a pair of electrodes (anode and cathode), thus promoting the transport of metals towards the electrodes (Cercato, M. and De Donno, G., 2020). SIP is a geoelectrical method that allows for non-invasive measurement and monitoring of the frequency-dependent complex conductivity of porous medium, ranging from millihertz to kilohertz. It provides information about the ability of the material to conduct electrical current (real component) and its propensity to becoming polarised (imaginary component) (Mendieta et al., 2021).

## SIP response of mine tailings subjected to an electrokinetic process

The experiment was conducted in an acrylic sample holder measuring  $35\text{ cm} \times 12\text{ cm} \times 12\text{ cm}$ . Within this holder, the sample measured  $20\text{ cm} \times 10\text{ cm} \times 10\text{ cm}$  and was equipped with graphite electrodes for both current injection (plates) and potential measurement (rods). At each end of the cell, two graphite plates served a double purpose as both the anode/cathode for electrokinetics and the SIP current injection electrodes. The sample was subjected to an EK process, maintaining a voltage

gradient of 0.6 V/cm, which was paused for approximately 20 min to conduct each SIP measurement. SIP results reveal a real component of the complex conductivity of approximately  $85 \times 10^{-3}$  Sm<sup>-1</sup>, measured immediately after the saturation of the sample with 0.1M citric acid (Day 1). Subsequent observations revealed a gradual increase, achieving a peak of  $95 \times 10^{-3}$  Sm<sup>-1</sup>, followed by a slight decrease to around  $90 \times 10^{-3}$  Sm<sup>-1</sup>. Towards the end of the experiment, the conductivity dropped further, reaching levels slightly below the initial value of  $85 \times 10^{-3}$  Sm<sup>-1</sup>, and eventually falling below  $70 \times 10^{-3}$  Sm<sup>-1</sup> at the end of the experiment. While geochemical samples are yet to be processed, the fluctuation in conductivity may be attributed to metal mobility, suggesting alterations in the conductive properties of the sample have changed over the course of the experimentation due to metal leaching and migration to the cathode. Additionally, phase peaks were observed in the different measurements from the beginning of the experiment (Day 1) until the end of it (Day 9), when the curve becomes relatively flat, suggesting that polarisation phenomena stopped, see Figure 1.

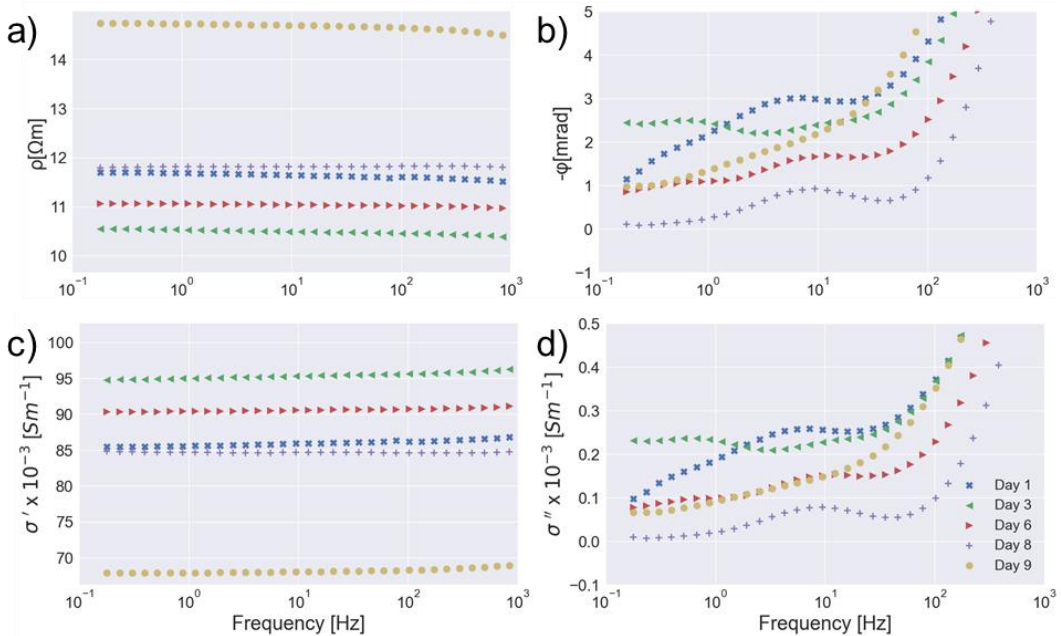


Figure 1: SIP results for a mine tailings sample. Markers represent measurements taken on different days. a) amplitude, b) phase, c) real component, and d) imaginary components of the complex conductivity.

## Conclusions

Our findings demonstrate the capability of SIP to effectively monitor changes in metal mobility within copper mine tailings. The observed decline in the real part of the conductivity following EK treatment is in line with expectations that the EK technique promotes metal mobility. Together, these results highlight the potential of integrating EK and SIP as complementary methodologies for undertaking and simultaneously monitoring metal recovery. This approach might offer more sustainable and efficient means to facilitate the transformation of discarded mine waste into a valuable asset, thus contributing to environmental restoration and sustainable development.

## References

- Cercato, M. and De Donno, G., 2020. Time-lapse monitoring of an electrokinetic soil remediation process through frequency-domain electrical measurements, *Journal of Applied Geophysics*, 175, 103980.
- Mendieta, A., Jougnot, D., Leroy, P., Maineult, A., 2021. Spectral induced polarization characterization of non-consolidated clays for varying salinities-an experimental study. *Journal of Geophysical Research: Solid Earth*, 126, 4.

# Experimental and numerical characterization of toluene transport and bioremediation processes using spectral induced polarization

Urie Luli Zohoré<sup>1,2</sup>, Isis Froment<sup>2</sup>, Aya Nianzou<sup>2</sup>, Pauline Kessouri<sup>2</sup>, Jacques Deparis<sup>2</sup>, Marc Crampon<sup>2</sup>, Roger Guérin<sup>1</sup>, Damien Jougnot<sup>1</sup>

<sup>1</sup> Sorbonne Université, CNRS, EPHE, UMR 7619 METIS, 75005 Paris, France, zohore.urie@gmail.com

<sup>2</sup> BRGM, Service Géologique National, 45060 Orléans, France, zohore.urie@gmail.com

Polluted soils are often the result of more or less recent anthropogenic activities, and constitute major societal issues. A recent study (Froger et al., 2021) estimates that 30% of the surface area of France has polycyclic aromatic hydrocarbon (PAH) concentrations in soils above  $100 \mu\text{g}.\text{kg}^{-1}$ . Once in the underground surface, these pollutants pose a risk to groundwater and drinking water supplies. Biodegradation in many regards can be an environmental-friendly remediation technique. This technique involves the decomposition of organic pollutants by micro-organisms. Many studies have highlighted the sensitivity of spectral induced polarization (SIP) to bacterial growth, biodegradation and bacterial activities such as mineral and biofilm production (e.g. Davis et al., 2006; Atekwana and Slater, 2009; Abdel Aal et al., 2010; Kessouri et al., 2019). All these studies focused on describing the influence of biodegradation on SIP without providing a method for quantification. To date, very little work has been done to quantitatively study the SIP response of bacteria in porous media. This work, part of the ANR project IMAGE, aims to develop: (i) petrophysical relationships at a column scale, linking complex conductivity to toluene biodegradation processes and (ii) a process-based inversion scheme coupled with a stochastic approach.

The experimental part uses two columns: one inoculated with *Rhodococcus wratislaviensis* which biodegrades toluene, and an abiotic control column. In fact, the columns form part of a more complete setup (see Figure 1).

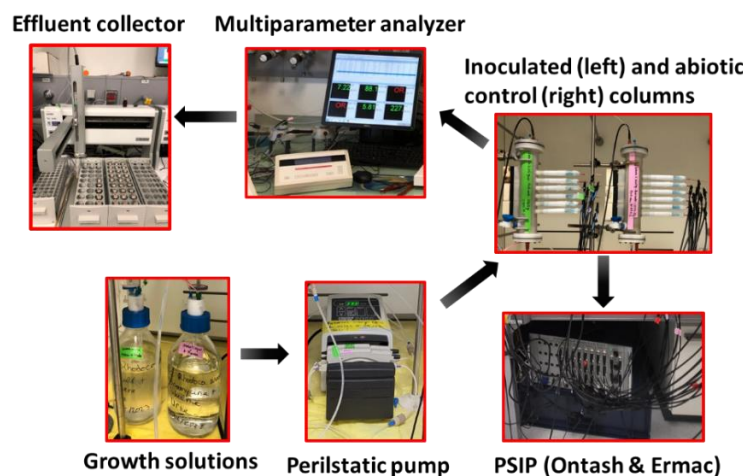


Figure 1: Experimental set-up of the open-loop circulation system.

This includes feeding bottles containing the growth media and toluene, a pressurised oxygen supply at 0.5 bar for oxygenation of the solutions, a multiparameter analyser (pH, Eh, dissolved oxygen and electrical conductivity of the fluid), and a peristaltic pump that allows the fluid to circulate at a constant flow rate through the system. Two configurations of fluid circulation were set up in this system. The first one is a closed-loop circulation: the fluid leaving the column flows back into the feed. The purpose of closed-loop circulation is to allow bacterial colonisation of the solid matrix (sand) in the column. The second configuration is an open-loop circulation: the fluid leaving the column (outflow fluid) does not return to the feed and is renewed regularly. This configuration comes close to natural conditions of biodegradation in groundwater. Moreover, in this configuration toluene concentration is monitored in the outflow fluid. Finally, at the end of the experiment, sand samples are collected at different heights in the column for DNA analysis.

It is worth mentioning that this experimental phase is in progress after a first attempt with technical difficulties. The first trial showed a DNA distribution higher at the bottom (194.4 ng/g) compared to the top (11.9 ng/g) of the inoculated column. This distribution is consistent with the expected distribution of toluene in the column. Indeed, bacteria tend to grow close to the point of entry of toluene in the column. The results also show a DNA concentration of 56.6 ng/g at the bottom of the abiotic column, thus revealing a contamination in the abiotic column. In the second trial, we have solved the issues previously encountered.

The second aspect of this work is devoted to forward modelling and inversion. The approach that we develop in this study aims to satisfy two criteria (i) to include in its expression the biogeochemical processes involved in biodegradation and (ii) to provide a more complete exploration of the solution space. In an effort to satisfy these two criteria, we are implementing a stochastic inversion approach. This approach is based on a Markov chain Monte Carlo algorithm. This method will allow the determination a quantitative relationship between complex resistivity and biodegradation parameters such as pollutant quantity, porosity and bacterial concentration.

## References

- Abdel Aal G.Z., Atekwana E.A., Rossbach S., Werkema D.D., 2010 – Sensitivity of geoelectrical measurements to the presence of bacteria in porous media. *Geophysical Research Letters*. 115(G3).
- Atekwana E.A., Slater L.D., 2009 – Biogeophysics: A new frontier in Earth science research. *Reviews of Geophysics*, 47, RG4004.
- Davis C.A., Atekwana E., Atekwana, E., Slater, L.D., Rossbach S., Mormile M.R., 2006 – Microbial growth and biofilm formation in geologic media is detected with complex conductivity measurements: microbial growth and geophysics. *Geophysical Research Letters*, 33, L18403.
- Froger C., Saby N., Jolivet C.C., Boulonne L., Caria G., Freulon X., de Fouquet C., Roussel H., Marot F., Bispo A., 2021 – Spatial variations, origins, and risk assessments of polycyclic aromatic hydrocarbons in French soils. *Soil*, 7, 161–178.
- Kessouri, P., Furman, A., Huisman, J. A., Martin, T., Mellage, A., Ntarlagiannis, D., ... & Placencia-Gomez, E. (2019). Induced polarization applied to biogeophysics: recent advances and future prospects. *Near Surface Geophysics*, 17(6-Recent Developments in Induced Polarization), 595-621.

# A new experimental setup for combination of SIP measurements with X-ray $\mu$ CT scanning: an application to the Gunnuhver geothermal system in Iceland

Hamdi Omar<sup>1,2,3</sup>, Tom Bultreys<sup>2</sup>, David Caterina<sup>3</sup>, Frédéric Nguyen<sup>3</sup>, Flore Rembert<sup>4</sup>, Sojwal Manoorkar<sup>2</sup>, Lore

Vanhooren<sup>1,5</sup>, and Thomas Hermans<sup>1</sup>

<sup>1</sup> Laboratory of applied Geology and Hydrogeology, Ghent University, Ghent, Belgium, [hamdi.omar@ugent.be](mailto:hamdi.omar@ugent.be)

<sup>2</sup> PProGRess/UGCT, Department of Geology, Ghent University, Ghent, Belgium

<sup>3</sup> Department Urban and Environmental Engineering, Liège University, Building B52, 4000 Sart Tilman, Belgium

<sup>4</sup> University of Orléans, CNRS, BRGM, ISTO, UMR 7327, Orléans, F-45071, France

<sup>5</sup> G-Time laboratory, Université libre de Bruxelles, Belgium

## **Abstract:**

Many volcanoes contain hydrothermal systems, which significantly contribute to the occurrence of volcanic eruptions. Unlike eruptions that emit magma, these events forcefully expel existing rock, volcanic gases (CO<sub>2</sub>, H<sub>2</sub>S, etc..), and steam, presenting a considerable danger to human safety. Recent devastating events highlight the challenges in predicting sudden hydrothermal explosions, revealing the limitations of current predictive capabilities. The main challenge is the lack of clear warning signs, which complicates the prediction of such eruptions. These phenomena can be initiated by the addition of mass and energy from magma, or by the formation of mineral seals over vents without direct magma involvement. It is crucial to enhance our understanding and prediction of these hydrothermal events to reduce their potential impacts on humans and the environment.

In the ERUPT research project, we investigate the geoelectrical behavior of volcanic hydrothermal systems (VHS) on a laboratory scale. Our research combines electrical properties, specifically Spectral Induced Polarization (SIP) measurements, with X-ray pore-scale (4D  $\mu$ CT) imaging to decipher the complex electrical signatures of volcanic systems through rock samples from the area of study. Spectral Induced Polarization (SIP) is a geophysical technique that assesses the complex electrical impedance of materials across a broad frequency range, offering valuable insights into the electrical characteristics of porous media. This method has been effectively applied to study rock samples from Volcanic Hydrothermal Systems (VHS). SIP responses are influenced by factors such as surface area, pore size distribution, and fluid content, as well as the movement of fluids within the rocks. Conversely, X-ray micro-CT is a technique that generates detailed, three-dimensional representations of a sample's internal structure, allowing for the examination of internal morphology, porosity, and other structural details at the micrometer scale, as well as the analysis of fluid pathways and dynamics.

By integrating these two techniques, we aim to achieve a deeper understanding of the geoelectrical properties and internal composition of rock samples. This is accomplished by examining SIP responses across various frequencies and linking them with  $\mu$ CT images to understand how changes

in geoelectrical properties correlate with fluid movement within the rock matrix and the effects of mineral alteration or precipitation. We have developed an innovative experimental setup that combines SIP and  $\mu$ CT techniques simultaneously. This novel prototype was meticulously designed with specific technical features to ensure optimal SIP signal acquisition under controlled temperature and pressure conditions, along with high-resolution 4D  $\mu$ CT analysis. The new experimental setup has enabled consistent Spectral Induced Polarization (SIP) measurements across various sample materials, showing no significant distortion of the SIP signal due to the combination of different materials (aluminum, brass, etc..) and/or the impact of its geometrical features. It has also been successfully tested for its pressure resistance under high confining liquid pressures. This approach holds significant potential for advancing research in geophysics, hydrogeology, reservoir characterization, and other related field.

## References

- Lévy, L., Maurya, P. K., Byrdina, S., Vandemeulebrouck, J., Sigmundsson, F., Árnason, K., ... & Labazuy, P. (2019). Electrical resistivity tomography and time-domain induced polarization field investigations of geothermal areas at Krafla, Iceland: comparison to borehole and laboratory frequency-domain electrical observations. *Geophysical Journal International*, 218(3), 1469-1489. Available at: <https://doi.org/10.1093/gji/ggz240>.
- Zimmermann, E., Kemna, A., Berwix, J., Glaas, W., Münch, H. M., & Huisman, J. A. (2008). A high-accuracy impedance spectrometer for measuring sediments with low polarizability. *Measurement Science and Technology*, 19(10), 105603.

# Exploring the Biogeobattery Phenomenon: Implications of Induced Polarization and Magnetic Susceptibility

Nicolette Filippone<sup>1</sup>, Dimitrios Ntarlagiannis<sup>1</sup>, Estella Atekwana<sup>2</sup>, Lee Slater<sup>1,3</sup>

<sup>1</sup>*Department of Earth & Environmental Sciences, Rutgers University Newark, United States, nicolette.filippone@rutgers.edu*

<sup>2</sup>*Department of Earth & Planetary Sciences, University of California Davis, United States*

<sup>3</sup>*Energy & Environment Directorate, Pacific Northwest National Laboratory, Richland, United States*

Crude oil spills pose significant ecological and environmental challenges, prompting the need for advanced techniques to characterize and monitor in-situ hydrocarbon degradation processes. This study explores the application of geophysical methods, including self-potential (SP), electrodic potential (EP), magnetic susceptibility (MS), and induced polarization (IP), to non-invasively investigate the long-term biochemical and physical transformations at a hydrocarbon-contaminated site. We specifically focus on understanding the influence of iron minerals on IP parameters in a crude oil-contaminated unconsolidated core sample retrieved from 5.3 meters below the land surface, within the water table fluctuation zone near Bemidji, Minnesota, United States. Our aim is to understand the interplay between geophysical signals and hydrocarbon degradation processes in the presence of a fluctuating water table. Our findings confirm the presence of a hypothesized biogeobattery, evidenced by a pronounced SP dipolar magnitude. Due to the polarization effect, the IP parameter (chargeability) shows a strong linear relationship with MS, indicating the presence of iron minerals (magnetite) that act as electron conductors. The observed strong spatial and temporal correlation between chargeability and MS, indicate that these associations evolve with fluctuations in environmental parameters, particularly water table levels. Overall, this integrated approach may aid in characterizing the locations and processes relevant to the hypothesized biogeobattery, thereby contributing to the assessment and management of hydrocarbon-contaminated sites.

# Electrical Characterization of Foam Used in Decontamination: Correlation between Foam Drainage and Resistivity

A. Shoker<sup>a,b,c</sup>, P. Kessouri<sup>a</sup>, A. Ahmadi-Senichault<sup>b</sup>, A. Maineult<sup>d</sup>

<sup>a</sup> BRGM (French Geological Survey), 45060 Orléans, France

<sup>b</sup> Institut de Mécanique et Ingénierie de Bordeaux (I2M), Arts et Métiers Institute of Technology, CNRS, Talence, 33405, France

<sup>c</sup> L'Unité Mixte de Recherche METIS, Sorbonne Université, 75252 Paris Cedex 05, France

<sup>d</sup> Laboratoire de Géologie, Ecole Normale Supérieure / CNRS UMR8538, PSL Research University, Paris, France

Aquifer pollution is a major problem with important consequences on human health, particularly hydrocarbon pollutants that permanently degrade soil and groundwater quality (Ramaswami et al., 2001). One of the methods for the decontamination of hydrocarbon-polluted aquifers is by injecting aqueous foams, known by their non-newtonian behavior, foam can be used as a (1) blocking agent: Foam diverts the fluid flow to other lower permeable layers and confines the pollutant, (2) mobilizing agent: Foam can be used to desorb and push the contaminants towards a recovery well, or (3) vectorizing agent: Foam can be used to transport additives enhancing the redox reactions such as chemicals, bacteria or nanoparticles (Davarzani et al., 2021). Aqueous foam is a two-phase system, where gas bubbles are dispersed in a continuous liquid phase (Bikerman, 1973). The liquid phase called contains the solvent (water) and surfactants. Surfactants, surface active agents, are used as a major foaming agent by reducing the surface tension between the two immiscible phases, such as gas and water (Xuhui Mao et al., 2015).

This work is aimed at using electrical geophysical tools to characterize foam flow in a porous medium, in a broadband frequency range. We performed a study to investigate the electrical properties of surfactant solutions, where we investigated the electrical behavior of surfactant solutions regarding the mixing and resting time by measuring DC resistivity using a conductivity meter (H19033). We used two types of surfactants: SDS (anionic) and CAHS (zwitterionic), in two types of solvents: Deionized and tap water. As a result, the mixing and resting time of surfactant solutions do not affect the solution's electrical properties over time. For the bulk aqueous foam study, we did resistivity and foam stability measurements for mentioned surfactants by the use of a foam analyzer (DFA100 by Kruss). The setup used to measure the electrical resistivity is a series of seven pairs of electrodes used both for injection and potential measurement at 500 kHz (capacitance probes). The seven pairs of electrodes are spread along the columns regularly. The first pair at the bottom measures the resistivity of the liquid used for the foam generation. The third pair is at the same height as the camera used for image analysis and is used for comparison with other foam parameters estimated by the image analysis, i.e. time-dependent analysis. We used these data to characterize foam properties with resistivity measurements.

Of the evolution of the electrical resistivity as a function of foam volume, Figure 1 shows the electrical resistivity changes in a distinct behavior (S-shape curve) in different experiments. We suppose this common behavior is related to the three drainage transitions (Magrabi et al., 2001). As a next step of this study, in addition to the modeling of electrical properties of the bulk foam, we will

investigate the electrical response of foam flow in a porous medium by conducting 2-D Tank experiments with SIP (low frequency) and TDR (high frequency) measurements.

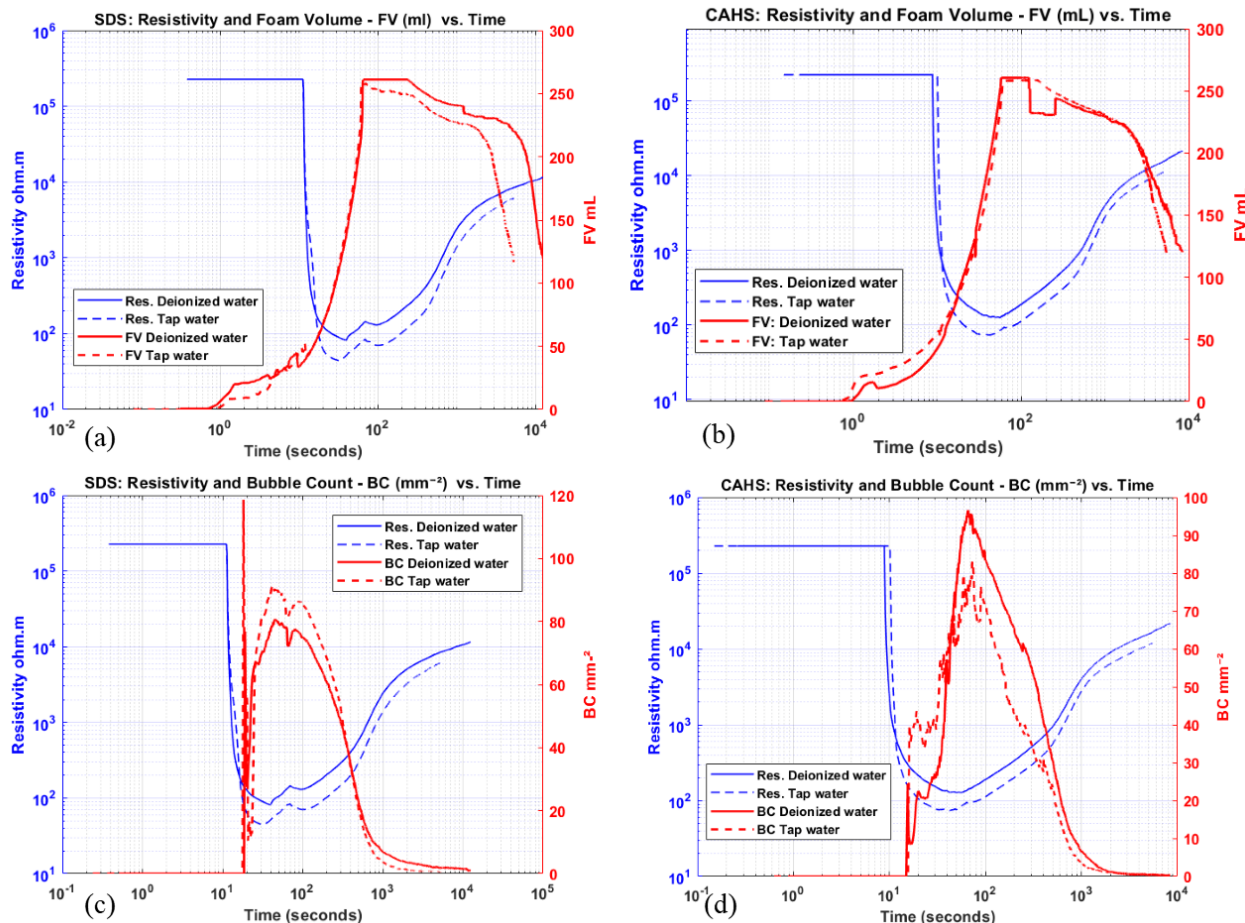


Figure 1. Resistivity (ohm.m) and foam volume (mL) vs. time (sec) (a): SDS anionic surfactant and (b) CAHS zwitterionic surfactant. Also, resistivity vs. Resistivity (ohm.m) and bubble count (mm<sup>-2</sup>) vs. time (sec) (c): SDS anionic surfactant and (d) CAHS zwitterionic. S-shaped curve is observed in different resistivity curves for both types of surfactants and solvents: Deionized and distilled water.

## References

- Bikerman, J.J., 1973. Measurement of Foaminess, in Foams. Springer Berlin Heidelberg, Berlin, Heidelberg, pp. 65–97. [https://doi.org/10.1007/978-3-642-86734-7\\_3](https://doi.org/10.1007/978-3-642-86734-7_3)
- Datye, A.K., Lemlich, R., 1983. Liquid distribution and electrical conductivity in foam. International Journal of Multiphase Flow 9, 627–636. [https://doi.org/10.1016/0301-9322\(83\)90112-X](https://doi.org/10.1016/0301-9322(83)90112-X)
- Davarzani, H., Aranda, R., Colombano, S., Laurent, F., Bertin, H., 2021. Experimental study of foam propagation and stability in highly permeable porous media under lateral water flow: Diverting groundwater for application to soil remediation. Journal of Contaminant Hydrology 243, 103917. <https://doi.org/10.1016/j.jconhyd.2021.103917>
- Magrabi, S.A., Dlugogorski, B.Z., Jameson, G.J., 2001. Free drainage in aqueous foams: Model and experimental study. AIChE Journal 47, 314–327. <https://doi.org/10.1002/aic.690470210>
- Ramaswami, A., Johansen, P.K., Isleyen, M., Bielefeldt, A.R., Illangasekare, T., 2001. Assessing Multicomponent DNAPL Biostabilization.I: Coal Tar. J. Environ. Eng. 127, 1065–1072. [https://doi.org/10.1061/\(ASCE\)0733-9372\(2001\)127:12\(1065\)](https://doi.org/10.1061/(ASCE)0733-9372(2001)127:12(1065))
- Xie, W., Neethling, S.J., Cilliers, J.J., 2004. A novel approach for estimating the average bubble size for foams flowing in vertical columns. Chemical Engineering Science 59, 81–86. <https://doi.org/10.1016/j.ces.2003.09.020>
- Xuhui Mao, Rui Jiang, Wei Xiao, 2015. Use of surfactants for the remediation of contaminated soils: A review.

# The complex electrical response to NaHCO<sub>3</sub> diffusion in non equilibrium systems

Arne Marvin Mansfeld<sup>1</sup>, Andreas Kemna<sup>1</sup>

<sup>1</sup>Geophysics Section Institute of Geosciences , University of Bonn, Germany, mansfeld@geo.uni.bonn.de

In near-surface waters, the fluid chemistry is controlled by equilibrium between atmospheric carbon dioxide and its aquatic species. These can either act as acid or base and thus control the pH of the system. The most common species is the hydrogencarbonate ion [HCO<sub>3</sub><sup>-</sup>]. The carbon-driven pH of water is not only important in agricultural fields as it controls nutrient availability but also in carbon storage and sequestering, given the chemical stability of the potential reservoirs. Even though the effects of high carbon concentrations on these systems are known and can be predicted, non-invasive monitoring and control of the pH in rocks and soils still face difficulty, due to inaccessibility of pore spaces. We propose the use of spectral induced polarisation (SIP) to measure the complex electrical conductivity of the subsurface. This method is based on the injection of alternating currents and can not only capture the real part conductivity used to estimate the salinity of the pore fluid, but also gain information on the structure of the porous medium via measuring the imaginary part or polarisation. The imaginary part is assumed to originate in the electrical double layer formed by the accumulation of dissolved ions, attracted by the surface charge of minerals. Charge migration in these layers in response to an external harmonic electrical field leads to relaxation processes, which can vary in strength and time in response to different properties of the sample. The timescales of these relaxation processes are controlled by the pore geometry and the mobility of the adsorbed ions. Information at which rates the relaxation times respond to changes in the surface assemblage and the pH however is limited.

In this study, we provide three sets of data obtained from diffusion experiments where the diffusion of a sodium hydrogen carbonate solution into quartz-rich sandstones was monitored with SIP at high temporal resolution. An example of the time-lapse measurements is shown in figure 1. The left side shows the evolution of the characteristic time constant received via debye decomposition of the complex electrical conductivity. The imaginary part of the sample's conductivity is shown on the right side of the figure. The imaginary part of the conductivity increases in response to the pH and salinity increase, following a trend similar to results from previous theoretical models and experiments on soils and rocks (Skold et al. (2011); Hördt et al. (2016); Schwartz et al. (2014)). The change in characteristic time follows a modified solution to the diffusion equation. With increasing pH and salinity the characteristic time of the samples increases forming higher and sharper peaks. We explain these results with a change in the mobility of the surface species in response to the diffusive flux, as bound hydrogen gets replaced with sodium ions, lowering the average ion mobility in the stern and diffusive layer. Our results show that even at high salinities with a corresponding reduction or stagnation in chargeability (as in figure 2), dynamic changes at the mineral water interfaces in response to the changing pH can be captured in the dominating

relaxation times of the electrical polarisation. This suggests that the SIP method remains a useful tool to characterize mineral water interfaces and pore space geometries even at high salinity.

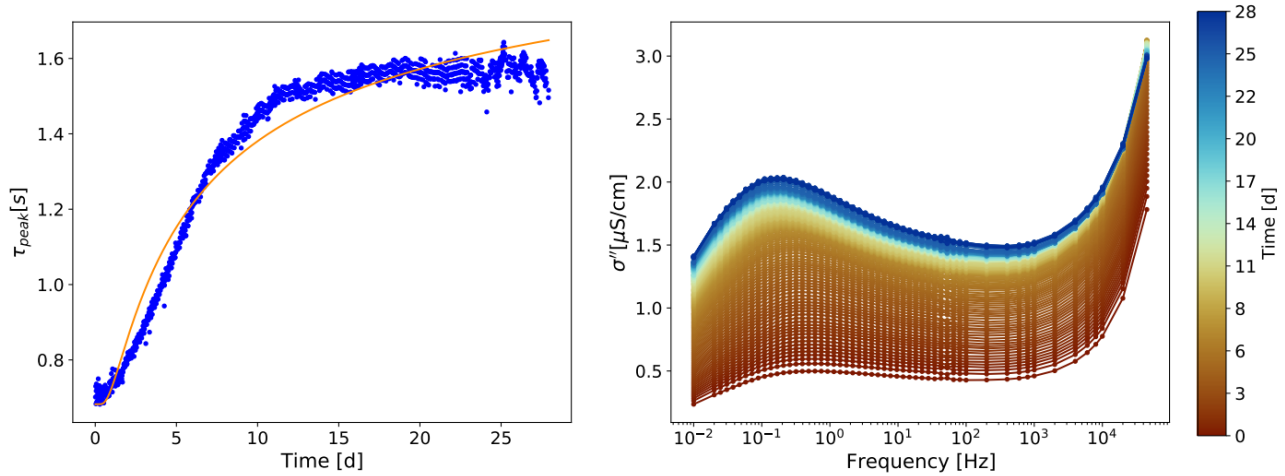


Figure 1: Exemplary temporal evolution of the characteristic time constant  $\tau_{peak}$  fitted by a diffusion equation (orange line) and the imaginary conductivity  $\sigma''$  of a sample.

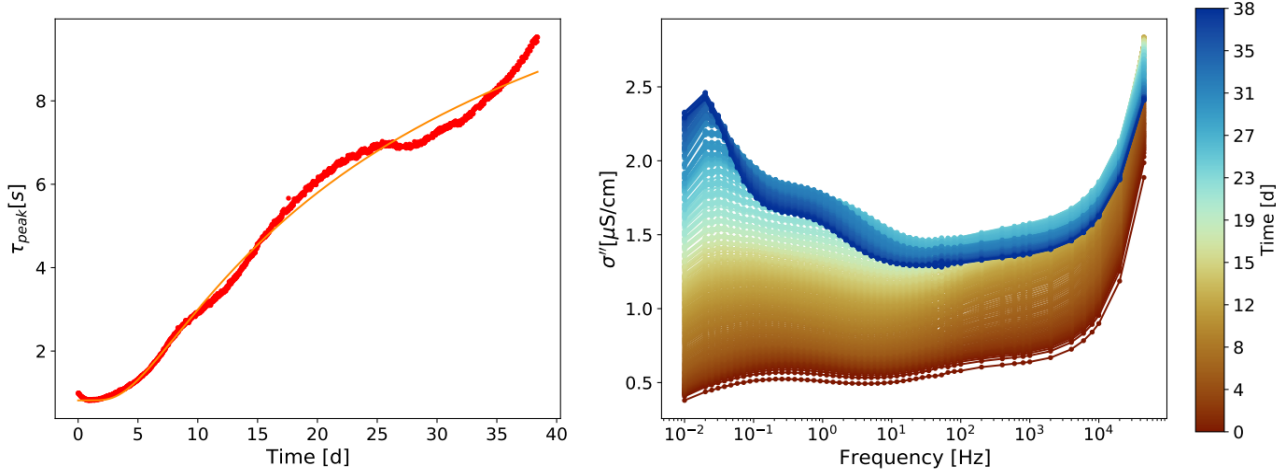


Figure 2: Exemplary data for the temporal evolution of the characteristic time  $\tau_{peak}$  and imaginary conductivity  $\sigma''$  of a sample reaching the salinity threshold for polarization reduction.

## References

- Hördt, A., Bairlein, K., Bielefeld, A., Bücker, M., Kuhn, E., Nordsiek, S. and Stebner, H., 2016, The dependence of induced polarization on fluid salinity and ph, studied with an extended model of membrane polarization, *Journal of Applied Geophysics* 135, 408–417.
- Skold, M., Revil, A. and Vaudelet, P., 2011 , The ph dependence of spectral induced polarization of silica sands: Experiment and modeling, *Geophysical Research Letters* 38(12).
- Schwartz, N., Shalem, T. and Furman, A., 2014, The effect of organic acid on the spectral-induced polarization response of soil, *Geophysical Journal International* 197(1), 269–276.

# Monitoring sulfur modified iron oxidation in sediments via spectral induced polarization

Hilary P. Emerson<sup>1</sup>, James E. Szecsody<sup>1</sup>, Judy Robinson<sup>1</sup>, and Lee Slater<sup>2</sup>

<sup>1</sup>Pacific Northwest National Laboratory, 902 Battelle Blvd, Richland, WA, USA, hilary.emerson@pnnl.gov

<sup>2</sup>Rutgers University-Newark, 195 University Ave, Newark, USA

Noninvasive geophysical approaches can provide evidence of subsurface conditions over large spatial extents during and after active environmental remediation. These indirect methods can support and complement direct characterization via conventional groundwater sampling and core characterization. While electrical resistivity (ER) is sensitive to changes in subsurface ionic chemistry in the pore fluid and sediments, bulk electrical conductivity from ER cannot separate the response from solution and solid phase reactions induced by an amendment (Johnson et al., 2013; Truex et al., 2018). However, spectral induced polarization measures the complex electrical conductivity, including the phase which allows for separation of the response based on (i) pore fluid electrolytic conduction and mineral surface conductivity and (ii) polarization of electron conducting minerals and temporary, reversible charge storage in the electrical double layer (Vinegar and Waxman, 1984; Revil, 2012).

Several studies have demonstrated the utility of SIP methods for physicochemical characterization of subsurface sediments (Revil et al., 2013; Kemna et al., 2012; Slater and Lesmes, 2002), including characterization and monitoring in preparation for and during remediation (Orozco et al., 2015; Sogade et al., 2006; Williams et al., 2009). However, spectral induced polarization (SIP) responses are not well understood within the context of remediation applications at contaminated sites. Systematic SIP studies are needed to gain further insights into the complex electrical response of dynamic, biogeochemical states to enable the use of SIP for subsurface site characterization and remediation monitoring. Although SIP measurements on zero valent iron have been previously published, the SIP response for sulfur modified iron (SMI), another potential subsurface reductive amendment, has not yet been reported. Hence, the purpose of this laboratory scale study was to evaluate SIP for nonintrusive monitoring of SMI in subsurface conditions. SMI was mixed with sediments from the Hanford Site (Washington, USA) and then packed into columns for geochemical and SIP analysis for up to 77 days under fully saturated conditions.

SMI exhibited distinguishable phase peaks between 0.1 and 1.0 Hz, which were detected as low as 0.3 wt.%. In the first few days (see Figure 1), the complex conductivity, phase maxima, and chargeability increased while the peak locations shifted to higher frequency (decreasing relaxation times), suggesting an initial increase in polarization and concurrent decrease in the length scales (or particle diameter). Then, after 77 days, the phase maxima and chargeability decreased with a concurrent increase in relaxation times, suggesting that over longer time periods, less polarizable phases are forming and particle size or connectivity of polarizable phases is increasing. These results demonstrate a unique SIP response to SMI oxidation over time that could be used for long-term monitoring of the efficacy of SMI emplaced as a subsurface barrier or injected in the field.

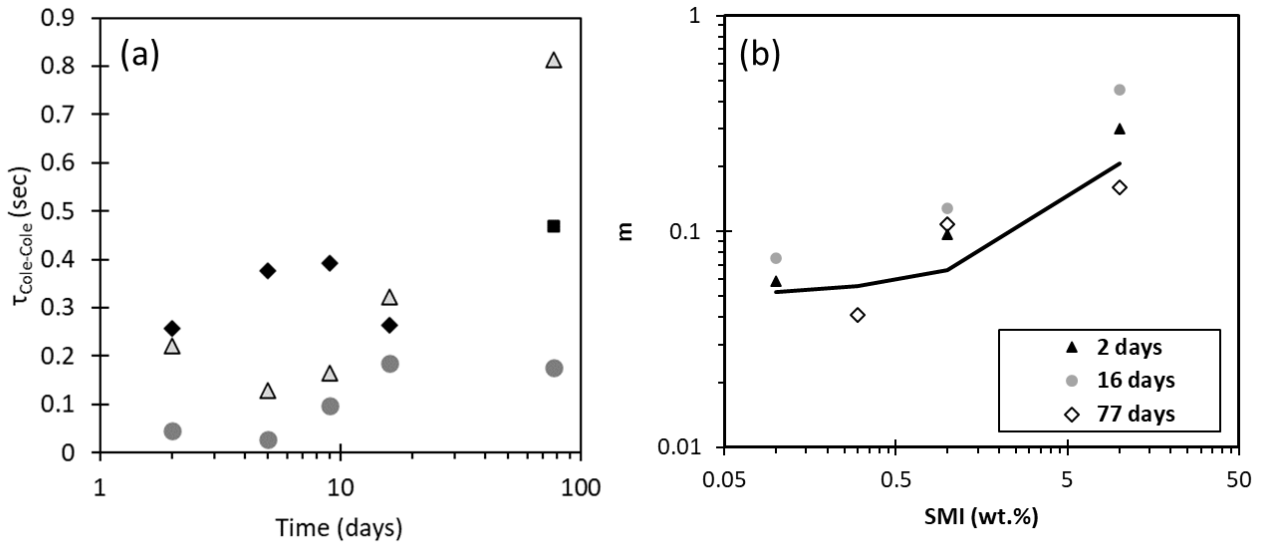


Figure 1: Comparison of SIP of variable SMI wt.% in Hanford sediments with time based on (a) time constants ( $\tau$ , sec) and (b) chargeability ( $m$ , unitless) as estimated with a standard Cole-Cole model fit (points) and compared to the theoretical correlation of intrinsic  $m$  with volumetric fraction (line).

## References

- Johnson, R.L., Nurmi, J.T., Johnson, G.S.O., Fam, D., Johnson, R.L.O., Shi, Z., Salter-Blanc, A.J., Tratnyek, P.G., and Lowry, G.V., 2013. Field-scale transport and transformation of carboxymethylcellulose-stabilized nano zero-valent iron. *Environmental Science and Technology* 47(3), 1573-80.
- Kemna, A., Biney, A., Cassiani, G., Niederleithinger, E., Revil, A., Slater, L., Williams, K.H., Orozco, A.F., Haegel, F.-H., Hordt A., Kruschwitz, S., Leroux, V., Titov, K., and Zimmermann, E., 2012. An overview of the spectral induced polarization method for near-surface applications. *Near Surface Geophysics* 10(6), 453-468.
- Orozco, A.F., Velimirovic, M., Tosco, T., Kemna, A., apion, H., Klaas, N., Sethi, R., and Bastiaens, L., 2015. Monitoring the injection of microscale zerovalent iron particles for groundwater remediation by means of complex electrical conductivity imaging. *Environmental Science and Technology* 49(9), 5593-5600.
- Revil, A. 2012. Spectral induced polarization of shaly sands: Influence of the electrical double layer. *Water Resources Research* 48(2).
- Revil, A., Eppehimer, J.D., Skold, M., Karaoulis, M., Godinez, L. and Prasad, M., 2013. Low-frequency complex conductivity of sandy and clayey materials. *Journal of Colloid and Interface Science* 398, 193-209.
- Slater, L.D. and Lesmes, D., 2002. IP interpretation in environmental investigations. *Geophysics* 67(1), 77-88.
- Sogade, J.A., Scira-Scappuzzo, F., Vichabian, Y., Shi, W., Rodi, W., Lesmes, D.P., and Morgan, F.D., 2006. Induced-polarization detection and mapping of contaminant plumes. *Geophysics* 71(3), B75-B84.
- Truex, M.J., Chronister, G.B., Strickland, C.E., Johnson, C.D., Tartakovsky, F.D., Oostrom, M., Clayton, R.E., Johnson, T.C., Freedman, V.L., Rockhold, M.L., Greenwood, W.J., Peterson, J.E., Hubbard, S.S., and Ward, A.L., 2018. Deep Vadose Zone Treatability Test of Soil Desiccation for the Hanford Central Plateau, PNNL-26902, Pacific Northwest National Laboratory, Richland, WA.
- Vinegar, H.J. and Waxman, M.H., 1984. Induced polarization of shaly sands. *Geophysics*, 49, 1267–1287.
- Williams, K.H., Kemna, A., Wilkins, M.J., Druhan, J., Arntzen, E., N'Guessan, A.L., Long, P.E., Hubbard, S.S., and Banfield, J.F., 2009. Geophysical monitoring of coupled microbial and geochemical processes during stimulated subsurface bioremediation. *Environmental Science and Technology* 43(17), 6717-6723.

# Spectral induced polarization signals of soils contaminated by aqueous film forming foam (AFFF) releases

Lee Slater<sup>1,2</sup>, Charles Schaefer<sup>3</sup>, Dale Werkema<sup>4</sup>, Dimitrios Ntarlagiannis<sup>1</sup>, Alex Avilar<sup>1</sup>, Ethan Siegenthaler<sup>1</sup>, Tara Moghtaderi<sup>1</sup> and Fred Day-Lewis<sup>2</sup>

<sup>1</sup>*Department of Earth & Environmental Sciences, Rutgers University Newark, USA, lslater@newark.rutgers.edu; lee.slater@pnnl.gov*

<sup>2</sup>*Energy & Environment Directorate, Pacific Northwest National Laboratory, USA*

<sup>3</sup>*CDM Smith, USA*

<sup>4</sup>*Environmental Protection Agency (EPA), USA*

The development of field-scale, in situ screening technologies is crucial for assessing aqueous film forming foam (AFFF) source zones at former fire training and storage sites, which are long-term sources of per- and polyfluoroalkyl substances (PFAS) contamination. Spectral induced polarization (SIP) may offer sensitivity to AFFF contamination due to the sorption of cationic/zwitterionic PFAS compounds and non-fluorinated surfactants to mineral surfaces. We explored the sensitivity of SIP to AFFF-contaminated soils with PFAS concentrations ranging from 2-30,000 ppb, confirmed by accepted analytical methods. Laboratory measurements were performed on soil samples from two AFFF source zones (Source Zone 1 and Source Zone 2), and field-scale SIP transects were conducted across these zones.

A statistically significant linear relationship between total PFAS concentration and laboratory-measured SIP response (phase angle) was observed for Source Zone 1, but based on only 10 samples (Figure 1). A visual correlation between field SIP response and sample PFAS contamination was noted but not statistically significant. In contrast, no significant relationship between SIP response and total PFAS concentration was found for Source Zone 2, where soil remediation activities had been undertaken, despite the availability of an extensive set of soil samples with PFAS analysis performed (>70 samples).

These findings indicate that SIP may provide a rapid and cost-effective means to map variations in contamination across AFFF source zones, guiding the selection of soil sampling locations and minimizing the risk of missing PFAS hotspots. However, the success of this technology will depend on the complexity of the site. While SIP may yield useful information on variations in PFAS contamination at undisturbed sites with native soils, its sensitivity may be compromised by soil heterogeneity at remediated sites. Ongoing research is focused on identifying the components of AFFF that most likely explain the observed dependence of SIP on soil PFAS concentrations.

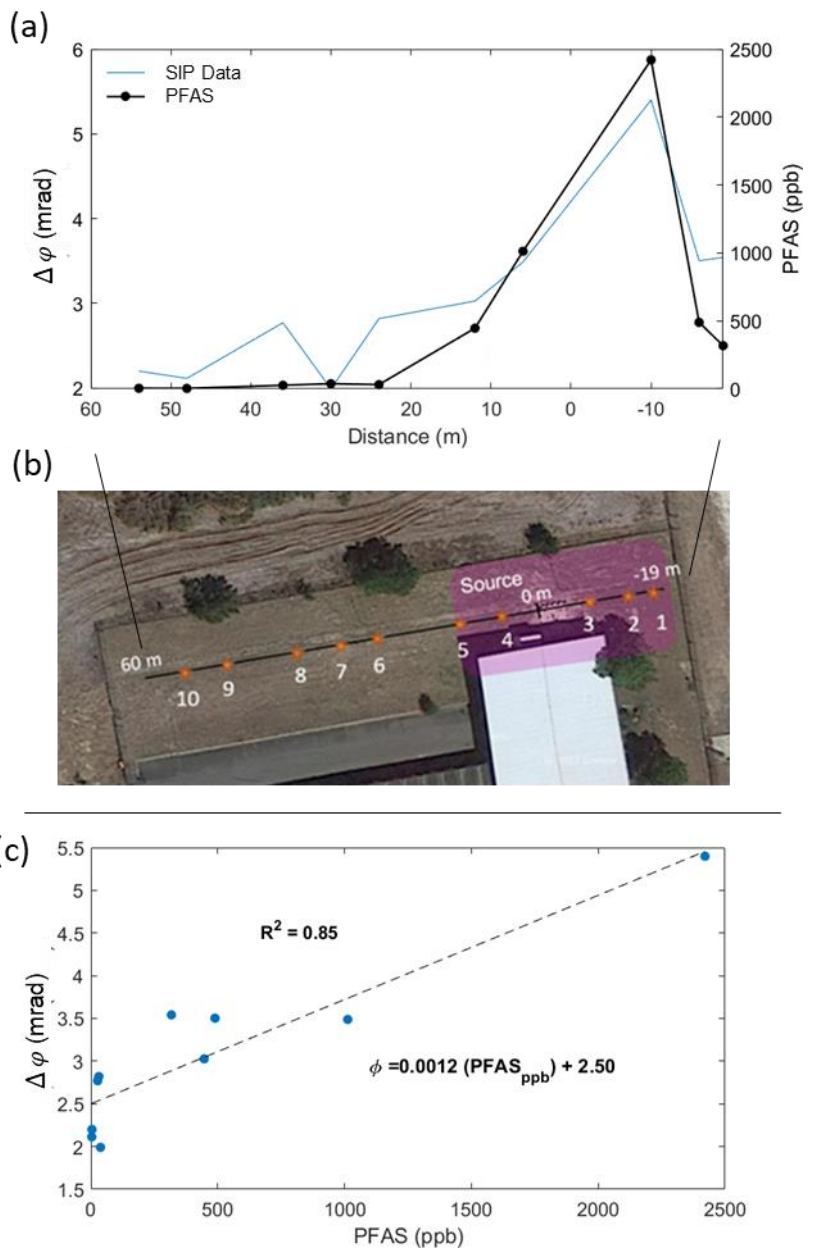


Figure 1: (a) laboratory-measured phase from SIP measurements compared with PFAS concentrations from ten samples taken on a transect crossing the source zone at the study site (b). The linear relationship between laboratory measured  $\varphi$  and the measured total soil PFAS concentration recorded is shown in (d) ( $p$ -value = 0.0009).

# DCIP monitoring of Älvkarleby test embankment dam

Reyhaneh Norooz<sup>1,2</sup>, Torleif Dahlin<sup>1</sup>, Thomas Günther<sup>3</sup>

<sup>1</sup>Engineering Geology, Lund University, Sweden, torleif.dahlin@tg.lth.se

<sup>2</sup>AFRY, Sweden

<sup>3</sup>Leibniz Institute of Applied Geophysics (LIAG), Hannover, Germany

A test embankment dam has been built (Figure 1) in Älvkarleby, Sweden, in order to assess the damage detection capability of several dam monitoring methods. The dam was built as a conventional zoned embankment dam, in a concrete container with the inner dimension of 20 m \* 16 m \* 4 m (Bernstone et al., 2021). The dam was designed with zones consisting of materials with different hydraulic properties and associated internal zones with large resistivity contrasts. A number of defects with secret locations were built into the pilot-scale embankment dam (Norooz et al. 2024).

Stainless steel plate electrodes are embedded in the embankment dam, in total 224, placed in the upstream and downstream fine filter and on the top of the core (Figure 2). The electrodes are used for automated acquisition of DCIP (direct current resistivity and induced polarization) tomography data sets. All data have been saved as full waveform. Measurement sequences with up to around 14 000 data including full range gradient, cross-line bipole-bipole and corner array are measured automatically every day with 3D coverage of the dam core.

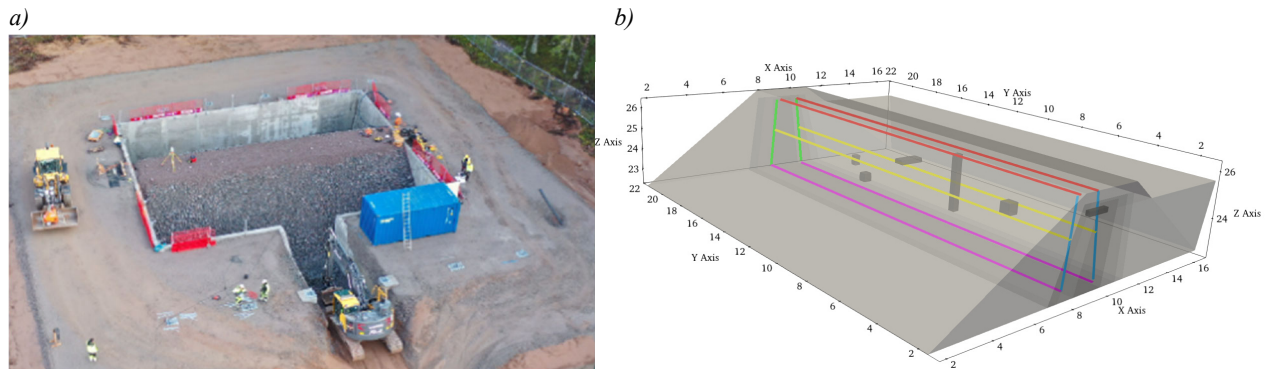


Figure 1: a) Aerial view of Älvkarleby test dam (Bernstone et al., 2021). b) Position of measurement lines and defects.

The pyBERT/pyGIMLi software package (Rücker et al. 2017) was used for the inversion. A 3D FEM (finite element) mesh was designed with the element structured based on the internal material zones of the dam, and the smoothness constrains decoupled at the known internal material borders.

The ERT part of the data for the first couple of years was inverted and revealed a strong layering in the resistivity of the core (Figure 2), which may be caused by e.g. differential wetting, and several anomalous zones that are not associated with the intentional defects were also discovered. A centrally placed horizontal permeable zone and the vertical loose zone were successfully discovered. These defects are mimicking zones affected by internal erosion that are expected to have higher resistivity values in comparison to the surrounding healthy core material in typical Swedish dams, and the results thus indicate the potential for detecting internal erosion. Strong seasonal resistivity variation is present with amplitude and phase differences between different zones (Norooz et al. 2024).

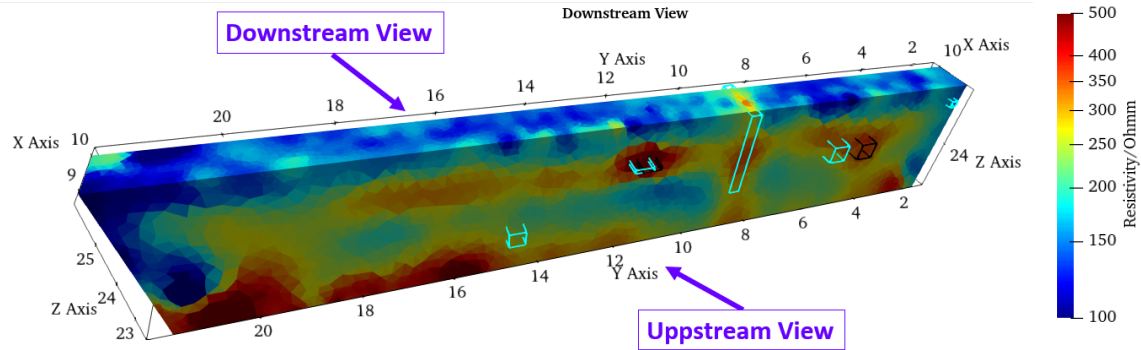


Figure 2: Inverted ERT data from the dam core of timeframe 2022-01-28. The location of the defects is shown by blue cuboids, whereas the predicted location is indicated by black cuboids. Several unintentional defects and layering of the material structure are prominent.

Preliminary inversion of a small part of the IP data (Figure 3) shows elevated chargeability in terms of phase in the left end of the dam (viewed from the upstream side), which appears to correlate with the position other sensor installations. There is furthermore a layering in the phase that has some similarity with the resistivity layering. The IP data will be inverted and analysed in depth including the spectral content and evaluated against reference data.

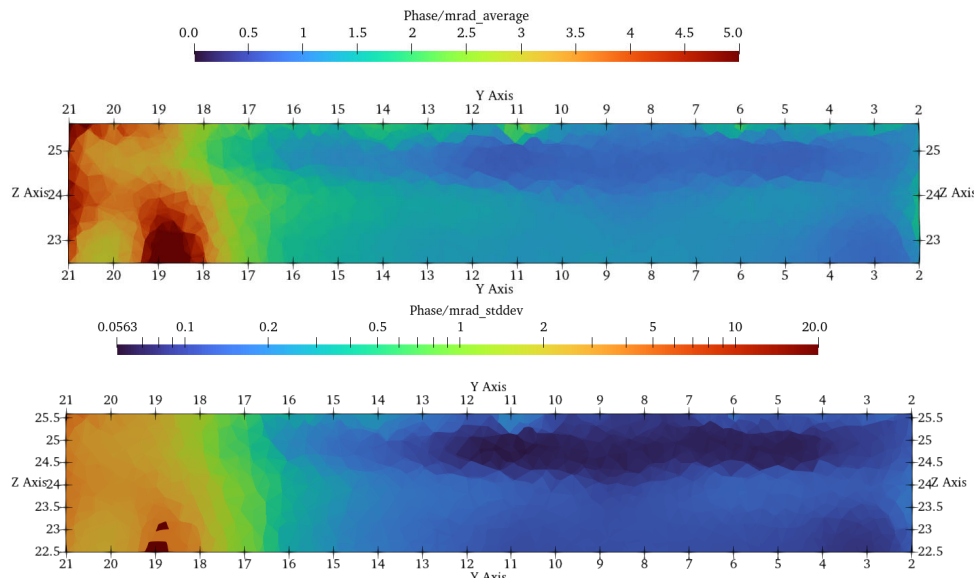


Figure 3: Average IP result for a period of 10 weeks (upper) and standard deviation during the period (lower).

## Acknowledgements

The research presented here was funded by Swedish Energy Agency (project 48411-1), Swedish Centre for Sustainable Hydropower- SVC (project VKU14177/VKU32021) and Vattenfall AB. The computations were performed on resources provided by the Swedish National Infrastructure for Computing (SNIC) at LUNARC. We wish to thank our colleagues at LUNARC for their valuable support in connection with the study.

## References

- Bernstone C., Lagerlund J., Toromanovic J. & Juhlin C. (2021). *Deformationer och portryck i en experimentell fyllningsdamm*, Report 2021:772, Energiforsk, Stockholm, ISBN 978-91-7673-772-9, 52p.
- Norooz R., Dahlin T., Nivorlis A., Olsson P.-I., Günther T. & Bernstone C. (2024) Monitoring internal erosion in embankment dams using 3D Electrical Resistivity Tomography: Älvkarleby test embankment dam, *Journal of Civil Structural Health Monitoring*, in press.
- Rücker C., Günther T. & Wagner F.M. (2017) pyGIMLI: An open-source library for modelling and inversion in geophysics, *Computers and Geosciences*, 109: 106-123.

# DCIP monitoring of a MAR infiltration pond at Vomb

Torleif Dahlin<sup>1</sup>, Per Hedblom<sup>1</sup>, Ankita Prayag<sup>1</sup>, Yaman Abu Jaish<sup>1</sup>, Matteo Rossi<sup>1</sup>, Kristofer Hägg<sup>2</sup> and Tina Martin<sup>1</sup>

<sup>1</sup>Engineering Geology, Lund University, Sweden, torleif.dahlin@tg.lth.se

<sup>2</sup>Sydvatten AB, Sweden

A DCIP system has been installed in and around an infiltration pond within the Vomb managed aquifer recharge (MAR) plant in southern Sweden. The objective of the installation is to monitor the water saturation and transport under the infiltration pond to create a better understanding of the infiltration process, in order to form a base for optimised operation of the water works. Another objective is to assess the possibility to monitor the growth of biofilm in the sand filter.

The installation consists of in total 416 electrodes in 3 lines with 128 to 160 each (Figure 1a). The electrodes consist of 10 cm x 10 cm stainless steel plates that were buried in trenches at 0.4 m depth, and connected alternately to two parallel cables that are separated by around 0.7 m (Figure 1b).

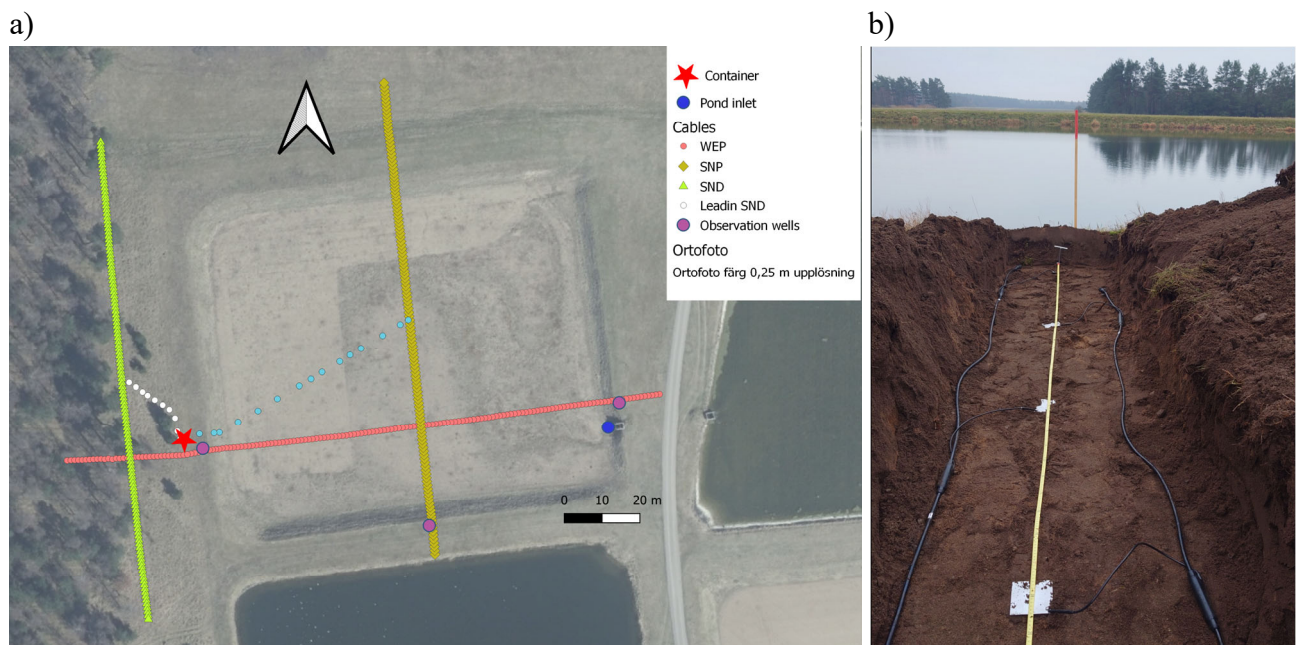


Figure 1: a) Positions of electrode spreads. b) Temporary trench for electrode installation in southern end of line SNP with neighbouring infiltration pond in the background.

Measurements are taken using 100% duty cycle IP (Olsson et al. 2015) with 4 s pulses, and data are saved as full waveform with a data rate of 3750 Hz to allow advanced signal processing (Olsson et al. 2016). A roll-along approach has been implemented, in which selected subsets of the electrode spreads are connected to the instrument in a sequence. Multiple gradient array adapted for separated spreads is used for the measurements, plus pole-dipole like array using the farthest electrode in the other end of the spread as “remote” electrode. Reciprocal measurements have been added for 10 % of the data. In total around 16 000 datapoints are measured daily.

A background series measured before water filling of the pond started shows electrode contact resistances that are mostly in the range 5-10 k $\Omega$ . Preliminary inversion of the apparent resistivity and integral chargeability data (Figure 2), without accounting for the burial depth of the electrodes, results in excellent data fit with mean residuals below 1 %. The sandy sediments above the groundwater level stand out with resistivities above 1 k $\Omega$ m, which drops to a few hundred  $\Omega$ m in the saturated zone (Figure 2a). The gradually decreasing resistivity with depth reflects changes in grain size of the sediments. In the southern end the line is close to the neighbouring water filled infiltration pond (Figure 1b) which is reflected by a steep increase in the level of the interface to lower resistivity associated with higher groundwater level. The chargeability is very low (Figure 2b), only a few mV/V, which is accentuated by the long interval for the integral IP.

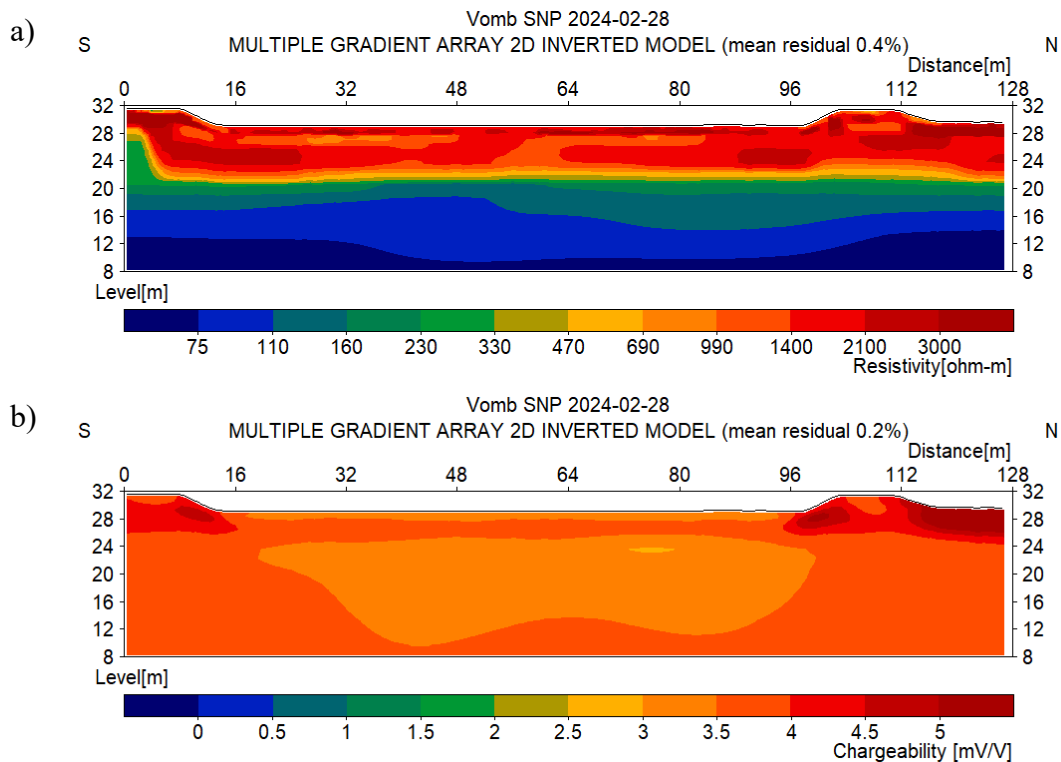


Figure 2: Example results from the south-north line through the infiltration pond; a) resistivity, and b) chargeability.

## Acknowledgements

The work is funded by the EU Interreg North Sea region via the “Blue Transition – how to make my region climate resilient” project, Sydvatten AB and Sweden Water Research (SWR). We thank Mike Torstensson and Stefan Svensson for excellent work and nice collaboration during the electrode installations.

## References

- Olsson P.-I., Dahlin T., Fiandaca G. and Auken E. (2015) Measuring time domain spectral induced polarization in the on-time – decreasing the acquisition time and increasing the signal levels, *Journal of Applied Geophysics*, 123, 316-321.
- Olsson P.-I., Fiandaca G., Juul Larsen J., Dahlin T. and Auken E. (2016) Doubling the spectrum of time-domain induced polarization by harmonic de-noising, drift correction, spike removal, tapered gating and data uncertainty estimation, *Geophysical Journal International*, 207(2): 774-784.

# Electrical Detection of Groundwater Leakage Channels by Spread Spectrum Induced Polarization (SSIP) Geophysical Method, Guizhou, China

Ijaz Ahmed<sup>1,2</sup>, Chen Rujun<sup>1,2\*</sup>, Cheng Shuang<sup>2</sup> and Shahid Ali Shah<sup>1,2</sup>

<sup>1</sup>School of Geosciences and Info-Physics, Central South University, Changsha, China, [chrujun@csu.edu.cn](mailto:chrujun@csu.edu.cn)

<sup>2</sup>AIoT Innovation and Entrepreneurship Education Centre for Geology and Geophysics, Central South University, Changsha, China

## Introduction

The main purpose of the study was to look into the extensive damage done to the environment by the constant release of wastewater from the slag yard in GZ, China. The implementation of leak detection and containment measures within an area of 500 meters of the facility has the potential to provide considerable cost savings by minimizing the expenses associated with the remediation of contaminated water. The main purpose of the research is to examine and provide effective methods to tackle the issue, with the goal of safeguarding the quality of groundwater, preserving the ecosystems of adjacent rivers. The study used an advanced geophysical technique called Spread Spectrum Induced Polarization (SSIP) to precisely identify and evaluate the pathways via which polluted water is leaking.

## Study area and methodology

The slag dump is in a karst development area, and the height difference between it and the nearby river bed is close to 300 meters. According to domestic and foreign karst development research, polluted water bodies' karst seepage channels maybe 150-250 meters below the surface. The detection is really challenging. Many domestic and international units near the slag yard failed to identify leaking because established karst leakage detecting systems cannot detect depths more than 50 meters Due to the foregoing, large-scale, high-precision, and high-accuracy detection technology research on slag field leakage channels are necessary. This study detects leakage in slag field channels using the SSIP technique, which has the characteristics of great interference resistance, large depth, high precision, and accuracy (Liu et al., 2017). With SSIP, the detection depth is at least 500 meters.

## Interpretation results

This study examined the SO<sub>4</sub>, PO<sub>4</sub>, Mg and Ca of water samples obtained from ZK02. As the concentration of sulfate in water rises, there is a corresponding increase in conductivity and reduction in resistivity. Additionally, the pH value tends to fall in the study area.

Table.1 water quality analysis of groundwater in ZK02.

F	SO <sub>4</sub>	PO <sub>4</sub>	Mg	Ca
mg/L	mg/L	mg/L	mg/L	mg/L
na	1216.680189	na	63.8485	394.132
na	1156.90442	na	60.944	389.2691
na	1014.858227	na	60.809	366.842
na	1080.153524	na	65.3427	368.7705
na	1080.13897	1.07811	70.4755	363.8268
na	1116.096869	na	66.1035	373.1297
na	1039.408871	0.76696	72.3558	374.3325

The resistivity contour in AL01 displays a structural fracture zone identified as the F1 fault. The reversed fault extends around 6 km with a north-south axis and an eastward dip of about  $80^\circ$ . The fault has a smooth, sloping structure in the horizontal distribution, with a fracture width ranging from 5 to 10 meters. The resistivity are consistent throughout all of the studied areas, with a notable rise in resistivity seen between 600 and 1200 meters down. The lithology of the AL02 segment is constant. The AL03 data indicates areas of low resistivity and poor polarizability on survey line. These regions may suggest the existence of water-filled or damp pathways, such as cracks or permeable zones. The survey line inversion data for AL04 shows a clear link between the location of the ZK02 drill hole and the low-resistance non-polarization zone. This region is the southern extension of the main chamber of Cave. Furthermore, there are noticeable low-resistance anomalies along the expansion path of the Cave auxiliary cave to the south. The conclusion is derived from geophysical prospecting findings and data obtained from hydrogeological exploration.

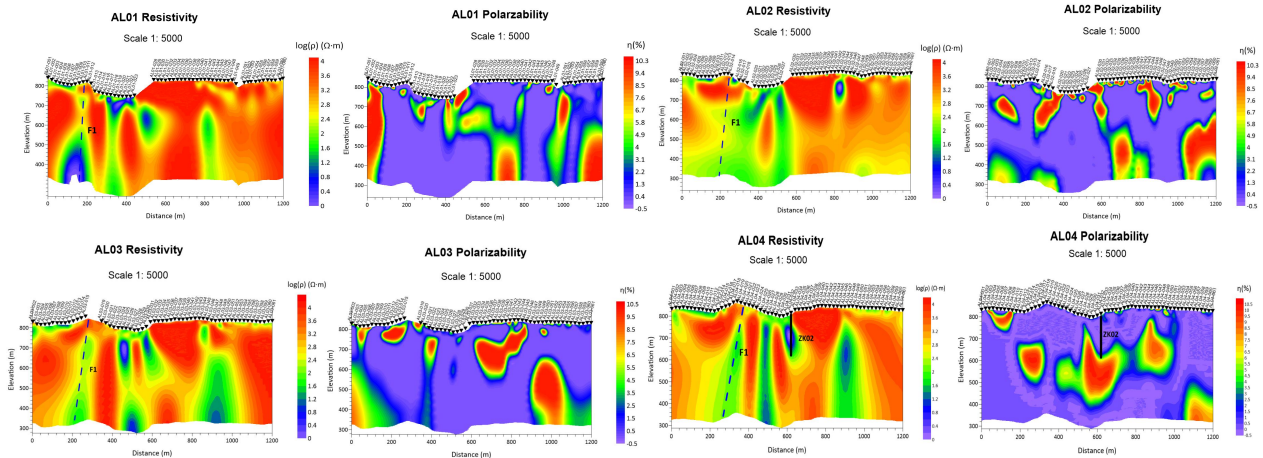


*Figure 1. AL01 - AL04 resistivity and polarizability contour diagrams*

The drilling at Well ZK02 reached a depth of 201.3 meters and found substantial rock cracks and fragmentation. TV camera tests conducted at a distance of 185 meters detected caves at depths ranging from 28 to 32 meters, along with significant fractures occurring between 130 and 150 meters. Geophysical data showed the existence of an aquifer with uncontaminated water in a fractured area, as well as a distinct fracture zone with contaminated water. Minerals such as calcite, dolomite, quartz, and clay minerals, including kaolinite, illite, and montmorillonite, were detected in the well samples by X-ray diffraction (XRD) examination. These minerals may influence the permeability and hydrogeological properties of the karst aquifer system.

## Conclusion

The present research aims to detect anomalies associated with water contamination in karst conduits through a SSIP investigation. According to the study, SSIP surveys can identify polluted water by its low resistance and non-polarization. The research shows that the SSIP investigation is successful in exploring considerable depths and producing accurate results. The work enhances comprehension of water pollution anomalies in karst pipes and provides significant perspectives for monitoring and managing water pollution in karst landscapes.

## References

- LIU, W., CHEN, R., CAI, H., LUO, W. & REVIL, A. 2017. Correlation analysis for spread-spectrum induced-polarization signal processing in electromagnetically noisy environments. *Geophysics*, 82, E243-E256.

# Capacitive coupling in spectral electrical impedance tomography (sEIT) measurements with a centralized multiplexer

Haoran Wang<sup>1</sup>, Johan Alexander Huisman<sup>1</sup>, and Egon Zimmermann<sup>2</sup>

<sup>1</sup> Agrosphere (IBG 3), Institute of Bio- and Geosciences, Forschungszentrum Jülich GmbH, Jülich, Germany. [h.wang@fz-juelich.de](mailto:h.wang@fz-juelich.de)

<sup>2</sup> Electronic systems (ZEA-2), Central Institute of Engineering Electronics and Analytics, Forschungszentrum Jülich GmbH, Jülich, Germany

## Abstract

We analysed capacitive coupling in sEIT measurements associated with different cable types (shielded and unshielded) and measurement approaches (active and passive electrodes) using circuit models and actual sEIT field measurements. The modelling results showed the intricate trade-offs between wire-wire, wire-shield, and shield-soil capacitive coupling for shielded and unshielded cables when using passive electrodes with a centralized multiplexer. The field measurements with a centralized multiplexer and a fan-shaped cable layout with elevated cables showed that unshielded cables showed lower capacitive coupling than shielded cables because of the dominance of wire-shield capacitive coupling. Analysis using the developed circuit models showed that this result is a consequence of the site conditions, and cannot be generalized.

## Introduction

Electromagnetic (EM) coupling effects, including both inductive and capacitive coupling, have long been an essential problem in broadband sEIT measurements. While data correction and filtering methods exist for inductive coupling, addressing capacitive coupling remains complex. Capacitive coupling usually refers to the leakage of electric current through possible capacitances wherever a potential difference exists. Typically, three types of capacitive coupling are considered. The first type is wire-to-wire coupling, which occurs between non-shielded cables with small separation. This type of capacitive coupling can be eliminated by using coaxially shielded cables. The use of coaxial cables results in the second type of capacitive coupling between the inner wire and shield (i.e. wire-to-shield capacity). This type of capacitive coupling can be avoided by using distributed amplifiers at the electrodes for voltage measurements (i.e. active electrodes), but most commercially available systems have a centralized multiplexer with amplifiers at the measurement system (i.e. passive set-up). The third type of capacitive coupling occurs between cable shield and soil and can be reduced by elevating cables above the ground surface. Recently, a fan-shaped cable layout has been proposed for sEIT field measurements, which separates cables for easier survey design and enables model-based corrections for inductive coupling. In such a case, capacitive coupling is the main remaining sources of errors for sEIT measurements in the kHz frequency range. Therefore, the aim of this study is to analyse the three types of capacitive coupling in sEIT measurements for different cable types (shielded and unshielded) and measurement approaches (active and passive set-up) using circuit models and actual sEIT field measurements.

## Methodology

Measurements were carried out at the campus of the Forschungszentrum Jülich using a customized sEIT measurement system. Eleven electrodes with 1 m electrode spacing were used, and the individual cables were arranged in a fan-shaped layout. Three different measurement setups were used for the field measurements. The first setup (active setup, reference measurement) used amplifiers

at the electrodes, which ensures that the voltage at the electrodes is known. The second setup (non-shielded passive setup) has amplifiers close to the system using a custom-made switchbox (i.e. a centralized multiplexer). Unshielded wires are used to connect the electrodes and the switchbox using the same fan-shaped lay-out. The third setup (shielded passive setup) also employs the switchbox, but coaxially shielded cables were used for the connection. This introduces an additional wire-shield capacity, and the developed circuit models showed that the voltage at the electrode can be estimated using a simple voltage divider that requires an estimate of the contact impedance. sEIT measurements were made using a skip-6 circulating measurement scheme from 1 Hz to 10 kHz for all three setups. Since the customized measurement system measures voltages at all electrodes except the electrodes used for current excitation, the potential differences of 396 selected electrode configurations were calculated during post-processing.

## Results

Fig. 1a-c shows the measured imaginary part of the complex impedance using the three measurement setups. Considering the measurements acquired with the active setup (Fig. 1a) as the reference here, it is clear from Fig. 1b that sEIT measurements using the passive setup with non-shielded cables in a fan-shaped layout resulted in accurate sEIT measurements. Based on the developed circuit models, the reasons for this can be analyzed. First of all, the unshielded wires have a large separation in the fan-shaped cable layout, which avoids significant leakage of current between wires. In this particular set of measurements, the cables were elevated about 5-10 cm above ground by the lush grass. This resulted in insignificant capacitive coupling between the shield and ground. Since there is no wire-shield capacitive coupling for unshielded cables, the effects of capacitive coupling were low. Measurements using the passive setup with shielded cables (Fig. 1c) showed larger variation at higher frequencies above 1 kHz. This is due to the high cable-shield capacity. After correction of the cable-shield capacity using the developed circuit model, the variation at 10 kHz has been largely reduced. Remaining errors are due to approximations in the correction approach.

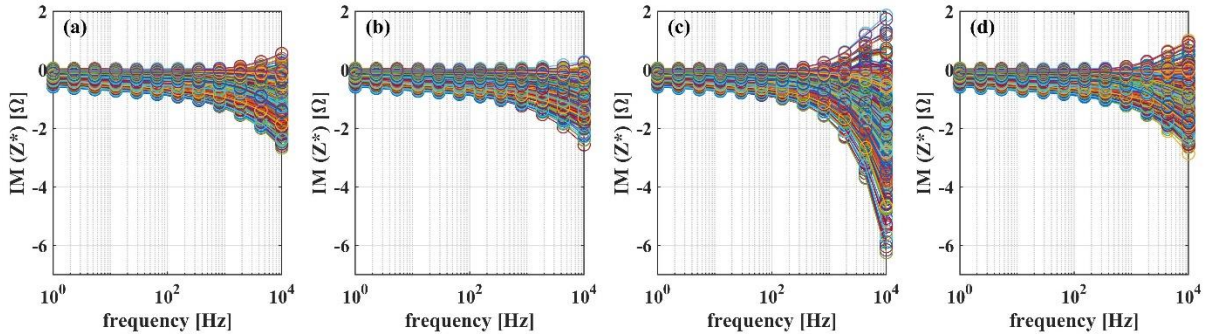


Fig. 1 Measured imaginary part of complex impedances using: (a) active setup, (b) passive setup with unshielded cables, (c) passive setup with shielded cables before and (d) after correction.

## Conclusions and outlook

The sEIT field measurements with a centralized multiplexer and a fan-shaped cable layout with elevated cables showed that unshielded cables showed lower capacitive coupling than shielded cables because of the dominance of wire-shield capacitive coupling. Analysis using the developed circuit models showed that this result is a consequence of the site conditions, and cannot be generalized. Overall, it was concluded that the combination of circuit models with sEIT measurements with different cable types and measurement approaches provided valuable insights in the intricate trade-offs between different types of capacitive coupling. Future research should focus on the quantitative evaluation of the correction approach for wire-shield capacity for shielded cables and 3D modelling of the passive set-up with unshielded cables to allow for sEIT measurements with this setup for larger layouts and in resistive soil environments.

# Induction effect removal in High-Frequency Induced Polarization data

R. Schulz<sup>1</sup>, M. Sugand<sup>1</sup>, A. Hördt<sup>1</sup>

<sup>1</sup>Institut für Geophysik und extraterrestrische Physik, TU Braunschweig, Germany, r.schulz@tu-braunschweig.de

In Induced Polarization (IP) data analysis, it is commonly assumed that the induction number

$Q = L * \sqrt{\frac{\mu_0 * \omega}{2\rho}}$  is small compared to one. The induction number depends on the investigation scale  $L$ , the angular frequency  $\omega$  and the resistivity  $\rho$  (McNeill et al., 1980). At low induction numbers, induction effects (IE) can be neglected in favor of polarization mechanisms. When operating with higher frequencies on field scale, particularly in areas with a relatively conductive subsurface, induction effects cannot always be disregarded.

The “Chameleon II” device, developed by Radic Research for field applications, performs High-Frequency Induced Polarization (HFIP) measurements by extending the frequency range typically used for IP measurements up to 230 kHz. A primary application of HFIP lies in estimating ice content in permafrost regions. In previous work by Przyklenk et al. (2016) and Mudler et al. (2019) it was argued that induction was negligible for the considered cases due to low induction numbers. However, artic permafrost mires are characterized by lower resistivities compared to other permafrost regions, such as high mountains. This combination of lower resistivities and high frequencies can lead to a potentially strong impact of induction effects.

The objective of our recent study is to interpret HFIP data while accounting for the influence by induction effects. We developed tools to do simulations with and without induction effects to assess the conditions under which induction can be considered negligible. Our simulation methods are based on CR1Dmod by Ingeman-Nielsen & Baumgartner (2006) combined with the complex resistivity model by Zorin and Ageev (2017). Simulations for typical models show that IE can be a disruptive factor in permafrost exploration. In unfavorable cases, the influence of IE can lead to the phase peak characteristic of the polarization of water ice between 100 Hz and 100 kHz (Petrenko, 1999) no longer being visible or its magnitude and peak frequency can be impacted (Figure 1).

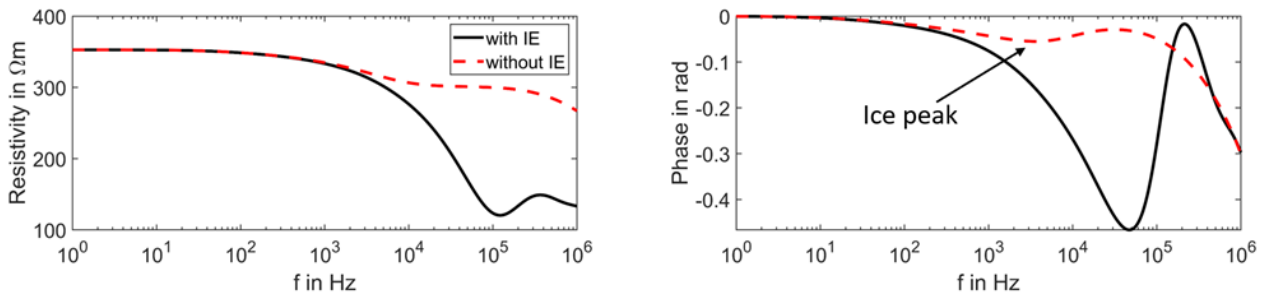


Figure 1: Resistivity (left) and phase shift (right) for a simulation with and without induction effects for a 1D model with the following parameters:  $\rho_{DC,m} = 100 \Omega\text{m}$ ,  $\epsilon_m = 30$ ,  $\alpha = 0.4$ ,  $k = 0.4$ ,  $\rho_{DC,i} = 10^7 \Omega\text{m}$ ,  $\epsilon_{HF,i} = 3.1$ ,  $\epsilon_{DC,i} = 91.5$ ,  $\tau_i = 2.2 * 10^{-5} \text{ s}$

To mitigate the impact of induction effects to our data, we developed a 1D inversion program based on the simulation methods. This inversion code is capable of fitting data with induction effects and using the result to calculate induction-free data, which can then be used in conventional Spectral Induced Polarization inversion codes. The program was tested with synthetic datasets, an example is shown in figure 2.

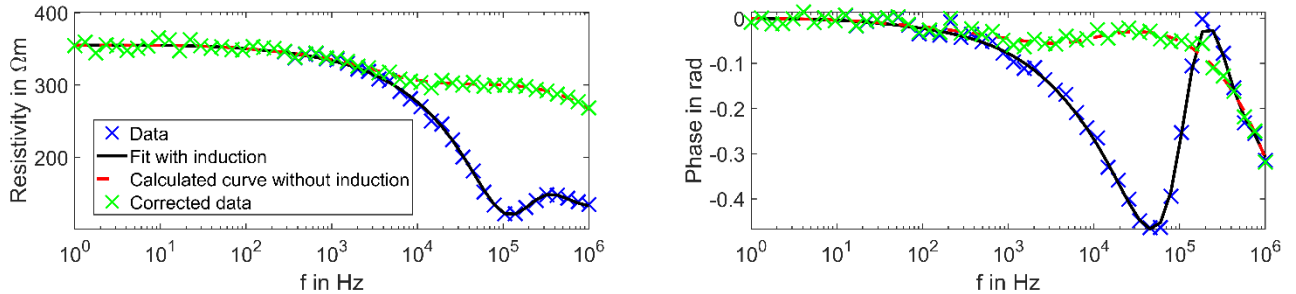


Figure 2: Resistivity (left) and phase shift (right). The noisy dataset (blue), simulated by using the same parameters as in figure 1, was fitted while accounting for IE (black). The final parameters are used to calculate a curve without induction (red). The difference between the fit and the calculated curve was subtracted from the dataset to get the corrected data (green).

We also analyse field data from different sites (permafrost and non-permafrost) and show that the data is affected by IE that may be well explained by our simulation codes. After the application of our correction procedure, the data is ready for processing with conventional IP interpretation tools, such as induction-free 2D inversion.

## References

- Ingeman-Nielsen, T., & Baumgartner, F. (2006). CR1Dmod: A Matlab program to model 1D complex resistivity effects in electrical and electromagnetic surveys. *Computers & Geosciences*, 32 (9), 1411–1419.
- McNeill, J. D., et al. (1980). Electromagnetic terrain conductivity measurement at low induction Numbers, Technical note TN-6, Geonics Ltd.
- Mudler, J., Hördt, A., Przyklenk, A., Fiandaca, G., Maurya, P. K., & Hauck, C. (2019). Two dimensional inversion of wideband spectral data from the capacitively coupled resistivity method—first applications in periglacial environments. *The Cryosphere*, 13 (9), 2439–2456.
- Petrenko, V. F., & Whitworth, R. W. (1999). Physics of ice. OUP Oxford.
- Przyklenk, A., Hördt, A., & Radić, T. (2016). Capacitively Coupled Resistivity measurements To determine frequency-dependent electrical parameters in periglacial environment—theoretical considerations and first field tests. *Geophysical Journal International*, 206 (2), 1352–1365.
- Zorin, N., & Ageev, D. (2017). Electrical properties of two-component mixtures and their application to high-frequency IP exploration of permafrost. *Near Surface Geophysics*, 15 (6), 603–613.

# High-frequency induced polarisation: Data inversion and ice-relaxation modelling

Madhuri Sugand<sup>1</sup>, Andreas Hördt<sup>1</sup>, Andrew Binley<sup>2</sup>

<sup>1</sup>*Institute of geophysics and extraterrestrial physics, Technical University of Braunschweig, Germany, [m.sugand@tu-braunschweig.de](mailto:m.sugand@tu-braunschweig.de)*

<sup>2</sup>*Lancaster Environment Centre, Lancaster University, United Kingdom*

In recent years, advances in instrument technology have allowed for measurement of Spectral Induced Polarisation (SIP) data in a wider frequency range. Conventionally, SIP is measured from 1 mHz to 1 kHz, focusing on the polarization of the electrical double layer. The motivation for extending measurements beyond this range is to capture the polarisation of ice which occurs between 1 kHz and 100 kHz. At these higher frequencies over resistive ground, the permittivity of materials has an influence on current flow, and specifically, permittivity of ice exhibits a characteristic temperature-dependent complex nature. Recent studies that measure polarisation of permafrost regions prove its feasibility to estimate ice-content (Grimm and Stillman, 2015; Mudler et al. 2022; Maierhofer et al. 2022). The method is termed high-frequency polarisation (HFIP) to distinguish it from conventional SIP measurements.

Field application of HFIP poses challenges during data acquisition. Ground type and temperature controls aspects such as: electrode type, survey configuration, signal quality, and cable-earth coupling. Furthermore, usual inversion routines inherently assume low phase shifts, however, in the presence of ice, phase shifts may theoretically reach up to -90° or greater than 1500 mrad (for pure ice). With this in mind, new insights from recent field campaigns conducted are presented with HFIP application in an ice-rich peat permafrost mire in northern Sweden.

The HFIP dataset is inverted as separate frequencies to control error propagation and understand the distribution of resistivity and phase shift without an assumed relaxation model. The 2-D inversion is performed with ResIPy, a Python wrapper around the R\* family of codes (Blanchy et al. 2020; Binley and Slater, 2020). Data error for each frequency is estimated based on a small set of reciprocal measurements, as presented in Binley and Slater (2020). It is observed that the inversion successfully accommodates high phase shifts, and the inversion error (calculated vs raw data) is deemed acceptable for every frequency.

Subsequently, the inverted dataset undergoes additional fitting with a petrophysical relaxation model, providing volumetric ice-content estimates (Zorin and Ageev, 2017). Notably, the fitting process is sensitive to starting model values, highlighting the importance of reasonable prior knowledge about the field site. Prior knowledge may include past ice-content estimates, lithology, soil moisture and vegetation, and insights learnt from the HFIP 2D inversion itself. The analysis of inverted spectra, including phase peak frequency, phase peak value, and the general shape of the phase spectrum, allows to differentiate zones within the 2D section. Correspondingly, these zones are assigned distinct starting model values. The results of this derived ice-content estimates are compared to a permafrost core extracted at the site and are found to be within 10% accuracy. Thus, the implemented objective approach for inverting HFIP data and subsequent quantitative analysis appears effective with an acceptable level of uncertainty in ice-rich peatland permafrost.

## References

- Blanchy, G., Saneiyan, S., Boyd, J., McLachlan, P. and Binley, A., 2020. ResIPy, an intuitive open source software for complex geoelectrical inversion/modeling. *Computers & Geosciences*, 137, p.104423.
- Binley, A. and Slater, L., 2020. Resistivity and induced polarization: Theory and applications to the near-surface earth. Cambridge University Press.
- Grimm, R.E. and Stillman, D.E., 2015. Field test of detection and characterisation of subsurface ice using broadband spectral-induced polarisation. *Permafrost and Periglacial Processes*, 26(1), pp.28-38.
- Maierhofer, T., Hauck, C., Hilbich, C., Kemna, A. and Flores-Orozco, A., 2022. Spectral induced polarization imaging to investigate an ice-rich mountain permafrost site in Switzerland. *The Cryosphere*, 16(5), pp.1903-1925.
- Mudler, J., Hördt, A., Kreith, D., Sugand, M., Bazhin, K., Lebedeva, L. and Radić, T., 2022. Broadband spectral induced polarization for the detection of Permafrost and an approach to ice content estimation—a case study from Yakutia, Russia. *The Cryosphere*, 16(11), pp.4727-4744.
- Zorin, N. and Ageev, D., 2017. Electrical properties of two-component mixtures and their application to high-frequency IP exploration of permafrost. *Near Surface Geophysics*, 15(6), pp.603-613.

# IP-distorted Transient Electromagnetic data modelling

Fereydoun Sharifi\*, Büлent Tezkan, Ismael M. Ibraheem, Pritam Yogeshwar, Rainer Bergers

*Institute of Geophysics and Meteorology, University of Cologne, Germany*

\* Corresponding author: F.Sharifi@uni-koeln.de, Sharifi.sena@gmail.com

## Abstract

Transient electromagnetic (TEM) methods are commonly employed for subsurface conductivity characterization in environmental investigation, hydrogeology, mineral exploration, as well as permafrost and glacier studies. The observed electromagnetic data are often associated with IP effect which distorts the observed TEM data (Weidelt, 1982; Seidel and Tezkan, 2017; Kozhevnikov and Antonov, 2021; Sharifi and Tezkan, 2023). Therefore a reliable interpretation needs to incorporate IP effect into the modelling of this data.

Beside enabling a more reliable interpretation of TEM data, considering the IP effect may provide a valuable insight into the electrical features, structure and texture of the subsurface chargeable target. However, the IP effect can pose a significant issue if overlooked, as it can distort model parameters that control the electromagnetic induction, namely the conductivity distribution of the subsurface model (Auken et al., 2017; Sharifi et al., 2020).

The objective of this study is to incorporate IP effects in the forward modelling and to recover the IP parameters from distorted TEM data using an efficient inversion algorithm. To achieve this aim, we developed a 1D forward and inversion code to investigate the incorporation of IP effects using different IP parameterizations including Cole-Cole, maximum phase angle (MPA), maximum imaginary conductivity (MIC) (Fiandaca et al., 2018) and the Jeffrey transform of Cole-Cole parameters (Ghorbani et al., 2007). For a 1D inversion of distorted TEM data we used the Levenberg-Marquardt algorithm. However, the result of inversion strongly depends on the starting model.

The result of 1D forward calculation and inversion of synthetic TEM data revealed that the Cole-Cole parametrization is more robust and reliable than MPA, MIC, and Jeffrey transform. Moreover, we performed a 3D TEM modelling to study the effect of 3D geometry which can cause a similar sign reversal in the TEM data as the IP effect.

To evaluate the performance of our algorithm using field data, we carried out a 1D inversion of TEM data acquired along a profile that traverses a landfill located near Cologne, Germany.

Furthermore, to obtain a priori information and validate the results of TEM data modelling, we conducted an electrical resistivity tomography (ERT) and time-domain IP (TDIP) survey along the TEM profile. A 2D inversion was used to retrieve the Cole-Cole parameters as input for TEM interpretation. By including the IP information, the TEM field data can be explained quantitatively, and a consistent and improved interpretation of the waste body is achieved.

**Keywords:** Transient Electromagnetic; Induced Polarization; Cole-Cole; Inversion; Landfill

## References

- Auken, E., Boesen, T., & Christiansen, A. V., 2017. A review of airborne electromagnetic methods with focus on geotechnical and hydrological applications from 2007 to 2017. *Advances in geophysics*, 58, 47–93.
- Fiandaca, G., Madsen, L. M., and Maurya, P. K., 2018. Re-parameterisations of the Cole–Cole model for improved spectral inversion of induced polarization data. *Near Surface Geophysics*, 16(4), 385–399.
- Ghorbani, A., Camerlynck, C., Florsch, N., Cosenza, P. and Revil, A., 2007. Bayesian inference of the Cole–Cole parameters from time-and frequency-domain induced polarization. *Geophysical prospecting*, 55(4), 589–605.
- Kozhevnikov, N. O., & Antonov, E. Y., 2020. Aftereffects in the transient electromagnetic method: inductively induced polarization. *Russian Geology and Geophysics*, 62(12), 1440–1448.
- Seidel, M., & Tezkan, B., 2017. 1D Cole-Cole inversion of TEM transients influenced by induced polarization. *Journal of Applied Geophysics*, 138, 220–232.
- Sharifi, F., & Tezkan, B., 2023. Recovering the Induced Polarization Effect from 1-D Coupled Inversion of TEM Data. In NSG2023 29th European Meeting of Environmental and Engineering Geophysics (Vol. 2023, No. 1, pp. 1–5). European Association of Geoscientists & Engineers.
- Sharifi, F., Arab-Amiri, A. R., Kamkar-Rouhani, A., & Börner, R. U., 2020. Development of a novel approach for recovering SIP effects from 1-D inversion of HEM data: Case study from the Alut area, northwest of Iran. *Journal of Applied Geophysics*, 174, 103962.
- Weidelt, P., 1982. Response characteristics of coincident loop transient electromagnetic systems. *Geophysics*, 47(9), 1325–1330.

# The use of Reciprocals for TDIP in volcanic areas

Lore Vanhooren<sup>1,3</sup>, Warre Dekoninck<sup>1</sup>, Adrian Flores-Orozco<sup>2</sup>, Corentin Caudron<sup>3</sup>, Thomas Hermans<sup>1</sup>

<sup>1</sup> Laboratory of applied Geology and Hydrogeology, Ghent University, Ghent, Belgium, [Lore.Vanhooren@ugent.be](mailto:Lore.Vanhooren@ugent.be)

<sup>2</sup>TU-Wien, Geophysics Research Group, Department of Geodesy and Geoinformation, Vienna, Austria.

<sup>3</sup>G-Time Laboratory, Universite Libre de Bruxelles, Brussels, Belgium.

Geo-electric methods such as ERT and IP have become increasingly important in the characterization of volcanic and geothermal systems. With the ERupT project, we aim to assess the suitability of these methods to visualize the dynamic behavior of volcanic hydrothermal systems, with the long-term aim of improving hazard assessment associated with phreatic/hydrothermal eruptions. The methods are sensitive to changes in temperature, saturation, mineralizations, and the presence of alteration clays, all of which can potentially change in time in this context.

The first phase of the project includes the characterization of our study site, followed by the installation of a semi-permanent ERT/IP profile measuring daily the resistance and chargeability. The study area is located in the Reykjanes geothermal field, Iceland, which is a relatively small (<2km<sup>2</sup>), high-temperature geothermal area, with reservoir temperatures reaching up to 200 °C. The area itself is unique due to its proximity to the ocean, as a result, the geothermal fluid is chemically altered seawater. Chemical analysis shows that almost no mixing occurs with meteoric water making it a purely seawater-fed geothermal system. Infiltrating rainwater forms a lens on top of the saline water of approximately 30 m thickness. The ERT inversion results (not shown here) clearly distinguish the high-temperature, high salinity groundwater at depth, the un-altered basalt in the freshwater zone, and surface alterations.

In both the characterization and monitoring phases, reciprocals are measured to assess the data quality and estimate the error level for subsequent inversion. The use of reciprocals has been well-established in the field. Relying on the reciprocity theorem, if the potential and current electrodes are interchanged, the response of the subsurface should be identical, given linear behavior of the subsurface (Parasis, 1988). Our data show a very good fit between the normal and reciprocal ERT measurements collected with a multiple-gradient array. However, the TDIP data tells a different story. Figure 1 shows pseudosections of the apparent chargeability of both the normal and reciprocal measurements before any advanced processing steps are done. On the image, the discrepancy between normal and reciprocal is abundantly clear, the normal profile shows an area of high chargeability between 250 and 320 m. The reciprocal also shows this, albeit not as pronounced, but has a second area of high chargeability between 0 and 100 meters, which is not present in the normal profile. We believe the difference between the normal and reciprocal does not stem from a systematic error but is founded in the non-linearity of the system in response to the different injection geometry with a normal and reciprocal multi-gradient array. We hypothesize the difference can be caused by oxido-reduction processes as is likely the case here due to the nature of the site. The high chargeability zone on the reciprocal between 0 and 100 meters coincides with an area of intense alteration and abundant

mineralizations. The area of high chargeability that is present on both profiles does not coincide with surface alterations but suggests activity deeper in the subsurface, which leads us to believe that this area is undergoing alteration processes that will in time be expressed on the surface.

Due to the discrepancy, the traditional use of reciprocals is not recommended as it would 1) remove many data points within these areas that are potentially of good quality and 2) it would not provide an accurate error model for the inversion. Hence methods relying fully on the analysis of decay curves are better suited. For example, Flores-Orozco et al, 2018, use decay curve analysis both for the removal of bad data points and the definition of the error model, omitting the need for reciprocal measurements completely. In this case, decay curves with a high signal-to-noise ratio are observed in both anomalies, for both normal and reciprocal data, but with different amplitudes. Our data set suggests that the measurement of reciprocals in nonlinear systems is still relevant as it can provide valuable information that would otherwise be missed.

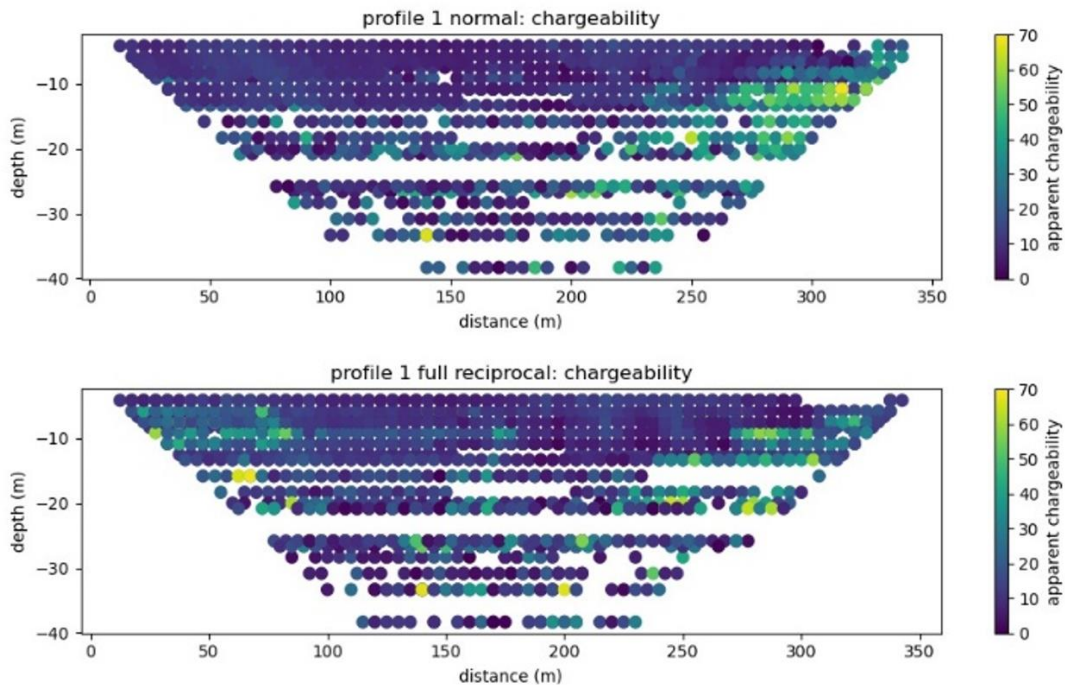


Figure 1: Apparent chargeability pseudosection for the normal (top) and its corresponding reciprocal (bottom) profile. The data has undergone minimal filtering, keeping only values between 0 and 70.

## References

- Flores Orozco, A., Gallistl, J., Bücker, M., Williams K.H., 2018, Decay curve analysis for data error quantification in time-domain induced polarization imaging. *Geophysics*, 83 (2), E75-E86
- Parasnis, D., 1988, Reciprocity theorems in geoelectric and geoelectromagnetic work. *Geoexploration*, 25(3), 177-198

# Variational Mode Decomposition for Estimating Uncertainties in Time-domain Induced Polarization Data

Khuram Naveed<sup>1</sup>, Line Meldgaard Madsen<sup>2</sup>, Denys Grombacher<sup>2</sup>, Jakob Juul Larsen<sup>1</sup>

<sup>1</sup>*Department of Electrical and Computer Engineering, Aarhus University, Denmark, knaveed@ece.au.dk*

<sup>2</sup>*Department of Geoscience, Aarhus University, Denmark*

Time-domain induced polarization (TDIP) data, like other geophysical methods, suffers from poor signal-to-noise ratio (SNR) problem due to the introduction of an overwhelming level of noise from natural and anthropogenic sources [1]. Hence, acquired data is pre-processed to mitigate the noise problem whereby prior information about the dominant anthropogenic and naturally occurring sources of noise is exploited to model and subtract the noise. This type of model-based (noise) subtraction (MBS) method for TDIP data denoising relies on well-defined noise models, e.g., powerline harmonics, spikes, drift noise etc. [2]. On the contrary, random noise components coming from electric devices and environmental factors along with the residues of the subtracted noise do not have such a well-defined model. That means, a significant part of noise still remains a big part of the recovered IP decay even after removal of harmonic, spikes and drift noise through the MBS method. Our recent work in [3] proposes the use of variational mode decomposition (VMD) to address this problem where a compromise on the initial part of the IP decay may be necessary to fully suppress noise components. The otherwise case requires permissibility of noise in the recovered signal. That results in the uncertainties within the gates and the fitted Cole-Cole (CC) models and inversion parameters [4]. A prior knowledge of uncertainties or error bars in the TDIP data allows the estimation of realistic CC fits and reliable inversion and interpretation. Existing error bar estimation methods are cumbersome and painfully time taking process because these require many repeated measurements of the data being acquired.

This abstract introduces a novel approach to this problem using the VMD that does not need repeated measurements of the IP waveform data. Since VMD algorithm retrieves most of the IP decay in its first IMF owing to the predominantly low frequency spectra of the IP decay [3]. Therefore, the rest of the IMFs are mostly composed of noise, which means a good estimate of the noise in the TDIP data can be obtained by adding the remaining IMFs. This way, noise from all the acquired TDIP data can be segregated from their respective IP decays (up to a high level of accuracy). A reasonable estimate of the uncertainties in the pre-processed TDIP data can be obtained by computing standard deviation (SD) of the retrieved noise records. For VMD to be suitable for error bar estimation, the SDs obtained through the VMD retrieved noise records must be close to the SDs obtained from the repeated measurements of TDIP data. To show that, we construct an experiment for a proof of concept via a synthetic experiment reported in Fig. 1 which is described in detail below.

We start by generating an IP decay waveform via AarhusInv software [6], that computes following Cole-Cole model [4] for the parameter values,  $\rho = 75$ ,  $m_0 = 50$ ,  $\tau_i = 3.5$  and  $C = 0.45$ . Next, we generate 1000 different random noise plus sinusoidal artefacts using the synthetic model described in

[3]. Note here we assume that harmonic noise has already been subtracted during preprocessing that leaves the random noise and the residues of the subtracted noise (modelled as low frequency sinusoids). Subsequently, we add these noise records to the IP decay to generate 1000 noisy examples of the same IP decay, to mimic the repeated measurements of 1000 stacks of TDIP data from the same electrode. Henceforth, we segregate the noise and the IP decay from each noisy example. Finally, we compute standard deviation of the VMD extracted noises from 1000 noisy TDIP examples and compare those against the estimated SDs of the noisy examples, see Fig. 1. Observe from Fig. 1d that, standard deviations estimated through the VMD of the segregated noise are very close to the true standard deviation estimates obtained by the 1000 noisy examples of same IP decay waveform, except at the earlier part where VMD underestimate the IP signal. The consistency of the error bars obtained using VMD with those from the true estimates proves that the VMD algorithm can isolates the noise from the IP decay (except the earlier part) and hence, it potential to be a reliable and a convenient way to estimate the uncertainties in the TDIP data.

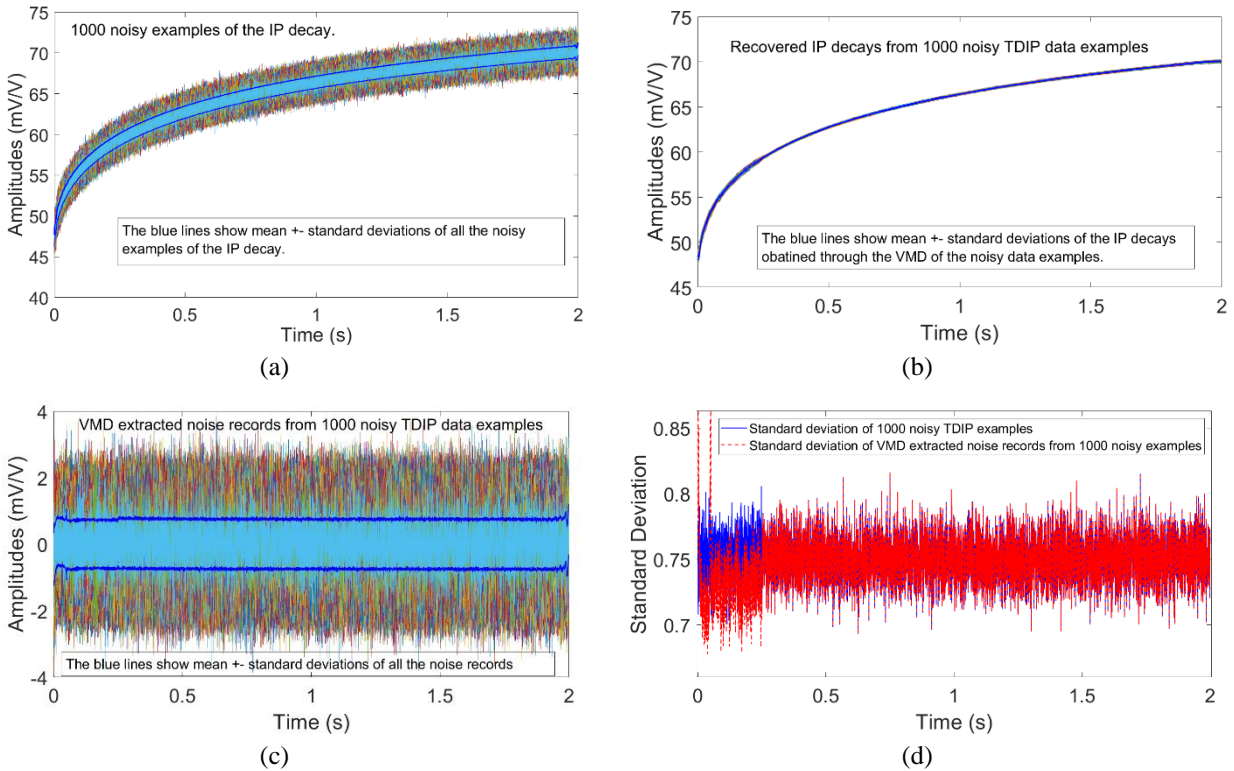


Figure 1: A proof of concept of how standard deviation of noise records extracted through VMD of 1000 noisy examples of TDIP data is close to the standard deviation of original noisy examples.

## References:

1. Everett, M. E. Near-surface applied geophysics. Cambridge University Press, 2013.
2. Butler, K. E. and Russell, R. D., "Subtraction of powerline harmonics from geophysical records," *Geophysics*, **58**(6), 898–903, 1993.
3. Olsson, P.-I., Fiandaca, G., Larsen, J. J., Dahlin, T. and Auken, E., "Doubling the spectrum of time-domain induced polarization by harmonic de-noising, drift correction, spike removal, tapered gating and data uncertainty estimation," *Geophysical Supplements to the Monthly Notices of the Royal Astronomical Society*, **207**(2), 774–784, 2016.
4. Naveed, K., Madsen, L. M., Grombacher, D., Larsen, J. J., "Processing time-domain induced polarization data using variational mode decomposition," *IEEE transactions on Geoscience and remote sensing*, **62**, pp. 1–13.
5. Pelton, W. H., Ward, S., Hallof, P., Sill, W. and Nelson, P. H. [1978] Mineral discrimination and removal of inductive coupling with multifrequency ip. *Geophysics*, **43**(3), 588–609.
6. Auken, E., Christiansen, A. V., Kirkegaard, C., Fiandaca, G., Schamper, C., Behroozmand, A. A., Binley, A., Nielsen, E., Effersø, F., Christensen, N. B. et al. [2015] An overview of a highly versatile forward and stable inverse algorithm for airborne, ground-based and borehole electromagnetic and electric data. *Exploration Geophysics*, **46**(3), 223–235.

# Investigating induced polarization in Floatem Data

S. Galli<sup>\*,1</sup>, A. Signora<sup>1</sup>, F. Schaars<sup>2</sup>, M. Grohen<sup>3</sup>, G. Fiandaca<sup>1</sup>

<sup>1</sup> The EEM Team for Hydro and eXploration, Dep. of Earth Sciences A. Desio, Università degli Studi di Milano, Milano (Italy)

<sup>2</sup> Artesia Water, Schoonhoven, The Netherlands, f.schaars@artesa-water.nl

<sup>3</sup> Wiertsema & partners, Tolbert, The Netherlands, michelgroenstaal@gmail.com

\* stefano.galli2@unimi.it

In this abstract, we present a case study where FloaTEM data (Maurya et al., 2022) are inverted within the EEMverter inversion suite (Fiandaca et al., 2024) accounting also for induced polarization, using the Maximum Phase Angle (MPA) re-parameterisation of the Cole-Cole model (Fiandaca et al., 2018).

The FloaTEM system (Fig. 1) is a dual moment TEM system in offset configuration, mounted on 3 boats for continuous acquisition: the front boat carries the instruments and tows the transmitter and receiver, mounted on mid and rear boats, respectively. An echo-sounder synchronized with a GPS was added to record bathymetry.

The survey consists of 65 km of FloaTEM data acquired in the IJsselmeer lake in Andijk, the Netherlands (Fig. 2). The inversion tests accounting for induced polarization have been carried out on a representative part of the survey (line 540) where the geology of the area is known: a ~5 m freshwater column overlays a few meters thick clay layer and a sandy aquifer filled with saline water (until 1932, when the Afsluitdijk was built, this area was part of the North Sea).

The data do not present the classic induced polarization signature: fast decays or polarity



Figure 1: deployed FloaTEM system in the Po River, Northern Italy



Figure 2: IJsselmeer survey area. In black the FloaTEM soundings, in yellow Line 540 used as an example for this abstract

Figure 3: resistivity only inversion (top), resistivity model with MPA Cole-Cole reparameterization (bottom). In red, the surface of the bottom of the lake.

inversion in the decays. In fact, a good misfit was reached in the resistivity only inversion; yet, being present a known polarizable medium, an inversion taking into account induced polarization was carried out, with the MPA reparameterization of the Cole-Cole formula.

The models (Fig. 3) obtained with and without accounting for

induced polarization are consistent with each other, with a small change in deeper resistivities and in the depth of investigation (DOI). However, looking at the phase distribution model (Fig. 4), a meaningful polarization contrast is evident: the water column results non-polarizable, while a chargeable 2 m thick layer exactly coincident with the conductive layer below the water is identified, i.e. clay.

Being able to identify polarizable layers in inductive data without sign-changes is not a given, but this example shows that, with the right modelling, subtle IP effects might be identified.

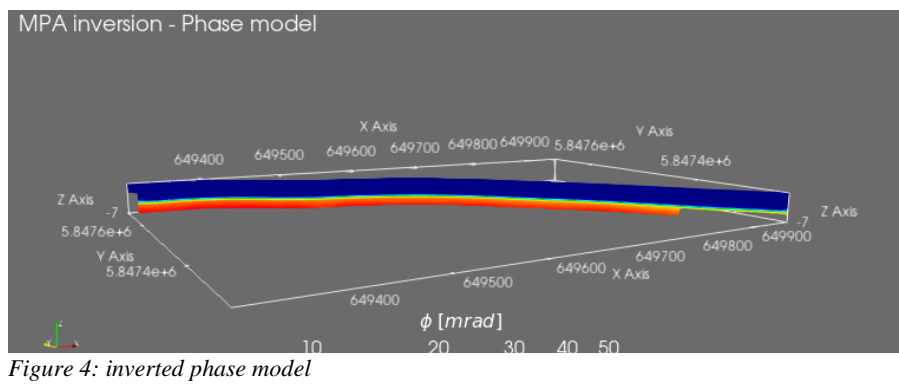
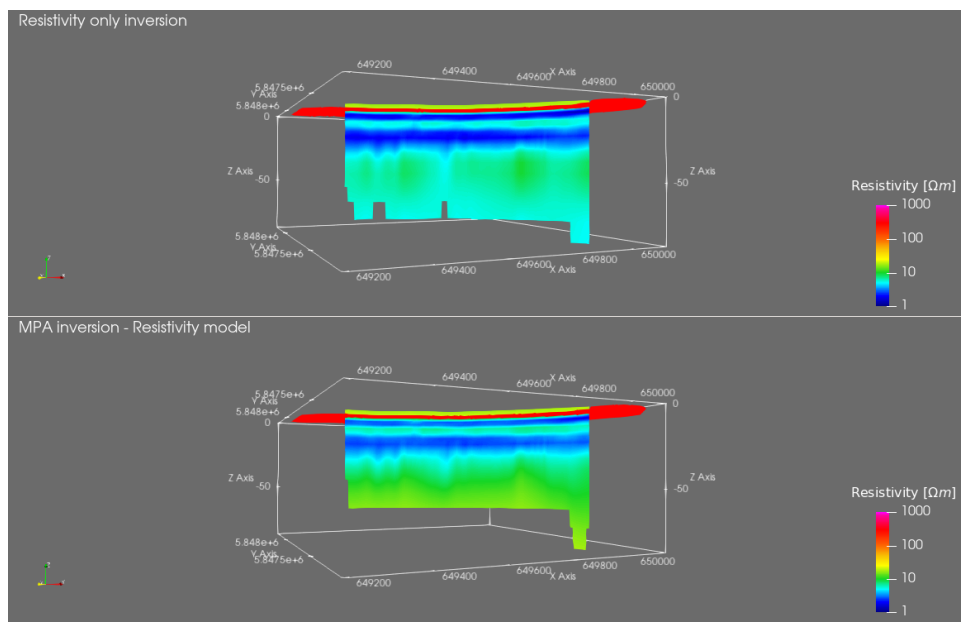


Figure 4: inverted phase model

## References

- Fiandaca, G., Madsen, L. M., & Maurya, P. K. (2018). Re-parameterisations of the Cole–Cole model for improved spectral inversion of induced polarization data. *Near Surface Geophysics*, 16(4), 385-399.
- Fiandaca, G., Zhang, B., Chen, J., Signora, A., Dauti, F., Galli, S., Sullivan, N.A.L., Bollino, A. and Viezzoli, A, 2024. Closing the gap between galvanic and inductive induced polarization: EEMverter, a new modelling tool for Electric and Electromagnetic data. *7th international IP workshop, 28-30 May 2024, Lund, Sweden*.
- Maurya, Pradip Kumar, et al. "Efficient imaging of hydrological units below lakes and fjords with a floating, transient electromagnetic (FloaTEM) system." *Hydrology and Earth System Sciences* 26.11 (2022): 2813-2827.
- Maurya, P. K., Grombacher, D., Lind, J., Lane, J. W., & Auken, E. (2022). Inversion of induced polarization-affected towed-transient electromagnetic data in a lateritic regolith geology: A case study from western Tanzania. *Geophysics*, 87(4), B247-B254.

# Inversion of galvanic time-domain IP data in terms of Debye-Warburg decomposition

Arcangela Bollino<sup>\*,1</sup>, Gianluca Fiandaca<sup>1</sup>

<sup>1</sup> The EEM Team for Hydro & eXploration, Department of Earth Sciences “Ardito Desio”, Università degli Studi di Milano, Milano (Italy)

\* [arcangela.bollino@unimi.it](mailto:arcangela.bollino@unimi.it)

The induced polarization (IP) method yields images of the complex resistivity (CR) of the subsurface, which provides information about the conduction and polarization properties of the measured soils or rocks. The measurements can be performed at different frequencies (typically below 10 kHz), in the so-called spectral IP (SIP) method, to obtain information about the frequency dependence of the CR. SIP data are usually analysed and related to petro-hydro, or biogeophysical properties by means of empirical or mechanistic models. Two types of empirical model approaches can be distinguished: The first type describes SIP data using one or a few polarisation peaks (i.e., local maxima) in the absolute phase spectrum (or imaginary conductivity spectrum) with corresponding, distinct relaxation times. This includes the Debye model (Debye, 1960) and the class of Cole-Cole-type models (Cole and Cole, 1941; Pelton *et al.*, 1978; Dias, 2000). The second approach describes the SIP response using a linear superposition of a large number of elementary Debye polarisation terms following a given distribution of relaxation times. This procedure of determining a relaxation time distribution (RTD) instead of a fixed number of relaxation times is referred to as Debye decomposition (DD) (Nordsiek and Weller, 2008). With this approach, the observed CR is represented as a superposition of a large number of Debye relaxation terms at relaxation times  $\tau_k$ :

$$\rho^*(\omega) = \rho_0 \left( 1 - \sum_{k=1}^N m_k \left[ 1 - \frac{1}{1 + (j\omega\tau_k)^c} \right] \right) \quad (1)$$

where  $N$  is the number of relaxation times (i.e., Debye polarization terms) used for the superposition,  $\rho_0$  is the DC resistivity,  $m_k$  is the  $k$ -th chargeability corresponding to the  $k$ -th relaxation time. The frequency dispersion of the kernel functions in the decompositions is controlled by the chosen fixed value for  $c$ , with the DD resulting for  $c=1$  and a Warburg decomposition (Revil *et al.*, 2014) resulting for  $c=0.5$ .

In this scenario, EEMverter (Fiandaca *et al.*, 2024), a novel software to model IP in electric and electromagnetic (EM) data, allows a parametric definition of electrical properties, such that the (complex) electrical conductivity/resistivity through functions, also integrating petrophysical relations. In particular, the Debye-Warburg decomposition parametrization is also available for inversion of field data, with selectable number of relaxation peaks per frequency decade: typically, one peak per frequency decade is enough for inverting field data.

A synthetic example mimicking unconsolidated sediments is presented in Figure 1. Following Römhild *et al.*, (2022), the forward response was computed by using the WhyCDF model space,  $\mathbf{m}_{WhyCDF} = \{\sigma_w, K, D_+, F\}$

where  $\sigma_w$  and  $K$  are water and hydraulic conductivity, respectively,  $D_+$  is the diffusion coefficient in the Stern layer and  $F$  is the formation factor. Full-decay time-domain IP are modelled with a multiple-gradient sequence, and the inversion is performed with a Warburg model space with three relaxation times at  $10^{-2}$ ,  $10^{-1}$  and  $10^0$  seconds:

$$\mathbf{m}_{Warburg} = \{\rho_0, m_1, m_2, m_3..\}$$

where  $\rho_0$  is the DC resistivity and  $m_1, m_2, m_3$  are the chargeabilities.

Figure 2 presents the inversion results of the Warburg decomposition, showing a good accordance with the spectral simulated spectral properties. We believe that this new inversion scheme will help in comparing laboratory and field results, offering a modelling framework that allow a direct comparison of the results.

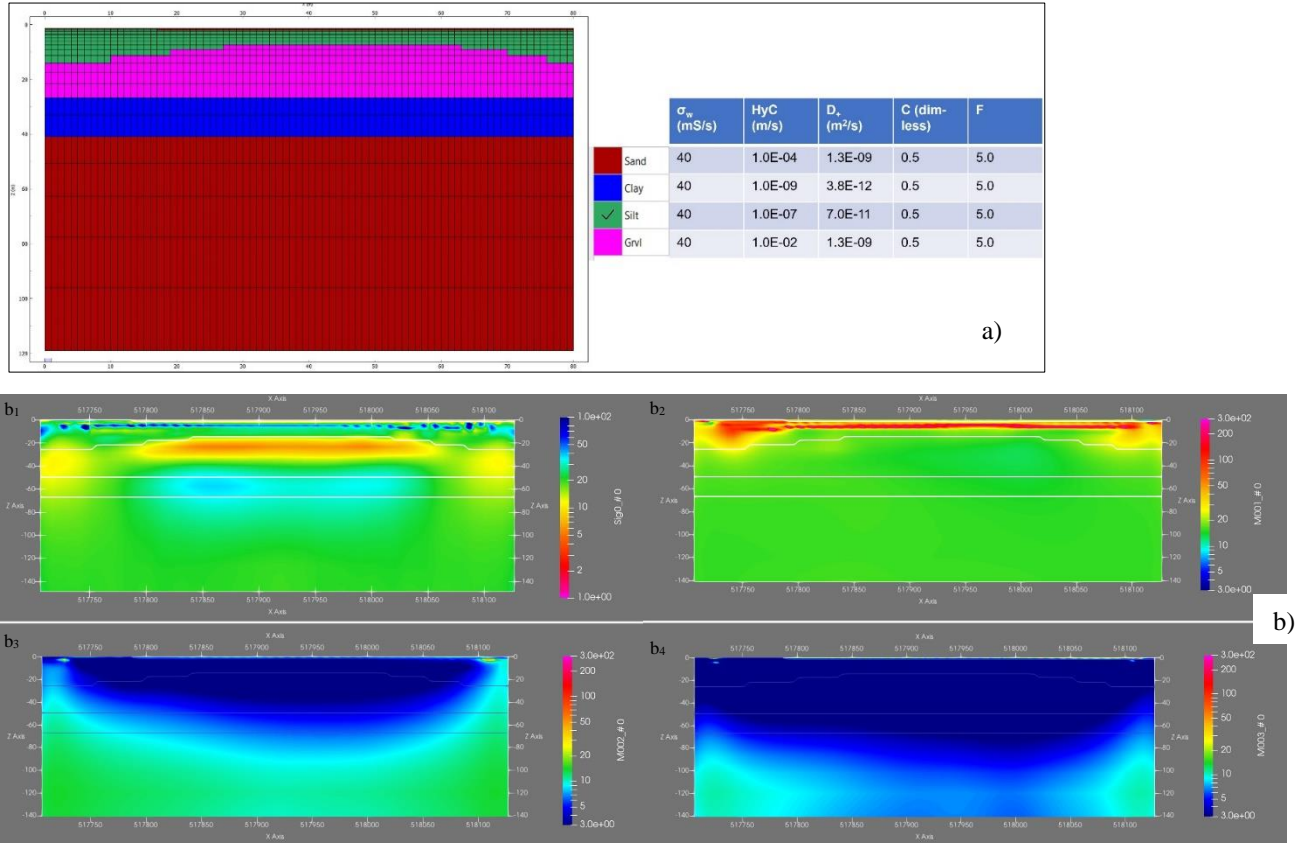


Figure 1: Inversion results of synthetic data. (a): The synthetic model built by using EEMstudio with four different lithologies; b1,b2,b3,b4: inversion parameters used in the Debye-Warburg decomposition re-parametrization (conductivity,  $m_1, m_2, m_3$ , respectively).

## References

- Cole, K. S., and R. H. Cole, 1941. Dispersion and absorption in dielectrics: The Journal of Chemical Physics, 9, 341–351, doi: 10.1063/1.1750906.
- Debye, P. 1929. Polar molecules. By P. Debye, Ph. D., Pp. 172. New York: Chemical Catalog Co., Inc., 1929. \$3.50. Journal of the Society of Chemical Industry, 48(43), 1036-1037.
- Dias, C. A. 2000. Developments in a model to describe low-frequency electrical polarization of rocks. Geophysics, 65(2), 437-451.
- Fiandaca, G., Zhang, B., Chen, J., Signora, A., Dauti, F., Galli, S., Sullivan, N.A.L., Bollino, A., Viezzoli, A. (2024). Closing the gap between galvanic and inductive induced polarization: EEMverter, a new modelling tool for Electric and Electromagnetic data. *7th international IP workshop, 28-30 May 2024, Lund, Sweden*.
- Nordsiek, S., and A. Weller, 2008. A new approach to fitting induced polarization spectra: Geophysics, 73, no. 6, F235–F245, doi: 10.1190/1.2987412.
- Pelton W.H., Ward S.H., Hallot P.G., Sill W.R. and Nelson P.H., 1978. Mineral discrimination and removal of inductive coupling with multi-frequency IP. Geophysics **43**, 588– 609.
- Revil, A., Florsch, N. and Camerlynck, C., 2014. Spectral induced polarization porosimetry. Geophysical Journal International, 198(2), 1016-1033.

Römhild, L., Fiandaca, G., Hu, L., Meyer, L. and Bayer, P., 2022. Imaging hydraulic conductivity in near-surface aquifers by complementing cross-borehole induced polarization with hydraulic experiments. *Advances in Water Resources*, 170, 104322.

# Three-dimensional vector finite element forward modeling and inversion for airborne electromagnetic data considering induced polarization effect

Jian Chen<sup>\*,1</sup>, Bo Zhang<sup>2</sup>, Gianluca Fiandaca<sup>1</sup>

<sup>1</sup>The EEM Team for Hydro & eXploration, Department of Earth Sciences "Ardito Desio", University of Milano, Milano (Italy).

[jian.chen@unimi.it](mailto:jian.chen@unimi.it).

<sup>2</sup>Institute of Earth exploration, Science and Technology, Jilin University, Changchun (China)

[\\*jian.chen@unimi.it](mailto:*jian.chen@unimi.it)

Modelling Induced polarization effects in airborne electromagnetic (AEM) data is becoming a standard tool in mineral exploration, but the industry standard is still based on one-dimensional (1D) forward and Jacobian modelling. We are developing a three-dimensional (3D) finite element electromagnetic forward and inversion method considering IP effects within the EEMverter modelling platform (Fiandaca et al., 2024). The computations are carried out in frequency domain, and then time-transformed in time domain through an Hankel transform. This allows to model any parameterization of the IP phenomenon, from the simple constant phase angle model to a full debye decomposition. Furthermore, 3D forward modeling mesh and inversion mesh are constructed separately: an Octree mesh is designed for efficient spatial segmentation for each sounding, while the inversion parameters are defined on a structured model mesh linked to the forward meshes through interpolation.

Each forward mesh only needs to be locally refined in the underground sensitive areas covered by the transmitter and receiver. This structure has good geometric flexibility, can easily simulate complex terrain, and greatly reduces the mesh size required to solve forward modeling problems. By separating the primary field  $\mathbf{E}^p$  and the secondary field  $\mathbf{E}^s$ , the background conductivity  $\sigma^p$  and the abnormal conductivity  $\sigma^s$ , and applying Dirichlet boundary conditions, the frequency domain electromagnetic double-curl partial differential equation is solved based on the vector finite element idea (Zhang et al. 2021):

$$\int_{\Omega} (\nabla \times \mathbf{N} \cdot \nabla \times \mathbf{E}^s - i\omega\mu(\sigma^s + \sigma^p)\mathbf{N} \cdot \mathbf{E}^s) dV = \int_{\Omega} (i\omega\mu\sigma^s \mathbf{N} \cdot \mathbf{E}^p) dV, \quad (1)$$
$$\mathbf{E}_s|_{\Omega} = 0.$$

Figure 1 and Figure 2 present the accuracy of forward and Jacobian computations as a function of frequency and resistivity.

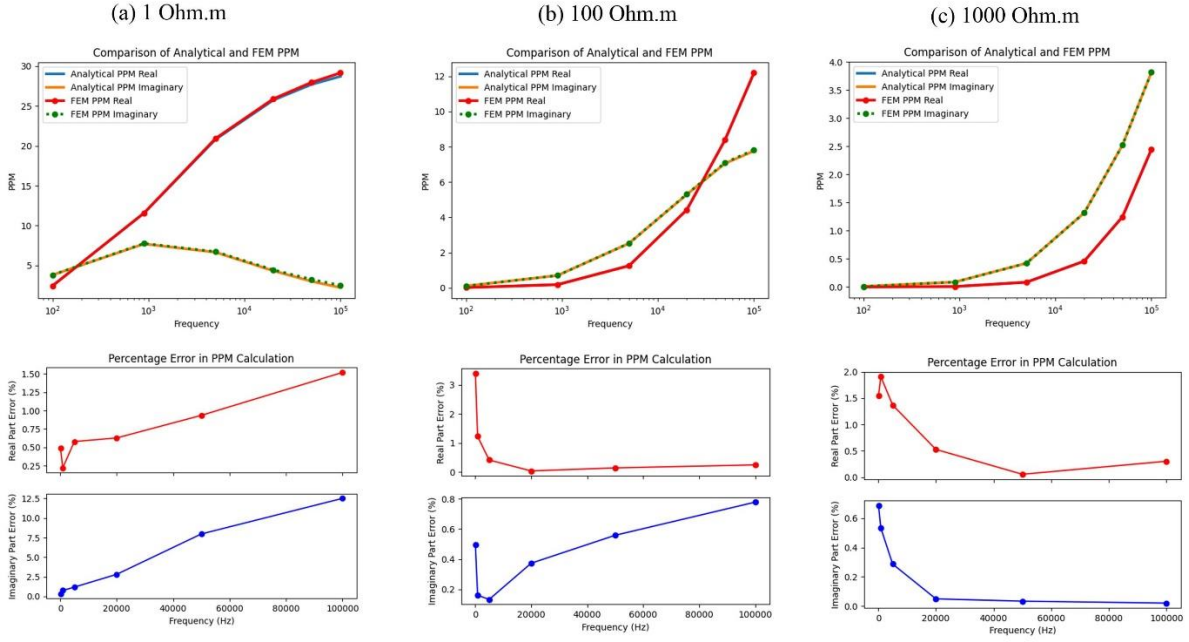


Figure 1: Comparison of calculation accuracy of three-dimensional finite element frequency domain electromagnetic forward modeling based on Octree mesh. The first row of graphs shows the comparison of PPM response values, and the second row shows the relative percentage error. (a) Half-space resistivity is 1 Ohmm; (b) Half-space resistivity is 100 Ohmm; (c) Half-space resistivity is 1000 Ohmm.

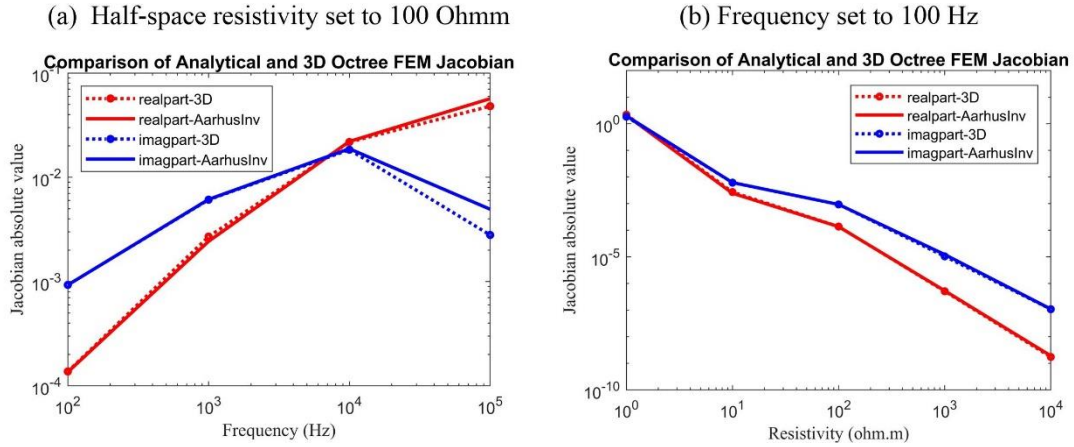


Figure 2: Comparison of calculation accuracy of the Jacobian. (a) Comparison of Jacobian values at different frequencies; (b) Comparison of Jacobian values at different resistivities.

## References

- Fiandaca, G., Zhang, B., Chen, J., Signora, A., Dauti, F., Galli, S., Sullivan, N.A.L., Bollino, A., Viezzoli, A. (2024). Closing the gap between galvanic and inductive induced polarization: EEMverter, a new modelling tool for Electric and Electromagnetic data. *7th international IP workshop, 28-30 May 2024, Lund, Sweden*.
- Zhang, B., Yin, C.C., Liu, Y.H., Ren, X.Y., Vikas C. B., and Xiong, B. (2021). 3D inversion of large-scale frequency-domain airborne electromagnetic data using unstructured local mesh. *GEOPHYSICS* 86: E333-E342.

# Closing the gap between galvanic and inductive induced polarization: EEMverter, a new modelling tool for Electric and Electromagnetic data

G. Fiandaca<sup>\*,1</sup>, B. Zhang<sup>2</sup>, J. Chen<sup>1</sup>, A. Signora<sup>1</sup>, F. Dauti<sup>1</sup>, S. Galli<sup>1</sup>, N.A.L. Sullivan<sup>1</sup>, A. Bollino<sup>1</sup>, A. Viezzoli<sup>3</sup>

<sup>1</sup> The EEM Team for Hydro & eXploration, Dept. of Earth Sciences “Ardito Desio”, Università degli Studi di Milano, Milano (Italy)

<sup>2</sup> Institute of Earth exploration, Science and Technology, Jilin University, Changchun (China)

<sup>3</sup> EMerge S.r.l., Cascina (Italy)

\* [gianluca.fiandaca@unimi.it](mailto:gianluca.fiandaca@unimi.it)

The phenomenon of Induced Polarization (IP) is commonly studied with galvanic methods, both in the field and in the laboratory. IP effects on inductive electromagnetic (EM) data have been reported since the early ‘80s, but the attention of the EM community in IP focuses mainly on exploration purposes, because strong chargeable anomalies trigger negative EM responses. However, Fiandaca et al. (2022) showed that the IP effect strongly affects EM data also in sand/clay environments, with a variety of acquisition systems, ranging from airborne EM to systems for continuous ground acquisitions. In this study we present a novel inversion software, EEMverter, specifically developed to model electric and electromagnetic data taking into account the IP phenomenon. Four distinctive features have been implemented in EEMverter: i) selectable IP parameterisations are allowed, ranging from Constant Phase Angle to Debye-Warburg decomposition, also making use of petrophysical relation for defining IP parameters in terms of hydraulic properties; ii) 1D, 2D and 3D forward modelling can be mixed sequentially or simultaneously in the iterative process within multiple inversion cycles, for diminishing the computational burden; iii) the joint inversion of Airborne IP (AIP), ground EM-IP and ground galvanic IP data is fully supported with a common IP parameterization; iv) time-lapse inversions of AIP, EM and galvanic IP data is possible with both sequential and simultaneous approaches.

Figure 1 presents the resistivity section of a synthetic model that mimics the electrical properties (both conduction and polarization) of sand, clay and consolidated formations, based on the petrophysical relations described in Weller et al. (2015), together with the inversion model of inductive and galvanic data. In particular, four different inversion results are presented: direct current and full-decay induced polarization (DCIP) galvanic data, with 10 m electrode spacing and 2D gradient sequence; AEM + ground EM data, with sounding distance of 40 m; AEM+ground EM + tTEM data (Auken et al., 2019), with tTEM soundings every 10 m; all data together in a joint inversion scheme.

The joint inversion presents much better resolution capability, with the inductive and galvanic data complementing each other in resolving both conductive and resistive layers. Examples of joint inversion of AEM, ground EM and galvanic IP data through EEMverter are presented in Dauti et al. (2024) in applications related to mineral exploration and in Signora et al. (2024) for the characterization of the HydroGeosITE, the Italian reference and calibration site for hydrogeophysical methods under development in Brescia, Italy.

We believe that EEMverter, with its common inversion environment for the IP inversion of inductive and galvanic data will help in closing the gap between galvanic and inductive IP.

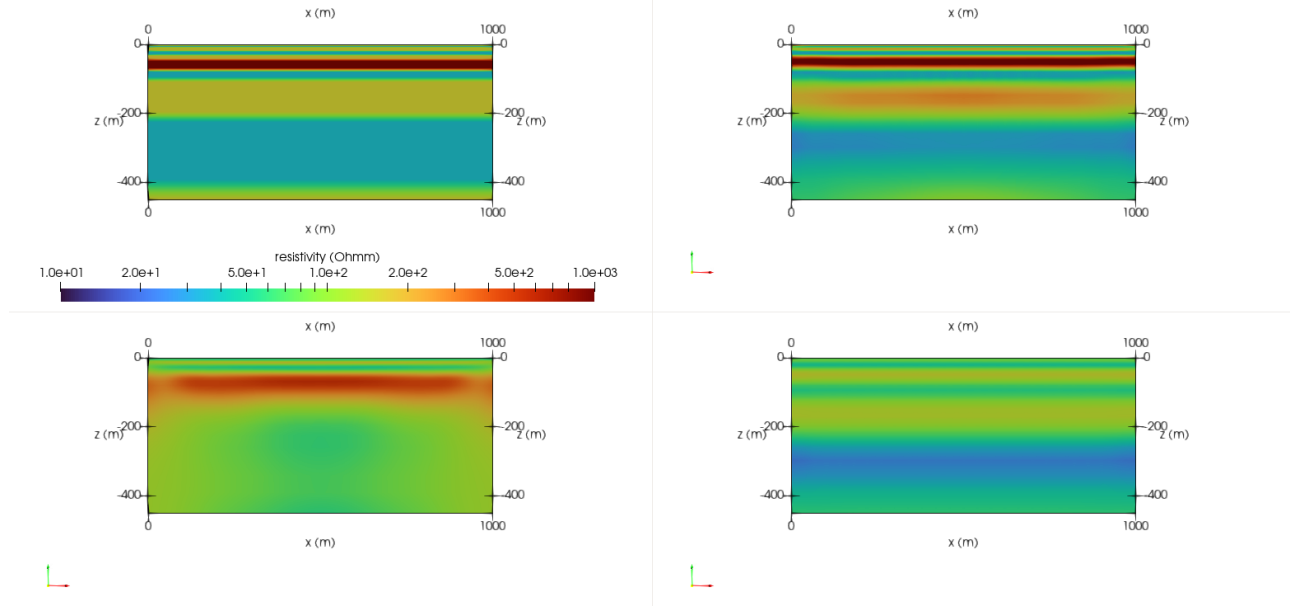


*Figure 1. Synthetic model and inversion results. Top left) resistivity section of a MPA IP simulation of electrical properties; Bottom left) inversion model of DCIP data; Bottom right) inversion model of AEM+ground EM data; Top right) joint inversion of all inductive and galvanic data.*

## References

- Auken E., Foged N., Larsen J.J., Trøllund Lassen K.V., Maurya P.K., Dath S.M., Eiskjær T.T., 2019. tTEM — A towed transient electromagnetic system for detailed 3D imaging of the top 70 m of the subsurface. *Geophysics*, 84 (1), E13-E22.
- Dauti, F., Viezzoli, A., Fiandaca, G., 2024. Inductive Induced Polarization: integration with galvanic DCIP and joint inversion. *7<sup>th</sup> International IP workshop, 28-30 May 2024, Lund, Sweden*.
- Fiandaca, G., Dauti F., Signora A., 2022. Effect of induced polarization on galvanic and inductive data: where does it matter most? *6<sup>th</sup> International Meeting on Induced Polarization WIP2022, 27-30 June 2022, Annecy, France*.
- Signora, A , Galli, S., Dauti, F., Sullivan, N. A. L., Lucchelli, A., Gisolo, M., Fiandaca, G., 2024. Joint inversion of E&EM data with IP modelling: The HydroGeosITE case study. *7<sup>th</sup> International IP workshop, 28-30 May 2024, Lund, Sweden*.
- Weller, A., Slater, L., Binley, A., Nordsiek, S., & Xu, S., 2015. Permeability prediction based on induced polarization: Insights from measurements on sandstone and unconsolidated samples spanning a wide permeability range. *Geophysics*, 80(2), D161-D173.

# Joint inversion of E&EM data with IP modelling: The HydroGeosITe case study

A. Signora<sup>\*,\*1</sup>, S. Galli<sup>1</sup>, F. Dauti<sup>1</sup>, A. L. Sullivan<sup>1</sup>, A. Lucchelli<sup>1</sup>, M. Gisolo<sup>2</sup>, G. Fiandaca<sup>1</sup>

<sup>1</sup>The EEM Team for Hydro & Exploration, Department of Earth Sciences, University of Milan (Italy), alessandro.signora@unimi.it

<sup>2</sup>A2A Ciclo Idrico S.p.a, Via Lamarmora 23, Brescia (Italy)

\* alessandro.signora@unimi.it

The HydroGeosITe project aims at the establishment of the first Italian calibration and reference site for airborne electromagnetic (AEM), ground EM and Electric Geophysical methods within the largest AEM campaign carried out in Italy for groundwater mapping and management (2021-2023,

>1800 km<sup>2</sup> survey area). The HydroGeosITe will serve as calibration site for future AEM campaigns, as well as for ground-based EM and galvanic surveys and its geophysical characterization combines galvanic direct current and full-decay induced polarization (DCIP), Airborne (AEM) and ground EM surveys (Figure 1).

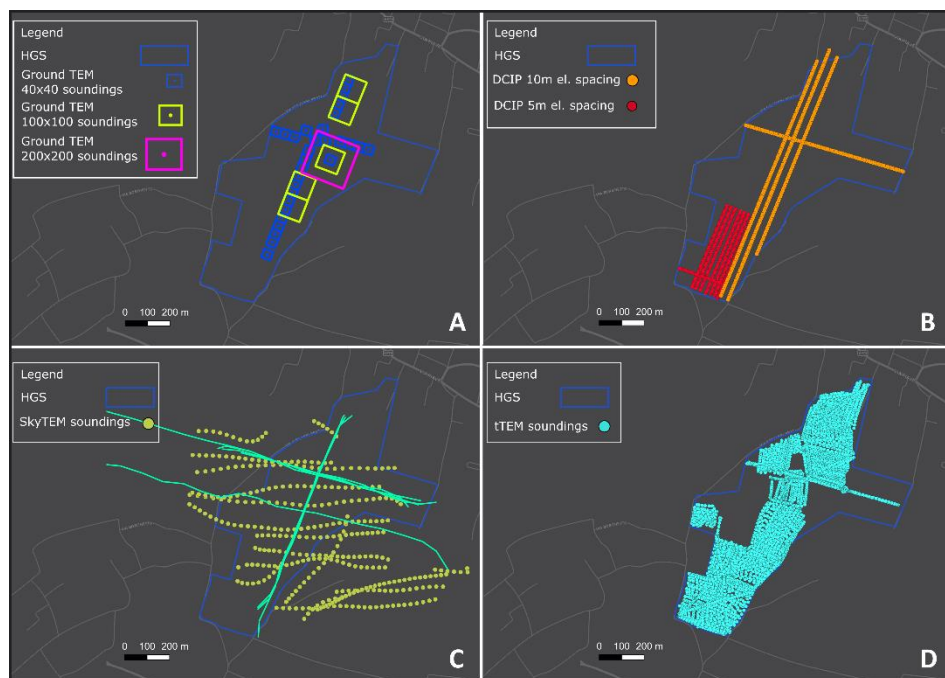


Figure 1: Maps reporting the geophysical surveys performed at the HydroGeosITe. A) Ground TDEM soundings (Thirty 40x40 m<sup>2</sup> Tx-Area; Five 100x100 m<sup>2</sup> Tx-Area; One 200x200 m<sup>2</sup> Tx-Area). B) Direct Current and Induced Polarization profiles (~7.4 km). C) SkyTem AEM System (350 soundings). D) tTEM EM system soundings (55 km).

All these different data have been inverted jointly taking into account induced polarization, for retrieving in a unique inversion process both conduction and polarization properties. In particular, the inversion is carried out in EEMverter (Fiandaca et al., 2024) modelling IP within a joint inductive/galvanic inversion where the EM data are modelled in 1D, while the galvanic DC and full-decay IP data are modelled in 2D in terms of the maximum phase angle (MPA) Cole-Cole re-parameterization (Fiandaca et al., 2018).

Two boreholes with lithological description and inductive resistivity logging are being drilled for validation down to 350 m, with the first borehole reaching a depth of 207 meters already completed.

Galvanic and Induced Polarization measurements on selected clay samples collected at various depths of the borehole have also been carried out.

The joint inversion scheme exhibits comparable data misfit when compared to the independent inversions, but shows significantly enhanced resolution (Figure 2), in strong agreement with the validation conducted through the borehole drilling and geophysical logging. These results open the way for a paradigm shift in E&EM imaging, closing the gap between galvanic and inductive methods in IP modelling.

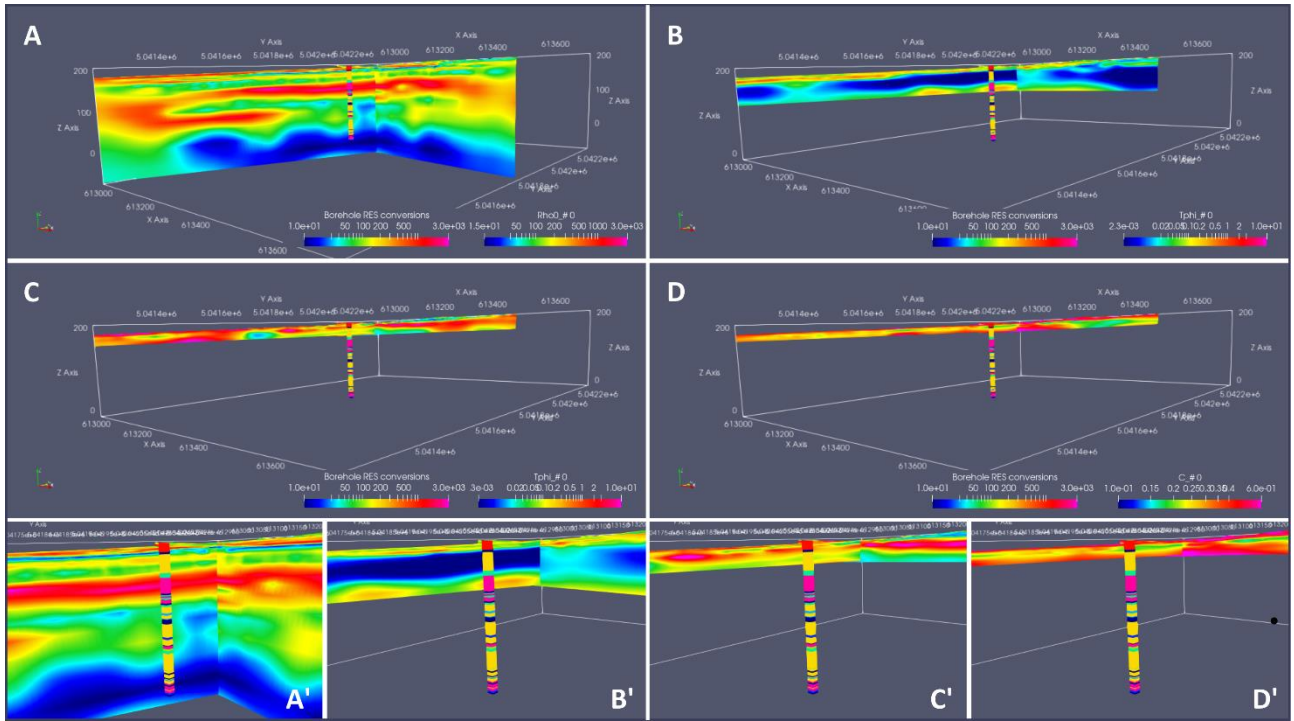


Figure 2: Joint Inversion models for the different Cole-Cole re-parametrized parameters (Fiandaca et., al 2018). On top of each model the resistivity conversion of the borehole stratigraphy is displayed. A) Resistivity parameter joint model (zoomed view in A' figure). B) Phi parameter joint model (zoomed view in B' figure). C) Tau parameter joint model (zoomed view in figure C'). D) C parameter joint model (zoomed view in figure C').

## References

- Fiandaca, G., Madsen, L. M., & Maurya, P. K. (2018). Re-parameterisations of the Cole–Cole model for improved spectral inversion of induced polarization data. *Near Surface Geophysics*, 16(4), 385-399.  
 Fiandaca, G., Zhang, B., Chen, J., Signora, A., Dauti, F., Galli, S., Sullivan, N.A.L., Viezzoli, A.; 2024: Closing the gap between galvanic and inductive induced polarization: EEMverter, a new modelling tool for Electric and Electromagnetic data. *7<sup>th</sup> International IP workshop, 28-30 May 2024, Lund, Sweden.*

# EEMstudio: a QGIS plugin for processing and modelling of electric and electromagnetic data with focus on induced polarization

N.A.L. Sullivan<sup>\*1</sup>, A. Viezzoli<sup>2</sup>, G. Fiandaca<sup>1</sup>

<sup>1</sup>*The EEM Team for Hydro & eXploration, Department of Earth Sciences “Ardito Desio”, Università degli Studi di Milano, Milano, Italy.*

<sup>2</sup> EMergo S.r.l., Cascina (PI), Italy

*\*nicole.sullivan@unimi.it*

In the workflow of electric and electromagnetic methods, processing is an essential step that have an influence on the outcome of the resulting models. IP effects in ground galvanic measurements are characterized by low signal-to-noise ratio, and effects generated by noise and interferences with anthropogenic infrastructures produce outliers on a significant fraction of the acquired IP data, which can be interpreted erroneously as geological features if not culled out during processing. Similarly, in inductive data, coupling results in artifacts in the models like spotted appearance and buried conductors (Viezzoli et al., 2013).

The preferred method for processing IP and inductive data is the visual inspection and manual culling of faulty data using ad hoc interfaces, possibly with the support of a georeferenced map, which helps in identifying man-made infrastructures like power lines, metal fences, guardrails and underground cables and pipes that generate coupling effects on both IP and inductive data.

EEMstudio is a QGIS plugin that gather visualization, processing and modelling tools within the QGIS environment (Fig. 1a). Processing is made in a designated tool configurated for both electric data (Fig. 1b) and electromagnetic data (not show in Fig. 1 for brevity). In this interface, various plots linked with the QGIS map allow a clear overview of the data, with a focus also on IP visualization. Here data can be inspected and removed where needed. In addition to data, it is possible also to upload, visualize and compare forward and model files to perform also quality control.

Regarding the modelling part, the inversions are handled using EEMverter, the inversion software developed by the EEM Team for Hydro & eXploration (Fiandaca et al., 2024), in 1D/2D/3D, also joint and timelapse. With EEMstudio is possible to gather and prepare all the files needed and launch directly the inversions.

One last app is the Model Builder (Fig. 1c), with the purpose of building 1D/2D/3D synthetic models to use as starting models or for forward computation.

EEMstudio was developed with the purpose of having all the necessary tools for processing and modelling of data in a unique environment, so that the workflow is optimized and convenient. Being it within QGIS, it is possible also to take advantage of all the functionalities of the most widespread open-source Geographic Information System software available.

It will be released open-source in a free version under the EUPL 1.2 software license, suitable for academic or professional use.

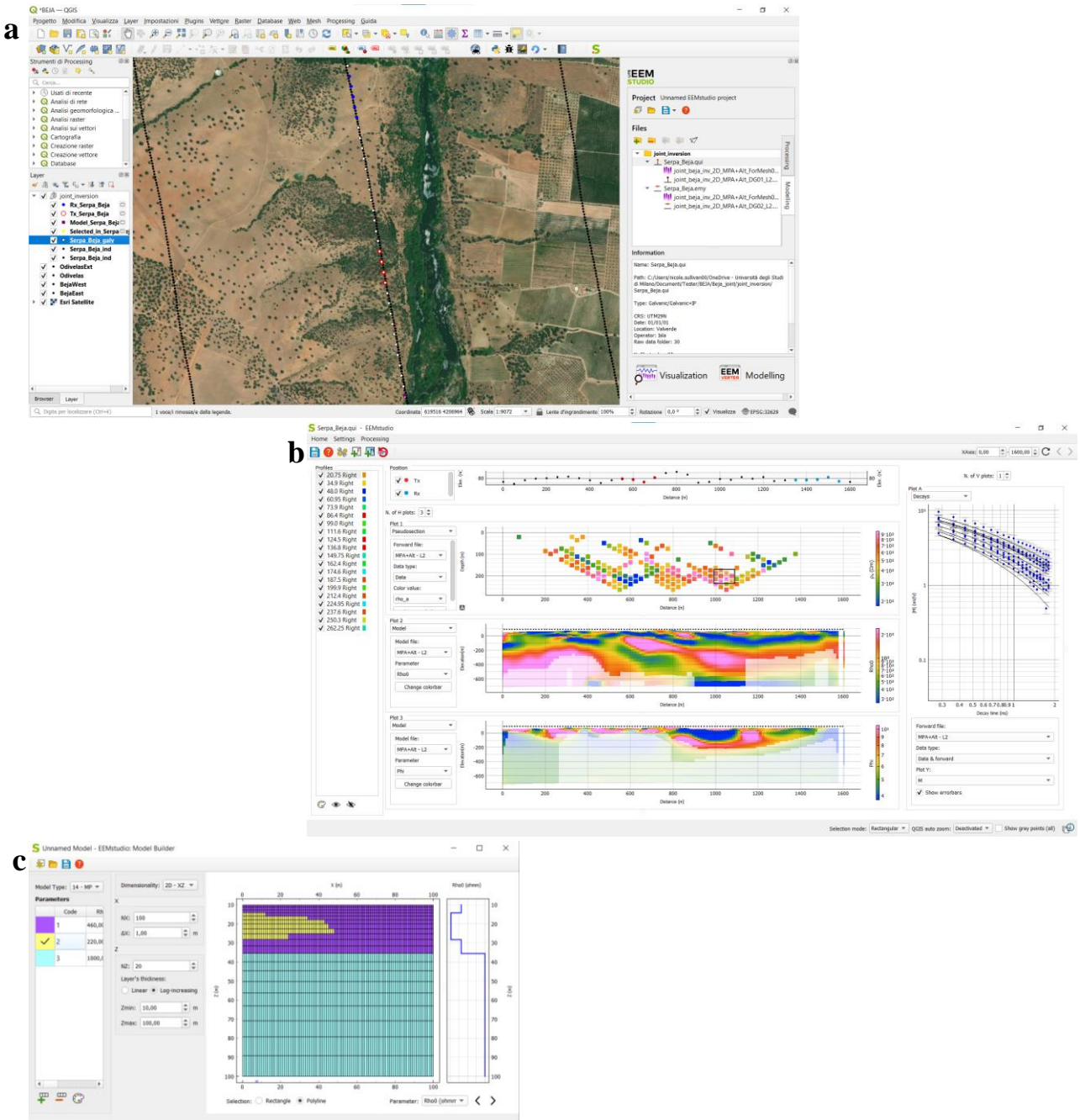


Figure 1: EEMstudio apps: a) QGIS main window with EEMstudio widget on the right and plotted layers from processing, b) processing and visualization app with galvanic data example, c) Model Builder to build synthetic models.

## References

- Fiandaca, G., Zhang, B., Chen, J., Signora, A., Dauti, F., Galli, S., Sullivan, N.A.L., Bollino, A. and Viezzoli, A, 2024. Closing the gap between galvanic and inductive induced polarization: EEMverter, a new modelling tool for Electric and Electromagnetic data. *7th international IP workshop, 28-30 May 2024, Lund, Sweden.*
- QGIS.org, % Y. QGIS Geographic Information System. QGIS Association. <http://www.qgis.org>
- Viezzoli, A., Jørgensen, F. and Sørensen, C., 2013. Flawed processing of airborne EM data affecting hydrogeological interpretation. *Groundwater*, 51, 191–202.

# Principle and application of array spread-spectrum IP technique for large depth of exploration

Chen Rujun \*<sup>1,2,3,4</sup>, Yao Hongchun <sup>1,2</sup>, Shen Ruijie <sup>1,2</sup>, He Lanfang <sup>5</sup>, Yang Lunkai <sup>6</sup>, Hu Hao <sup>6</sup>, Farid Ullah <sup>1,2</sup>

<sup>1</sup>*School of Geosciences and Info-Physics, Central South University, China, chen.rujun@foxmail.com*

<sup>2</sup>*AIoT Innovation and Entrepreneurship Education Center for Geology and Geophysics, Central South University, China*

<sup>3</sup>*Hunan Key Laboratory of Nonferrous Resources and Geological Hazards Exploration, China*

<sup>4</sup>*Key Laboratory of Metallogenetic Prediction of Nonferrous Metals, Ministry of Education, Central South University, China*

<sup>5</sup>*Key Laboratory of Mineral Resources, Institute of Geology and Geophysics, Chinese Academy Science, China*

<sup>6</sup>*Institute of Geochemical Exploration and Marine Geological Survey, Jiangsu Geological Bureau, China*

Induced polarization method (IP) is the main exploration method for metal sulfide deposits and is also widely used in groundwater exploration and evaluation. However, the IP method has long been restricted by problems such as small exploration depth, low exploration efficiency, and the inability to distinguish graphitized formation and pyrite haloes, which cause interference IP anomalies. Although the emergence of spectral induced polarization (SIP) has solved the problem of distinguishing sources of IP anomalies to a certain extent, SIP is less efficient than traditional IP exploration and is more susceptible to electromagnetic interference. In view of the practical problems faced in the application of the IP method, we proposed the spread spectrum IP (SSIP) method and developed related instruments. The SSIP method uses pseudo-random signals as the excitation field source, and then despreads the collected pseudo-random signals into amplitudes and phases of several controllable frequency points at the receiving end based on the idea of spread spectrum(Liu et al. 2017). The characteristics of the source of IP anomalies are distinguished through the amplitude and phase of multiple frequencies. The above method can greatly improve the exploration depth and anti-interference ability, and also includes the advantages of SIP (Liu et al., 2017, 2019). In terms of instruments, we have implemented synchronous real-time acquisition of massive SSIP receivers based on the wireless Internet of Things using ZigBee, thereby greatly improving exploration efficiency; based on the series and parallel technology of multiple controllable DC sources, the transmitter also takes into account high voltage and sending large currents (1000-2000V, 3-30A). The base frequency of spread spectrum waveform is controllable with frequency range as 1/1024 - 1024Hz.

SSIP instrument is an IP exploration and observation equipment that uses spread spectrum signals as transmitting, receiving and processing objects. It takes advantage of the inherent anti-interference ability and multi-frequency characteristics of spread spectrum signals to achieve high quality, high efficiency and high precision. SSIP instrument consists of a transmitting system, a receiver array, a current acquisition unit, and wireless networking components (figure 1). The receiver uses ZigBee wireless networking technology, capable of array observation.

The above-mentioned SSIP instruments have the advantages of large exploration depth, high exploration efficiency, and strong anti-interference ability (Liu et al., 2017, 2019; Xi et al, 2013). It has repeatedly achieved major prospecting breakthroughs in the exploration of various mineral deposits such as chromite (Xi et al., 2013), copper-molybdenum, lead-zinc (Liu et al., 2017, 2019), and copper-gold deposits in China. For example, in the Chushawan copper-molybdenum mining area in Nanyang City, Henan Province, the terrain is complex and pyrite is developed in shallow areas. SSIP exploration results found that the ore body causes low resistivity area, but there are multiple

low resistivity areas with no relationship with ore body. It was found that the F2 (1/8 Hz) SSIP anomalies are mainly caused by porphyry-type ore bodies, and the abnormal area and the ore body shape is basically the same. It has been verified that deep porphyry copper-molybdenum ore bodies have been discovered, of which molybdenum resources amount to 100,000 tons.

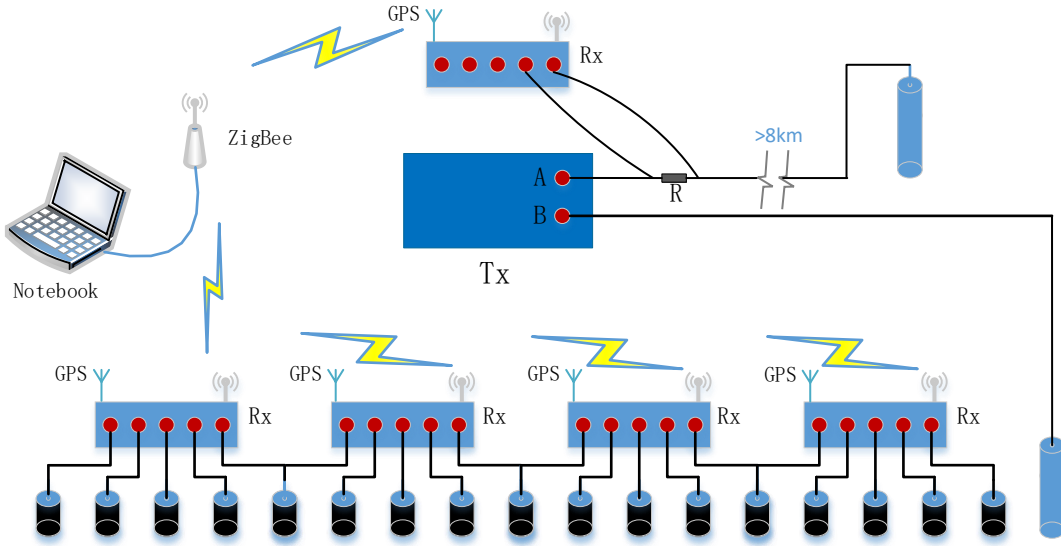


*Figure 1: Distributed SIP measurement system based on ZigBee and GPS synchronization. The receiving system is composed of multiple 4-channel receivers Rx supporting ZigBee wireless sensor networks. The transmitter Tx can transmit a spread spectrum signal. The transmitter uses a 4-channel receiver Rx to collect the current signal (only one channel is used). The notebook computer uses ZigBee network to control all current and voltage acquisition.*

In the west of Gucheng Lake, Gaochun District, Nanjing City, Jiangsu Province, where electromagnetic interference is strong, we used a power supply current of about 6A to achieve a depth of 1,000 m of SSIP sounding. The sounding results were verified by drilling and found 13 layers of copper, lead, zinc, gold, and silver polymetallic ore bodies. This proves that the results of our SSIP sounding are reliable.

## References

- Liu, W., Chen, R., Cai, H., Luo, W. and Revil, A., 2017. Correlation analysis for spread-spectrum induced-polarization signal processing in electromagnetically noisy environments. *Geophysics*, 82(5), pp.E243-E256.
- Liu, W., Lü, Q., Chen, R., Lin, P., Chen, C., Yang, L. and Cai, H., 2019. A modified empirical mode decomposition method for multiperiod time-series detrending and the application in full-waveform induced polarization data. *Geophysical Journal International*, 217(2), pp.1058-1079.
- Xi, X., Yang, H., He, L. and Chen, R., 2013, March. Chromite mapping using induced polarization method based on spread spectrum technology. In *Symposium on the Application of Geophysics to Engineering and Environmental Problems 2013* (pp. 13-19). Society of Exploration Geophysicists and Environment and Engineering Geophysical Society.

# Inverting time-domain induced polarization field data using Debye discretization

Thomas Günther<sup>1</sup>, Tina Martin<sup>2</sup>

<sup>1</sup>*Leibniz Institute for Applied Geophysics, Hannover, Germany, Thomas.Guenther@leibniz-liag.de*

<sup>2</sup>*Engineering Geology, Lund University, Sweden*

## Introduction

Induced polarization measurements (IP) in the field scale can contribute to imaging the subsurface, in both the frequency domain (FD) and the time domain (TD). In practice, for the data analysis still single-frequency or total-chargeability inversion is common. However, the spectral information contained in the data, i.e. by measuring multiple frequencies or time windows, can bear additional information on the underlying material and enable deriving important parameters like hydraulic conductivity (e.g., Maurya et al. 2018) or mineral types and contents (e.g., Martin et al. 2021).

Therefore it is beneficial to invert the whole data, and rather jointly than sequentially. In the frequency domain, one can constrain the neighboring frequencies (Günther & Martin 2016), but this cannot be easily transferred to time domain. There are approaches, however, mostly assuming a Cole-Cole behavior for every model cell (Fiandaca et al. 2012; Madsen et al. 2020). However, this assumption is not universally true and can lead to severe inversion artifacts if subsurface effects with skewed or multi-modal spectra is affecting the data. We present a new inversion algorithm based on a Debye decomposition in the modelling that can be applied to both FD and TD data.

## Debye decomposition

A Debye decomposition (DD) is the natural IP space splitting a spectrum or decay into a sum of exponential (Debye) relaxation terms, called the relaxation time distribution (RTD). Nordsiek & Weller (2008) introduce DD in the FD, minimizing the number of non-zero RTD. Tarasov & Titov (2007) discuss the Debye decomposition of a signal in the time-domain by using smoothness constraints along the relaxation time axis. We follow the latter approach. From the RTD, one can derive a total chargeability and a characteristic log-mean relaxation time for further analysis.

## Full-waveform processing

TDIP data provides high-resolution (10 kHz sampling rate) time series that are contaminated by noise of different sorts. Olsson et al. (2016) process the data sequentially by removing an offset ( $u_0$ ), a linear drift, harmonic noise cancelling and a Cole-Cole term leaving the DC resistance and a Decay. We fit all parameters simultaneously

$$u = RI + u_0 + dt + \sum_{k=1}^K e^{-t/\tau_k} + \sum_{l=1}^L a_l \cos(\omega_l t) + b_l \sin(\omega_l t)$$

Additionally, we account for the effect of different measuring pulses superposing each other (Tarasov & Titov 2007) so that the Debye sum is summed over all pulses. Additionally, a Cole-Cole term over the whole wave train accounts for slowly decaying electrode polarization. Result of the processing is a resistance value  $R$  and a data RTD that can be used to describe the decay using arbitrary time axis instead of integrating over gates. Alternatively, the data space can stay in the Debye space thus avoiding a subjective gating. The forward operator finally iterates over the relaxations.

## Inversion

We extend the DD to the modelling domain, so that every model cell is described by an RTD. Consequently, a 2D resistivity problem becomes a 3D inverse problem. For regularization, we use smoothness constraints both in the spatial domain (between neighboring cells of the same relaxation time) and in the spectral domain (between neighboring relaxation times of the same cells), similar to the frequency constraint approach used by Günther & Martin (2016). This is already implemented numerically efficient in the pyGIMLi (Rücker et al. 2017) framework *MultiFrameModelling* by using block matrices for both the Jacobian matrix and the regularization matrix.

## Application

We apply the method to data from the Mjölkalånga site in Sweden where good contrasts can be seen and the new approach be used for (e.g.) calculating hydraulic properties (see abstract/poster Martin et al.) from the total chargeability (TC) and the mean relaxation time.

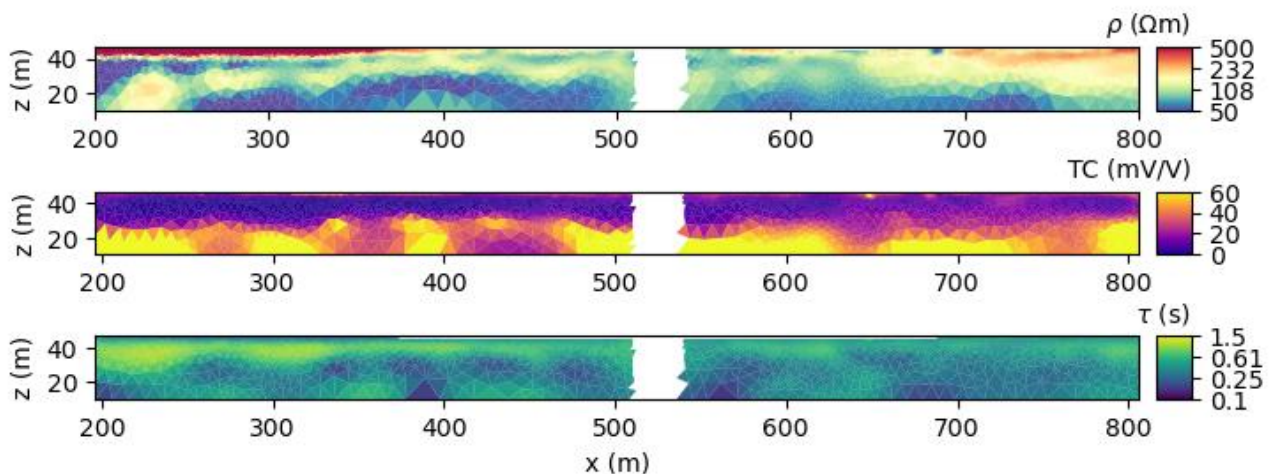


Figure 1: Inversion result from Mjölkalånga P1: resistivity (top), total chargeability (center) and logmean relaxation time (bottom).

## References

- Fiandaca G, Ramm J, Binley A, Gazoty A, Christiansen A V and Auken E. 2013. Resolving spectral information from time domain induced polarization data through 2-d inversion. *Geophys. J. Int.* 192. 631-646. [doi:10.1093/gji/ggs060](https://doi.org/10.1093/gji/ggs060)
- Günther T and Martin T. 2016. Spectral two-dimensional inversion of frequency-domain induced polarization data from a mining slag heap. *J. of Applied Geophysics*. 135. 436-448. [doi:10.1016/j.jappgeo.2016.01.008](https://doi.org/10.1016/j.jappgeo.2016.01.008)
- Madsen L M, Fiandaca G and Auken E. 2020. 3-d time-domain spectral inversion of resistivity and full-decay induced polarization data -- full solution of Poisson's equation and modelling of the current waveform. *Geophys. J. Int.* 223. 2101-2116. [doi:10.1093/gji/ggaa443](https://doi.org/10.1093/gji/ggaa443)
- Martin T, Günther T, Weller A and Kuhn K. 2021. Classification of slag material by spectral induced polarization laboratory and field measurements *J. Appl. Geoph.* 194. [doi:10.1016/j.jappgeo.2021.104439](https://doi.org/10.1016/j.jappgeo.2021.104439)
- Maurya P K, Fiandaca G, Christiansen A V and Auken E. 2018. Field-scale comparison of frequency- and time-domain spectral induced polarization. *Geophys. J. Int.* 214, 1441-1466. [doi:10.1093/gji/ggy218](https://doi.org/10.1093/gji/ggy218)
- Olsson P-I, Fiandaca G, Larsen J J, Dahlin T and Auken E. 2016. Doubling the spectrum of time-domain induced polarization by harmonic de-noising, drift correction, spike removal, tapered gating and data uncertainty estimation. *Geophys. J. Int.*. 207, 774-784. [doi:10.1093/gji/ggw260](https://doi.org/10.1093/gji/ggw260)
- Rücker C, Günther T and Wagner F. 2017. pyGIMLi: An open-source library for modelling and inversion in geophysics. *Computers & Geosciences* 109, 106-123. [doi:10.1016/j.cageo.2017.07.011](https://doi.org/10.1016/j.cageo.2017.07.011)
- Tarasov A and Titov K. 2007. Relaxation time distribution from time domain induced polarization measurements, *Geophys. J. Int.* 170, 31-43. [doi:10.1111/j.1365-246x.2007.03376.x](https://doi.org/10.1111/j.1365-246x.2007.03376.x)

# Processing of Time-Domain Induced Polarization datasets with reciprocal measurements

Matteo Rossi<sup>1</sup>, Aristeidis Nivorlis<sup>1</sup>, Torleif Dahlin<sup>1</sup>

<sup>1</sup>Engineering Geology, Lund University, Sweden, matteo.rossi@tg.lth.se

Induced Polarization (IP) is often a weak and noisy signal to be recorded, both in frequency- and time-domain. For this reason, dealing with reciprocal measurements is not as straightforward as processing the direct-current electrical resistivity (e.g. see Flores Orozco et al., 2012).

The present work focuses on surface and cross-hole datasets, acquired in time-domain (TD) with a dipole-dipole configuration. The main goal is to streamline a processing framework to analyze the voltage signal of full-waveforms and obtain a reliable IP response together with an estimation of the uncertainty of the measurements.

Pairs of reciprocal measurements can have different superimposed noise, as magnitude and frequency. Moreover, the voltage response in charging and discharging pulses can be altered by a drifting trend due to some polarization that occurs at the electrode/soil interface. After some preliminary processing steps to clean the data from these types of noise (similar to Olsson et al., 2016), the reciprocal full waveforms are statistically analyzed for each time pulse. Only the pulses that pass a statistical test are further considered in the processing, since the noise level can vary towards the total acquisition time of a full waveform.

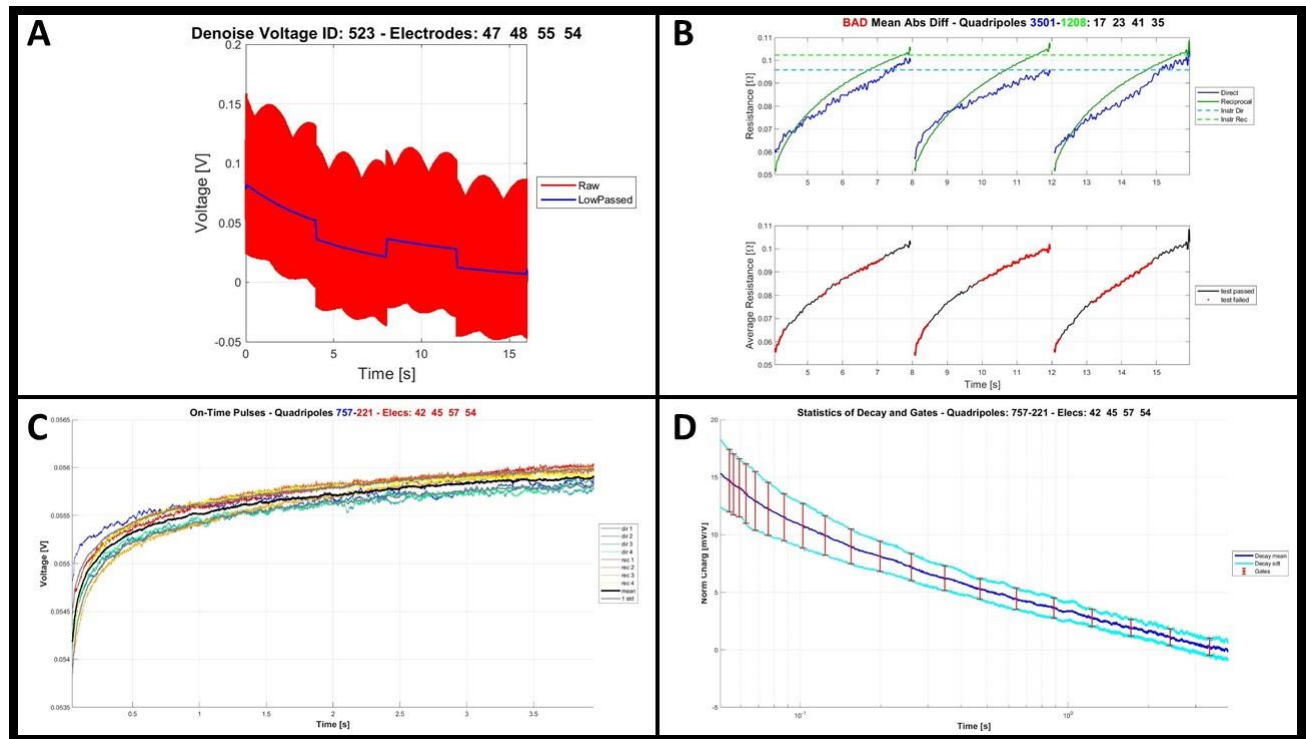


Figure 1. Some of the processing steps for analysing the reciprocal full waveforms: A) denoise; B) statistical test for each pulse; C) collection of pulses that passed the statistical test; D) final decay curve with relative uncertainty.

The quality of resistivity and IP measurements are treated simultaneously, since they are correlated in the same full waveform, and an accurate estimation of the uncertainties can be quantified.

The processed full waveforms can also be analyzed to directly extract the complex resistivity of some frequencies (depending on the pulse length). This frequency domain information is then statistically analyzed for each reciprocal pair and finally compared with the results of the time-domain processing.

## Acknowledgements

Funding has been provided by the Swedish Research Council Formas – A Swedish Research Council for Sustainable Development (ref. 2016-20099), SBUF (Svenska Byggbranschens Utvecklingsfond) – The Development Fund of the Swedish Construction Industry (ref. 13336 and 13938), ÅForsk (ref. 14-332), SGU – Geological Survey of Sweden, Sven Tyréns Stiftelsen, Västra Götlandsregionen, The Crafoord Fundation (id. 20190869), and Lund University. We wish to thank our project partners at SGU and Tvätteriet Alingsås for the fruitful collaboration and valuable help provided.

## References

- Flores Orozco A., A. Kemna, E. Zimmermann, 2012, Data error quantification in spectral induced polarization imaging, *Geophysics*, 77 (3), pp. E227-E237.
- Olsson, P.I., Fiandaca, G., Larsen, J.J., Dahlin, T. and Auken, E., 2016. Doubling the spectrum of time-domain induced polarization by harmonic de-noising, drift correction, spike removal, tapered gating and data uncertainty estimation. *Geophysical Supplements to the Monthly Notices of the Royal Astronomical Society*, 207(2), pp.774-784.

# An open-source suite for deployment of automated DCIP monitoring: towards real-time monitoring applications

Aristeidis Nivorlis<sup>1,2</sup>, Torleif Dahlin<sup>2</sup>, Per Hedblom<sup>2</sup>

<sup>1</sup> Deltares, 2600 MH Delft, The Netherlands, aris.nivorlis@deltares.nl

<sup>2</sup> Engineering Geology, Lund University, Sweden

Geoelectrical monitoring is time-consuming, labor-intensive, and prone to human error if carried out manually. Therefore, the measurement process (from data collection to inversion) needs to be automated to reduce the time and effort required to conduct monitoring experiments (Dimech et al., 2022). Including Induced Polarization (IP) data, most commonly in the time-domain, adds another layer of complexity because the full waveform data (Olsson et al., 2016) and the chargeability decays (Flores Orozco et al., 2018) need to be meticulously evaluated.

We present an open-source Python suite that offers a complete solution for autonomous and automated monitoring experiments. The suite contains three major components i) data acquisition and handling ii) processing and inversion of DCIP data iii) a template for interactive visualization and reporting (Figure 1). Furthermore, the components can be used independently and modified to accommodate different experiments and use-cases.

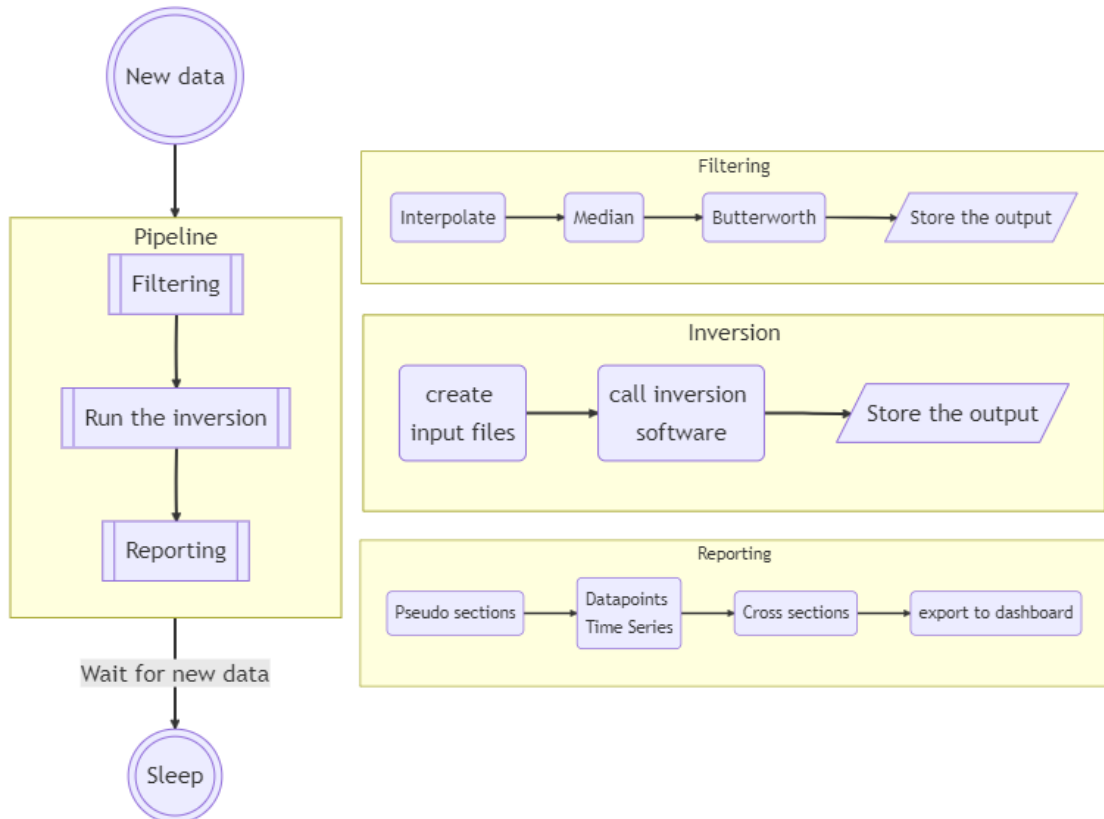


Figure 1: The proposed data pipeline can be adopted and used to automate the processing and inversion of geoelectrical data, effectively enabling real-time monitoring.

The proposed methodology has been evaluated in multiple scenarios and successfully implemented at four test sites, with results presented by e.g. Nivorlis et al. (2024) and Norooz et al. (2023). It is robust and may be implemented without substantial programming expertise. It can significantly reduce the time and effort required to conduct geoelectrical monitoring surveys, especially in large areas, and offers a complete and scalable solution that enables close to real-time geoelectrical monitoring. Following the open-source example of other geoelectrical libraries (Cockett et al., 2015; Rücker et al., 2017), the aim is to create a central framework for geophysical monitoring tools and attract further contributions.

## References

- Cockett, R., Kang, S., Heagy, L. J., Pidlisecky, A., & Oldenburg, D. W. (2015). SimPEG: An open source framework for simulation and gradient based parameter estimation in geophysical applications. *Computers & Geosciences*, 85, 142–154. <https://doi.org/10.1016/j.cageo.2015.09.015>
- Dimech, A., Cheng, L., Chouteau, M., Chambers, J., Uhlemann, S., Wilkinson, P., Meldrum, P., Mary, B., Fabien-Ouellet, G., & Isabelle, A. (2022). A Review on Applications of Time-Lapse Electrical Resistivity Tomography Over the Last 30 Years: Perspectives for Mining Waste Monitoring. *Surveys in Geophysics*, 43(6), 1699–1759. <https://doi.org/10.1007/s10712-022-09731-2>
- Flores Orozco, A., Gallistl, J., Bücker, M., & Williams, K. H. (2018). Decay curve analysis for data error quantification in time-domain induced polarization imaging. *Geophysics*, 83(2), E75–E86. <https://doi.org/10.1190/geo2016-0714.1>
- Nivorlis, A., Sparrenbom, C., Rossi, M., Åkesson, S., & Dahlin, T. (2024). Multidisciplinary monitoring of an in-situ remediation test of chlorinated solvents. *Science of The Total Environment*, 922, 170942. <https://doi.org/10.1016/j.scitotenv.2024.170942>
- Norooz, R., Dahlin, T., Olsson, P., Nivorlis, A., Günther, T., & Bernstone, C. (2023). Monitoring Internal Erosion in Embankment Dams Using 3D Electrical Resistivity Tomography: Älvkarleby Test Embankment Dam. 2023(1), 1–5. <https://doi.org/10.3997/2214-4609.202320112>
- Olsson, P.-I., Fiandaca, G., Larsen, J. J., Dahlin, T., & Auken, E. (2016). Doubling the spectrum of time-domain induced polarization by harmonic de-noising, drift correction, spike removal, tapered gating and data uncertainty estimation. *Geophysical Journal International*, 207(2), 774–784. Scopus. <https://doi.org/10.1093/gji/ggw260>
- Rücker, C., Günther, T., & Wagner, F. M. (2017). pyGIMLi: An open-source library for modelling and inversion in geophysics. *Computers and Geosciences*, 109, 106–123. Scopus. <https://doi.org/10.1016/j.cageo.2017.07.011>